Indian Journal of Natural Sciences www.tnsroindia.org.in ©IJONS

Vol.9 /Issue 52 / February / 2019 *International Bimonthly* *ISSN: 0976 – 0997*

RESEARCH ARTICLE

Ameliorating Effects of *Morus alba* Leaves Extract on Nephrotoxicity - Induced by Gentamicin in Male Rats

Mojtaba I. Hashim[1]*and Salma J. Askar[2]

Department of Physiology, Biochemistry and Pharmacology, College of Veterinary Medicine, University of Baghdad, Iraq.

Received: 13 Nov 2018 Revised: 15 Dec 2018 Accepted: 17 Jan 2019

*Address for Correspondence
Mojtaba I. Hashim
Department of Physiology,
Biochemistry and Pharmacology,
College of Veterinary Medicine,
University of Baghdad, Iraq.
Email: saif1998-2008@yahoo.com

ABSTRACT

The present study was designed to evaluate the ameliorating effect of methanolic extract of *Morus alba* L. leaves on nephrotoxicity induced by intramuscular injection of gentamicin in order to give an experimental evidence for its established use. The experiment was involved the extraction of *Morus alba* leaves by using 70% methanol solvent. The yielding percentage of methanolic extract of *Morus alba* L. leaves was (27%). To study the ameliorating effect of leaves methanolic extract of *Morus alba* on nephrotoxicity induced by gentamicin, (75) Swiss albino male rats were used weighing (200-230)gm. which were divided randomly into five equal groups, 15 rats in each group as follows: G1 (control) which was received distilled water orally daily for 5 and 10 days. G2: received gentamicin sulphate (5mg/kg) intramuscularly once daily for 5 and 10 days. G3: received co-administration of gentamicin (5mg/kg) intramuscularly + 200 mg/kg of leaves methanolic extract orally daily for 5 and 10 days. G4: received co-administration of gentamicin (5mg/kg) intramuscularly + 400 mg/kg of methanolic leaves extract orally daily for 5 and 10 days respectively, while the G5: received gentamicin + Vitamin C 200mg/kg orally. All the treatments were given in amounts levels of (0.1/100gm) B.W. Five rats from each group were left 10 days more without any additional treatments as recovery period. Animals of each group were sacrificed at the end of 5, 10 and 20 days and bloods were collected and sera were separated for biochemical and antioxidant analysis. The results showed significant increase at ($P<0.05$) in serum levels of creatinine, BUN, uric acid ,MDA oxidative enzyme and significant decrease at ($P<0.05$) in the serum levels of GSH antioxidant enzyme in the group (G2) in the periods of treatment 5,10 and 20 days recovery, while there were significant decrease at ($P<0.05$) in serum levels of creatinine, BUN, uric acid, MDA and increase in GSH antioxidant enzyme in the groups G3,G4 and G5 which return to normal levels. These findings revealed that the co-administration of gentanicin + methanolic extract of *Morus alba* leaves has been

exhibited more activity as antioxidant in treating of nephrotoxicity induced by gentamicin and indicate that the methanolic leaves extract of *Morus alba* displays a good therapy against nephrotoxicity and nephrotoxicant agents.

Keywords: *Morus alba*, Extract, Nephrotoxicity, Rats

INTRODUCTION

Gentamicin is an aminoglycoside antibiotic that is widely used for treating infections of gram negative bacteria (Bentley *et al*. 2010). The specificity of gentamicin renal toxicity is related to its accumulation in the renal proximal tubules and in lysosomes (Nagai and Takano, 2004) which lead to direct tubular necrosis and loss of tubular brush border integrity (Pedraza-Chaverri *et al*., 2003). The mechanism of gentamicin-induced nephrotoxicity is not completely known. Balakumar *et al*, (2010) reported that gentamicin induced nephrotoxicity by inhibiting protein synthesis in renal proximal tubular cells resulting in acute tubular necrosis followed by acute renal failure. Moreover gentamicin has been shown to increase the generation of reactive oxygen species (ROS) like superoxide anion (O_2^-), hydroxyl radicals (OH) and hydrogen peroxide (H_2O_2) as well as reactive nitrogen species (RNS) in the renal cortex that lead to renal structural and functional deterioration (Wang *et al*., 2006, Martinez- Salgado *et al*., 2007 and Balakumar *et al*., 2008). *Morus alba* Linn (mulberry) is an nontoxic natural therapeutic agent which belongs to Moraceae family is an example that contains more than 150 species and *Morus alba* L. (white mulberry) is the most important among them(Srivastava *et al*., 2006 and Zafar *et al*., 2013). Because of its highly therapeutic effects and low toxicity *Morus alba* has been widely used as anti-inflammatory (Chen *et al*., 2013), neuroprotective, skin tonic, strong antioxidant, antihyperglycemic, antibacterial, antihypertensive and antihyperlipidemic effects (Nomura *et al*., 1980, Chu *et al*., 2006, Butt *et al*., 2008 and Sun *et al*., 2011), diuretic astringent and antioxidant (Yang *et al*., 2010 and Kobayashi *et al*., 2010). In recent years numerous data indicate that phytochemicals rich-mulberry extract related exhibit wide range of protective and therapeutics role in pathogenesis of brain disease due to the presence of phenolic compounds such as Alzheimer's disease (Song *et al*., 2014, Qiao *et al*., 2015 and El-Sayyad, 2015), parkinson diseases (Kim *et al*.,2010, Khan *et al*., 2013 and Strathearn *et al*., 2014), neuroprotective activity (Weber *et al*., 2012, Wang *et al*., 2014 and Seo *et al*., 2015) and depression (Lee *et al*., 2013). *Morus alba* is rich in polyphenolic compounds especially the flavonoids and among the flavonoids quercetin 3-(6-malonylglucoside) which is the most significant for antioxidant potential of mulberry plant (Butt *et al.,* 2008). The leaves of mulberry contains higher amount of quercetin which is responsible for reduction of oxidation process in vivo and in vitro (Iqbal *et al.,* 2012). More previously studies used the toxic dose of gentamicin to induce nephrotoxicity and there were few studies that used the clinical dose of gentamicin so we have interest to study the the ameliorating of Morus alba methanolic leaves extract against nephrotoxicity induced by using the clinical dose of gentamicin in rats**.**

MATERIALS AND METHODS

Animals

This study was performed under the guidelines supervision of Ethical Committee for lab. Animals work in the College of Veterinary Medicine, University of Baghdad. Seventy five male Wister albino rats about five months of age and with body weight ranged 200-230gm.were used to perform the experiment of the present study. Rats were housed in plastic cages 20×50 ×75 cm dimensions, placed in a special housing room belongs to the Department of Physiology ,Biochemistry and Pharmacology / College of Veterinary Medicine /University of Baghdad for two weeks for acclimatization. Standard rodent diet (Commercial feed pellets) and tap water were freely available. Housing condition were maintained at 20-25 ^oC in air-conditioned room, while the light/ dark cycle was 12/12.

Plant Material

Freshly leaves of *Morus alba* L. collected from local trees of Salah-AL-Din in Tuz city, Iraq during September and October 2017. The leaves were cleaned from soils and dust, which washed with tap water and dried about (1-7) days in room temperature at shade .The dried leaves were pounded to a fine powder by an electrical grinder and kept in glass container .The plant classification was done in the Ministry of Agriculture/ State Board for Seeds Testing and Certification S.B.S.T.C in Abu-Graib /Baghdad at certificate No. 3585 in 13 / 09 /2018**.**

Extraction of *Morus alba* L. Leaves

The powder of *Morus alba* L. leaves was extracted with methanol 70% . 100 gram of the leaves powder was placed in 1 liter flask with 1000 ml of 70% methanol, with stirring by using magnetic stirrer hot plate for 8 hrs. The extraction temperature was 35-40C°, then the mixture was filtered via sterilized gauze to acquire free of rough particulars and then filtered by Whatmann filter paperd. The filtered solution evaporated at 45C° in incubator for 3 days. The dried final extract was kept frozen at –20 C° until use (Anwar *et al*., 2015).

Preparation of *Morus alba* Leaves Extract Concentrations

Stock solution was prepared by mixing (5000mg) from dried extract with distilled water and completed the volume to (10ml) to get a concentration of (500mg/ml). Then the concentration of (200mg/ml) was prepared by mixing (1ml) from stock solution and completing to (2.5ml) of distilled water and each rat was given a dose volume of (0.1ml/100g) B.W. (Dkhil *et al*., 2015).

Preparation of Gentamicin Solution

Gentamicin Sulphate injection (80mg/2ml) ampoule was used. The solution was prepared by taking 1ml (40mg) of gentamicin sulphate from the ampoule and completing to (8ml) of normal saline to get a concentration of (5mg/ml) and it was given to rats intramuscularly at a dose of 5mg/kg B.W. (Zahid *et al*., 2013).

Preparation of Vitamin C Solution

Vitamin C (500mg) tablet was used. The solution was prepared by dissolving tablet (500mg) in (2.5ml) of distilled water to get a concentration of (200mg/ml), which was given to rats at a dose of 200mg/kg orally (Yousef *et al*., 2012).

Experimental Design

The experiment was designed to evaluate the ameliorating effect of methanolic extract *Morus alba* leaves on nephrotoxicity induced by gentamicin. Total of (75) male rats were divided randomly into five groups, (15) rats in each group. Treatments began with schedules as follows:

Group 1 (Control): was received distilled water (0.1ml/100gm) orally daily for periods of (5) and (10) days.

Group 2: was received gentamicin sulphate (5mg/kg) intramuscularly daily for (5) and (10) days.

Group 3: was received co-administration of gentamicin sulphate (5mg/kg) intramuscularly + (200mg/kg) of methanolic extract of *Morus alba* leaves orally daily for (5) and (10) days.

Group 4: was received co-administration of gentamicin sulphate (5mg/kg) intramuscularly + (400mg/kg) of methanolic extract of *Morus alba* leaves orally daily for (5) and (10) days.

Group 5: was received co-administration of gentamicin sulphate (5mg/kg) intramuscularly + (200mg/kg) of standard naturally antioxidant vitamin C orally daily for (5) and (10) days.

Five rats from each group were left for 10 days periods without any additional treatment as a recovery period. All the treatments were given at adose volume of (0.1ml/100)gm.B.W.

Parameters Studied

After the end of 5, 10 days and 10 days of recovery period of treatments of each group, the blood samples were collected. Blood was obtained via the heart puncture from each rat using syringes. Blood were kept in gel tubes and serum was isolated after centrifugation at a speed of 3000 revolution/minute (rpm) for (15) minutes, and then serum samples were stored in freezer at (-20C^0) until analysis for:

I.Biochemical tests

- Serum BUN levels
- Serum creatinine levels
- Serum uric acid levels

II.Parameter related to oxidant-antioxidant status

- Serum reduced glutathione concentration (GSH) levels.
- Serum Malondialdehyde (MDA) levels.

Statistical Analysis

Data are presented as mean ± S.E. which were analyzed by using completely randomized design in factorial experimental (One-way) ANOVA SPSS package(2008).A probability of ($P < 0.05$) was considered as significant differences (Steel and Torrie,1980).

RESULTS

The Effect of Gentamicin and *Morus alba* Leaves Methanolic Extract on Serum Blood Urea Nitrogen (BUN) mg/dl.

The concentration of serum blood urea nitrogen (BUN) mg/dl in different groups are illustrated in table **(3.1)** which reveal significant ($P<0.05$) increase in serum urea nitrogen levels in group (G2) in periods of 5, 10 days and 10 days recovery periods as compared to control group (G1) and there were significant ($P<0.05$) decrease in the levels of serum BUN in the groups (G3,G4 and G5) as compared to gentamicin(G2) group.

The Effect of Gentamicin and *Morus alba* Leaves Methanolic Extract on Serum Creatinine Levels (mg/dl)

The values represented in table (3.2) reveal significant ($P<0.05$) increase in serum creatinine levels (mg/dl) in the rats those received gentamicin at the periods 5, 10 days and 10 days recovery periods as compared to the normal values of (G1) group. From the other hand there were significant ($P<0.05$) decrease in serum creatinine levels of groups (G3, G4 and G5) as compared to gentamicin group (G2).

The Effect of Gentamicin and *Morus alba* Leaves Methanolic Extract on Serum Uric Acid Levels (mg/dl).

The concentrations of serum uric acid (mg/dl) in different groups are represented in table (3.3). There were significant ($P<0.05$) increase in the levels of uric acid in the serum of rats that treated with gentamicin (G2) group in the periods

5, 10 days and 10 days recovery periods as compared to control group (G1). On the other hand there were significant ($P<0.05$) decrease in the levels of serum uric acid in the groups (G3, G4 and G5) in treated periods and recovery as compared to gentamicin group (G2).

The Effect of Gentamicin and *Morus alba* Leaves Methanolic Extract on Serum Reduced Glutathione (GSH) Levels (µmol/L).

Table (3.4) shows the levels of serum reduced glutathione (GSH) of all groups. The results show there were significant ($P<0.05$) decrease in GSH levels in serum of rats group (G2) as compared to (G1) control group, while there were significant ($P<0.05$) increase in GSH levels in (G3, G4 and G5) groups in comparison with (G2) group that treated with gentamicin.

The Effect of Gentamicin and *Morus alba* Leaves Methanolic Leaves Extract on Serum Malondialdehyde (MDA) Levels (µmol/L).

Concerning the levels of serum (MDA), there were significant ($P<0.05$) increase levels of these values in the (G2) group in the periods of 5, 10 days and recovery periods as compared to (G1) group that received distilled water and there were significant ($P<0.05$) decrease in the values of (MDA) in serum rats of (G3, G4 and G5) groups as compared to (G2) group.

DISCUSSION

Effect of Gentamicin and *Morus alba* Leaves Methanolic Extract on Serum Levels of BUN, Uric Acid and Creatinine.

The results of the present study corroborated the findings of previous investigations in which nephrotoxicant effects of gentamicin were observed. The study showed an increase in serum levels of blood urea nitrogen (BUN), uric acid and creatinine in gentamicin treated group (G2), while rats of (G3,G4 and G5) treated groups showed significant decrease of serum blood urea nitrogen, uric acid and creatinine levels which return to the normal levels. Our findings are in agreement with previous studies that found gentamicin caused marked renal dysfunction by significant increase in serum BUN, uric acid and creatinine levels (Cronin and Thompson, 1991 and Silan *et al*., 2007). The marked increase of these values indicates to the reduction in glomerular filtration rate as well as impairment of renal blood flow. In addition uric acid is the primary catabolic product of protein and non-protein nitrogen, kidney excretes uric acid primarly by tubular excretion and uric acid increases in massive tissue destruction and renal disease (Sonnenwirth and Jarret, 1980). Gentamicin induced increase the levels of serum BUN, uric acid and creatinine as a result of membrane lipid peroxidation due to stimulation of reactive oxygen species (ROS) such as H_2O_2 and O_2 which potentially induce the contraction of mesangial cells which lead to change in filtration surface area and ultrafiltration coefficient that causes retardation in glomerular filtration rate (Derakhshanfar *et al*., 2007). These values will be decreased in serum and began to return to normal control (G1) after the co- administration of *Morus alba* methanolic leaves extract with gentamicin and vitamin C with gentamicin groups (G3, G4 and G5) by the fact that the methanolic leaves extract has the potent antioxidant activity which increase proportionally with the increase of polyphenolic contents and a highly positive relationship between total phenols and antioxidant activity which appear to be in many plant species (Oktay *et al*., 2003 and Khan *et al*., 2013). The same studies reported that methanolic extract of *Morus alba* had the free radical scavenging activity by proton-donating ability of the extract which could serve as free radical inhibitors and inhibit lipid peroxidation (Khan *et al*., 2013). Nephrotoxicity induced by gentamicin is a complex phenomenon which characterized by an increase in serum BUN, uric acid and creatinine levels and severe proximal renal tubular necrosis that followed by renal failure (Al-Majed *et al*., 2002). The reduction in glomerular filtration rate which is indicated by the increase in serum creatinine levels would be accompanied by

an increase in BUN levels when a marked renal parenchymal injury occurs (Erdem *et al*., 2000). Our findings also are in agreement with recent studies (Lakshmi and Sudhakar, 2010; Pitchai *et al*., 2017 and Vagh *et al*., 2017) which showed that higher values of plasma uric acid were found in rats on day (7) of treatment with gentamicin which associated with renal dysfunction and severe proximal renal tubular necrosis followed by renal failure. In the present study the elevation in serum values of BUN, uric acid and creatinine in rats treated with gentamicin were brought to normal levels in the rats treated with *Morus alba* leaves extracts and vitamin C by reducing the effects of gentamicin induced nephrotoxicity may be due to potent antioxidant effects and diuretic property of this plant and that are in agreement with (El-Ghiaty *et al*., 2014 and Reddy *et al*., 2016). The mechanism behind elevation serum urea and creatinine might be that gentamicin increases the entry of Ca^{+2} in the mesengeal cells leading to reduced glomerular filtration rate (Stojiljkovic *et al*., 2008). The increase in BUN levels in gentamicin treated group is might due to high level of ROS that might be alter the protein synthesis and catabolism (Ishaq *et al*., 2015). The co-administration of plant extract along with gentamicin in our study reduced the levels of raised serum BUN and creatinine suggesting that the contents of *Morus alba* leaves extract protected the integrity of kidney tissue.

Effect of Gentamicin and *Morus alba Leaves* Methanolic Extract on Serum Reduced Glutathione (GSH) and Malondialdehyde (MDA) µmol/L in Rats.

It has been demonstrated that gentamicin generates reactive oxygen species (ROS) that mediate biomolecules oxidation in the kidney (Walker *et al.,* 1999). In the present study *Morus alba* leaves extract improves the serum levels of glutathione (GSH), the antioxidant defense against gentamicin induced oxidative damage and this may be due to free radical scavenging property of the extract as well as direct antioxidant activity (Schmid *et al*., 2008). Our findings are in agreement with (Alqasoumi, 2013) which reported that plant extract attenuated the harmful effects of gentamicin both by inhibiting free radical formation or by restorations of antioxidant systems due to presence of flavonoids and tannins that possess potent antioxidant and free radical scavenging properties. The antioxidant activity increased with increasing polyphenols content and there are highly relationship between total polyphenols and antioxidant activity in many plant species (Oktay *et al*., 2003) which play free radical neutralization and lipid peroxidation inhibition. Also increased levels of antioxidant enzyme (GSH) in our study are in agreement with previous studies (El-Beshbishy *et al*., 2006 and Sadighara *et al*., 2013) which demonstrated that *Morus alba* 70% methanolic leaves extract could be a natural antioxidant sources and powerful antioxidant properties, while (Dkhil *et al*., 2015) reported that *Morus alba* methanolic extract which administered to mice induce a highly reduction in serum levels of malondialdehyde (MDA) and highly elevation in glutathione levels (GSH). The presence of flavonoids and phenols in *Morus alba* leaves could be responsible for hydroxyl radical (OH) scavenging activity thus it is quite clear that changes observed in GSH could be attributed to the enhancement in antioxidant status in serum of rats (Madhumitha and Indhuleka, 2012). The decrease in the serum levels of GSH in (G2) group may be due to its increased utilization for scavenging gentamicin or oxygen derived radicals and administration of *Morus alba* leaves extract restored the GSH levels to the normal values which indicated the antioxidant effects of the plant extract (Ishaq *et al*., 2015).

CONCLUSION

From the data of our study, we could conclud that renal damage due to gentamicin is associated with oxidative stress and the primary site of damage was renal proximal convoluted tubules. The curative effects of *Morus alba* leaves extract on gentamicin - induced nephrotoxicity by normalization the serum concentration of BUN, creatinine and uric acids. The curative effects of *Morus alba* leaves extract against gentamicin - induced nephrotoxicity possibly by attenuating the oxidative stress induced by administration of gentamicin, by inhibiting lipid peroxidation and enhancing serum glutathione antioxidant enzyme activity.

Recommendations

From our data we can recommended that the serum BUN, creatinine and uric acid levels should be monitored during the course of treatment with gentamicin and if found unusual should be corrected accordingly. *Morus alba* leaves extract could lead to discover a novel pharmaceutical formulation which will be useful for treatment of drug - induced nephrotoxicity or use as a health - care food supplement. Additional studies are necessary to explore other possible mechanisms of *Morus alba* leaves extract by using other extract solvents and in other species of animals.

ACKNOWLEDGMENTS

The author would like to thank Assist. Prof.Dr.Luma W. Khalil, Head of Department of Physiology , Biochemistry and Pharmacology , College of Veterinary Medicine , University of Baghdad ,Iraq for assistance in completing this work.

REFERENCES

1. Bentley, M.L. Corwin, H.L. and Dasta, J. (2010). Drug - induced acute kidney injury in the critically ill adult : Recognition and prevention strategies. Critical Care Medicine, 38: 169- 174.
2. Nagai, J. and Takano, M. (2004). Molecular Aspects of Renal Handling of Aminoglycosides and Strategies for Preventing the Nephrotoxicity. Drug Metabolism and Pharmacokinetics, 19 (3) : 159-170.
3. Pedraza-Chaverri, J. Gonzales-Orozco, A.E. Maldonado, P.D. Medina-Campos, O.N. and Hernandez-Pando, R. (2003). Diallyl disulphide ameliorates gentamicin - induced oxidative stress and nephropathy in rats. European Journal of Pharmacology, 473: 71-78.
4. Balakumar, P. Rohilla, A. and Thangathirupathi, A. (2010). Gentamicin-induced nephrotoxicity: Do we have a promising therapeutic approach to blunt it? Pharmacological Research, 62(3): 179-186.
5. Wang, Z. Liu, L. Mei, Q. Liu, L. Ran, Y. and Zhang, R. (2006). Increased expression of heat shock protein 72 protects renal proximal tubular cells from gentamicin-induced injury. Journal of Korean medical science, 21 (5): 904-910.
6. Martinez-Salgado, C. Lopez-Hernanddez, F.J. and Lopez-Novoa, J.M. (2007). Glomerular nephrotoxicity of aminoglycosides. Toxicology and Applied pharmacology, 223: 86-98.
7. Balakumar, P. Chakkarwar, V.A. Reddy, J. and Singh, M. (2008). Experimental models of nephropathy. Journal of Renin - Angiotensin - Aldosterone System, 9: 189-195.
8. Srivastava, S. Kapoor, R. Thathola, A. and Srivastava, R.P. (2006). Nutritional quality of leaves of some genotypes of mulberry (*Morus alba*), Int. J. Food Sci. Nutr., (57): 305–313.
9. Zafar, M.S. Muhammad, F. Javed, I. Akhtar, M. Khaliq, T. Aslam, B. Waheed, A. Yasmin, R. and Zafar H. (2013). White Mulberry (Morus alba): A Brief Phytochemical and Pharmacological Evaluations Account. Int. J. Agric. Biol., 15 (3): 612-620.
10. Chen, Y.C. Tien, Y.J. Chen, C.H. Beltran, F.N. Amor, E.C. Wang, R.J. Wu, D.J. Mettling, C. Lin, Y.L. and Yang, W.C. (2013). *Morus alba* and active compound oxyresveratrol exert anti-inflammatory activity via inhibition of leukocyte migration involving MEK/ERK signaling. Chen et al. BMC Complementary and Alternative Medicine, 13: 45.
11. Nomura, T. Fukai, T. and Kuwanon, G. (1980).A New Flavone Derivative from the Root Barks of the Cultivated Mulberry Tree (Morus alba L.). Chem. Pharm. Bull., 28(8): 2548- 2552.
12. Chu, Q. Lin, M. Tian, X. and Ye, J. (2006). Study on capillary electrophoresis - amperometric detection profiles of different parts of Morus alba L. J.Chromatogr. A., 1116 (1-2): 286- 90.
13. Butt, M.S. Nazir, A. Sultan, M.T. and Schroën K. (2008). *Morus alba* L. nature's functional tonic, Trends Food Sci. Technol., (19): 505–512.

14. Sun, F. Shen, L.M. and Ma, Z.J. (2011).Screening for ligands of human aromatase from mulberry (Mori alba L.) leaf by using high-performance liquid chromatography/tandem mass spectrometry. Food. Chem., 126(3): 1337 - 1343.
15. Yang, Y. Gong, T. Liu, C.H. and Chen, R.Y. (2010). Four New 2-Arylbenzofuran Derivatives from Leaves of *Morus alba*L. Chem. Pharm. Bull., 58(2): 257- 260.
16. Kobayashi, Y. Miyazawa, M. and Kojima, T. (2010). The use of *Morus alba* L. (mulberry) : and *Eucommiaulmoides* (Tochu) : leaves as functional foods : a promising approach in the management of hyperlipidemia. J. Trad. Med., 27: 227 -230.
17. Song, N. Yang, H. Pang, W. Lian, F. and Jiang, Y. (2014). Mulberry Extracts Alleviate a β25-35- Induced Injury and Change the Gene Expression Profile in PC12 Cells. Evid Based Complement Alternat Med., 150 - 617.
18. Qiao, A. Wang, Y. Zhang, W. and He, X. (2015). Neuroprotection of Brain-Targeted Bioactive Dietary Artoindonesianin O (AIO) from Mulberry on Rat Neurons as a Novel Intervention for Alzheimer's Disease. J. Agric. Food Chem., 63(14): 3687-3693.
19. El-Sayyad, H.I. (2015).Cholesterol overload impairing cerebellar function: The promise of natural products. Nutrition, 31(5): 621 - 630.
20. Kim, H. G. Ju, M.S. Kim, M.C. and Lee, S.H. (2010).Mulberry fruit protects dopaminergic neurons in toxin-induced Parkinson's disease models. Br. J. Nutr., 104 (1):
21. Khan, M.A. Abdur, R.A. Islam, S. Haque, M. and Khurshid, A.H. (2013). A comparative study on the antioxidant activity of methanolic extracts from different parts of *Morus alba* L. (Moraceae). BMC. Res. Notes., 6: 24.
22. Strathearn, K.E. Gad, Y. Grace, M.H. and Lila, M.A. (2014). Neuroprotective effects of anthocyanin and proanthocyanidin-rich extracts in cellular models of Parkinson s disease. Brain Res., 1555: 60-
23. Weber, J. T. Lamont, C.L. and Slemmer, J.E. (2012). Potential neuroprotective effects of oxyresveratrol against traumatic injury. Eur. J. Pharmacol.,680(1-3): 55-62.
24. Wang, C.P. Zhang, L.Z. Li, G.C. Ding, F. and Liang, X. M. J. (2014). Mulberroside A protects against ischemic impairment in primary culture of rat cortical neurons after oxygen-glucose deprivation followed by reperfusion. J. Neurosci. Res., 92 (7): 944 - 54.
25. Seo, K.H. Lee, D.Y. Jeong, R.H. Hong, E.K. and Baek, N.I. (2015). Neuroprotective effect of prenylatedarylbenzofuran and flavonoids from morus alba fruits on glutamate-induced oxidative injury in HT22 hippocampal cells. J. Med. Food., 18(4): 403 - 8.
26. Lee, M.S. Park, W.S. Kim, Y.H. Morita, K. and Her, S. (2013). Antidepressant-like effects of Cortex Mori Radicis extract via bidirectional phosphorylation of glucocorticoid receptors in the hippocampus. Behav. Brain. Res., 236 (1):56-61.
27. Iqbal, S. Younas, U. Chan, K.W. Sarfraz, R.A. and Uddin, K. (2012). Proximate composition and antioxidant potential of leaves from three varieties of Mulberry (Morus sp.) : a comparative study. Int. J. Mol. Sci., 13(6): 6651- 6664.
28. Anwar, F. Kanwal, S. Shabir, G. Alkharfy, K.M. and Gilani, A.H. (2015). Antioxidant and Antimicrobial Attributes of Different Solvent Extracts from Leaves of Four Species of Mulberry. International Journal of Pharmacology, 11(7): 757-765.
29. Dkhil, M. Bauomy, A.A. Diab, M.S.M. and Al-Quraishy, S. (2015). The antioxidant effect of Morus alba leaves extract on kidney, testes, spleen and intestine. Pakistan J. Zool., 47 (2): 393 - 397.
30. Zahid, M. Ahmed, S. and Anjum, S. (2013). Electrolyte imbalance associated with aminoglycosides - An experimental study. PJMHS., 7(4): 1090 - 1093.
31. Yousef, J.M. Chen, G. Hill, P.A. and Li, J. (2012). Ascorbic acid protects against the nephrotoxicity and apoptosis caused by colistin and effects its pharmacokinetics. J. Antimicrob. Chemother., 67: 452- 459.
32. 32 .Steel, R. G. D. and Torrie, J. H. (1980). Principles and procedures of statistic. A biometrical lab roach (2nd edition).
33. Cronin, R.E. and Thompson, J.R. (1991). Role of potassium in pathogenesis of acute renal failure. Miner Electrolyte Metab., 17: 100- 105

34. Silan, C. Uzun, O. Comunoglu, N.U. and Cengiz, M. (2007). Gentamicin - induced nephrotoxicity in rats ameliorated and healing effects of resveratrol. Biol. Pharm. Bull., 30: 79 - 83.
35. Sonnenwirth, A.C. and Jarett, L.(1980). Gradwohl Clinical Laboratory Methods and Diagnosis. 8 th Ed. The C.V. Mosby Co., St.Louis.
36. Derakhshafar, A. Bidadkosh, A. and Kazeminia, S. (2007). Vitamin E Protection against gentamicin - induced nephrotoxicity in rats : a biochemical and histopathologic study. Iranian J. Vet., 8: 231- 238.
37. Oktay, M. Gulcin, I. and Kufrevoiglu, O.I. (2003). Determination of in vitro antioxidant activity of funnel (FoeniculumVulgare) seed extracts. LWT - Food Sci. Technol., 36: 263- 271.
38. Al-Majed, A.A. Mostafa, A.M. Al-Rikabi, A.C. and Al-Shabanah, O.A. (2002). Protective effects of oral Arabic gum administration on gentamicin - induced nephrotoxicity in rats. Pharmacol. Res., 46: 445- 451.
39. Erdem, A. Gundogan, N.U. Kara, A. and Bozkurt, A. (2000). The protective effect of taurine against gentamicin-induced acute tubular necrosis in rats. Nephrology Dialysis Transplantation, 15(8): 1175-1182.
40. Lakshmi, B.V. and Sudhakar, M. (2010). Protective effect of Zingiber officinale on gentamicin - induced nephrotoxicity in rats. Intl. J. Pharmacol., 6 (1): 85- 62.
41. Pitchai, B. Witnesskoe, W.E. Gan, Y.S. and Bahari, M.B. (2017). Effects of pre and post - treatment with dipyridamole in gentamicin - induced acute nephrotoxicity in the rat. Regulatory Toxicol. Pharmacol., 84: 35 - 44.
42. Vagh, A.A. Patel, R.M. Mavadiya, S.A Mehta, C.T. and Varia, R.D. (2017). Clinico - Biochemical and Nephroprotective effects of medicinal herbs on gentamicin induced nephrotoxicity in Wistar rats. Indian J. Vet. Sci. Biotech., 13(1): 62 - 69.
43. El- Ghiaty, M.A. Ibrahim, M.H. Abdou, S.M. and Hussein, F.Z. (2014). Evaluation of the protective effect of Cystone against cisplatin - induced nephrotoxicity in cancer patients, and its influence on cisplatin antitumor activity. Intl. Urol. Nephrol., 46 (7): 1367 - 1373.
44. Reddy, R.Y. Sujatha, C. and Raghavendra, H.G. (2016).Nephroprotective effect of Hibiscus plant ifolius in gentamicin induced nephrotoxicity in rats. Cre. J. Res., 2(2): 26 - 33.
45. Stojiljkovic, N. Mihailovic, D. Veljkovic, S. and Jovanovic, I. (2008). Glomerular basement membrane alterations induced by gentamicin administration in rats. Exp. Toxico. Pathol., 60:69-75.
46. Ishaq, B. Murtaza, S. Khan, J. and Anwar, H. (2015). Protective potentialof Trachyspermum ammi seeds in gentamicin- induced nephrotoxicity in rabbit model. Boletin Latinoamericano y del Caribe de Plantas Medicinales y Aromaticas, 14(4):280-286.
47. Walker, P. D. Barri ,Y. and Shah, S.V. (1999). Oxidant mechanisms in gentamicin nephrotoxicity. Ren.Fail., 21:433-442.
48. Schmid, U. Stopper, H. Heidland, A. and Schupp, N. (2008). Benfotiamine exhibits direct antioxidant capacity and prevents induction of DNA damage in vitro. Diabetes Metab. Res. Rev., 24: 371- 377.
49. Alqasoumi, S. (2013). Protective effect of Ipomeaaquaticafrosk Protective effect of Ipomoea aquaticaForsk on gentamicin - induced oxidative stress and nephropathy in rats. Topclass J. Herb Med., 2: 13-19.
50. El-Beshbishy, H.A. Singab, A.N. Sinkkonen, J. and Pihlaja, K. (2006).Hypolipidemic and antioxidant effects of Morus alba L. (Egyptian mulberry) root bark fractions supplementation in cholesterol - fed rats. Life Sci., 78: 2724- 2733.
51. Sadighara, P. Jafari, A.M. Khaniki, G.J. and Lotei, A.A. (2013). Potential therapeutic effects of Morus alba leaf extract on modulation oxidative damage induced by hyperglycemia in cultured fetus fibroblast cells. Glob. Vet., 10: 35- 38.
52. Madhumitha, S. and Indhuleka, A. (2012).Cardioprotective effect of *Morus alba* L. leaves in isoprenaline induced rats. Int. J. Pharm. Sci. Res., 3: 1475- 1480.

Table 1. The Effect Of Gentamicin And *Morus Alba* Leaves Methanolic Extract On Serum Blood Urea Nitrogen (BUN) mg/dl In Rats

Group	Mean ± SE		
	5 Day	10 Day	Recovery periods
G1 : Control D.W orally	46.00 ± 1.58 A a	45.40 ± 2.08 A a	45.40 ± 2.23 A a
G2 : Gentamicin (5mg/kg) B.W. I/M	70.80 ± 0.86 B a	96.00 ± 2.00 B b	81.00 ± 0.63 B c
G3 : Gentamicin (5mg/kg) B.W. I/M + *Morus alba* leaves extract (200mg/kg) B.W. orally	66.00 ± 0.71 C a	60.00 ± 1.14 C b	55.00 ± 0.70 C c
G4 : Gentamicin (5mg/kg) B.W. I/M + *Morus alba* leaves extract (400mg/kg) B.W. orally	55.00 ± 0.71 D a	50.00 ± 0.70 D b	48.00 ± 0.71 AD b
G5: Gentamicin (5mg/kg) B.W. I/M + Vit C (200mg/kg) B.W. orally	50.00 ± 0.83 D a	44.40 ± 0.81 A b	45.40 ± 1.93 AD b

♦ Values are presented as mean ± SE
♦ Small different letters denoted to (P<0.05) significant differences within groups.
♦ Capital different letters denoted to (P<0.05) significant differences between groups.

Table 2. The Effect Of Gentamicin And *Morus alba* Leaves Methanolic Extract on Serum Creatinine Levels (mg/dl)

Group	Mean ± SE		
	5 Day	10 Day	Recovery periods
G1 : Control D.W orally	0.30 ± 0.04 A a	0.34± 0.04 A a	0.36± 0.05 A a
G2 : Gentamicin (5mg/kg) B.W. I/M	2.00 ± 0.15 B a	4.50 ± 0.17 B b	4.30 ± 0.07 B b
G3 : Gentamicin (5mg/kg) B.W. I/M + *Morus alba* leaves extract (200mg/kg) B.W. orally	1.50 ± 0.03 C a	1.30 ± 0.07 C a	0.94 ± 0.06 C b
G4 : Gentamicin (5mg/kg) B.W. I/M + *Morus alba* leaves extract (400mg/kg) B.W. orally	0.50 ± 0.07 AD a	0.56± 0.04 AD a	0.40 ± 0.03 AD b
G5: Gentamicin (5mg/kg) B.W. I/M + Vit C (200mg/kg) B.W. orally	0.40± 0.03 AD a	0.30 ± 0.01 AD b	0.30 ± 0.04 AD b

♦ Values are presented as mean ± SE
♦ Small different letters denoted to (P<0.05) significant differences within groups.
♦ Capital different letters denoted to (P<0.05) significant differences between groups.

Table 3. The Effect of Gentamicin and *Morus alba* Leaves Methanolic Extract on Serum Uric Acid Levels (mg/dl)

Group	Mean ± SE		
	5 Day	10 Day	Recovery periods
G1 : Control D.W orally	0.20 ± 0.03 A a	0.22± 0.02 A a	0.21 ± 0.01 A a
G2 : Gentamicin (5mg/kg) B.W. I/M	1.26 ± 0.06 B a	3.00 ± 0.10 B b	2.90 ± 0.07 B b
G3 : Gentamicin (5mg/kg) B.W. I/M + *Morus alba* leaves extract (200mg/kg) B.W. orally	1.00 ± 0.03 B a	0.80 ± 0.03 C ab	0.60± 0.04 C b
G4 : Gentamicin (5mg/kg) B.W. I/M + *Morus alba* leaves extract (400mg/kg) B.W. orally	0.40 ± 0.07 A a	0.40 ± 0.03 A a	0.44± 0.04 AC a
G5: Gentamicin (5mg/kg) B.W. I/M + Vit C (200mg/kg) B.W. orally	0.42 ± 0.03 A a	0.23 ± 0.02 A a	0.25 ± 0.02 AC a

♦ Values are presented as mean ± SE
♦ Small different letters denoted to (P<0.05) significant differences within groups.
♦ Capital different letters denoted to (P<0.05) significant differences between groups.

Table 4. The Effect of Gentamicin and *Morus alba* Leaves Methanolic Extract on Serum Reduced Glutathione (GSH) Levels (µmol/L).

Group	Mean ± SE		
	5 Day	10 Day	Recovery periods
G1 : Control D.W orally	4.64 ± 0.14 A a	4.61 ± 0.29 A a	4.62 ± 0.33 A a
G2 : Gentamicin (5mg/kg) B.W. I/M	3.00 ± 0.22 B a	2.52 ± 0.44 B b	3.12 ± 0.41 B b
G3 : Gentamicin (5mg/kg) B.W. I/M + *Morus alba* leaves extract (200mg/kg) B.W. orally	3.20 ± 0.24 B a	3.40 ± 0.52 C a	4.01 ±0.59 C b
G4 : Gentamicin (5mg/kg) B.W. I/M + *Morus alba* leaves extract (400mg/kg) B.W. orally	3.63 ± 0.25 C a	4.04 ± 0.30 D b	4.36 ± 0.63 AC b
G5: Gentamicin (5mg/kg) B.W. I/M + Vit C (200mg/kg) B.W. orally	4.42 ± 0.84 A a	5.18 ± 0.95 E b	4.84 ± 0.44 ACD b

♦ Values are presented as mean ± SE
♦ Small different letters denoted to (P<0.05) significant differences within groups.
♦ Capital different letters denoted to (P<0.05) significant differences between groups.

Table 5. The Effect of Gentamicin and *Morus alba* Leaves Methanolic Leaves Extract on Serum Malondialdehyde (MDA) Levels (µmol/L)

Group	Mean ± SE		
	5 Day	10 Day	Recovery periods
G1 : Control D.W orally	4.44 ± 0.14 A a	4.40 ± 0.19 A a	4.36 ± 0.16 A a
G2 : Gentamicin (5mg/kg) B.W. I/M	6.61 ± 0.13 B a	7.82 ± 0.16 B b	6.20 ± 0.21 B c
G3 : Gentamicin (5mg/kg) B.W. I/M + *Morus alba* leaves extract (200mg/kg) B.W. orally	5.30 ± 0.26 C a	4.62 ± 0.12 A b	4.60 ± 0.14 C b
G4 : Gentamicin (5mg/kg) B.W. I/M + *Morus alba* leaves extract (400mg/kg) B.W. orally	4.52 ± 0.10 A a	4.46 ± 0.12 A a	4.22 ± 0.06 A a
G5: Gentamicin (5mg/kg) B.W. I/M + Vit C (200mg/kg) B.W. orally	3.90 ± 0.10 D a	3.82 ± 0.04 C a	4.02 ± 0.11 AD a

♦ Values are presented as mean ± SE
♦ Small different letters denoted to (P<0.05) significant differences within groups.
♦ Capital different letters denoted to (P<0.05) significant differences between groups.

Indian Journal of Natural Sciences www.tnsroindia.org.in ©IJONS

Vol.9 /Issue 52 / February / 2019 *International Bimonthly* *ISSN: 0976 – 0997*

RESEARCH ARTICLE

Developing Materials and Activities for an ESP Physical Therapy Course

Wasim Hassan[1]* and Mamuna Ghani[2]

[1]Lecturer in English, National Textile University Faisalabad, Pakistan
[2]Incharge, Faculty of Arts/Director Advanced Studies and Research Board, The Islamia University of Bahawalpur, Pakistan.

Received: 19 Nov 2018 Revised: 21 Dec 2018 Accepted: 23 Jan 2019

*Address for Correspondence
Wasim Hassan
Lecturer in English,
National Textile University Faisalabad,
Pakistan.
Email: meemash504@gmail.com

ABSTRACT

The study 'Developing materials and activities for an ESP Physical Therapy Course' brings to light the need of developing material and activities for an ESP physical therapy course for the ESL learners. The materials and activities for teaching ESP Physical Therapy course proved very useful in improving the proficiency of English language of the ESL learners at the College of Physical Therapy of Government College University Faisalabad as they helped the ESL learners in fulfilling the deficiencies of communication skills in physical therapy. The materials and activities for teaching ESP Physical therapy course were designed in close coordination with the management, faculty and the ESL learners. Testing techniques (pre-test and post-test) were used for data collection. The material and activities were taught to the ESL learners who were later evaluated with post-test for the effectiveness of materials and activities of ESP physical therapy course. The results of pre-test and post-test were compared and it was found that these materials and activities were more useful and helpful in enhancing the proficiency of English language than the general English currently taught. The research was quantitative in nature. Data was analysed with SPSS 20.0 and presented in tabular and graphical form.

Keywords: English for Specific Purpose, Course Designing, Materials Development, Physical Therapy.

INTRODUCTION

English as an International Language

Anderson quotes Ethnologue (published by SIL International) to describe the number of languages spoken in the world in the following words "there are 6909 distinct languages spoken in the world today" (2012:1). A very few of

them are international languages while most of them national or local languages. English is one of the most frequently used international languages and its significance is rapidly increasing in daily life. According to Talbot "English is a major language of commercial communication generally. It is also the world's language of the internet and global access to knowledge" (2009:4). The concept of English as a foreign language is dwindling now rather it has become the language of the whole world. In Pakistan, English is the second most important language. It is used as an official language and is used vastly in different areas from education to business and from administration to international trade. English is the dire need of the time. In education sector, English is a compulsory subject from class one to graduation level. Similarly, the medium of instruction of all technical and scientific subjects is English from secondary to higher education level. It is almost impossible to make any progress in the world without English in 21st century. English is a global language, and without it, it is even difficult to survive in a global world. It is essential for us to give due worth to English language to compete in the ever growing market of international trade. Specific courses are designed and developed to improve the ability of communication of learners to meet the particular needs of the time.

English for Specific Purpose (ESP)

English for specific purpose (ESP) courses are concerned with the specialized English language teaching to the ESL/ EFL students according to their specific academic and professional needs. Human knowledge has expanded significantly over the past few centuries which gave birth to the specialized activities of human life. These specific activities demand specific language needs. Villata describes ESP in the following words: "ESP is taught as part of academic curriculum in educational institutions. On the other hand, ESP is also needed among experienced professionals to improve their communication" (2003:30).

Physical Therapy

Physical Therapy is a branch of medical and rehabilitation sciences which has its language structure based on particular lexicon and terminologies. Physical Therapy is based on clinical examination, diagnosis and treatment of cardiovascular, neurological, musculoskeletal, physiological and psychosomatic diseases. Physical therapists serve the community by putting theory of human health into practice. They also take part in research based activities to solve the problems of physical disorder. Physical therapist has to conduct a range of activities like measuring the strength of muscle and joint, testing the sensation loss, analyzing movement and posture, evaluating the disorder in circulatory and respiratory system, performing electrical tests on muscles and nerves and educate the community/communities with healthy life style. The language used in the field of physical therapy is a specific language different from general English therefore the students of physical therapy need to learn English used in their own field to improve their academic and professional capabilities.

Statement of the Problem

The undergraduates of physical therapy are not proficient enough in English language to deal with the technical language used in the field of physical therapy and hence there is a need of designing materials and activities of ESP Physical therapy.

Objective of Study

The objective of the present research is to design materials and activities of ESP physical therapy course.

Hypothesis

ESP physical therapy based materials and activities result in better proficiency of English than general English course which is currently taught to undergraduates of physical therapy. H_0 : Average marks of ESP PT course > Average marks of General English course

Significance of Study

The current research endeavors to help the students execute their communicative needs in academic and professional fields but it will also help the other universities to follow the guidelines and suggestions for designing ESP courses in their respective fields.

Delimitations of Study

As the main purpose of the present study is to develop materials and activities for an ESP Physical Therapy course at the College of Physical Therapy at Government College University Faisalabad, Pakistan there are delimitations in the study because all the undergraduates across different universities of Pakistan where Physical therapy is being taught are not part of the research.

Literature Review

Emergence of ESP

ESP emerged as one of the most prominent areas of TEFL in the early 1960s. The universities and colleges in UK and other parts of the world started offering ESP diplomas and degrees in the late 1970s and onward. Some instructors see ESP as a way of developing English for a particular field of knowledge while many others see it as teaching English to fulfill the needs of professionals. Notably, ESP emerged due to three different reasons as pointed out by Hutchinson and Waters "there are three reasons common to the emergence of all ESP: the demands of a Brave New World, a revolution in linguistics, and focus on the learner" (1987:6). According to them there are two most significant periods in the history which paved the way for emergence of ESP. First, the end of the Second World War brought with it "an age of enormous and unprecedented expansion in scientific, technical and economic activity. For various reasons, most notably the economic power of the USA in the post war-world, the role (of international language) fell to English. Second, the oil crisis of the early 1970s resulted in Western money and knowledge flowing into the oil-rich countries. The language of this knowledge became English." (1987:ibid). Hutchinson and Waters identify Ewer et. al as a few of the prominent descriptive EST pioneers. Similarly, another reason was seen very significant for the emergence of ESP by Hutchinson and Waters. This last reason was more concerned with psychology instead of language teaching. According to them there are specific set of skills an individual has to cope with and psychologically, a learner is more fascinated by the fulfillment of particular needs he has in his profession and academics, it was for this reason that ESP got fame amongst the learners and instructors that it met the professional and academic needs of them. According to Howatt as quoted in Kim "the expedited expansion of international business led to a huge growth in English for business purposes (EBP) all over the world, from the United Kingdom, North America, Oceania to Middle East and Asia. ESP became a vital and innovative field in the TESOL movement by the 1980s" (2008:5).

Branches of ESP

Basturkmen (2010) presents three branches of ESP i.e. English for Academic Purpose (EAP), English for professional purpose and English for occupational purpose. EAP is subdivided into English for general academic purpose and English for specific academic purpose. Second branch of ESP (English for professional purpose) is also divided into two types i.e. English for general professional purpose and English for specific professional purpose. Likewise, third branch of ESP (English for occupational purpose) is also divided into two types i.e. English for general occupational purpose and English for specific occupational purpose. According to Hutchinson and Waters (1987) ESP is divided into two branches; EAP involves training students to use language appropriately at a higher level. It is based on the training of use of language in the core areas and teaching four skills of English language with a focus on grammar and vocabulary while EOP means English for Occupational Purposes. It prepares the English language learners to work in the vocational or occupational fields like English for science and technology, English for hotel management, English for medical sciences, English for aeronautical engineering etc. Kim asserts that "EOP particularly concerns with adult language acquisition as well as with aspects of general training for adult learners; the purpose of EOP training is to enhance workplace performance, with special attention to how adults learn a language to communicate better in job-related contexts" (2008:2). Hutchinson and Waters (1987) illustrate two types of ESP i.e. EAP and EOP in a tree diagram of ELT which is presented in the following:

Carter has a different view about the types of ESP. According to him following are the three types of ESP: "i) English as a restricted language, ii) English for Academic and Occupational Purposes iii) English with specific topics" (1983:23).The language used by air traffic controllers or by waiters are examples of English as a restricted language. Mackay and Mountford describe the difference between a language and restricted language in the following words: "the language of international air-traffic control could be regarded as 'special', in the sense that the repertoire required by the controller is strictly limited and can be accurately determined situationally, as might be the linguistic needs of dining-room waiter or air-hostess. However, such restricted repertoires are not languages, just as a tourist phrase book is not grammar. Knowing a restricted 'language' would not allow the speakers to communicate effectively in novel situations, or in contexts outside the vocational environment" (1978:4).

Characteristics of ESP Courses

Carter identifies three common features to ESP courses which are as follow: "a) authentic material, b) purpose-related orientation and c) self-direction" (1983:134). Dudely-Evans (1997) also assert the same that using authentic learning material to teach ESP is entirely feasible. By authentic materials we mean that the ESP practitioners conduct needs analysis and then according to the needs courses including text of particular field of learners should be designed and taught to the English language learners. Purpose-related orientation refers to the simulation of communicative tasks required of the target setting. Self-direction is another of characteristics of ESP courses as defined by Carter "point of including self-direction…is that ESP is concerned with turning learners into users" (1983:134). For the self-direction to take place the ESP learners should have a certain liberty to decide about their learning in that they should decide themselves what, how, and when they will study.

Difference between ESP (English for Specific Purpose) and ESL (English as a Second Language/ General English)

There are several differences between ESP and ESL as students of English for specific purpose are adults with some familiarity of English and learn English language and use it to perform particular job-related task while ESL is based on teaching of basics of English language to the learners of any age group. The focus of ESP is teaching language in context i.e. it copes with the topics from different fields of knowledge as tourism, business and administration,

journalism, engineering and medical sciences. On the other hand, ESL courses present the students topics of general nature. The lexicon and grammar are taken from day to day life instead of particular fields. Holme describes the difference between ESP and General English in the following: "The General English syllabus is based on a conception of the kind of reality that the student has to deal with in English. ESP is simply a narrowing of the needs spectrum. The ESP process of specialization should not result in the complete separation of one part of the language from another" (1996:3).

Syllabus

Oxford dictionary defines syllabus in the following words "The subjects in a course of study or teaching." According to Julia Cresswell "An early syllabus was 'a concise table of headings of a text' It was derived from modern Latin it was originally a misreading of Latin *Sittybas* from Greek *Sittuba* meaning 'title slip, label'. The use of the word in educational context for a program of study is recorded from the late 19th century" (2009:432). According to Yalden syllabus is a "summary of the content to which learners will be exposed" (1987: 87). Naeem describes the difference between a course and a syllabus in the following words: "syllabus can be taken to be something rather than more abstract, with fewer details of the blow by blow conduct of the individual lessons. Thus you and I might quite properly write rather different courses, with different materials but based on the same syllabus" (2009:468). A skill-based syllabus is the one that focuses on the language skill(s) necessary to perform a task in academic or professional setting. The language skills are four in number i.e. listening, speaking, reading and writing. Listening and reading are considered receptive skills while speaking and writing are considered as productive skills of language. A syllabus which makes analysis of the skill(s) to be used by the language learners, designing and teaching a course accordingly is called skill-based syllabus. The focus of Skill-based syllabus can be any or all of the four skills of language.

Designing an ESP Course

According to Basturkmen"ESP courses are narrower in focus than ELT courses-----ESP views learners in terms of their work or study roles and that ESP courses focus on work or study-related needs, not personal needs or general interests" (2010:3). Yalden (1987) provides the following model outlining the basic steps necessary for designing an English for Specific Purpose course:

Physical Therapy

According to Cambridge Dictionary physical therapy is "the treatment of muscle stiffness, pain, and injury, especially by rubbing and moving the sore parts" (2009:213). According to American Physical Therapy Association "Physical therapists (PTs) are highly-educated, licensed health care professionals who can help patients reduce pain and improve or restore mobility - in many cases without expensive surgery and often reducing the need for long-term use of prescription medications and their side effects"(2005:80). As a profession, Physical Therapy emerged in the 20th century. The basic reasons which prompted the need of Physical therapy as a profession was the innovations in science and technology in medical sciences as well as the World War I and World War II. It was very late in the twentieth century that physical therapy was acknowledged as a profession in Pakistan that meant patient health care needs were not met. Even today, there is a scope for a physical therapist in Pakistan due to the shortage of graduates in the field. Realization of this fact has attracted many students towards the field of Physical therapy which can be vividly seen by the number of entrants to the academic degree 'DPT (Doctor of Physical Therapy)' over the last few years in Pakistan.

On the reasons of academic failure of nursing students Bosher and Smalkoski (2002) conducted a needs analysis. The findings of the study included that communicating with the patients in English was the biggest difficulty for the professionals of medical sciences. Rattanapinyowong et al. (1988) conducted needs analysis of an ESP course for the

learners of health care at Mahidol University, Bangkok. From the collected data it was clear that health care professionals were in need of an ESP health care course. Lockwood (2012) highlighted the needs for an ESP Course for the employees of call centers in India and Philippines. Alfehaid (2011) in his doctoral thesis titled 'Developing an ESP Curriculum for Students of Health Sciences through Needs Analysis and Course Evaluation in Saudi Arabia' presented course evaluation and needs analysis. He elicited the data through questionnaires and interviews for health professionals and learners. The data shows that the four skills were very important for the learners and professional of health sciences. Kandil (2008) conducted needs analysis of Arab learners of high school level. The research revolves around Teaching English for No Obvious Reason which is faced by most of the Arab educational organizations. Elkilic (1994) also conducted Needs Analysis research which was aimed at identifying the needs of ESP course for the learners of medical students of Selcuk University, Turkey. Reading was rated as the important language skill for reading scholarly journals, magazines and reports. Chan (2009) presented the difference between the theories and their implication in teaching business English. He developed two types of check-lists to for the enhancement of use of ESP materials with evaluation. Lepetit and Cichocki (2002) investigated a needs analysis on 165 subjects (healthcare professionals) at the College of Health, Education and Human Development USA. According to the findings of the study, students thought that oral communicative skill was more important than writing and reading literature. Kassim and Ali (2010) studied the needs of an ESP course for the graduates of Engineering of different universities of Malaysia. The study found out that though the graduates around the country were unable to find jobs due to their poor communication skills.

RESEARCH METHODOLOGY

Procedures of Study

Tests (Pre-test and post-test) have been conducted for data elicitation. Percentage method has been used and the data has been presented in tabular as well graphical form.

Population of Study

Population of study was 500 undergraduates of physical therapy of the College of Physical Therapy at Government College University Faisalabad, Pakistan.

Sample of Study

As per the rules of statistics minimum 10% sample of the total population must be selected that is why 67 undergraduates of Physical Therapy were randomly selected from 500 undergraduates for pedagogy and evaluation of ESP Physical Therapy based materials and activities.

Tools of Data Elicitation

Quantitative techniques have been used in the analysis and interpretation of data. Pre-test and post-test were conducted to evaluate the effectiveness of the materials and activities of ESP Physical Therapy course.

Tools of Data Analysis

Statistical Package for Social Sciences (SPSS) 20.0 has been used for data analysis. As per the characteristics of paired sample T-Test, sample remains the same while data is collected two times in the form of pre-collected data and post-collected data. Paired Sample T-Test is the most appropriate test for data analysis in the situation of the current research because the current research demands pre-test and post-test to be conducted to verify the results of pedagogy of materials and activities of ESP PT and the general English course.

Data and Interpretation of Data

Data of Pre-Test and Post-Test

Figure 3 sums up the improvement of scores from pre-test to post-test of the undergraduates of physical therapy. It also presents a comparison of pre-test and post-test scores of the undergraduates of physical therapy. It can be seen that 1.49% of the undergraduates of physical therapy improved 2% scores from pre-test to post while 4.47% showed an improvement of 4% marks from pre-test to post-test scores whereas 23.88% undergraduates who were pre-tested and after pedagogy of ESP Physical Therapy Course showed an improvement of 6% marks in their post-test whereas 23.88% undergraduates showed a betterment of 8% marks from their pre-test to post-test scores. 13.43% of the undergraduates of physical therapy showed an improvement of 10% marks from their pre-test to post-test scores of English similarly 11.94% of the undergraduates showed an improvement of 12% marks from their marks of pre-test to those of post-test. 8.95% of the undergraduates jumped to 14% marks from their pre-test to post-test. 1.49% of the undergraduates showed a massive improvement of 20% in their scores from pre-test to post-test while the same trend of massive improvement of 22% was also observed in the marks of 1.49% undergraduates of physical therapy. 5.97% of the undergraduates were consistent with their scores and did not show any improvement of scores from their pre-test to pos-test. While 1.49% undergraduates showed a decline of -2 marks% from their pre-test to post-test scores similarly 1.49% also showed a decline of -6% scores from pre-test to post-test.

It is evident from the statistical comparison of pre-test and post-test scores of ESP Physical therapy Course that the materials and activities of ESP physical therapy have brought a marked proficiency of English language of the undergraduates of physical therapy as the mean of scores of pre-test has risen drastically from 58% to 67%in the post-test after pedagogy of ESP Physical Therapy Course. It is expected that ESP Physical Therapy Course would bring better results once it is implemented and a continuity of its pedagogy will open new horizons of improvement in this course.General Statistics was applied to 67 undergraduates of physical therapy whose data was collected in the form of pre-collected data and post-collected data. The pre-test average marks of the undergraduates of physical therapy are 58.84 and post data average marks of the undergraduates of physical therapy are 67.04. It shows that the undergraduates after learning ESP Physical Therapy course showed improved proficiency of English language as compared to the general English course. Standard deviation/variation of pre-test of the undergraduates of physical therapy was 6.850 while it was 6.124 in post-test which shows that post-test variation is lesser than pre-test. Standard Error mean of pre-test was .837 in pre-test while it was .748 in post-test which means that ESP Physical therapy Course has less standard error than general English Course.

Relationship between sample of pre-test and post-test is .739 which means samples have better relationship. 0.000 Significance of pre-test and post-test shows that samples have a good relationship. Mean value of paired sample T-Test is -8.209. Standard deviation/variation of pre-test and post-test of the undergraduates of physical therapy is 4.737. Standard Error mean of pre-test and post-test is .579. Confidence interval of upper value is -7.053 and lower value is -9.364 and this interval is calculated 95% confidence interval. Significance level of pre-test and post-test is 0 that shows ESP Physical Therapy Course has helped the undergraduates of physical therapy achieve better proficiency in English than general English course.

FINDINGS AND CONCLUSIONS

Findings from Comparative Analysis of Pre-Test and Post- Test

A comparative analysis of pre-test and post-test shows a marked improvement of proficiency in English of the undergraduates of physical therapy. It is clear that apart from the 2.98% undergraduates who showed a decline of scores from pre-test to post-test all undergraduates of physical therapy showed a prominent improvement in proficiency of English language because the overall mean of scores of pre-test has risen drastically from 58% to 67% in the post-test after pedagogy of ESP Physical Therapy Course. Amongst the undergraduates who showed a noticeable difference in their pre-test to post-test scores are 23.88% undergraduates who showed an improvement of 6% marks in their post-test and also those 23.88% undergraduates who showed a betterment of 8% marks from their pre-test to post-test scores. Similarly 13.43% of the undergraduates of physical therapy showed an improvement of 10% marks from their pre-test to post-test scores of English similarly 11.94% of the undergraduates showed an improvement of 12% marks from their marks of pre-test to those of post-test. Moreover, 8.95% of the undergraduates jumped to 14% marks from their pre-test to post-test. 1.49% of the undergraduates showed a massive improvement of 20% in their scores from pre-test to post-test while the same trend of massive improvement of 22% was also observed in the marks of 1.49% undergraduates of physical therapy. It is evident from the above statistical comparison of pre-test and pre-test scores that ESP Physical therapy Course has brought a

Findings from the Analysis of Currently Taught English Course

'Functional English (ENG-321)' is taught to the undergraduates of 1st semester. This course has the contents based on English grammar e.g. parts of speech and use of articles, sentence structure, active and passive voice, practice in unified sentence (synthesis), analysis of phrase, clause and sentence structure, transformation, inversion of sentences, analysis of complex sentences, subject, predicate, complements, direct & indirect objects, direct and indirect speech. This course also consists of functions of English language like making introductions, expressing requests and enquiries, greetings, gratitude, invitations, regrets, following and giving directions, sharing narratives and sharing unique experiences etc. The Second course of English is 'English Comprehension and Composition (ENG-322)'is taught to the undergraduates of Physical therapy in 2nd Semester. The contents of this course are relevant to reading comprehension skills, Reading techniques, vocabulary building skills, pre-writing techniques, writing techniques, paragraph writing, types of Writing, essay writing techniques, paraphrasing, précis writing and expansion of a sentence into paragraph etc. Currently taught courses of English at the College of Physical Therapy are i.e. Functional English (ENG-321) and English Comprehension and Composition (ENG-322) are aptly written and implemented but the fact of matter is that the undergraduates of physical therapy are not proficient enough in English to cope with the academic and professional communicative needs in English in their field of study. The results of pre-test testify that the undergraduates of physical therapy were unable to understanding the particular jargon and register of physical therapy and therefore were unable to show better scores in pre-test. Both of the currently taught English courses are comprehensive in covering the basic knowledge and skill of English language. They can be fruitful to any student of any field of knowledge but ESP Physical Therapy Course has been designed for the undergraduates to enhance the field knowledge of Physical Therapy as well to improve proficiency of language skills, the post-test scores of the undergraduates of physical therapy strengthen this claim. ESP Physical Therapy Course covers the four skills of English language while general English courses taught currently deal only with reading and writing skills. The contents, materials and activities of ESP Physical Therapy are better than general English courses because they are more relevant to English used in the field of Physical Therapy. ESP Physical therapy Course has been designed to improve the four skills of English language instead of just reading and writing skills.

Acceptance of Hypothesis

It was hypothesized that the proficiency of the undergraduates of physical therapy who were taught ESP Physical Therapy Course will be better than those who are taught general English Course. The hypothesis was :H_0 : Average marks of ESP PT course > Average marks of General English course Paired Sample T-Test is significant that shows ESP Physical Therapy Course is better than general English course in fulfilling the academic and professional communicative needs of the undergraduates of physical therapy.

Recommendations

Recommendations have been suggested for the undergraduates of physical therapy and English teachers of the college of physical therapy in the lines below:Students should be provided familiarity with English for Specific Purpose Course for Physical Therapy. They should be provided understanding of technical terms and vocabulary in physical therapy. They should seek opportunities for social and professional interaction with the seniors and professionals. The course books and materials provided to them should fulfill the communicative needs in English in the domain Physical Therapy. Communicative competence in English in the field of Physical Therapy should be the ultimate goal of teaching-learning process. They should not ignore the importance of learning functions of English language in physical therapy. As far the English language teachers are concerned, they should focus on developing speaking skills of their students for improved communication skills in the field of Physical Therapy. They should develop proficiency in the four skills of English instead of just reading and writing skills. They should themselves possess a sound communicative competence to teach ESP Physical Therapy Course. They should provide the students with the chances to communicate with classmates and senior doctors. They should adopt direct method to teach the materials and activities of ESP Physical Therapy.

ACKNOWLEDGEMENTS

This research paper has been extracted from the PhD Thesis entitled "Designing an ESP (English for Specific Purpose) Course for the Undergraduates of Physical Therapy at Government College University Faisalabad, Pakistan" by Mr. Wasim Hassan, supervised by Prof. Dr. Mamuna Ghani (Incharge, Faculty of Arts/Director Advanced Studies and Research Board, The Islamia University of Bahawalpur Pakistan) and has been published in the partial fulfillment of requirement of the degree of Doctorate of Philosophy in Linguistics from the department of English, The Islamia University of Bahawalpur Pakistan.

REFERENCES

1. Adams, M.J. (1990). *Beginnig to Read. The New Phonics in Context. A Précis of the Classic Text.*Heinemann. London.
2. Anderson, Stephen R. (2012). *Languages: A Very Short Introduction.* Oxford: Oxford University Press.
3. Basturkmen, H. (2008). *Ideas and Options in English for Specific Purposes.* Lawrence ErlbaumAssociates, Publishers. New Jersey.
4. Basturkmen, H. (2010). *Developing Courses in English for Specific Purposes.* Palgrave Macmillan.Hampshire.
5. Broughton, G., Brumfit, C., Flavell, R., Hill, P. and Pincas, A. (1978). *Teaching English as a Foreign Language (Second Edition).* Routledge & Kegan Paul Ltd. New York.
6. Carter, R., & Nunnan, D. (2001).*The Cambridge Guide to Teaching English for the Speakers of Other Languages.* Cambridge University Press. Cambridge.
7. Cresswell, J. (2009).*A Delightful Dictionary of Derivations_Oxford dictionary of word origins.* Oxford University Press. Oxford.

8. Evans, T.D. & St. John, M. (1999).*Developments in ESP: A multidisciplinary approach.* Cambridge University Press. Cambridge.
9. Holme, R. (1996) *ESP Ideas.* Harlow, Essex: Longman.
10. Hutichinson, T. & Waters, A. (1987).*English for Specific Purpose: A Learning Centered Approach.* Cambridge University Press. Cambridge.
11. Kim, D. (2008). *English for Occupational Purposes -One Language?.* Continuum Books. Norfolk. Mackay, R., & Mountford, A. (Eds.). (1978). *English for Specific Purposes: A case study approach.* London: Longman.
12. Naeem, M. (2009). *TESOL (Teaching of English to the Speakers of Others Languages).* Famous Products. Lahore.
13. Richards, J.C & Rodgers, T.S. (1986).Approaches and Methods in Language Teaching (A Description and Analysis). Cambridge University Press. New York.
14. Richards, J.C. (1990). The Language Teaching Matrix. Cambridge University Press. Cambridge.
15. Richards, J.C. (2001). *Curriculum Development in Language Teaching.* Cambridge University Press. Cambridge.
16. Richards, J.C. & Richard, S. (2002). *Longman Dictionary of Language Teaching and Applied Linguistics.* Pearson Education. London.
17. Rodgers, T. (1989).*Syllabus design, curriculum development and polity determination. In R.K. Johnson (ed.), The Second Language Curriculum.* Cambridge Press. New York.
18. Rogers, C. (1983). *Freedom to learn for the 80's.* Columbus, OH: Charles Merrill.
19. Russell, B. (1976).*The impact of Science on Society*. Routledge. London.
20. Saraswat, M. (2009).*Speak English Fluently.* Upkar Prakashan. Agra-2.
21. Selinker, L., Tarone, E., &Hanzeli, V. (Eds.). (1981). *English for Academic and Technical Purposes: Studies in honor of Louis Trimble.* London: Newbury House.
22. Strevens, P. (1988). *ESP after twenty years: A re-appraisal. In M.Tickoo (Ed.), ESP: State of the Art* (pp.1-13). Singapore: SEAMEO Regional Centre.
23. Stryker, S., & Leaver, B. (Eds.). (1997). *Content-based instruction in foreign language education: Models and Methods.* Washington, D.C: Georgetown University Press.
24. Tomlinson, B. (2003). *Developing Materials for Language Teaching.* Cromwell Press. Wiltshire. Vanpatten, B., & Lee, J. (1990).*Second language acquisition- Foreign language learning.* Avon:Multilingual Matters.
25. Worthern, B.R. & Sanders, J.R. (1973).*Educational Evaluation: theory and Practice.* Ob.Jones Publishing company. Columbus.
26. Yalden, J. (1987).*Principles of Course Design for Language Teaching.* Cambridge University Press. Cambridge.
27. Yogan, J., & Kaylani, C. (1996).*ESP program design for mixed level students.* English for specific purposes, 15, 311-24.

Table 1. Comparison of Pre-Test and Post-Test Scores of the Undergraduates of Physical Therapy

Sr. No.	Pre-test Score (%)	Post-test Score (%)	Difference of Score (%)	Sr. No.	Pre-test Score (%)	Post-test Score (%)	Difference of Score (%)
1	58	66	8%	35	58	64	6%
2	54	66	12%	36	60	68	8%
3	56	68	8%	37	72	76	4%
4	68	78	10%	38	58	72	14%
5	54	66	12%	39	66	72	6%
6	64	72	8%	40	58	64	6%
7	58	70	12%	41	40	62	22%
8	58	74	12%	42	56	70	14%
9	60	74	14%	43	56	64	8%
10	70	78	8%	44	56	58	2%
11	66	72	6%	45	68	74	6%
12	52	66	14%	46	60	74	14%

13	64	70	6%	47	50	58	8%
14	44	64	20%	48	64	72	8%
15	58	70	12%	49	52	62	10%
16	58	68	10%	50	50	62	12%
17	62	68	6%	51	66	72	6%
18	58	66	8%	52	44	54	10%
19	60	66	6%	53	58	70	12%
20	64	58	-6%	54	58	62	4%
21	60	60	0%	55	60	58	-2%
22	62	68	6%	56	56	64	8%
23	60	70	10%	57	52	52	0%
24	66	70	4%	58	54	64	10%
25	42	54	12%	59	60	68	8%
26	58	64	6%	60	46	52	6%
27	60	66	6%	61	64	70	6%
28	68	74	6%	62	56	64	8%
29	62	70	8%	63	56	66	10%
30	60	74	14%	64	66	74	8%
31	58	66	8%	65	78	78	0%
32	58	66	8%	66	56	66	10%
33	60	66	6%	67	66	76	10%
34	62	62	0%				

Table 2. Paired Samples Statistics

		Mean	N	Std. Deviation	Std. Error Mean
Pair 1	Pre	58.84	67	6.850	.837
	Post	67.04	67	6.124	.748

Table 3: Paired Samples Correlations

		N	Correlation	Sig.
Pair 1	pre & post	67	.739	.000

Table 4. Paired Samples T-Test

	Paired Differences					T	Df	Sig. (2-tailed)
	Mean	Std. Deviation	Std. Error Mean	95% Confidence Interval of the Difference				
				Lower	Upper			
Pair 1 pre – post	-8.209	4.737	.579	-9.364	-7.053	-14.184	66	.000

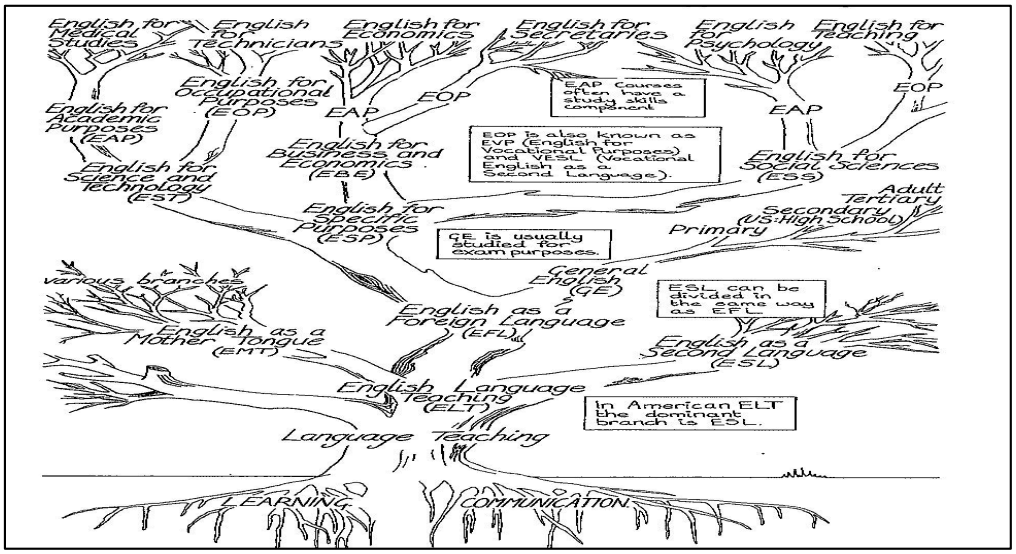

Figure 1. Tree Diagram of Types of English for Specific Purpose

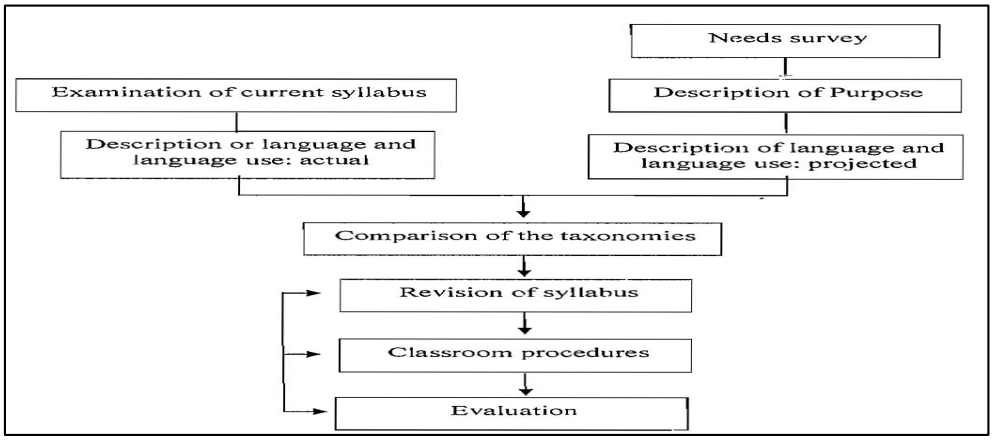

Figure 2: Yalden's (1987) Model for Designing an ESP Course

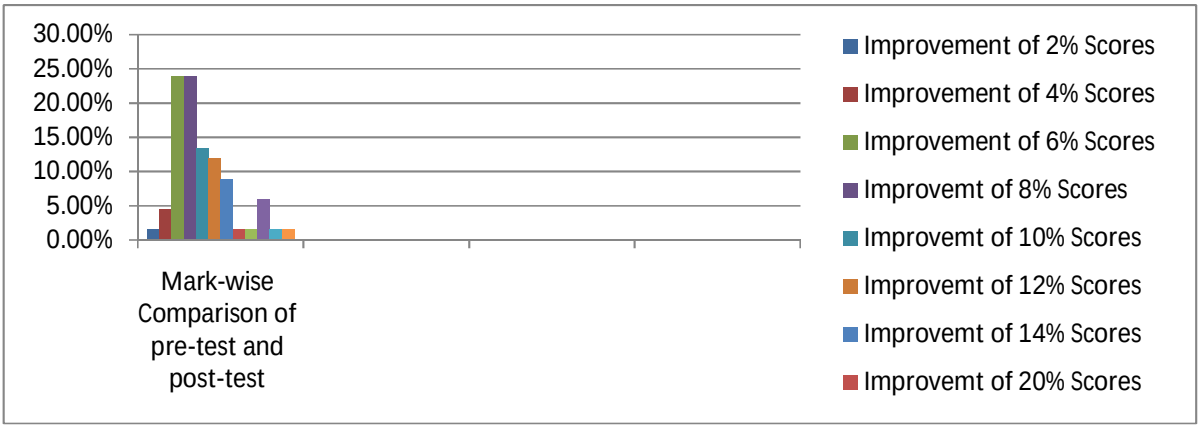

Figure 3. Mark-Wise Comparison of Pre-Test And Post-Test

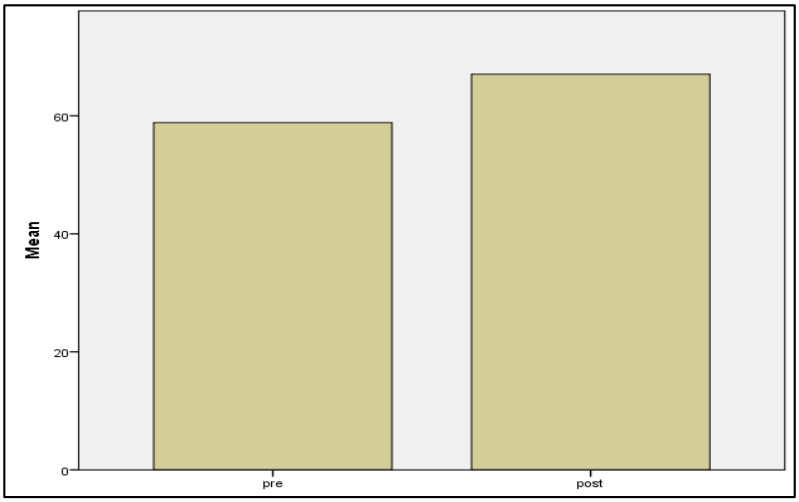

Figure 4. Mean of Pre-Test Score and Post-Test Scores

Indian Journal of Natural Sciences www.tnsroindia.org.in ©IJONS

Vol.9 /Issue 52 / February / 2019 *International Bimonthly* *ISSN: 0976 – 0997*

RESEARCH ARTICLE

Study of Some Thermal Properties of [PVA:PVP] Polymer Blends Films and the Feasibility of a Biotic Application on the (PVA-PVP-Ag) Nano Polymer Composite Solution

Sabah A. Salman*, Ammar A. Habeeb and Ali A. Sallal

Department of Physics, College of Science, University of Diyala, Diyala, Iraq

Received: 20 Nov 2018 Revised: 22 Dec 2018 Accepted: 24 Jan 2019

***Address for Correspondence**
Sabah A. Salman
Department of Physics,
College of Science,
University of Diyala,
Diyala, Iraq

ABSTRACT

In this study pure (PVA) polymer film and films of [PVA:PVP] polymer blends at weight ratios (([100:0], [90:10], [80:20], [70:30]), [60:40], [50:50], [40:60], [30:70], [20:80], [10:90]) wt%) preparation using the casting method**.** The effect of the weight ratio of the polymer blend on the thermal properties of [PVA:PVP] polymer blends films have been studied, the practical results have shown that the thermal conductivity coefficient of [PVA:PVP] polymer blends films behaves irregularly compared with pure (PVA) polymer film by increasing the weight ratio of the (PVP) polymer. The differential scanning calorimetric (DSC) test has showed that the glass transition of the [PVA:PVP] polymer blends films in which increases in most of the weight ratios of the polymer blend compared with pure (PVA) polymer film while decreases in weight ratios (([40:60], [30:70], [20:80]) wt%) of the polymer blend compared with pure (PVA) polymer film with absent of the glass transition at the weight ratio ([90:10] wt%) for the polymer blend, also, the crystalline melting point showed irregular behavior compared with pure (PVA) polymer film by increasing the weight ratio of the (PVP) polymer with absent of the crystalline melting point at the weight ratio ([40:60] wt%) for the polymer blend. In this study as well, a (PVA-PVP-Ag) nano polymer composite solution has been prepared where a test of the bacteria (E.Coli, Proteus) sensitivity has conducted for this solution, in addition the practical results have exhibited that mentioned nano polymer composite solution is highly effective in terminating and constraining the stated bacteria.

Keyword: Polyviny Alcohol (PVA), Polyviny Pyrrolidone (PVP), Silver (Ag) Thermal Properties**,** Polymer Blends, Nano Polymer, Antimicrobial Properties, E-Coli, Proteus.

INTRODUCTION

Polymers have increasingly become attractive because of a large number of applications. The blending of different polymers or inorganic materials with polymers represents a strategic route to improve the performance of a material, and allows the realization of novel composite systems that enhance the performance of the parent blend [1]. The solution blending of different polymers is one of the methods used to get new material with a variety of properties, which mainly depend on characteristics of the parent homo polymers and the blend composition [2]. Poly vinyl alcohol (PVA), a semicrystalline polymer, has been studied extensively because of its many interesting physical properties, which arise from the presence of OH groups and the hydrogen bond formation with other polymers or metals. Poly vinyl pyrrolidone (PVP) is a vinyl polymer possessing planar and highly polar side groups due to the peptide bond [3]. It is amorphous polymer and possesses high (T_g) due to the presence of rigid pyrrolidone group, which is strong on drawing the group. The nanomaterials are the class of advanced materials that can be produced to measure the dimensions and dimensions of their internal granules between (1-100)nm. These small materials have different characteristics than the larger materials. The material is a corner of the technology. The nanomaterials vary in terms of origin and differ in different proportions, such as organic or inorganic, natural or different (manufactured) [4]. Biochemical or chemical nanoparticles can be obtained from bacteria and fungi that have the ability to produce nanoparticles with antimicrobial properties [5].

EXPERIMENTAL PART

We are used polymer Polyvinyl alcohol (PVA) in the preparation of polymer blends films, which product by Central House (P) Ltd of India with molecular weight (13000-23000) g/mol, and polymer Polyviny Pyrrolidone (PVP) K-30, is product by (HIMEDIA) company with molecular weight (40,000 g / mol). A pure (PVA) polymer film and [PVA:PVP] polymer blends films were prepared using the casting method by using special molds made from glass. The preparing of pure (PVA) polymer film is by adding a certain weight ratio of (PVA) polymer to distilled water using a magnetic sterrier for (1h) at (80°C) to obtain a homogeneous solution and then pour the solution in a special glass mold on a mild surface until the solvent evaporates to obtain the pure (PVA) polymer film. In order to prepare the [PVA:PVP] polymer blends films, certain weight ratios of (PVA) polymer were mixed with specific weight ratios of (PVP) polymer then adding the distilled water using the magnetic stirrer for (1h) at (80°C) to obtain a homogeneous solutions, then the solutions poured into special glass molds placed on a mild surface and left until the solvent evaporates to produce the [PVA:PVP] polymer blends films.

Thermal Properties

Thermal tests (T_g, T_m) for [PVA:PVP] polymer blends films were conducted using a Differential Scanning Colarymeter (DSC), type (STA. PT-1000 Linseis) of origin (Linseis Company Germany). The thermal conductivity coefficient (k) was performed using the Lee's Disc method for calculating the thermal conductivity of insulating materials using the device manufactured at the English company (Griffen and George).

Bioactivity Test

The sensitivity test of (E. coli - Proteus) for (PVA-PVP-Ag) nano polymer composite solution with volume ratios ((0.5, 1, 1.5) vol %) from silver nanomaterial, where used the (Disc Diffusion Method).

RESULTS AND DISCUSSION

Thermal Properties

Thermal Conductivity

The thermal conductivity coefficient (k) is calculated by using the Lee's Disc Method, Figure (1) shows the thermal conductivity coefficient of pure (PVA) polymer film and [PVA:PVP] polymer blends films with different weight ratios, we note from the figure that the thermal conductivity coefficient value of pure (PVA) polymer film is ($2.4x10^{-4}$ W/m.K), and when mixing the (PVA) polymer and (PVP) polymer with different weight ratios the thermal conductivity coefficient value changes where it behaves irregularly, and we note from the figure that the value of the thermal conductivity coefficient increases at the weight ratios (([90:10], [70:30], [60:40], [40:60], [20:80]) wt%) for the polymer blend compared with pure (PVA) polymer film and it's decrease at the weight ratios (([80:20], [50:50], [30:70], [10:90]) wt%) for the polymer blend compared with the pure (PVA) polymer film, the irregularity of the thermal conductivity coefficient value may be due to the heterogeneity between (PVA) polymer and (PVP) polymer due to the large surface area of (PVP) polymer [6], and that the difference in the thermal conductivity values indicates that the thermal conductivity coefficient behaves independently of the heat capacity [7]. Table (1) shows the thermal conductivity coefficient values for all polymer blends films.

Glass Transition Temperature

The glass transition temperature (T_g) of pure (PVA) polymer film and [PVA:PVP] polymer blends films with different weight ratios was calculated using the Differential Scanning Colarymeter (DSC), Figure (2) explains the values of glass transition temperature for all the polymer blends films as shown in Table (2), where we note that the glass transition temperature value of pure (PVA) polymer film is (110.28 ºC), and when mixing the (PVA) polymer and (PVP) polymer with different weight ratios, we note the value of the glass transition temperature increases at the weight ratios (([80:20], [70:30], [60:40], [50:50], [10:90]) wt%) for the polymer blend compared with the pure (PVA) polymer film, while their value is decreases at the weight ratios (([40:60], [30:70], [20:80]) wt%) for the polymer blend compared with pure (PVA) polymer film, this irregular value in the glass transition temperature is due to the mixing of (PVA) polymer and (PVP) polymer which leads to reduce the flexibility of polymer chains of the (PVA) polymer and (PVP) polymer [8,9], and also we note the disappearance of the glass transition temperature at the weight ratio ([90:10] wt%) for the polymer blend where they cannot be interpreted correctly considering it reflection for the blend mixing [10]. It is worth mentioning that at the beginning of all the figures we see the presence peak of the top (exothermic), symbolized by (T_w), which lies before the glass transition temperature, and the reason for the emergence of this top is the presence of a small amount of moisture in all prepared samples [11] .

Crystalline Melting Temperature

The crystalline melting temperature (T_m) of pure (PVA) polymer film and [PVA:PVP] polymer blends films with different weight ratios was calculated using Differential Scanning Colarymeter (DSC). The crystalline melting temperature is used to determine the nature of the material and its purity [12], Figure (2) shows the values of the crystalline melting temperature of all polymer blends films as shown in Table (3), where we note the crystalline melting temperature value of pure (PVA) polymer film is (220.25 °C), and when mixing the (PVA) polymer and (PVP) polymer with different weight ratios we note that the value of the crystalline melting temperature at the weight ratios (([90:10], [30:70]) wt%) of the polymer blend increases compared with pure (PVA) polymer film, and its decrease at the weight ratios (([80:20], [70:30], [60:40], [50:50], [20:80], [10:90]) wt%) for the polymer blend compared with pure (PVA) polymer film, this increase and decrease in crystalline melting temperature value compared with pure (PVA) polymer film indicates that the higher crystallization and regularity of the crystal

structure decreases with the increase of texture degree [12]. We note at the weight ratio ([40:60] wt%) for the polymer blend disappearing crystalline melting temperature, this disappearance is due to the strong interaction between (PVA) polymer and (PVP) polymer (covalent and hydrogen bonds) that weaken crystallization in (PVA) polymer and (PVP) polymer [13], as well as due to the decrease or increase in non-crystallized regions in prepared samples.

Bioactivity Test

The sensitivity test of bacteria (E. coli - Proteus) for (PVA-PVP-Ag) nano polymer composite solution with volume ratios ((0.5, 1, 1.5) vol %) from silver nanomaterial, where used the (Disc Diffusion Method), the study showed that the nano polymer composite solution have highly effective on bacteria (E.Coli - Proteus), and increases the effectiveness of (PVA-PVP-Ag) nano polymer composite with solution increase the concentration of silver nanomaterial, the small size of nanoparticles and its large surface area (whenever the size of nanoparticles was smaller it has been collected in larger numbers on the surface of the cells, which increases the toxicity of nanoparticles on the microorganisms) effect on the permeability of the plasma membrane of the bacteria and thus due to the death of the cell. The mechanism in which the nano polymer composites interact with the bacterial cells is that the microorganisms carry negative charges, while the nano metallic oxides carry positive charges, thus creating an electromagnetic attraction between the bacteria and the surface of the nanoparticles, this nanoparticles release ions which interact with the thiol group (SH-Group) of proteins transport foods that emerge from the bacterial cell membrane due to reduced permeability of the membrane which resulting to the cell death, in other words, the mechanism of inhibition of (DNA) susceptibility to replication and genetic gene expression of different cellular proteins and necessary enzymes to production of an (ATP) enzyme becomes ineffective which is lead to the attacking of (PVA-PVP-Ag) nano polymer composite the surface of the cell membrane and disrupts the permeability process and cell breathing or interferes with the electronic transmission system of the bacteria [14]. Figure (3) shows the image of bioactivity test of the (PVA-PVP-Ag) nano polymer composite on bacteria (E. coli) and (Proteus).

CONCLUSIONS

The thermal conductivity coefficient of [PVA:PVP] polymer blends films has an irregular behavior compared with (PVA) pure polymer film by increasing the weight ratio of (PVP) polymer, and found that the thermal conductivity coefficient of [PVA:PVP] polymer blends films with different weight ratios is very small, therefore this polymer blend can be used as a thermal insulator shield at all weight ratios. The differential Scanning Colarymeter (DSC) test of pure (PVA) polymer film and [PVA:PVP] polymer blends films with different weight ratios showed:

1. The glass transition temperature of [PVA:PVP] polymer blends films is increased at most weight ratios of the polymer blend compared with pure (PVA) polymer film, while its decreasing at the weight ratios (([40:60], [30:70], [20:80]) wt%) of the polymer blend compared with pure (PVA) polymer film, but we note at the weight ratio ([90:10] wt%) for the polymer blend disappearance the glass transition temperature.
2. The crystalline melting temperature of [PVA:PVP] polymer blends films showed irregular behavior compared with pure (PVA) polymer film by increasing the weight ratio of (PVP) polymer, and also we note disappearance the crystalline melting temperature at the weight ratio ([40:60] wt%) for the polymer blend The bioactivity test showed the success possibility of (PVA-PVP-Ag) nano polymer composite solution to the exteniction and killing the twice types of bacteria (E.Coli, Proteus).

REFERENCES

1. S.A.Salman,N.A.Bakr, M. R. Jwameer, "Effect of Annealing on the Optical Properties of (PVA-CuCl) Composites", International Letters of Chemistry, Physics and Astronomy, Vol.63, pp.98-105, (2016).

2. R. Singh and S. G. Kulkarin, "Morphological and Mechanical Properties of polyvinyl alcohol Doped with Inorganic Fillers", International Journal of Polymeric Materials and Polymeric Biomaterial, Vol.62, No.6 pp.351-357, (2013).
3. P. J. Liu, W. H. Chen, Y. Liu, S. B. Bai and Q. Wang, "Thermal Melt Processing to Prepare Halogen-Free Flame Retardant Polyvinyl Alcohol", Polymer Degradation and Stability, Vol.109, pp.261-269, (2014).
4. G. R. Tuttle, "Size and Surface Area Dependent Toxicity of Silver Nanoparticles in Zebrafish Embryos (Danio rerio)", Master of Science, Oregon State University. (2013).
5. N. Duran, P. D. Marcato, R. D .Conti, O. L. Alves, F. M. Costa and M. Brocchi, "Potential use of Silver Nanoparticles on Pathogenic Bacteria, their Toxicity and Possible Mechanisms of Action", J. Braz. Chem. Soc., Vol. 21, No.6, pp.949-959, (2010).
6. V. Kovacevic, M. Leskovac and S. Blagojevic, "Morphology and Failure in Nanocomposites. Part II: Surface Investigation", Journal of Adhesion Science and Technology, Vol. 16, pp. 1915-1921 (2002).
7. K, Hemalatha, H. Somashekarappa and R. Somashekar, "Micro-Structure, Ac Conductivity and Spectroscopic Studies of Cupric Sulphate Doped PVA/PVP Polymer Composite", Scientific Research Publishing, Vol.5, pp.408-418, (2015).
8. H. Yu, X. Xu, X. Chen, T. Lu, P. Zhang and X. Jing, "Preparation and Antibacterial Effect of PVA-PVP Hydrogels Containing Silver Nanoparticals", Journal of Applied Polymer Science, Vol.103, pp. 125-133, (2006).
9. L. C. Shen, "Studies on the Effect of Nanosized Ceramic Filler Polyvinyl Alcohol/Lithium Perchlorate Based Polymer Electrolytes", Msc, Thesis, University of Malaya, Faculty of Science, Department of Physics, (2012).
10. C. Chen, J. Chueh, H. Tseng, H. Huang and S. Lee, "Preparation and Characterization of Biodegradable PLA Polymeric Blends", Biomaterials, Vol. 24, pp. 1167-1173, (2003).
11. I. S. Elashamwi, E. M. Abdelrazek and A.Y. Yassin, "Influence of $NiCl_2$/ $CdCl_2$ as Mixed Filler on Structural, Thermal and Electrical Properties of PVA/ PVP Blend", British Journal of Applied Science & Technology, Vol. 4, No. 30, pp. 4263- 4279, (2014).
12. O. W. Guirguis, and M. T. H. Moselhey, "Thermal and Structural Studies of Poly vinyl Alcohol and Hydroxypropyl Cellulose Blends", Natural Science, Vol. 4, No. 1, pp. 57- 67, (2012).
13. I. R. Rodrigues, M. M. C. Forte, D. S. Azambuja and K. R. L. Castagno, "Synthesis and Characterization of hybrid Polymeric Networks (HPN) Based on Polyvinyl Alcohol/Chitosan", Reactive & Functional Polymers, Vol. 87, pp. 708-715, (2007).
14. H. A. Abod, Kh. A. Bander and S. S. Zain-Al-Abdeen, "Effect of Silver Nanoparticles Prepared by Streptomyces. Spp on Some Pathogenic Bacteria", Tikrit Journal of Pure Sciences, Vol. 22, No.3, pp.17-26, (2017).

Table 1. Values of thermal conductivity coefficient of [PVA:PVP] polymer blends films with the weight ratio of the blend

Blending Ratio of [PVA:PVP] (wt%)	k (W/m.K)
[100:0]	$2.4x10^{-4}$
[90:10]	$2.8x10^{-4}$
[80:20]	$1.65x10^{-4}$
[70:30]	$2.78x10^{-4}$
[60:40]	$1.68x10^{-3}$
[50:50]	$1.66x10^{-4}$
[40:60]	$5.58x10^{-4}$
[30:70]	$2.38x10^{-4}$
[20:80]	$2.79x10^{-4}$
[10:90]	$2.09x10^{-4}$

Table 2. Values of the glass transition temperature of [PVA: PVP] polymer blends films with the weight ratio of the blend

Blending Ratio of [PVA:PVP] (wt%)	T_g (°C)
[100:0]	110.28
[90:10]	–
[80:20]	118
[70:30]	119
[60:40]	123.4
[50:50]	111.2
[40:60]	108
[30:70]	90.4
[20:80]	91.5
[10:90]	116.3

Table 3. Values of the crystalline melting temperature of [PVA: PVP] polymer blends films with the weight ratio of the blend.

Blending Ratio of [PVA:PVP] (wt%)	T_m (°C)
[100:0]	220.25
[90:10]	221.38
[80:20]	216.35
[70:30]	215.47
[60:40]	205.76
[50:50]	216.71
[40:60]	–
[30:70]	224.81
[20:80]	164.18
[10:90]	213.30

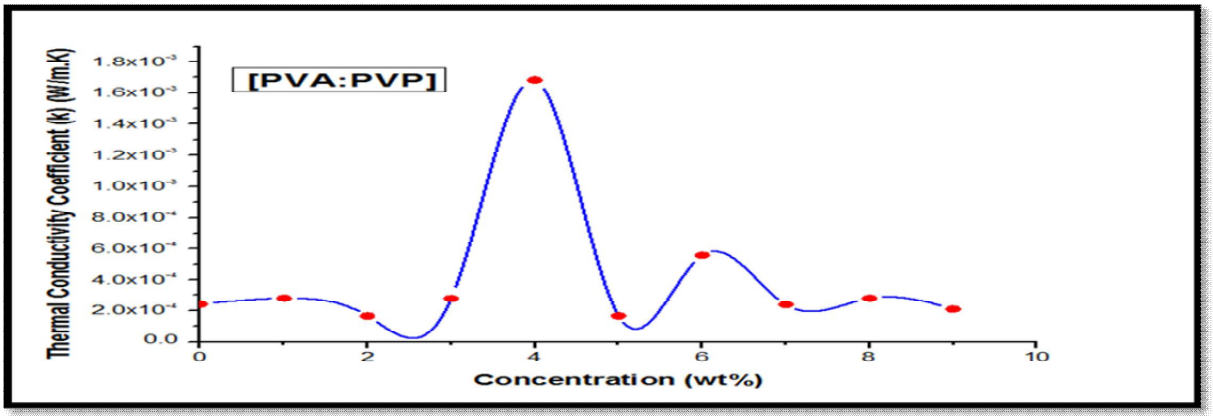

Figure 1. Thermal conductivity coefficient of [PVA:PVP] polymer blends films as a function of the weight ratio of the blend

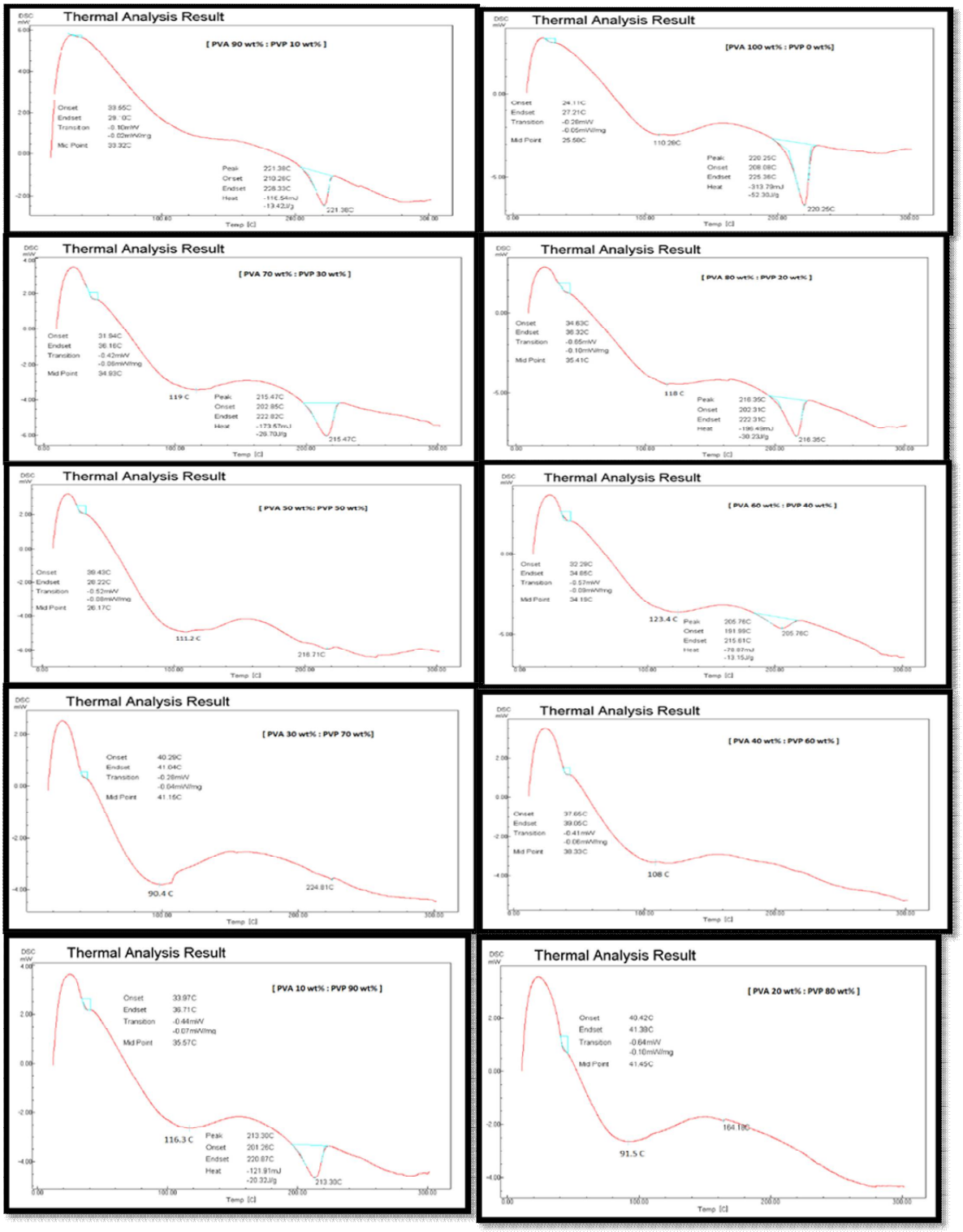

Figure 2. Thermal (DSC) schemes for [PVA-PVP] polymer blends films with different weight ratios.

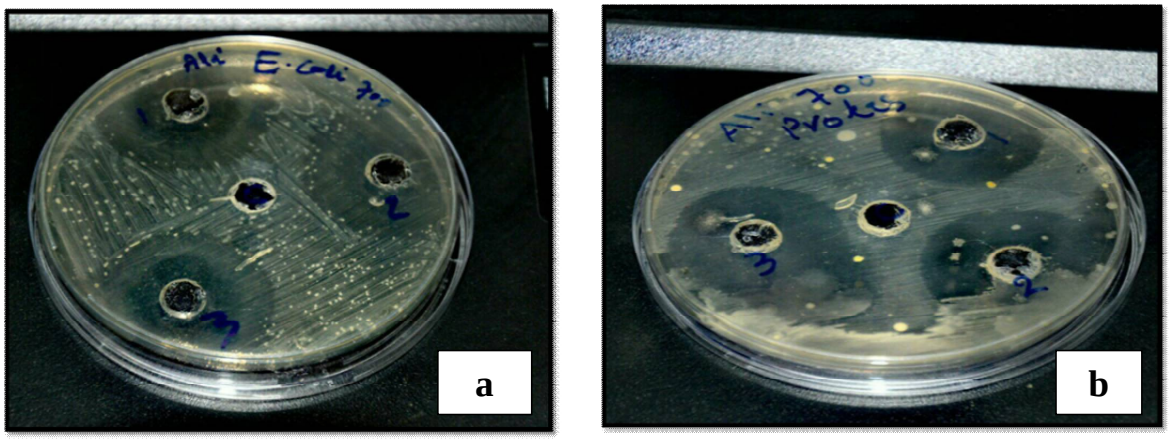

Figure 3. Image of the bioactivity test of (PVA-PVP-Ag) nano polymer composite on bacteria

a) *E.Coli* **b) *Proteus***

Indian Journal of Natural Sciences www.tnsroindia.org.in ©IJONS

Vol.9 /Issue 52 / February / 2019 *International Bimonthly* *ISSN: 0976 – 0997*

REVIEW ARTICLE

Peak Calling Algorithms and Their Applications for Next-Generation Sequencing Technologies

Hamdan A. Taleb[1*], Aisha AL-Dherasi[2], Sultan Al-Mosaib[3], Mohammed Alnoud[4] and Vilaphong Souksavanh[5]

[1]Department of Computer Science and Technology, Tongji University, Shanghai, China.
[2]Center of Genome and Personalized Medicine, Institute of Cancer Stem Cell, Dalian Medical University, Dalian, Liaoning, China.
[3]Department of Computer Science, KuvempuUniversity, Shimoga, India.
[4]School of Life Science and Technology, Tongji University, Shanghai, China.
[5]School of Software Engineering, Tongji University, Shanghai, China.

Received: 17 Nov 2018 Revised: 20 Dec 2018 Accepted: 23 Jan 2019

[*]**Address for Correspondence**
Hamdan A. Taleb
Department of Computer Science and Technology,
Tongji University,
Shanghai, China.
Email: hamdan.ha44@gmail.com

ABSTRACT

Next-generation sequencing (NGS) technologies have grown significantly since their introduction, and the focus has been on developing sophisticated analytical tools to handle a massive amount of data. Peak calling for NGS technologies has become one of the most important issues in bioinformatics. Peak calling is an increasingly popular approach for finding and studying regions in a genome that have been enriched with aligned reads, these regions are those where a protein interacts with DNA. Current peak calling algorithms are typically inapplicable to non-bioinformaticians. In this Review, we present the current development of peak calling algorithms for the Next-Generation sequencing technologies and available softwares.

Keywords: Next-Generation Sequencing; Peak calling; Peak detection; Peak calling Algorithms; peak caller.

INTRODUCTION

NGS (Next-Generation Sequencing) technologies have been useful to many scientific and clinical areas including detection of genetic variations. Recent developments in the NGS have allowed researchers and scientists to study a variety of molecular events active on the genome with high accuracy[1]. Extensive peak calling algorithms for NGS data demonstrate the evolving and diverse needs of the research community.The chromatin-based NGS techniques

such as Chip-seq, DNase-seq, MNase-seq …etc, have been recognized and adopted by various research projects. DNase I hypersensitive regions sequencing (DNase-Seq) is a technique which depends on a firm DNase I footprinting protocol[2]. This technique is a widely used method for profiling cis-regulatory components in open chromatin areas [1]. ChIP–seq (Chromatin Immunoprecipitation Followed by NGS) is one of the widely used techniques for the genome-wide locations of DNA binding proteins such as transcription factors or modified histones [1, 3, 4]. MNase-seq is a technique in which micrococcal nuclease digestion of chromatin is followed by NGS to determine the locations of high nucleosome occupancy[5]. In 2013 a new technique as a complementary to MNase-seq called ATAC (Transposase-Attainable Chromatin by Sequencing) was introduced to study chromatin accessibility [6]. Advances in these techniquesvaried between experimental approaches and computational approaches. Peak calling method is generally the first step in the analysis of these data [7].

Recently, there are more than 30 peak calling algorithms for the NGS data have been developed as of now. Most of this algorithms are developed for the ChIP-seq data analysis. Generally, most peak callers are based on negative binomial model, Poisson model or Kernel Density Estimator to address the count data. For example, MACS uses a Poisson model to test the significance of tag enrichment adjusting the local mapping structure [8];ZINBA applies a Kernel Density Estimator to estimate local read density and identifies enriched areas [9] etc.The number of literature increasingly grows, which keeps enriching our understanding of the experimental data. In this review, we will summarize the widely-used peak calling algorithms for the NGS technologies. We first present an overview of the NGS technologies and peak calling algorithms.Secondly, we will introduce the general workflow of peak calling algorithms.Thirdly, we will introduce the peak calling algorithms that have been developed for identifying areas in a genome-wide enriched with aligned reads. Finally, some technical issues will be outlined.

Overview of the NGS Technologies and Peak calling Algorithms

Massively parallel sequencing is a feature of the NGS, which has revolutionized recent genomic research[10].The technologies like ATAC-seq,DNase-seq, ChIP-seq, MNase-seq, and FAIRE-seq, combine the NGS with new biochemical techniques or modulations of established methods. An enormous range of chromatin phenomena can be further investigated [4]. Before discussing the peak calling algorithms, we will introduce the NGS techniques first:

ChIP–seq technique

The CHIP-seq is the most common method for identifying the binding sites for single-stranded DNA or modified histones. It is one of the early techniques of the NGS that offers higher resolution and clearer data at a lower cost in several areas, especially in genome-wide of identifying the locations and biochemical modifications of bound proteins [11-13]. In recent years, ChIP-seq technique has become the main technique to the genome-wide study of histone modifications and protein–DNA interactions [14, 15]. Several methods and algorithms have been developed for ChIP-seq analysis. The Peak calling is one of those methods that have been developed to identify areas where sequence reading is enriched in the genome

FAIRE-seqtechnique

The FAIRE-Seq (Formaldehyde-Assisted Isolation of Regulatory Elements) is an NGS technique used for identifying the DNA sequences related to the regulatory activity. Compared with other techniques, the FAIRE-Seq does not need the permeabilization of cells or segregation of nuclei, which is applicable to any kind of cells[16, 17].

DNase-seq technique

The DNase-seq is a technique used to determine the sites of regulatory regions, which is sensitive to the gap of (DNase) I [18, 19]. DNase I hypersensitive locations are normally enriched in the highly expressed gene bodies and is clearly enriched in a functional regulatory chain such as promoters and enhancers, which are targeted by numerous transcription-factors (TFs). The ENCODE (Encyclopedia of DNA Elements) [20] and the NIH Roadmap Epigenomics[21]offered the DNase-seq data of numerous human and mouse cell lines and tissues.

MNase-seq technique

Micrococcal nuclease followed by NGS (MNase-seq) is a technique in which assimilation of chromatin is followed by NGS. It is The most common technology utilized to identify the position of high nucleosome occupancy[22].

ATAC-seq technique

The ATAC-seq is the most common technique used to study chromatin accessibility. As a complementary technique to DNase-seq, MNase-seq, and FAIRE-seq, the technology was first reported in 2013 [6]. The ATAC-seq is used with a number of methods for cell separation and isolation, which likewise works on a diversity of cells, and applicable to human lymphoblastoidcells [23]. The requirement on the number of cells is also lower, the precision of which is likewise higher than other techniques like DNAse-Seq.

Peak calling

Peak calling is a computational technique used to identify regions in a genome that have been enriched with aligned reads. These regions are the positions where proteins are connected with DNA[24]. Figure 1 illustrates how these regionsare shown in areas of the genome. Recently, several peak calling algorithms have been developed and optimized for identifying enriched genomic regions from NGS technologies experiments (some widely available peak-calling algorithms for NGS technologies are listed below in table1 and the other algorithms in table2). But there is a wide field of discordance among the peak calls from different algorithms. The algorithmic engine has to be general enough in order to be applicable across datasets from many different *-seq technologies (i.e. ChIP-seq, DNase-seq, etc.). The properties of enriched areas differ between different NGS technologies, For example, DNase-seq data, in contrast, it doesn't appear as sharp as those in TFBS ChIP-seq nor as wide as in a model histone modification ChIP.

Aims of peak calling algorithms for NGS technologies

Given the recent developments in the field of bioinformatics and especially in NGS a number of literature offer a diverse peak calling algorithms. Here we formulate the core requirements for a peak calling algorithms for NGS in this manner: In order to keep up with the steadily rising number of experimental protocols that require peak calling algorithms for data-analysis,these algorithmshave to be wide-ranging sufficient in order to be applicable across datasets from many different NGS technologies (i.e. ChIP-seq peak calling algorithms applied to MNase-seq, DNase-seq, and ATAC-seq etc.). Regardless of the algorithmic and statistical complexity of the data-analysis mission, the implementation needs to be suitable for a general audience.

General Workflow of peak calling algorithms

In general, variant Peak calling algorithms needs several steps to analyze the data to get the final peak list (Figure 2 illustrate that)Which are described in the following steps:

Read shifting

The aligned reads are from fragments of 150-500 bp in length and, as most of this data is from single-end sequencing, only one end of a fragment is read. The readings are offset and the data is merged from both points to determine the most likely bases involved in protein binding. Reads therefore align with both the sense, antisense strands and the 3 or 5 extremes of the DNA fragments. The readings are shifted and the data is merged from both points to determine the most likely bases for protein binding.

Background estimation

Control data is processed in same method to allow for each genomic background to be specified by input controls or for enriched areas. Some peak calling algorithms work do not need control data to work[25]and assume a background signal, so others use blacklist tools for those masksof the genome For instance, "The Duke Excluded Regions" was developed for the ENCODE project, which mapped sequence tags were filtered out before peak calling for Open Chromatin (FAIRE and DNase) data sets.

Identifying peaks

The peak is the point/value that is higher than its surroundings. Therefore we can assume that in (1, 5, 1), the 5 is the peak.A Peak is called when the number of readings exceeds a predetermined threshold value or when there is a minimum enrichment value compared to the background signal, frequently in a sliding window through the genome. Some algorithms apply both methods. The parameters can be adjusted to determine the peaks, sometimes resulting to very different numbers of tops being called. The user needs to determine if fewer high-quality peaks are preferred over lower quality peaks.

Significance analysis

Many peak calling algorithms calculate a P value for called peaks, and the others usethe height of the peaks or/and enrichment above background to rank peaks. However, these do not provide statistical significance values. FDR (The false discovery rate) is often used to provide a truest peak list, and it can be calculated from the available P values. Some packages make use of the control data to determine an empirical FDR and generate a ratio of peaks in the sample vs. control.

Redundanciesremoval

Sum of redundant reads are kept for analysis, for instance: Redundant reads refer to reads with the same genomic location and direction. To remove these Redundancies, generally it is done by removing the redundancy and retaining only 1 read for each set of redundant reads.

Which algorithm is best for analysis?

If we ask different bioinformaticians which algorithms are best,we will probably get different answers. The answer greatly depends on the type of data which used in the experiments. Several algorithms have been developed for use with high-throughput sequencing data.Most of these algorithms developed for ChIP-seq and also utilized to other techniques such as MACS algorithm developed for ChIP-seq and also possible used for DNase-seq data.
Here we provide a brief description of the widest peak calling algorithms for NGS technologies. More details about these algorithms and the list of most common peak calling algorithms are shown in Table 2:

MACS Algorithm

MACS (Model-based Analysis of ChIP-Seq) is one of the most commonly used peak calling algorithms, it is still in development until now which makes it an effective algorithm, it is an algorithm for identifying genome-wide protein–DNA interaction from ChIP-Seq data [8]. Also it is possibly used for DNase-seq[26]. It has been benchmarked and reviewed in a number of studies, including many effective works[27-31]. MACS can be run with or without an input control dataset. MACS is widely available as both source code (http://github.com/taoliu/MACS) and through the Galaxy software platform (https://usegalaxy.org/) and has been shown to have an accurate and efficient performance [32, 33]. A Poisson model is employed for identification of statistically significant enriched regions:

$$\lambda_{local} = \max(\lambda_{BG}, [\lambda_{Region}, \lambda_{1k}], \lambda_{5k}, \lambda_{10k})$$

Steps of the MACS for calling peaks:

1- Removing redundancy: MACS removes redundant reads Depending on user-defined variables without changing the input data files that contain the mapped ChIP-seq reads and control reads. Automatically, MACS saves no more than one read For each genomic position [34].
2- Regulating read location based on fragment size distribution. (Algorithm 1 show TheMACS algorithm for Estimate ChIP-seq Fragment Size)
3- Computing peak enrichment using local background normalization.

Calculating the estimated value FDR for every peak.

We present an example for MACS peak caller output in Table1.
Thomas, R., et al.in their paper [35], performed a comparative study and systematic evaluation of the characteristics of macs2 and five other chip seq peak calling algorithms and they noted that The algorithm MACS2 and BCP do the best performance on simulated transcription factor binding data.

ZINBA Algorithm

ZINBA (Zero-Inflated Negative Binomial Algorithm) is an algorithm developed to call areas of the genome enriched for sequencing reads originating from a diverse array of biological experiments. It's applied to FAIRE-seq and ChIP-seq of CCCTC-binding factor, RNA polymerase II (RNA Pol II), and histone (H3K36me3), ZINBA Compared to F-seq, Macs and Hotspot less suitable for DNase-seq data analysis.[26]. ZINBA performs three procedures: data preprocessing, data analysis by identifying significantly enriched regions, and an elective limits refinement for more narrow sites[36].

step 1: data preprocessing
- Calculation of signal values
- Calculation of covariate values

step 2: data analysis
- Mixture regression to select enriched regions
- Model initialization
- Convergence
- Selecting relevant covariates using BIC

Step 3: peak boundary refinement
- Isolating exact peak boundaries within merged regions

F-SeqAlgorithm

F-Seq algorithm has been developed specially for use with DNase-seq data. Also has been used for FAIRE-seq and ChIP-seq data [26, 37]. F-Seq is suggested in which a Kernel Density Estimator is applied to obtain the distribution of reads.

$$\hat{g}(x) = \frac{1}{nb}\sum_{i=1}^{n} K\left(\frac{x - x_i}{b}\right)$$

F-Seq algorithm shows the best performance for DNase-seq data by comparison with Hotspot, MACS and ZINBA [26]. F-Seq has been implemented in Java, which made it easy to use.

BCP Algorithm

BCP (Bayesian Change-Point) is a multipurpose algorithm that can be useful to all histone modifications data types [38]. BCP algorithm uses a Poisson distribution $\mathrm{Pois}(\theta_t)$ with a Gamma conjugate prior, which accounts for the inherent over-dispersion described in ChIP-seq data.

$$f(\theta_t|y_n) = \sum_{1\le t\le j\le n} y_{ijt}\,\mathrm{Gamma}\,(x_{ij}, \beta_{ij}).$$

Where: θ can be estimated by different window sizes, n is the number of ''windows'' or blocks in the chromosome [33].The BCP algorithm successfully applies to both punctate peak and diffuse island identification with robust accuracy and limited user-defined parameters.

MUSIC Algorithm

MUSIC is a peak calling algorithm developed for identification of enriched regions at multiple scales in the read depth signals from ChIP-Seq experiments. the significant advantage of this algorithm is that users can identify the scales that they want to concentrate on, which is done by using the start and end scale parameters for the multiscale filtering [39, 40].

iNPS Algorithm

iNPS (Improved nucleosome-positioning) is a widely used algorithm for identifying nucleosome locations from MNase-seq data.iNPS algorithm is based on the cutoff of peak shape and the P-value of Poisson approximation for identifying and peak filtering from MNase-seq data experiments [41].

Hotspot Algorithm

Hotspot is an algorithm developed for detecting areas of local enrichment of short-read sequence tags mapped to the genome by a binomial distribution [42]. It has been applied extensively in DNase-seq and ChIP-seq data, with transcription factor and histone modification (H3K36me3, H3K27me3, and H3K4me3) data [26, 42].

SISSRs Algorithm

SISSRs (Site Identification from Short Sequence Reads), is a peak finder algorithmdeveloped for precise identification of binding sites from short reads generated from ChIP-Seq experiments [43]. The latest version of the Perl application

of the SISSRs algorithm isavailable at http://dir.nhlbi.nih.gov/papers/lmi/epigenomes/sissrs/. SISSRs is taken as input in a data file containing genomic coordinates of the mapped reads in BED file format.

Other algorithms

Afterward, we present some other peak calling algorithms for NGS data found in the literature, these algorithms are listed in Table 3. Ambrosini, G., et al. [44] presented in their paper a new command line tools and web server for ChIP-seq data analysis, one of these tools is "ChIP-Peak" which is a peak finder suitable for finding transcription factor binding sites. This tool is available at http://ccg.vital-it.ch/chipseq/.Fejes, A.P., et al. [45] developed a "FindPeaks" algorithm. The FindPeaks is a software application for determined theareas of enrichment from short-read in sequencing technology. The greatest number of papers and protocols for algorithms in table 2 and table 3 belongs to NGS peak calling. In summary, every day there are new algorithms and protocols. This fact proves that the development of peak calling algorithms for Next-Generation sequencing techniques is very diverse and rapidly expanding.

Technical issues

Data format

SAM, BAM or BED format are usually the most common accepted input formats by several calling softwares, also some algorithms support other input data formats such as GFF, FPS, SGA … etc[44]. For instance, ZINBA allowed three input formats BED, tagAlign and bowtie. Here we will show more details about these formats and in Table 5 we give a recommendation for data requirements for a peak calling applications:

SAM (Sequence Alignment Map) **format** is a common format for saving biological sequences aligned datagenerated by NGS technologies, it supports short and long reads (up to 128Mbp), the format contains one header segment and one alignment segment [46].

BAM format is the compressed binary version of the SAM format. Many peak callers for NGS and analysis software's work with BAM/BED format [44].

BEDformat: is a data format used by the UCSC genome browser for defining genomic areas. It offers a flexible way to describe the data lines that are put on show in an annotation track. BED format consists of 3-12 columns of data [47], We show an example of BED format data in Table 4, Where columns are: 1) The name of the chromosome, 2) The starting position, 3) The ending position, 4) The name of the BED line, 5) A score between 0 and 1000, 6) The strand, either +, - or (" . " = no strand. 7) The starting thick position, 8) the ending thick position, 9) An RGB value which determine the display color of the data. 10) The number of blocks. 11) the block sizes. 12) A list of block starts. Note. The first three columns in each feature line are essential and the others are optional.

GFF format: is a type of format data utilized for describing the data of genes and other DNA and protein sequences, now there exist two types of the GFF file format in general use (GFF2/GFF3). Many softwares accept this format.

Alignment and Convert data formats

When we use these peak callers, sometimes we need to convert the data format to conform with input requirements or to alignment results such as merging files. SAMtools software package [46] provides useful operations for convert from other alignment formats, sort and merge alignments. BWA [48], Bowtie [49], or any other or alignment software is needed to map *-Seq reads to the reference genome.

Visualization data

After obtaining the final peak list of data, we need to visualize the data.To visualizee data,most Users view their data either as called peaks or as signal profiles on a genome browser. UCSC: The most extensively used visualization environment is UCSC (the University of California Santa Cruz) genome browser, available via this link (https://genome.ucsc.edu/) [50], or IGV (Integrative Genome Viewer) http://www.broadinstitute.org/igv/[51], Figure 1 a screenshot for IGV show the results. Some peak callers have a visualization screen to display the histogram for the data like Nseq algorithm [52].

CONCLUSION

With the rapid progression of NGS technologies, the peak calling algorithms is quietly developing. Currently, several peak calling algorithms are available for the identification regions in a genome, these regions are those where DNA interacts with protein. But still peak calling algorithms has not grown to a point where it can be applied for more than one technique (i.e. ChIP-seq, MNase-seq, DNase-seq etc.) and addressed for different format data (i.e. SAM, BAM, GFF etc.), Although there are some algorithms that can be applied to other techniques but they are still deficient in some aspects.This paper presented a review of peak calling algorithms for NGS analysis in the communities of bioinformatics and computational biology. The aim of this review is to provide guidance for bioinformatics researchers to select the most suitable algorithms for their applications. We wish that this review for this active area of bioinformatics provides a useful starting point for your *_seq data analysis.

ACKNOWLEDGMENTS

Many thanks to the DMB lab at Tongji Universityfor suggestions on the manuscript.

REFERENCES

1. Shin, H., et al., *Computational methodology for ChIP-seq analysis.* Quantitative Biology, 2013. **1**(1): p. 54-70.
2. J.Galas, D. and A. Schmitz, *DNase footprinting. a simple method for the detection of protein-DNA binding specificity.* Nucleic Acids Res, 1978: p. 3157-3170.
3. Gupta, R. and A. Sathyanarayanan, *Calling narrow and broad peaks from ChIP-Seq data in Strand NGS.* Strand NGS, 2015.
4. Meyer, C.A. and X.S. Liu, *Identifying and mitigating bias in next-generation sequencing methods for chromatin biology.* Nature Reviews Genetics, 2014. **15**(11): p. 709-721.
5. Strino, F. and M. Lappe, *Identifying peaks in *-seq data using shape information.* BMC Bioinformatics, 2016. **17 Suppl 5**: p. 206.
6. Buenrostro, J.D., et al., *Transposition of native chromatin for fast and sensitive epigenomic profiling of open chromatin, DNA-binding proteins and nucleosome position.* Nat Methods, 2013. **10**(12): p. 1213-8.
7. Thomas, R., et al., *Features of ChIP-seq data peak calling algorithms with good operating characteristics.* 2016.
8. Zhang, Y., et al., *Model-based analysis of ChIP-Seq (MACS).* Genome Biol, 2008. **9**(9): p. R137.
9. Rashid, N.U., et al., *ZINBA integrates local covariates with DNA-seq data to identify broad and narrow regions of enrichment, even within amplified genomic regions.* Genome Biology, 2011. **12**.
10. Behjati, S. and P.S. Tarpey, *What is next generation sequencing?* Archives of disease in childhood - Education & practice edition, 2013. **98**(6): p. 236-238.
11. Park, P.J., *ChIP-seq: advantages and challenges of a maturing technology.* Nat Rev Genet, 2009. **10**(10): p. 669-80.
12. Liu, E.T., S. Pott, and M. Huss, *Q&A: ChIP-seq technologies and the study of gene regulation.* 2010.
13. Furey, T.S., *ChIP-seq and beyond: new and improved methodologies to detect and characterize protein-DNA interactions.* Nat Rev Genet, 2012. **13**(12): p. 840-52.

14. Xu, H., et al., *A signal-noise model for significance analysis of ChIP-seq with negative control.* Bioinformatics, 2010. **26**(9): p. 1199-204.
15. Barski, A., et al., *High-resolution profiling of histone methylations in the human genome.* Cell, 2007. **129**(4): p. 823-37.
16. Giresi, P.G., et al., *FAIRE (Formaldehyde-Assisted Isolation of Regulatory Elements) isolates active regulatory elements from human chromatin.* Genome Res, 2007. **17**(6): p. 877-85.
17. Song, L., et al., *Open chromatin defined by DNaseI and FAIRE identifies regulatory elements that shape cell-type identity.* Genome Res, 2011. **21**(10): p. 1757-67.
18. Madrigal, P. and P. Krajewski, *Current bioinformatic approaches to identify DNase I hypersensitive sites and genomic footprints from DNase-seq data.* Front Genet, 2012. **3**: p. 230.
19. Crawford, G.E., et al., *Genome-wide mapping of DNase hypersensitive sites using massively parallel signature sequencing (MPSS).* Genome Res, 2006. **16**(1): p. 123-31.
20. Consortium, E.P., *A user's guide to the encyclopedia of DNA elements (ENCODE).* PLoS Biol, 2011. **9**(4): p. e1001046.
21. Bernstein, B.E., et al., *The NIH Roadmap Epigenomics Mapping Consortium.* Nat Biotechnol, 2010. **28**(10): p. 1045-8.
22. Hu, S., et al., *CAM: A quality control pipeline for MNase-seq data.* PLoS One, 2017. **12**(8): p. e0182771.
23. Buenrostro, J.D., et al., *ATAC-seq: A Method for Assaying Chromatin Accessibility Genome-Wide.* Curr Protoc Mol Biol, 2015. **109**: p. 21 29 1-9.
24. Valouev, A., et al., *Genome-wide analysis of transcription factor binding sites based on ChIP-Seq data.* Nat Methods, 2008. **5**(9): p. 829-34.
25. Nix, D.A., S.J. Courdy, and K.M. Boucher, *Empirical methods for controlling false positives and estimating confidence in ChIP-Seq peaks.* BMC Bioinformatics, 2008. **9**: p. 523.
26. Koohy, H., et al., *A Comparison of Peak Callers Used for DNase-Seq Data.* Plose, 2014(A Comparison of Peak Callers Used for DNase-Seq Data).
27. Pepke, S., B. Wold, and A. Mortazavi, *Computation for ChIP-seq and RNA-seq studies.* Nat Methods, 2009. **6**(11 Suppl): p. S22-32.
28. Kim, H., et al., *A short survey of computational analysis methods in analysis Chip-seq data.* HUMAN GENOMICS, 2010. **5**: p. 117-132.
29. Spyrou, C., et al., *BayesPeak: Bayesian analysis of ChIP-seq data.* BMC Bioinformatics, 2009. **10**: p. 299.
30. Nakato, R., T. Itoh, and K. Shirahige, *DROMPA: easy-to-handle peak calling and visualization software for the computational analysis and validation of ChIP-seq data.* Genes Cells, 2013. **18**(7): p. 589-601.
31. Wilbanks, E.G. and M.T. Facciotti, *Evaluation of Algorithm Performance in ChIP-Seq Peak Detection.* PLoS ONE, 2010.
32. Goecks, J., et al., *Galaxy: a comprehensive approach for supporting accessible, reproducible, and transparent computational research in the life sciences.* Genome Biology 2010.
33. Xing, H., et al., *Genome-wide localization of protein-DNA binding and histone modification by a Bayesian change-point method with ChIP-seq data.* PLoS Comput Biol, 2012. **8**(7): p. e1002613.
34. Feng, J., et al., *Identifying ChIP-seq enrichment using MACS.* Nat Protoc, 2012. **7**(9): p. 1728-40.
35. Thomas, R., et al., *Features that define the best ChIP-seq peak calling algorithms.* Briefings in Bioinformatics, 2016: p. bbw035.
36. 36.Rashid, N.U., et al., *ZINBA integrates local covariates with DNA-seq data to identify broad and narrow regions of enrichment, even within amplified genomic regions.* Genome Biology, 2011.
37. Boyle, A.P., et al., *F-Seq: a feature density estimator for high-throughput sequence tags.* Bioinformatics, 2008. **24**(21): p. 2537-8.
38. Xing, H., et al., *A Novel Bayesian Change-point Algorithm for Genome-wide Analysis of Diverse ChIPseq Data Types.* 2012(70): p. e4273.
39. Harmanci, A., J. Rozowsky, and M. Gerstein, *MUSIC: identification of enriched regions in ChIP-Seq experiments using a mappability-corrected multiscale signal processing framework.* Harmanci et al. Genome Biology
40. Nakato, R. and K. Shirahige, *Recent advances in ChIP-seq analysis: from quality management to whole-genome annotation.* Briefings in Bioinformatics, 2016: p. bbw023.
41. Chen, W., et al., *Improved nucleosome-positioning algorithm iNPS for accurate nucleosome positioning from sequencing data.* Nat Commun, 2014. **5**: p. 4909.
42. John, S., et al., *Chromatin accessibility pre-determines glucocorticoid receptor binding patterns.* Nat Genet, 2011. **43**(3): p. 264-8.
43. Jothi, R., et al., *Genome-wide identification of in vivo protein-DNA binding sites from ChIP-Seq data.* Nucleic Acids Res, 2008. **36**(16): p. 5221-31.

44. Ambrosini, G., et al., *The ChIP-Seq tools and web server: a resource for analyzing ChIP-seq and other types of genomic data.* BMC Genomics, 2016. **17**(1).
45. 45.Fejes, A.P., et al., *FindPeaks 3.1: a tool for identifying areas of enrichment from massively parallel short-read sequencing technology.* Bioinformatics, 2008. **24**(15): p. 1729-30.
46. Li, H., et al., *The Sequence Alignment/Map format and SAMtools.* Bioinformatics, 2009. **25**(16): p. 2078-9.
47. Karolchik, D., et al., *The UCSC Table Browser data retrieval tool.* Nucleic Acids Res, 2004. **32**(Database issue): p. D493-6.
48. Li, H. and R. Durbin, *Fast and accurate short read alignment with Burrows-Wheeler transform.* Bioinformatics, 2009. **25**(14): p. 1754-60.
49. Langmead, B. and S.L. Salzberg, *Fast gapped-read alignment with Bowtie 2.* Nat Methods, 2012. **9**(4): p. 357-9.
50. Kent, W.J., et al., *The human genome browser at UCSC.* Genome Res, 2002. **12**(6): p. 996-1006.
51. Nicol, J.W., et al., *The Integrated Genome Browser: free software for distribution and exploration of genome-scale datasets.* Bioinformatics, 2009. **25**(20): p. 2730-1.
52. Nellore, A., et al., *NSeq: a multithreaded Java application for finding positioned nucleosomes from sequencing data.* Front Genet, 2012. **3**: p. 320.
53. McCarthy, M.T. and C.A. O'Callaghan, *PeaKDEck: a kernel density estimator-based peak calling program for DNaseI-seq data.* Bioinformatics, 2014. **30**(9): p. 1302-4.
54. Woo, S., et al., *PING 2.0: an R/Bioconductor package for nucleosome positioning using next-generation sequencing data.* Bioinformatics, 2013. **29**(16): p. 2049-50.
55. Zhang, Y., et al., *Identifying positioned nucleosomes with epigenetic marks in human from ChIP-Seq.* BMC Genomics, 2008. **9**: p. 537.
56. Narlikar, L. and R. Jothi, *ChIP-Seq data analysis: identification of protein-DNA binding sites with SISSRs peak-finder.* Methods Mol Biol, 2012. **802**: p. 305-22.
57. Flores, O. and M. Orozco, *nucleR: a package for non-parametric nucleosome positioning.* Bioinformatics, 2011. **27**(15): p. 2149-50.
58. Zang, C., et al., *A clustering approach for identification of enriched domains from histone modification ChIP-Seq data.* Bioinformatics, 2009. **25**(15): p. 1952-8.
59. Xu, S., et al., *Spatial clustering for identification of ChIP-enriched regions (SICER) to map regions of histone methylation patterns in embryonic stem cells.* Methods Mol Biol, 2014. **1150**: p. 97-111. 6
60. Ji, H., et al., *An integrated software system for analyzing ChIP-chip and ChIP-seq data.* Nat Biotechnol, 2008. **26**(11): p. 1293-300.
61. Zhang, Y., et al., *PePr: a peak-calling prioritization pipeline to identify consistent or differential peaks from replicated ChIP-Seq data.* Bioinformatics, 2014. **30**(18): p. 2568-75.
62. Rozowsky, J., et al., *PeakSeq enables systematic scoring of ChIP-seq experiments relative to controls.* Nature Biotechnology, 2009. **27**: p. 66.
63. Newkirk, D., et al., *AREM: aligning short reads from ChIP-Sequencing by expectation maximization.* Comput. Biol., 2011: p. 1-15.
64. Chen, K., et al., *DANPOS: dynamic analysis of nucleosome position and occupancy by sequencing.* Genome Res, 2013. **23**(2): p. 341-51.
65. Schep, A.N., et al., *Structured nucleosome fingerprints enable high-resolution mapping of chromatin architecture within regulatory regions.* Genome Res, 2015. **25**(11): p. 1757-70.

Table 1. illustrates the output of Macs peak caller

1	2	3	4	5	6	7	8	9
chr1	137660	138139	480	153	62	635.75	41.05	0.00
chr1	138380	139613	1234	680	118	1038.81	41.05	0.00
chr1	712724	715549	2826	1877	433	3100.00	98.27	0.00
chr1	752449	752902	454	151	15	83.67	12.44	6.45
chr1	905080	905697	618	385	18	54.29	8.13	15.71
chr1	760913	763271	2359	1901	296	2878.46	83.33	0.00
chr1	839086	841012	1927	465	175	1154.41	24.76	0.00

where columns are: 1) Chromosome, 2) Start, 3) End, 4) length of peak region, 5) summit location related to the peak start position, 6) number of reads in peak region, 7) Fold-change (compared to the expectation from Poisson distribution with local lambda) 8) -$\log_{10}$*P*-value 9) FDR (false discovery rate).

Table 2. The most popular peak calling algorithms for NGS technologies

Name of algorithm	*_seq data	URL	Notes	Depended environment	Ref.
MACS	Chip – seq Dnase – seq [26]	http://liulab.dfci.harvard.edu/MACS/	MACS is specifically Developed for Chip – seq data.	Python	[8]
ZINBA	FAIRE-seq ChIP-seq DNase-seq	http://code.google.com/p/zinba/	ZINBA developed for analyzing DNA-seq experiments。	R	[36]
F-Seq	DNase-seq Chip-seq	https://www.encodeproject.org/publications/f57ccb1c-d002-401d-bce5-548a443d0118/	F-Seq originally developed for DNase-seq data, it has also been used for ChIP-seq peak detection	Java	[37]
BCP	ChIP-Seq	http://rulai.cshl.edu/BCP	BCP is especially suited for analysis of diffuse histone ChIP-seq data.	C++	[33]
MUSIC	ChIP-Seq	https://github.com/gersteinlab/MUSIC	Developed for ChIP-Seq data.	C++	[39]
PeaKDEck	DNase-seq	https://www.ccmp.ox.ac.uk/peakdeck	Developed for DNase-Seq data	Perl	[53]
iNPS	MNase-seq	http://www.picb.ac.cn/hanlab/iNPS.html	iNPS was designed for MNase-seq data.	Python	[41]
PING & PING 2.0	MNase-seq ChIP-Seq	http://www.bioconductor.org/packages/release/bioc/html/PING.html	For nucleosome locating by NGS data.	R	[54]
NPS	MNase-seq ChIP-seq	http://liulab.dfci.harvard.edu/NPS/	For identifying peaks from MNase-seq data.	Python	[55]
Hotspot	DNase-seq Chip-seq	https://github.com/rthurman/hotspot	A new algorithm of Hotspot named ‘‘Dnase2hotspots’’	C++ And R (the statistical Analyses)	[42]
SISSRs	Chip-seq	http://sissrs.rajajothi.com/	SISSRs-identified binding sites: CTCF, NRSF, STAT1	Perl	[43] [56]
nucleR	MNase-seq	http://mmb.pcb.ub.es/nucleR/	For MNase-seq data	R	[57]

Table 3.This table shows a number of peak calling algorithms also developed for NGS data analysis

Name of algorithm	***_seq data**	**URL**	**Ref.**
ChIP-Peak	Chip-seq	https://ccg.vital-it.ch/chipseq/chip_peak.php	[44]
FindPeaks	Chip-seq	http://www.bcgsc.ca/platform/bioinfo/software/findpeaks	[45]
SICER	Chip-seq	https://home.gwu.edu/~wpeng/Software.htm	[58, 59]
CisGenome	Chip-seq	http://www.biostat.jhsph.edu/~hji/cisgenome/	[60]
PePr	Chip-seq	https://code.google.com/archive/p/pepr-chip-seq/	[61]
PeakSeq	Chip-seq	http://info.gersteinlab.org/PeakSeq	[62]
QUEST	Chip-seq	http://www-hsc.usc.edu/~valouev/QuEST/QuEST.html	[24]

AREM	Chip-seq	https://cbcl.ics.uci.edu/doku.php/software/arem	[63]
USeq	Chip-seq	http://useq.sourceforge.net/	[25]
CAM	MNase-seq	http://www.tongji.edu.cn/~zhanglab/CAM	[22]
NSeq	MNase-seq	https://github.com/songlab/NSeq	[52]
DANPOS	MNase-seq	http://code.google.com/p/danpos/	[64]
NucPosSimulator	MNase-seq	http://bioinformatics.fh-stralsund.de/nucpos/	[54]
Perl Scripts	ATAC-seq	https://github.com/GreenleafLab/NucleoATAC	[65]

Table 4. Example for BED format data

1	2	3	4	5	6	7	8	9	10	11	12
chr1	1000	5000	clonA	960	+	1000	5000	0	2	567. 489	0.3513

Table 5. Recommendation for data requirements for a peak calling applications

***_seq data**	**URL for data**
DNase-seq data	http://hgdownload.cse.ucsc.edu/goldenPath/hg19/encodeDCC/wgEncodeUwDnase/
Chip-seq data	http://hgdownload.cse.ucsc.edu/goldenPath/hg19/encodeDCC/wgEncodeBroadHistone/
MNase-seq data	http://dir.nhlbi.nih.gov/papers/lmi/epigenomes/hgtcellnucleosomes.aspx http://dir.nhlbi.nih.gov/papers/lmi/epigenomes/hgtcellnucleosomes.aspx
FAIRE-seq	http://www.bios.unc.edu/~nur2/

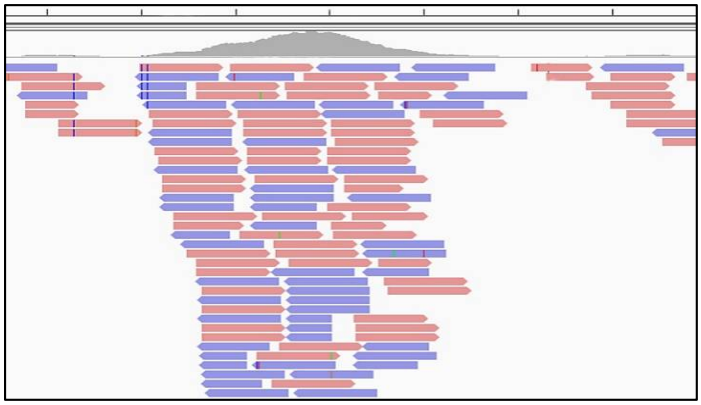

Figure 1.Illustrationof how peak regions are shown in areas of the genome

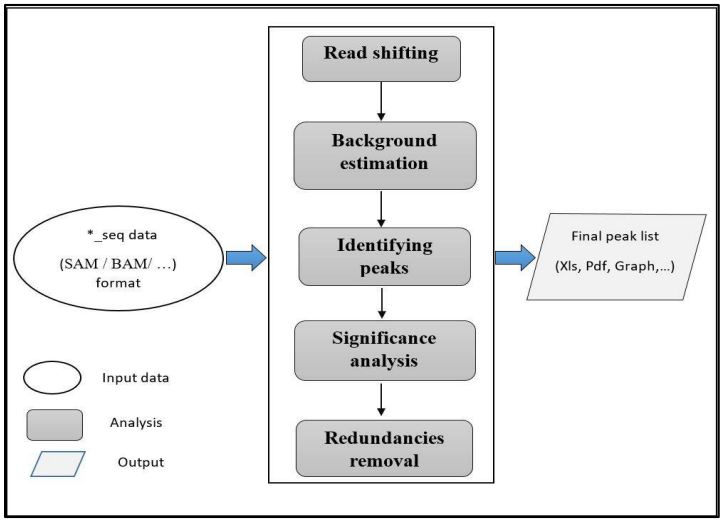

Figure 2. A flowchart illustrating the Peak calling algorithms steps to analyze the data to get the final peak list.

Indian Journal of Natural Sciences www.tnsroindia.org.in ©IJONS

Vol.9 /Issue 52 / February / 2019 *International Bimonthly* *ISSN: 0976 – 0997*

REVIEW ARTICLE

Accurate Diagnosis of Pathogenic Parasites Based on Modern Techniques

Khadeeja Abees Hmood Al-khalidy*

Department of Environment, College of Sciences, University of Al-Qadisiyah, Iraq.

Received: 18 Nov 2018 Revised: 21 Dec 2018 Accepted: 24 Jan 2019

***Address for Correspondence**
Khadeeja Abees Hmood Al-khalidy
Department of Environment,
College of Sciences,
University of Al-Qadisiyah, Iraq.

ABSTRACT

Parasites are characterized by the ability of many of them to cause injuries ranging from severe to mild impact on different neighborhoods. It is therefore very important to investigate these parasitic infections to address them and to limit their increased susceptibility, Molecular diagnostics are based on amplification of genes and allow for very small amounts of parasitic DNA to be investigated with a specificity of 97%. One of the most important developments in recent years in molecular biology is the discovery of polymerase chain reaction (PCR) technique by Karymullisin1985; this technique can amplify the exact amounts of DNA to millions of replicas. This technique has received considerable attention in various fields of research, especially in molecular biology and clinical medicine, the polymerase chain reaction method is used to investigate and diagnose organisms that are difficult to diagnose in appearance and form this technique has a high sensitivity of up to 97.4% and its specificity reaches 100%.

Keywords: Parasites, injuries, increased, technique, DNA, PCR, clinical, medicine.

INTRODUCTION

Parasites cause various health problems for humans and their animals. Parasites, such as protozoa and worms, are dangerous pathogens. Parasites are of great health importance to doctors and veterinarians for their wide spread and parasitism on a wide range in man andother hosts [1, 2], especially in tropical and sub-tropical climates, which are no less important than other microscopic pathogens because they can infect most organs of the body and lead to sometimes fatal complications. (In addition to its ability to multiply and in great numbers, which led to its failure to completely eliminate [3, 4], there is widespread interest in the need to control these parasites and reduce their impact on humans .Diagnosis of the majority of parasites in traditional methods is sometimes very difficult,and there are many parasites similar in terms of external appearance such as *Sarcocystis spp*., *Leishmaniaspp, Toxoplasma gondii*[5, 6] so must adopt molecular diagnostic methodssuch as Conventional –PCR,Nested–PCR, Real-time PCR…etc[7,8].

The molecular methods one of the most recent methods of diagnosis and identification of parasites and the distinction between them, that are characterized by accuracy of their results, privacy and high sensitivity compared to other methods such as cellular farms and microscopic examinations [9,10]. [11] They can identify small amounts of parasitic DNA and are characterized by their speed, through which resistance to treatment can be distinguished and used for scientific research [12]., there are many types of polymerase chain reaction, some of them:

Conventional-PCR reaction

The polymerase chain reaction method is used mainly after isolating and multiplying the parasite by tissue culture or by experimental lesions in mice [13, 14]. The Conventional polymerase chain reaction process amplifies the amount of DNA extracted by a number of cycles so that the amount of DNA increases at each cycle, this amount of DNA is then passed through Agaros gel, DNA packages dyed with an atheidium dye can be observed after being examined under ultraviolet light [15, 16]. The basic principle of polymerase chain reaction technology is based on the replication of a DNA sequence, which may be a gene or part of a gene or a simple extension of nucleotides in a sequence of known DNA, but the function of this sequence may be unknown [17],the discovery of overgrown chains by migration on gel agarose. If the nucleotide sequence of DNA is not present in the sample, this means that the primers added do not find anything to combine with it, so amplification does not occur in this case ,there are three main steps in the polymerase chain reaction, which are repeated 30 or 40 cycles through the automated cycler, which heat and cool the tubes containing the reaction mixture in a short period of time [18, 19, 20].

Nested-PCR

The interlocking polymerase chain reaction technique is used to solve detection problems associated with tissue samples that contain a small number of DNA copies. The target, which is present with large amounts of host DNA, may inhibit the work of the polymerase, the typical work method of this technique involves two cycles ,and the first cycle is a first round of amplification using a pair of primer called "outer primers." This cycle includes 35-30 cycles. After that, the product uses the first cycle as a template for the second round using the other pair of primer called Inner primers. Best and most the success of the method of dilution and re-amplification using the same primer (as in the conventional polymerase chain reaction technique),the internal pair of primers is a specific factor for the sensitivity and specificity of the test [21].

Real-time-PCR

A new scientific technique combining the amplification of the DNA sample with the detection of the amount and quality of the amplification output in a single reaction tube, which protects the samples from contamination by opening and closing the reaction tubes [22,23]. This technique is based on double dinucleotide reagents, which are a radioactive dye associated with each detector that has a sequence complementary to one of the resulting tapes. A fluorescent dye, called a Reporter, is connected to the 5-end reagent of the reagent is associated with a dye called Quencher. When the laser or halogen dye is stimulated, this dye absorbs the energy of the photons and then transfers it to the absorbent dye via the Fluoresce resonance energy transfer (FRET) [24].

Many real-time PCR amplification chemicals, including Probe, fluorescent labeled Oligonucleotide, glow in special conditions, glow indicates the presence of the probe and DNA sequences, and molecular methods have proved efficient in distinguishing pathogens from non-pathogens As well as in identifying the genes of harmful strains and finding potential relationships between genotypes and phenotypic patterns [25]. The probe is made up of radio labeled nucleotide sequences, which complements a portion of parasitic DNA and is highly specific and re-replicable [12]. Parasites are characterized by the ability of many of them to cause injuries ranging from severe to mild impact on different neighborhoods. It is therefore very important to investigate these parasitic infections to address them

and to limit their increased susceptibility [26, 27], Because of their health damage to humans and other animals as well as spread in soil [28, 29, 30], and water [31], so very important to investigate these parasitic infections.

REFERENCES

1- Jones, J.; Lopez, A. & Wilson, M. (2003). Congeital Toxoplasmosis. Am. Eam. Physician., 67: 2131-2145.
2- Al-Abodi, H. R. J. (2018). Pathological Effects Associated with Parasitic Infections. *Indian Journal of Natural Sciences*, Vol.9 /Issue 51, 16146-16151.
3- Al-Kubaisi, A.H. M. (2001). Study of epidemiological classifications of intestinal parasites in Babylon Governorate / Iraq. Thesis / Faculty of Science / Babylon University: 48 .
4- Hamzah, H. M. and Jameel, H. R. (2017). Epidemiology study of Entamoebaspesies in AL-Qadisiya governorate. Al-qadisiyah Journal for pure science, Vol.9, No. 3.
5- Darabus, G. H.; Oprescu, I.; Morariu, S.; &Narcisa, M. (2006).Parasitology and parasite diseases, Mirton Timisoara.
6- Al-abodi, H. R. J. (2017). Serological and molecular detection of Toxoplasma gondii in Columba livia hunting pigeons of AL- Qadisiyah province. AL-Qadisiyah Journal of Vet. Med. Sci; 16 (1):128-133
7- Brenier-Pinchart, P.; Morand-Bui V.; Fricker-Hidalgo H.; Equy V.; Marlu R.; Pelloux H. (2007).Adapting aconventional PCR assay for Toxoplasma gondii detection to real-time quantitative PCR including a competitive internal control, Parasite, 14(2): 149-154.
8- Al-Abodi, H. R. J. (2018). Suspicion in the form of infection is the basis for selecting the appropriate method for examining the toxoplasmosis disease of bends that have no symptoms from patients. Int. J. Adv. Res. 6(9), 655-662.
9- Van den Bossche, D., Cnops, L., Verschueren, J., & Van Esbroeck, M. (2015). Comparison of four rapid diagnostic tests, ELISA, microscopy and PCR for the detection of Giardia lamblia, Cryptosporidium spp. and Entamoebahistolytica in feces. Journal of microbiological methods, 110, 78-84.
10- Al-Abodi, H. R. J.; Al-Mayali, H. M. H. and Ali, M. J. (2015). Molecular study to most important virulence factor of Entamoebahistolytica in Diwaniyah province. International Journal of Advanced Research, Volume 3, Issue 8, 231-236.
11- Verweij, J. J., &Stensvold, C. R. (2014). Molecular testing for clinical diagnosis and epidemiological investigations of intestinal parasitic infections. Clinical microbiology reviews, 27(2),418.
12- Sastry, A.S; Bhat, S. (2014).Essentials of medical parasitology. First Edition. Jaypee Brothers Medical Publishers (P) Ltd.5-6.
13- Garcia ,J. L.; Gannari, S. M.; Machado, R. Z. & Navarro, I. T. (2006).Toxoplamagondii: detection by mouse bioassa, histopathology and polymerase chain reaction in tissues from experimentally infected pigs. J.Experiment .Parasitol., 113:267-271.
14- Al-Mayali, H. M. H. and Al-abodi, H. R. J. (2017). Molecular characterization of Entamoeba spp. In Al-Qadisiya province, Iraq. Al-Kufa University Journal for Biology, VOL.9 / NO.1 : 374-386.
15- AL-NASHI, A.P.Ali Abed Raheem; AL-AOSI, G. R. L (2013). Isolate and diagnose the bacteria present in the hospital in the city of Diwaniyah and the statement of the mechanisms to control the use of antibiotics and antiseptics. Al-Qadisiyah Journal Of Pure Science, V. 18 (3): 11-20.
16- AL-Shaibani, K. T. M. , Al-abodi, H. R. J. and Mahmood, H. R. (2018). Effect of Two Species of Ticks and Lice on Some Blood and Biochemical Parameters and their Role in the Transmission of Toxoplasma Gondii to Turkey MeleagrisGallopavo during Spring and Summer Seasons in AL-Diwaniyah Province – Iraq. Journal of Global Pharma Technology, 10(06):273-280.
17- White,T. J. (1996). The future of PCR technology: of technogyies and applications. Trends Biotechnol., 14: 478 - 483.
18- Al-Grawi, E.D.C., and G.R.L. Al-Awsi. 2018. "Expression of CDKN2A (P16/Ink4a) among Colorectal Cancer Patients: A Cohort Study." Journal of Pharmaceutical Sciences and Research 10 (5).

19- Al-Abodi, H. R. J. (2019). Molecular and expermentaldianostic study of coccidisis in hubbred chicken. *Eco. Env. & Cons. 25 (1)*, pp. (172-177).

20- Al-Abodi, H. R. J. (2018). Use of rapid cassette test and polymerase chain reaction technique to investigate toxoplasmosis in *Columba livia* birds in Al-Muthanna governorate. Proceeding of 6th International Scientific Conference, College of Veterinary Medicine, University of Basrah,Iraq, *Basrah Journal of Veterinary Research,*Vol.17, No.3: 45-50

21- Mohammad .F. I..; & Al-Khalidy , K, A, H.(2018). Detection of Leishmaniaspp .by Nested-PCR and virulence factors GIPLs, GP63 in L. major by conventional-PCR. Journal Biochemical and Cellular Archives Vol.18,No.2.

22- Bustin, S. A. (2002). Absolute quantification of mRNA using real time reverse transcriptase polymerase chain reaction assay. J. Mol. Endocrinal, 25: 169 – 193.

23- Al-Abodi H R J and Al-zayadi W A A (2017) The use of traditional methods and the most recent molecular methods to investigatethe presence of parasite Giardia lambia in infants with diarrhea and study some factors affecting its spread in Qadisiyah governorate. Al-Kufa University Journal for Biology 9(1), 365-373.

24- AL-Khalidy, K.A.H .(2016).Detection of Entamoebahistolytica in patients an infected infants with diarrhea in born and children's hospital by classic methods and Real time Polymerase Chain Reaction. Al -Qadisiyah Journal of Pure Sciences, Vol. 21, No. 2.

25- Shamran, A. R, Shaker, Z. H, Al-Awsi, G. R. L, Khamis, A .S , Tolaifeh, Z. A. and Jameel, Z. I, 2018. RAPD-PCR IS A GOOD DNA FINGERPRINTING TECHNIQUE TO DETECT PHYLOGENETIC RELATIONSHIPS AMONG STAPHYLOCOCCUS AUREUS ISOLATED FROM DIFFERENT SOURCES IN HILLA CITY, IRAQ. Biochemical and Cellular Achieves. Vol. 18, Supplement 1, pp. 1157-1161 .

26- Al-Abodi, H. R. J. (2018). EFFECT AND SPREAD OF GIARDIA PARASITE ON CHILDREN IN PRIMARY DEVELOPMENT STAGES IN SOUTHERN IRAQ. Biochem. Cell. Arch. Vol. 18, No. 2, pp. 1537-1541.

27- Al-Ammash, M. S. J.; KhaledThamerMatar Al-Shaibani, K. T. M. and Al-Abodi, H. R. J. (2018). INVESTIGATING THE PREVALENCE OF INFECTION WITH TOXOPLASMA GONDII IN MEN AND WOMEN IN SAMARRA CITY, IRAQ. Plant Archives Vol. 18 No. 2, pp. 2501-2508.

28- Ana,S. A.; Al-Khalidy.K. A H. ; Ana .S. A. (2018). Description of parasitic infections in honeybees Apissp In the Middle Euphrates region of Iraq. Indian Journal of Public Health Research & Development, Vol.9, No.3.

29- Shaker, E. M., Al-Shaibani, K. T. M. and Al-abodi, H. R. J. (2018). Effect of Alcohol extract of green tea plant Camellia sienensis as a therapeutic of parasite Entamoebahistolytica. Plant Archives Vol. 18 No. 1, pp. 953-959.

30- Al-Khalidy , K, A, H; Al-Egali, K. A. D. ; AL-Mayali, H.M .(2017). Detection of Toxoplasma gondii in the soil of the home gardens of some residential neighborhoods in AL-Diwaniyah city. Al-Kufa University Journal for Biology / VOL.9 / NO.1 .

31- AL-Khalidy, K.A.H .(2015).Identification study of Giardia lamblia which associated with drinking water in some areas in AL-Diwaniyah city by flotation methods and conventional-PCR. Al -Qadisiyah Journal of Pure Sciences, Vol. 20, No. 2.

Indian Journal of Natural Sciences www.tnsroindia.org.in ©IJONS

Vol.9 /Issue 52 / February / 2019 *International Bimonthly* *ISSN: 0976 – 0997*

RESEARCH ARTICLE

Identification of *iha* and *kpsMT* Virulence Genes in *Escherichia coli* Isolates with Urinary Tract Infection in Iraqi Patients

Rana Kadhim Mohammed and Ali Attallah Ibrahim*

Department of Biotechnology, College of Science, University of Baghdad, Baghdad, Iraq.

Received: 18 Nov 2018 Revised: 21 Dec 2018 Accepted: 25 Jan 2019

*Address for Correspondence
Ali Attallah Ibrahim
Department of Biotechnology,
College of Science,
University of Baghdad,
Baghdad, Iraq.
E-mail:aliatta52@gmail.com

ABSTRACT

The present study aimed theidentification of *iha*, and *kpsMT* virulence genes in uropathogenic *Escherichia coli* (UPEC)**,** also appearance relationship between this genes and **s**usceptibilitytodifferent antimicrobials**.** One hundred and thirty samples of mid-stream urine in sterilized containers were collected from patients with urinary tract infections (UTIs) and who attended to two hospitals are AL-Yarmouk Educational hospital, Al-Kadhimyia Educational hospital for duration from December / 2017 to April/ 2018. *Escherichia coli* (*E.coli*) isolates were identified according to the cultural, morphological characteristics, biochemical tests, and genetically identified. The results showed the dominance of *E.coli* over other causative agent since it achieved 60 isolated (54.54%) from 110 sample give positive growth after cultured. The distribution of *E.coli* isolated 42 isolates (70%) of them were isolated from female while 18 (30%) were from male. Antibiotic susceptibility testing showed the results for eight antibiotics appear the isolates were high resistant to Tetracycline (76.7%), followed by Nalidixic Acid (73.3%), Trimeth-Sulfamethox (70%).Virulence genes were distribution within the UPEC, *iha* 51 isolates (85%), and *kpsMT* 48 isolates (80%).The *E.coli* is most frequency bacterial distributed in pationts with UTIs, and there are adhesion and capsular polysaccharidesvirulence genes was high frequency.

Keywords: Urinary Tract Infection, *E.coli*, UPEC, virulence genes.

INTRODUCTION

Urinary tract infections (UTIs), is infection along urinary tract at anywhere. UTIs had various names depending on the urinary tract part is infected(Najib*et al.*, 2009). In children and adults the UPEC most frequent agent causing UTI(Anvarinejad*et al.*, 2012). Female most than male to be infacted to UTIs with about 55% of female during their

lifetime are sufferance from these infections (Foxman, 2003; Rahn, 2008). At least 45-85% of UTIs there are caused by *E.coli* followed by *Klebsiella spp*., *Proteus spp*, *Pseudomonas spp* and *Enterobacter spp*.(Rai *et al.*, 2008). While gram positive bacteria caused 15% of UTIs include *Staphylococci spp., Streptococci spp*.,and *Enterococci spp.*(Arisoy*et al.*, 2006). Dependent on the virulence factors (VFs) are appearance, the potency of pathogenic E. coli strains is presence, which are located either on chromosome or on plasmid of bacteria. The UPEC associated with virulence genes most usually include afimbrialadhesin I (*afaI*), P fimbriae (*pap*), hemolysin (*hly*), aerobactin (*aer*), cytotoxic necrotizing factor 1 (*cnf1*), S fimbriae (*sfa*), , adhesins (*iha*) and capsular polysaccharide production (*kpsMT*)(da Silva and Mendonça, 2012). There are virulence factors location on such genetic mobile elements may to be virulence properties spread facilitate within bacterial organism communities(Dromigny*et al.*, 2005). The uropathogens when and where increasing rates of antibiotics resistance, have caused growing worry in all world countries(Farshad*et al.*, 2012). Understanding molecular characterization of plasmids, antibiotic resistance patterns, and other genetic elements is beneficial in the epidemiological(Sawalha, 2009). Allow of the genetic material movement there are by Plasmids, including genes responsible for resistance of antimicrobial between bacterial species and genera(Snyder, Champness and Champness, 2007).

A numbers virulence genes of *E. coli* that have been possibility involved as substantial in allowing some UPEC isolates to establishment of UTIs, involved *iha*, and *kpsMT* virulence genes. *iha* (IrgA homolog adhesion) function as adherence factor(Bauer *et al.*, 2002; Kanamaru *et al.*, 2003), *kpsMT* (group II capsule), function as Capsular polysaccharide production(Marrs*et al.*, 2002; Kanamaru *et al.*, 2003). *iha* gene encodes the IrgA homologue adhesin (an outer membrane protein) associated with uropathogenic and enterohemorrhagic strains, which confers adherence to non-adherent bactrial strains, iha in UPEC strains occurs frequently(Johnson *et al.*, 2000; Tarr *et al.*, 2000; Johnson, O'Bryan, Delavari, *et al.*, 2001; Johnson, O'Bryan, Kuskowski, *et al.*, 2001; Johnson, Parissa Delavari, Kuskowski and Stell, 2001; Johnson, Parissa Delavari, Stell, Whittam, *et al.*, 2001; Bauer *et al.*, 2002; Kanamaru *et al.*, 2003). Originally identified of iha gene as part of a tellurite resistance correlated pathogenicity islands (PAI) from an E. coli O157:H7 isolate and is comparable to the iron-regulated gene A in V. cholerae. A HeLa cell adherent phenotype in vitro observed, when in the non-adherent *E. coli* K-12 strain the *iha* gene was expressed in this strain(Tarr*et al.*, 2000).

Bacteria produced the capsular polysaccharides are actually in various size. In *E.coli* capsules, the outer most protective cell surface layer which constitute from this, based on biosynthetic criteria and genetic there are classified into four groups. group ii capsule (encoded by *kpsMT* gene is one of three functional regions) is one of four capsular types described in *E.coli* (produced by most UPEC), which accustom of charged polysaccharidic polymers, and high molecular weight. *kpsMT* gene in group ii capsule, encode proteins required for ABC-depended export there for conserved in all group ii capsulated bacteria and(Marrs*et al.*, 2002; Kanamaru *et al.*, 2003; Whitfield, 2006).

MATERIALS AND METHODS

Urine samples collected, UPEC isolation and identification

The urine samples were collected from AL-Yarmouk Educational Hospital, and Al-Kadhimyia Educational hospital, during the period from December/ 2017 to April/ 2018. Total number were 130 samples, collected in sterile container and immediately transfer to laboratory for culturing. Samples were cultured on blood agar for isolation, there was *E.coli* identification by culturing on MacConky agar, Eosin methyl blue (EMB) agar,and by biochemical test (Indol test, Oxidase test, Catalase test, Methyl-Red, and Vogas-Broskaor tests), and at lastgenetically by *16S rRNA* gene.

Antibiotic susceptibility testing

Susceptibility testing for antibiotic is done by disk diffusion method(Kirby-Bauer method)(Atlas, Brown and Parks, 1995), by measured the inhibition zone around the antibiotic disk. There were eight antibiotics used in this study were Amikacin (AK 30µg), Amoxicillin-clavulanate (AUG 20-10µg)Ciprofloxacin (CIP 5µg), Doxycycline (DXT 30µg), NalidixicAcid (NA 30µg), Streptomycin (S 10µg), Tetracycline (T 30µg), Trimeth-Sulfamethox (TS 1.25-23.75µg)

DNA extraction, and genes detection of UPEC isolates

Extraction DNA of *E.coli* by used DNA Extraction Kit (Bioneer, Korea), depended on the steps involved in kit from company. The set of primers used in this study were for *16S rRNA* gene (identification of *E.coli*) forward primer was 5′-GGAAGAAGCTTGCTTCTTTGCTG-3′, and the reveres primer was 5′-GAGCCCGGGGATTTCACAT-3′ the amplification product was 546 base pear (bp)(Sabat*et al*., 2000), and for virulence genes of *E.coli*, for*iha* gene the forward primer was 5′-CTGGCGGAGGCTCTGAGATCA-3′, and the reveres primer was 5′-TCCTTAAGCTCCCGCGGCTGA-3′ the amplification product was 827 base pear (bp)(Johnson *et al*., 2000), for *kpsMT* gene the forward primer was 5′-CCATCGATACGATCATTGCACG-3′, and the reveres primer was 5′- ATTGCAAGGTAGTTCAGACTCA -3′the amplification product was 400 base pear (bp)(Kanamaru *et al*., 2003).

The reaction in polymerase chain reaction (PCR) (MultiGene, Labnet, USA) for monoplex were performed in a total volume of 25µl, including 12.5µl of Go Taq®Green Master mix (2X) (Promega, USA), 1µl for each primers (Alpha DNA, USA), 2µl of DNA template, 8.5µl of Nuclease free water.Were the program for the amplification gene carried out using PCR as follows: for *16S rRNA* gene, initial denaturation one cycle 8 min. at 95ºC, 35 cycle each cycle of 1 min. at 94ºC, 1.5 min at 55ºC, and 1 min. at 72ºC, followed by a final extension 10 min. at 72ºC, for *iha* gene, Initial Denaturation one cycle in 5 min. at 94ºC, 30 cycle each cycle of 45 sec. at 94ºC, 1 min. at 58ºC, and 1.5 min. at 72ºC, followed by a final extension one cycle in 10 min. at 72ºC, for *kpsMT* gene, Initial Denaturation one cycle in 5 min. at 94ºC, 30 cycle each cycle of 45 sec. at 94ºC, 45 sec. at 60ºC, and 1 min. at 72ºC, followed by a final extension one cycle in 10 min. at 72ºC.The Detected result of PCR amplification by using gel electrophoresis in agarose gel (1.5%), stained by ethidium bromide and used transilluminator ultraviolet for visualized. The result of PCR amplification product for each gene was compared with DNA ladder 100bp (Solarbio, China).

Statistical analysis

The results of these studies were statistically analysis by used IBM SPSS (Statistical Package for the Social Sciences) software program Version 23, (2015).

RESULTS

Distribution of UPEC from Sample Collection

Among 130 sample collected from urine sample after cultured and stained with gram stain there were 87 sample (66.9%) give gram negative bacteria, wile 23 sample (17.7%) give gram positive bacteria, and 20 sample (15.4%) without growth.A total results of gram negative bacteria 87 sample there were isolated of *E.coli* was 60 isolate (69%) depended on culture characters, biochemical tests result (Indole, Catalase, and Methyl-Red tests was positive, Oxidase, and Vogas-Broskaor tests was negative), and genetically.The distribution of *E.coli* isolated depending on the gender were 42 isolate (70%) from female, and 18 isolate (30%) from male. The distribution of *E.coli* isolated depending on the age (range of age was 1-80 years distribution into four group) were 19 isolates (31.7%) in 1-20 years, 19 isolates (31.7%) in 21-40 years, 15 isolates (25%) in 41-60 years, and 7 isolates (11.6%) in 61-80 years.

Antimicrobial susceptibility testing

The isolated were tested to eight antibiotic, the results of antibiotic susceptibility testingfor the UPEC isolates shown in table (1). UPEC isolates exhibited the highest level of resistance to Tetracycline 46 isolates (76.7%), followed byNalidixic Acid44 isolates (73.3%), Trimeth-Sulfamethox42 isolates (70%), Ciprofloxacin41 isolates (68.3%), and Amoxicillin-clavulanate37 isolates (61.7%). UPEC multi-drug resistant were distribution in patientsat 7 isolates (11.7%), 15 isolates (25%), 7 isolates (11.7%), 13 isolates (21.7%), 6 isolates (10%), 1 isolates (1.7%) for three, four, five, six, seven, and eight antibiotics resistant respectively,

Molecular Assay, Identification of *E.coli* and Distribution of Virulence Genes

Genetically identification of *E.coli* by *16s rRNA*gene on agarose gel shown in figure (1). The virulence genes were distribution within the UPEC isolated from patientsfor *iha* gene 51 isolates (85%), and *kpsMT* gene 48 isolates (80%), and cross-tabulationbetween them show in table(2).In general, the result for *iha*gene, and *kpsMT*gene on agarose gel show in figure (2), and in figure (3) respectively.The cross-tabulation between virulence genes and results of antibiotic susceptibility in UPEC isolated from patients shown in table (3). While the cross-tabulation between virulence genes in UPEC isolated with age, and gender of patients show in table (4), and table (5) respectively.

DISCUSSION

In this study the results show the *E.coli* was the most important causing UTI, due to the *E.coli* have many factors facilitatethe infection like virulence factor, resisting to antibiotic, etc.... The prevalence was high in female than in male due relationship with wide and short urethra, and host factors (normal vaginal flora) that potential explanation higher risk of female for UTI(Jadhav*et al*., 2011; Vollmerhausen *et al*., 2011). Were with age of patients show the prevalence of UTI in primary ages of patients and then followed in middle ages and decreased with age. The results finding for antibiotic resistance distribution in UPEC important investigation. *E.coli* isolated of these study had high resisting to Tetracycline (76.7%), followed by Nalidixic Acid (73.3%), Trimeth-Sulfamethox (70%), Ciprofloxacin (68.3%), and Amoxicillin – clavulanate (61.7%).The explanations there were resistance to Antimicrobial Class Tetracyclines, Fluoroquinolones, Folate pathway inhibitors, and β -Lactamase Inhibitor Combinations. UPEC in thus study showed multi-drug resistant were distribution in isolates from patients. The potential explanation there were rare of medical and laboratory consultation to take antibiotics. Also The transfer of determinants antibiotics resistance by mobile genetic elements (transposons, gene cassettes, and plasmids) potential important factors that can contribute to the increase in the propagation of bacteria resistance to antibiotics(Hall and Collis, 1998).

iha gene 51 isolates (85%) there encoding adhesion virulence factor were most commonly occurring in UPEC, the adhesion factor response for invasion, replication, and colonization within UPEC. *kpsMT* gene 48 isolates (80%) there encoding group II capsule virulence factor were also distribution but less than *iha* gene, were *kpsMT* gene response for Capsular polysaccharide production. High distribution of virulence factors in the UPEC isolates there was potential there were isolates high pathogenic.In Japan, a prevalence rate of *iha*: 38.7%, and *kpsMT* 90.2% was reported by (Kanamaru *et al*., 2003), in Uruguay, a prevalence rate of *iha*: 54%, and *kpsMT* 59%was reported by (Poey *et al*., 2012), in USA, a prevalence rate of *iha*: 42%, and *kpsMT* 71%was reported by (Marschall *et al*., 2012),in Iran, a prevalence rate of *iha*: 62.1%, and *kpsMT*9%was reported by(Mashayekhi *et al*., 2014), in Mexico, a prevalence rate of *iha*: 64.9%, and *kpsMT*92.2% was reported by (Paniagua-Contreras *et al*., 2017).The result in the table (3) showing the relationship between virulence genes and the antibiotic susceptibility test, both genes show that their appearance in the bacteria was close when compared with antibiotic susceptibility test results. There were *iha*, and *kpsMT* genes present mostly high in *E.coli* sensitive to Amikacin, Streptomycin, and Doxycycline antibiotics, and present mostly high in *E.coli* resistant to Ciprofloxacin, NalidixicAcid, Tetracycline, Trimeth-Sulfamethox, and Amoxicillin-

clavulanic Acid antibiotics. *Iha*, and *kpsMT* genes present in female most than in male there are show in table (4). Also *Iha*, and *kpsMT* genes present in 1-20years and in 21-40 years more than other ages of patients are show in table (5).

CONCLUSION

The *E.coli* is most frequency bacterial distributed in pationts with UTIs, also *E.coli* was most resisting to Tetracycline, followed by Nalidixic Acid, and Trimeth-Sulfamethox antibiotics. There were *iha*, and *kpsMT* virulence genes was high distribution, were *iha*gene, more frequency distribution than *kpsMT* gene.

ACKNOWLEDGMENTS

For very kindly for the accomplishment of this work, we are grateful to Head of the Biotechnology Department and College of Science in Baghdad University, and for AL-Yarmouk Educational Hospital, and Al-Kadhimyia Educational hospital.

REFERENCES

1. Anvarinejad, M. *et al.* (2012) 'Genotypic analysis of E. coli strains isolated from patients with cystitis and pyelonephritis', *Iranian Red Crescent Medical Journal*. Kowsar Medical Institute, 14(7), p. 408.
2. Arisoy, M. *et al.* (2006) 'Detection of virulence factors of Escherichia coli from children by multiplex polymerase chain reaction', *International journal of clinical practice*. Wiley Online Library, 60(2), pp. 170–173.
3. Atlas, R. M., Brown, A. E. and Parks, L. C. (1995) *Laboratory manual of experimental microbiology*. Mosby.
4. Bauer, R. J. *et al.* (2002) 'Molecular epidemiology of 3 putative virulence genes for Escherichia coli urinary tract infection–usp, iha, and iroNE. coli', *Journal of Infectious Diseases*. The University of Chicago Press, 185(10), pp. 1521–1524.
5. Dromigny, J. A. *et al.* (2005) 'Risk factors for antibiotic-resistant Escherichia coli isolated from community-acquired urinary tract infections in Dakar, Senegal', *Journal of Antimicrobial Chemotherapy*. Oxford University Press, 56(1), pp. 236–239.
6. Farshad, S. *et al.* (2012) 'Microbial susceptibility, virulence factors, and plasmid profiles of uropathogenic Escherichia coli strains isolated from children in Jahrom, Iran.', *Archives of Iranian Medicine (AIM)*, 15(5).
7. Foxman, B. (2003) 'Epidemiology of urinary tract infections: incidence, morbidity, and economic costs', *Disease-a-month*. Elsevier, 49(2), pp. 53–70.
8. Hall, R. M. and Collis, C. M. (1998) 'Antibiotic resistance in gram-negative bacteria: the role of gene cassettes and integrons', *Drug resistance UPDATES*. Elsevier, 1(2), pp. 109–119.
9. Jadhav, S. *et al.* (2011) 'Virulence characteristics and genetic affinities of multiple drug resistant uropathogenic Escherichia coli from a semi urban locality in India', *PloS one*. Public Library of Science, 6(3), p. e18063.
10. Johnson, J. R. *et al.* (2000) 'Molecular epidemiological and phylogenetic associations of two novel putative virulence genes, iha and iroNE. coli, among Escherichia coli isolates from patients with urosepsis', *Infection and immunity*. Am Soc Microbiol, 68(5), pp. 3040–3047.
11. Johnson, J. R., O'Bryan, T. T., Delavari, P., *et al.* (2001) 'Clonal relationships and extended virulence genotypes among Escherichia coli isolates from women with a first or recurrent episode of cystitis', *The Journal of infectious diseases*. The University of Chicago Press, 183(10), pp. 1508–1517.
12. Johnson, J. R., Delavari, P., Stell, A. L., Whittam, T. S., *et al.* (2001) 'Molecular comparison of extraintestinal Escherichia coli isolates of the same electrophoretic lineages from humans and domestic animals', *The Journal of infectious diseases*. The University of Chicago Press, 183(1), pp. 154–159.
13. Johnson, J. R., O'Bryan, T. T., Kuskowski, M., *et al.* (2001) 'Ongoing horizontal and vertical transmission of virulence genes and papA alleles among Escherichia coliblood isolates from patients with diverse-source bacteremia', *Infection and immunity*. Am Soc Microbiol, 69(9), pp. 5363–5374.

14. Johnson, J. R., Delavari, P., Kuskowski, M. and Stell, A. L. (2001) 'Phylogenetic distribution of extraintestinal virulence-associated traits in Escherichia coli', *The Journal of infectious diseases*. The University of Chicago Press, 183(1), pp. 78–88.
15. Kanamaru, S. *et al.* (2003) 'Distribution and genetic association of putative uropathogenic virulence factors iroN, iha, kpsMT, ompT and usp in Escherichia coli isolated from urinary tract infections in Japan', *The Journal of urology*. Elsevier, 170(6), pp. 2490–2493.
16. Marrs, C. F. *et al.* (2002) 'Variations in 10 putative uropathogen virulence genes among urinary, faecal and peri-urethral Escherichia coli', *Journal of medical microbiology*. Microbiology Society, 51(2), pp. 138–142.
17. Marschall, J. *et al.* (2012) 'Both host and pathogen factors predispose to Escherichia coli urinary-source bacteremia in hospitalized patients', *Clinical infectious diseases*. Oxford University Press, 54(12), pp. 1692–1698.
18. Mashayekhi, F. *et al.* (2014) 'Molecular characterization and antimicrobial resistance of uropathogenic Escherichia coli', *Iranian Journal of Biotechnology*. National Institute of Genetic Engineering and Biotechnology, 12(2), pp. 32–40.
19. Najib, K. H. *et al.* (2009) 'Renal scar formation in children with recurrent urinary tract infections', *Iran Red Crescent Med J*, 11, pp. 93–95.
20. Paniagua-Contreras, G. L. *et al.* (2017) 'Virulence factors, antibiotic resistance phenotypes and O-serogroups of Escherichia coli strains isolated from community-acquired urinary tract infection patients in Mexico', *Journal of Microbiology, Immunology and Infection*. Elsevier, 50(4), pp. 478–485.
21. Poey, M. E. *et al.* (2012) 'Virulence profiles in uropathogenic Escherichia coli isolated from pregnant women and children with urinary tract abnormalities', *Microbial pathogenesis*. Elsevier, 52(5), pp. 292–301.
22. Rahn, D. D. (2008) 'Urinary tract infections: contemporary management', *Urologic nursing*. Anthony J. Jannetti, Inc., 28(5), p. 333.
23. Rai, G. K. *et al.* (2008) 'Causative agents of urinary tract infections in children and their antibiotic sensitivity pattern: a hospital based study', *Nepal Med Coll J*, 10(2), pp. 86–90.
24. Sabat, G. *et al.* (2000) 'Selective and sensitive method for PCR amplification of Escherichia coli 16S rRNA genes in soil', *Applied and environmental microbiology*. Am Soc Microbiol, 66(2), pp. 844–849.
25. Sawalha, R. M. H. (2009) 'Prevalence of urinary tract infection among children of primary schools in Nablus'.
26. da Silva, G. J. and Mendonça, N. (2012) 'Association between antimicrobial resistance and virulence in Escherichia coli', *Virulence*. Taylor & Francis, 3(1), pp. 18–28.
27. Snyder, L., Champness, W. and Champness, W. (2007) *Molecular genetics of bacteria*. Asm Press Washington, DC.
28. Tarr, P. I. *et al.* (2000) 'Iha: a novel Escherichia coli O157: H7 adherence-conferring molecule encoded on a recently acquired chromosomal island of conserved structure', *Infection and immunity*. Am Soc Microbiol, 68(3), pp. 1400–1407.
29. Vollmerhausen, T. L. *et al.* (2011) 'Population structure and uropathogenic virulence-associated genes of faecal Escherichia coli from healthy young and elderly adults', *Journal of medical microbiology*. Microbiology Society, 60(5), pp. 574–581.
30. Whitfield, C. (2006) 'Biosynthesis and assembly of capsular polysaccharides in Escherichia coli', *Annu. Rev. Biochem.* Annual Reviews, 75, pp. 39–68.

Table 1. Antibiotic susceptibility testing for the UPEC isolates.

Antibiotic	Resistant No. (%)	Sensitive No. (%)	Intermediate No. (%)
Amikacin (AK)	9 (15%)	38 (63.3%)	13 (21.7%)
Amoxicillin-clavulanate(AUG)	37 (61.7%)	14 (23.3%)	9 (15%)
Ciprofloxacin (CIP)	41 (68.3%)	4 (6.7%)	15 (25%)
Doxycycline (DXT)	18 (30%)	25 (41.7%)	17 (28.3%)
NalidixicAcid (NA)	44 (73.3%)	14 (23.4%)	2 (3.3%)
Streptomycin (S)	19 (31.7%)	29 (48.3%)	12 (20%)
Tetracycline (T)	46 (76.7%)	14 (23.3%)	0 (0%)
Trimeth-Sulfamethox (TS)	42 (70%)	18 (30%)	0 (0%)

Table 2. Cross tabulation for *iha* gene with *kpsMT* gene.

		kpsMT gene		Total (%)
		Absent (%)	Present (%)	
iha gene	Absent (%)	3 (5%)	6 (10%)	9 (15%)
	Present (%)	9 (15%)	42 (70%)	51 (85%)
Total (%)		12 (20%)	48 (80%)	60 (100%)

Table 3. The cross-tabulation between virulence genes and results of antibiotic susceptibility.

Antibiotic		*iha* -gene		*kpsMT* -gene	
		Present No. (%)	Absent No. (%)	Present No. (%)	Absent No.(%)
Amikacin	R*	9 (15%)	0 (0%)	9 (15%)	0 (0%)
	S*	31 (51.7%)	7 (11.7%)	29 (48.3%)	9 (15%)
	I*	11 (18.3%)	2 (3.3%)	10 (16.7%)	3 (5%)
Amoxicillin-clavulanic Acid	R*	33 (55%)	4 (6.7%)	31 (51.7%)	6 (10%)
	S*	13 (21.7%)	1 (1.7%)	10 (16.7%)	4 (6.7%)
	I*	5 (8.3%)	4 (6.7%)	7 (11.7%)	2 (3.3%)
Ciprofloxacin	R*	35 (58.3%)	6 (10%)	34 (56.7%)	7 (11.7%)
	S*	4 (6.7%)	0 (0%)	2 (3.3%)	2 (3.3%)
	I*	12 (20%)	3 (5%)	12 (20%)	3 (5%)
Doxycycline	R*	14 (23.3%)	4 (6.7%)	13 (21.7%)	5 (8.3%)
	S*	22 (36.7%)	3 (5%)	20 (33.3%)	5 (8.3%)
	I*	15 (25%)	2 (3.3%)	15 (25%)	2 (3.3%)
NalidixicAcid	R*	38 (63.3%)	6 (10%)	37 (61.7%)	7 (11.7%)
	S*	12 (20%)	2 (3.3%)	9 (15%)	5 (8.3%)
	I*	1 (1.7%)	1 (1.7%)	2 (3.3%)	0 (0%)
Streptomycin	R*	17 (28.3%)	2 (3.3%)	15 (25%)	4 (6.7%)
	S*	25 (41.7%)	4 (6.7%)	23 (38.3%)	6 (10%)
	I*	9 (15%)	3 (5%)	10 (16.7%)	2 (3.3%)
Tetracycline	R*	39 (65%)	7 (11.7%)	36 (60%)	10 (16.7%)
	S*	12 (20%)	2 (3.3%)	12 (20%)	2 (3.3%)
	I*	0 (0%)	0 (0%)	0 (0%)	0 (0%)
Trimeth-Sulfamethox	R*	37 (61.7%)	5 (8.3%)	34 (56.7%)	8 (13.3%)
	S*	14 (23.3%)	4 (6.7%)	14 (23.3%)	4 (6.7%)
	I*	0 (0%)	0 (0%)	0 (0%)	0 (0%)

* R: resistant, S: sensitive, I: intermediate.

Table 4. Cross-tabulation between virulence genes in UPEC isolated with gender.

		kpsMT gene		Total No.(%)	*iha* gene		Total No. (%)
		PresentNo.(%)	Absent No. (%)		Present No.(%)	Absent No.(%)	
Gender	Female	34 (56.7%)	8 (13.3%)	42 (70%)	36 (60%)	6 (10%)	42 (70%)
	Male	14 (23.3%)	4 (6.7%)	18 (30%)	15 (25%)	3 (5%)	18 (30%)
Total No. (%)		48 (80%)	12 (20%)	60(100%)	51 (85%)	9 (15%)	60 (100%)

Table 5. Cross-tabulation between virulence genes in UPEC isolated with age.

		kpsMT gene		Total No. (%)	*iha* gene		Total No. (%)
		Present No. (%)	Absent No. (%)		Present No.(%)	Absent No. (%)	
Age	1-20 years	16 (26.7%)	3 (5%)	19 (31.7%)	17 (28.3%)	2 (3.3%)	19 (31.7%)
	21-40 years	15 (25%)	4 (6.7%)	19 (31.7%)	14 (23.3%)	5 (8.4%)	19 (31.7%)
	41-60 years	12 (20%)	3 (5%)	15 (25%)	13 (21.7%)	2 (3.3%)	15 (25%)
	61-80 years	5 (8.3%)	2 (3.3%)	7 (11.6%)	7 (11.7%)	0 (0%)	7 (11.6%)
Total No. (%)		48 (80%)	12 (20%)	60 (100%)	51 (85%)	9 (15%)	60 (100%)

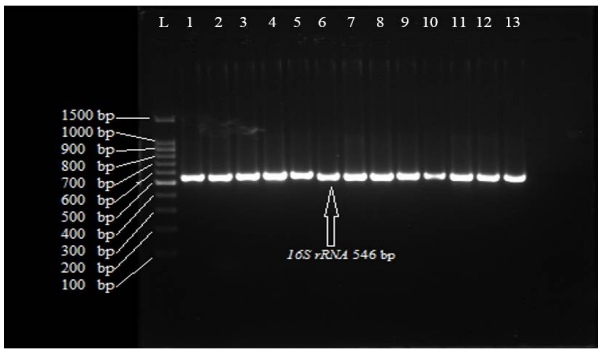

Figure 1. PCR detection for *E.coli* by *16s rRNA* identification gene*L: DNA ladder, 1-13: the No. of *E.coli* isolates from 1 to 13isolates.

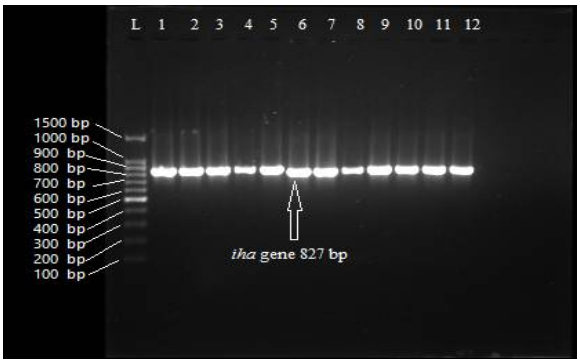

Figure 2. The amplification product of PCR results for *iha* gene (827 bp). *L: DNA ladder, 1-13: the No. of *E.coli* isolates from 26 to 37isolates

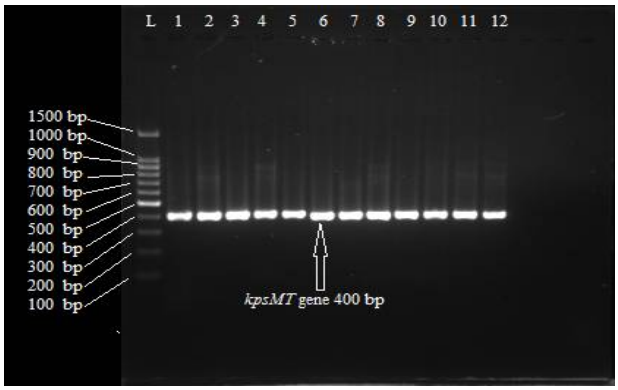

Figure 3. The amplification product of PCR results for *kpsMT*gene(400 bp).
*L: DNA ladder, 1-13: the No. of *E.coli* isolates from 1 to 12isolates

Indian Journal of Natural Sciences www.tnsroindia.org.in ©IJONS

Vol.9 /Issue 52 / February / 2019 *International Bimonthly* *ISSN: 0976 – 0997*

RESEARCH ARTICLE

Hardness and Impact Strength of Functionally Graded Nanocomposites

Ali A. Abbas* and Zainab R. Muslim

Physics Department, College of Science, University of Baghdad, Iraq.

Received: 22 Nov 2018 Revised: 24 Dec 2018 Accepted: 26 Jan 2019

***Address for Correspondence**
Ali A. Abbas
Physics Department,
College of Science,
University of Baghdad, Iraq.
E-mail: aliadilabbas@yahoo.com

ABSTRACT

Functionally graded polymer nanocomposites were prepared by hand lay–up technique by addition graphene and carbon nanotubes with different weight fraction (1and 3)wt.% to epoxy resin. Hardness and impact strength of functionally graded polymer nanocomposite for each weight fraction were determined and tested for pure and composites side.The results show that hardness and impact strength loaded from composite side higher than when samples loaded from pure epoxy side and generally higher was observed for carbon nanotubes composites than graphene composites.

Keywords: technique, nanocomposites, weight, polymer, graded, carbon.

INTRODUCTION

The demand for advanced materials with improved properties to meet new requirements, or to replace existing materials, has been steadily increasing. Among advanced materials, polymer composites possess superior strength, stiffness, toughness, hardness, and heat distortion temperature compared with the material properties of metals [1]. Currently, polymer composites are being investigated for use in a wide range of applications, including products and components in the biotech, automotive, and aerospace industries.For a long time that nanoparticles are used as fillers in polymer composite to improve the mechanical and physical properties of the polymer.The epoxy resins are used ina variety of engineering applications since their properties, such as thermal stability, good mechanical response, low density and electrical insulator, can be varied considerably[2].

Functionally graded material (FGM)belong to a class of composite materials thathave been prepared by using special technique developed to attain properties that cannot be achieved by monolithic materials[3].FGMcan be characterized by the variation in composition and structure gradually over volume.Results are corresponding changes in the properties of the material like hardness, elasticity module, wear resistance or biocompatibility. The

concept of FGM was first proposed in 80's to develop heat-resistant materials for the propulsion system and air frame of space planes. Some fields of activities–like aeronautical or biomedical industry are concerned by FGM developments [4]. Krumovaetal., studied hardness of functionally graded polymer composites based on an epoxy resin matrix and SiC filler particles were prepared by controlling the preparation conditions during centrifugation, a high gradient in the particle distribution (from 0 to 45 vol.%) could be achieved. The results presented in this study demonstrate that with an epoxy matrix and SiC particles special materials with a gradient in the mechanical properties can be prepared. For example, al high particle volume content, reached by centrifugation, leads to very high hardness values at one end of the samples. The aimed continuous variation of the hardness over the length of the samples was also achieved [5]. Nardiet al.,in this study the nanoindentation tests were carried out on the surface of polymer nanocomposites exhibiting either graded or homogeneous distributions of Fe3O4@ silica core-shell nanoparticles in a photocurable polymeric matrix. The results reveal a complex interplay between graded morphology, indentation depth, and calculated modulus and hardness values, which was elucidated through numerical simulations where noticed that modulus and hardness of graded polymer nanocomposites were found to depend on enhanced concentrations of particles near the surface and on the indentation depth.For small Indentations, large increases in modulus and hardness to very high values were obtained for graded composites with an average 8%vol of NPs, compared with their homogeneous[6].

Bafekrpour et al., studied thermo mechanical and viscoelastic properties of functionally graded nanocomposites with phenolic matrix and synthetic graphite (SG) as nanofillers were fabricated using a combined powder stacking and compression molding techniques. Ball milling was used to homogeneously distribute nanofillers within the phenolic matrix. The results show that this properties were highly affected by the distribution patterns of SG within the matrix[7].

MATERIALS AND METHODS

Materials Used

1- Epoxyand hardener type (HT 2000were provided by Renksan Group, turkey) were in the ratioof 3:1 for curing as a matrix.
2- The materials used as filler like Multi-wall carbon nanotubes (CNTs) (Cheap Tubes Inc., USA) purity 90% with particle size < 10 nm, graphene (GR) (sky spring nanomaterials, Inc., USA)) purity 99% with particle size 40-60 nm.

Preparation of Nanocomposites

The mixing process consisted of three steps. Firstly, graphene and carbon nanotubes were stirrer mixed with the epoxy resin, with different weight ratios (1and 3) wt. %, the mixing was done at 40 ^{o}C with a magnetic stirrer for 45 min to have good distribution and the mixture left to cool then hardener was added to the mixture then the sample were kept in container under vacuum to remove the bubbles before cast the composites.

Preparation of Graded Nanocomposites

Hand lay–up technique was used to prepare graded nanocomposites, subsequently the first layer which was poured into mould. Then succeeding layers with different content were poured into the mould. Before pouring succeeding layers,the gelation time were one hours were made to allow pre-curing of previous layer.The list of samples prepared with different composition are shown in Tables (1)and (2) .

Hardness Test

Shore durometer hardness test apparatus (digital, Italy, typeTH210) was used to measure the hardness values of the samples under study. This test was carried out by fixing penetration tool of the Shore D apparatus on surface of samples, the number value of hardness exhibits on the electronic screen of the instrument, the test carried out on composites side and pure side.

Impact test

The test was done by un-notched Charpy impact test machine manufactured bythe Testing Machines (Amityville, NY) was used for the sakeof performing impact test on the prepared samples. This instrument consists mainly of pendulum and energy gauge. Charpy impact test consists of standard test piece that would be broken with one flow of a swinging hammer. The test piece is supported at both ends in a way that the hammer strikes it at the middle. The testing method of this instrument includes lifting of the pendulum to its maximum height and fixing it firmly. Thesample is fixed in its pertaining place, and then the energy gauge is initialized (on zero position), after that the pendulum is freed whereas its potential energy would be changed to kinetic energy. Some of this kinetic energy is utilized to fracture the sample, while the energy gauge reads the value of fracture energy for the sample under test.Impact strength (I.S) is calculated by applying the following relation [8]:

I.S=U/A (J/m^2) ……..(1)

Where

U= Energy of fracture in(Joule)

A=cross section area in (m^2).

RESULTS AND DISCUSSION

HardnessTest Results

Although hardness is one of the properties most widely used to distinguish between various kinds of materials, there is no single, universally applicable measure or definition of it. There is however a number of characteristics associated with hardness, these include resistance to indentation resistance to scratching, resistance to wear, and abrasion [9]. From the figure (3) ,it can be observed that the incorporation of nanoparticles into epoxy matrix results in improvement in hardness of nanocomposites. Mechanical properties of nanocomposites generally depend on factors such as particle shape, filler type, size, content ratio, and adhesion between matrix and fillers and the dispersion of fillers within the matrix. The reason for improvement in the hardness isthe inclusion of surface treated hard nanoparticles and uniform dispersion in theepoxy matrix. that nanoparticles have significantly large specific surface area, which greatly facilitates the transfer of load from polymer matrix to nanoparticles. As a result, hard nanoparticles in the epoxy effectively restrict indentation and increase the hardness of the nanocomposites[10,11].The highest value was record for [CNT1%,3%]3 (84.76).

From figure (4 and 5), It is noticed that hardness of functionally graded nanocomposites of all samples from composites side was higher than pure side to face that hardness is resistance of the surface to indentation therefore hardness from composites exhibit high values where observed from non graded nanocomposites, fig. (3), where fillers being hard and brittle compared with the matrix material, the added filler particles increases the hardness of the composite because of increasing the wettability or the bonding between the matrix and the filler particles.

ImpactTest Results

Impact test determines the amount of energy absorbed by a material during fracture. it is different from other mechanical tests because it is very fast, where the sample is subjected to the rapid stress leading to change in the behavior of material[12]. In general, it is noticed that the impact strength was highest at 3% wt. in all types,fig. (6). In fact, there is almost a constant rate of increase in impact energy with the increasing of fillers content. This is justified by the reports that the physicochemical inter action between the particle and the matrix plays asignificant role in the obtained composites. Moreover, the strong chemical bonding improves the mechanical properties of the composites such high increase in values could be due to generation of more interfacial surface due to nanoparticles with high modulus lead to absorb higher mechanical stresses,where nanoparticles acts a strong stress concentrators which resist crack propagation where increaseof crack deflections (creating more than one crack propagation direction) which means crack propagation resistance and increase of chains supporting resulting from nanoparticles existence[13,14].

The carbon nanotubes composites exhibit higher impact strength than the composites containing grapheme particles, due to the multi-walled nanotube absorbed more energy and it is dissipated within the area of nanotubes and take more timeto penetrate inside the sample. But, in the case of graphene, impactenergy spread easily all over the sample because graphene dispersed in the plate form. Thereduced in absorbed energy may be caused by stress concentration in the vicinity of the graphene; this typically occurs when hard filler sare incorporated intoa brittle matrix. However, the impact strength is generally better for carbon nanotubes composites than for graphene composites[15]. From fig. (7 and 8) Impact strength of the functionally graded nanocomposites are higher when loaded from the composites side for all types because in pure epoxy onthe opposite side,the impact load leads to agreater elongation to break, while the composites loading side improves the resistance to impact. These two phenomena may be responsible for the higher impact strengths for this samples [16]. The highest value was record for [CNT1%,3%]3(19.50 kJ/m$^{2)}$.

CONCLUSIONS

Hardness and impact strength of non- graded nanocomposites increase with increase weight fraction of nanoparticles. In functionally graded nanocomposites impact strength increase with number of layers of composites and with increase weight fraction, hardness increase with increase weight fraction. carbon nanotubes composites exhibit higher mechanical properties than graphene composites for graded and non graded types.

REFERENCES

1. S. Lee, S. Cho and Y. Lee"Mechanical and thermal properties of MWCNT-reinforced epoxy nanocomposites by vacuum assisted resin transfer molding", Carbon Letters,15(1), 32-37 (2014).
2. M. Park, S. Lee and Y.Lee"Mechanical properties of epoxy composites reinforced withammonia-treated graphene oxides",Carbon Letters ,21, 1-7 (2017).
3. N.Misra, G. Kapusetti, D. K. Pattanayak and A. Kumar"Fabrication and characterization of epoxy/silicafunctionally graded composite material", indian J. Phys., 85(9),1393-1404(2011).
4. P. J. Bartoloet al."Innovative Developments in Virtual and Physical Prototyping",CRC Press,2011.
5. M. Krumova, C. Klingshirn, F. Haupertand K. Friedrich"Microhardness studies on functionally graded polymer composites", Composites Science and Technology, 61, 557-563(2001) .
6. T. Nardi, C.Hammerquist, J. A. Nairn, A. Karimi, J. E. Månson and Y.Leterrier,"Nanoindentation of functionally graded polymer nanocomposites: assessment of the strengthening parameters through experiments and modeling ", Frontiers in Materials,2,2015.

7. X. Wan"Nanocomposites: Synthesis, Characterization and Applications",Nova Science Publishers, 311-327(2013).
8. V. K. Thakur ," Green Composites from Natural Resources", CRC Press, 2014.
9. J. P. Mittal, I. Kaur and R. C.Sharma "Industrial Engineering and Materials",Mittal Publications,1992.
10. I. Ozsoy , A. Demirko, A. Mimaroglu, H. Unal ,Zafer Demir,"The Influence of Micro- and Nano-Filler Contenton the Mechanical Properties of Epoxy Composites"Journal of Mechanical Engineering 61(10),601-609(2015).
11. M.G.Veena ,"Effect of the type and content of filler on electrical,mechanical and thermal properties of epoxynanocomposites for electrical insulation", Ph.D. thesis, University of Mysore,2012.
12. M. L. Gambhir and N. Jamwal,"Building and Construction Materials: Testing and Quality Control" McGraw-Hill Education (india) private limited,2014.
13. N.A.Ali , S. I. Hussein , M. K. Jawad and I. A. AL-Ajaj,"Effect of Al_2O_3 and SiO_2Nanoparticle on Wear, Hardness and Impact behavior of Epoxy composites",Chemistry and Materials Research ,7(4),34-39(2015).
14. Z. Guo,T. Pereira, O. Choi, Y. Wang and H. T. Hahn,"Surface functionalized alumina nanoparticle filled polymericnanocomposites with enhanced mechanical properties",Journal of Materials Chemistry,16, 2800-2808(2006).
15. S. Singh,V. K. Srivastava and R. Prakash"Influences of carbon nanofillers on mechanical performanceof epoxy resin polymer", Appl Nanosci,2014.
16. P. Tsotra and K. Friedrich " Electrical and mechanical properties of functionally graded epoxy-resin/carbon fibre composites," Composites Part A Applied Science and Manufacturing, 34(1),75-82(2003) .

Table 1. non-graded composites.

Sample No.	Sample ID	Composition
1	Ep	Epoxy
2	[CNT1%]1	Epoxy+1%wt. CNTs
3	[CNT3%]1	Epoxy+3%wt. CNTs
4	[GR1%]1	Epoxy + 1% wt. GR
5	[GR3%]1	Epoxy + 3% wt. GR

Table 2. functionally graded nanocomposites.

SampleNo.	Samples ID	Composition		
		1st layer	2nd layer	3rd layer
1	[CNT1%]2	Epoxy	Epoxy+1%wt. CNTs	/
2	[CNT3%]2	Epoxy	Epoxy+3%wt. CNTs	/
3	[CNT1%,3%]3	Epoxy	Epoxy+1%wt. CNTs	Epoxy+3%wt. CNTs
4	[GR1%]2	Epoxy	Epoxy + 1% wt. GR	/
5	[GR3%]2	Epoxy	Epoxy + 3% wt. GR	/
6	[GR1%,3%]3	Epoxy	Epoxy + 1% wt. GR	Epoxy + 3%wt. GR

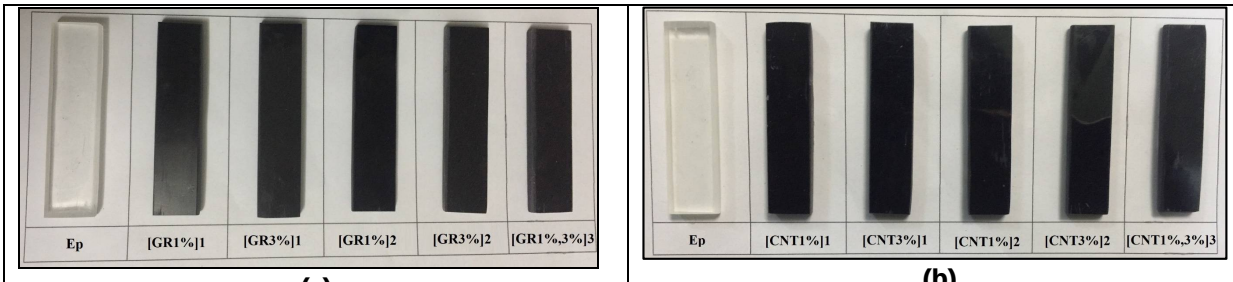

(a) **(b)**

Fig.1. (a)(b) hardness and impact of functionally graded and non-graded graphene and carbon nanotubes composites samples

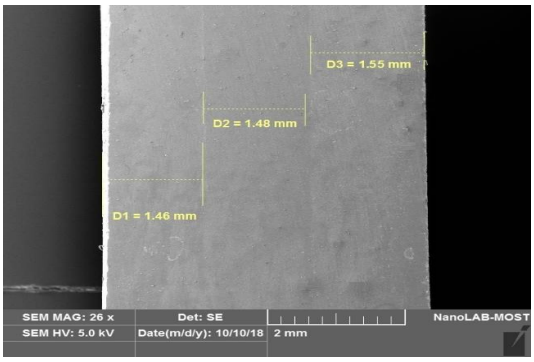

Fig.2. SEM photo to cross section of functionally graded nanocomposite sample to show the layers

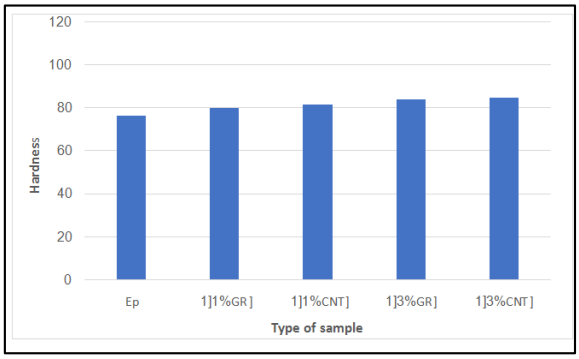

Fig..3 Hardness of non-graded grapheneand carbon nanotubes nanocomposites.

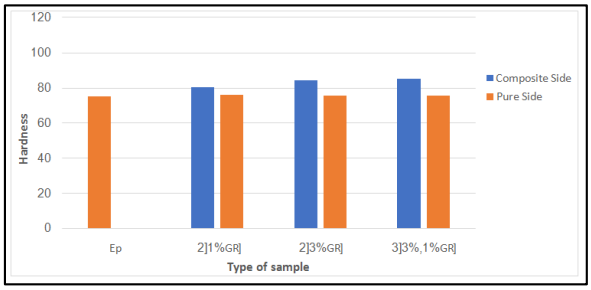

Fig.4.Hardness of functionally graded graphene nanocomposites.

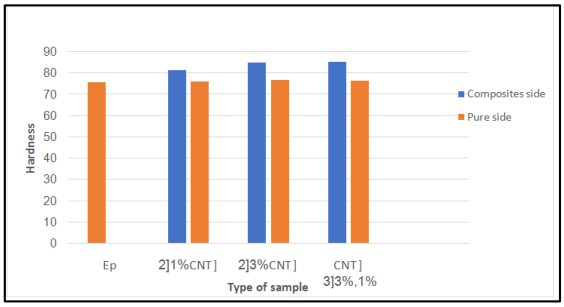

Fig.5. Hardness of functionally graded carbon nanotubes nanocomposites.

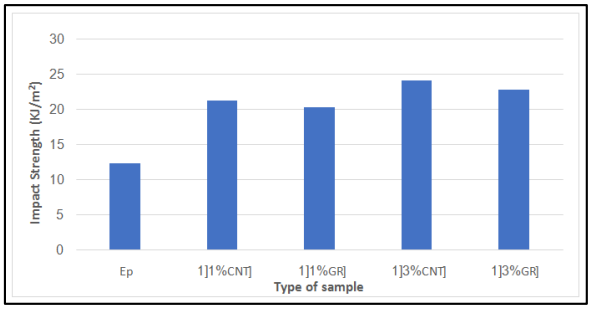

Fig.6. Impact strength of non-graded graphene, carbon nanotubes nanocomposites.

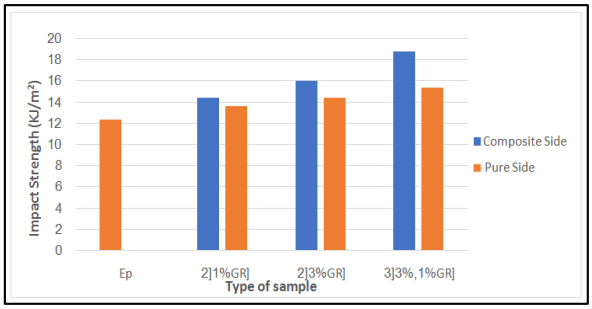

Fig.7.Impact strength of functionally graded graphene nanocomposites.

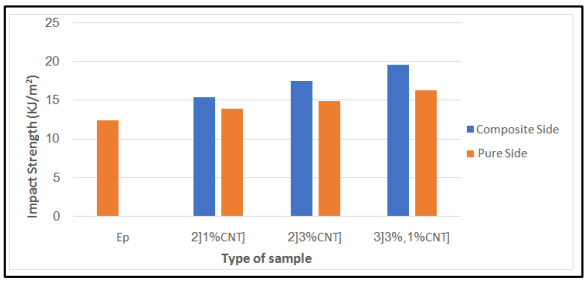

Fig. 8.Impact strength of functionally graded carbon nanotubes nanocomposites

Indian Journal of Natural Sciences www.tnsroindia.org.in ©IJONS

Vol.9 /Issue 52 / February / 2019 *International Bimonthly* *ISSN: 0976 – 0997*

RESEARCH ARTICLE

Efficiency Boosting by using Dissimilar Cations Mixture in Polymer Electrolyte

Mustafa Kadhum Abid[1]*, Mohammed Kadhim Jawad[1] and Mustafa Sami Al-Salmani[2]

[1]Department of Physics, College of Science, University of Baghdad, Baghdad, Iraq.
[2]Department of Molecular and Medical Biotechnology, College of Biotechnology, Al-Nahrain University, Baghdad ,Iraq.

Received: 18 Sep 2018 Revised: 20 Oct 2018 Accepted: 22 Nov 2018

***Address for Correspondence**
Mustafa Kadhum Abid
Department of Physics,
College of Science, University of Baghdad, Baghdad, Iraq.
E-mail: tophy_007@yahoo.com

ABSTRACT

The conduction of iodide ions in quasi-solid-state polymer electrolytes containing such electrolytes can be enhanced by incorporating iodides having appropriate cations. Gel electrolytes have been synthesized using solution cast technique based on Polyacrylonitrile (PAN) and Poly (methyl methacrylate) (PMMA) and a mixture of salts potassium iodide (KI) and sodium iodide (NaI), in addition to incorporating ethylene carbonate (EC) and propylene carbonate (PC) as plasticizers. The salt composition in the double mixture was varied in order to optimize good ionic conductivity. We report the effect of mixed iodide salt system with two dissimilar cations to enhance the conductivity of gel polymer electrolytes (GPEs). All the electrolytes based on double salts have shown conductivity enhancement compared to their single cation counterparts. The ionic conductivity of electrolytes with relatively large cations, K^+ and Na^+, was higher and essentially constant. The highest ionic conductivity forsample D8 with single iodide (KI) was (3.11×10^{-3}S.cm^{-1}) at room temperature,whereas the sample D6 with double iodide was (2.28×10^{-3} S.cm^{-1}) at room temperature.The temperature dependence conductivityhas been performed in the range of 298–373 K and it is observed that it obeys the Arrhenius behavior. It has been observed that the dielectric constant, increases with temperature in the lower frequencyregion and is almost negligible in the higher frequency region. This behavior can be explained on the basis of electrodepolarization effects.Eight different solar cells were fabricated employing different electrolyte compositions. The best cell using the electrolyte sample D4 has efficiency (2.014 %) with binary iodide salt (KI15/NaI20%). The enhancement of the solar cellperformance with increasing size of the cation is discussed in terms of the effect of the cations on theTiO2 anode and ion transport in the electrolyte.

Keywords: Ionic conductivity, Polymer electrolyte, Potassium iodide, Sodium Iodide.

INTRODUCTION

In the past three decades, the progress of the portable consumer electronic devices has made it an urgent need to develop new batteries with a high energy density and design flexibility[1].Polymer electrolytes introduced in the 1970s consist of an appropriate salt dissolved in a polymer matrix signifying a unique class of electrolytes. They are very attractive materialsto be used in applications such as batteries, photoelectrochemical(PEC) solar cells, electrochromic devices, supercapacitorsand fuel cells due to the favorable mechanicalproperties, ease of fabrication and minimum side reactions [2]. Gel polymer electrolytes (GPEs) exhibit high ionic conductivity at ambient temperature and thus can be a good candidate for practical use [1].Renewable energy sources that gain their energy conversion from the sun, such as solar cells, are expected to be capable of supplying the endless energy for mankind [3]. The development of renewable and clean energy sources isimportant in order to fulfill future energy needs withoutdepleting our fossil fuels and without polluting our environment. It's important toenhance the performance of DSSCs. By the improvementof the photo-electrode and the electrolyte[4]. The nature and the concentration of ionicspecies also have a profound influence on the conductivity ofthese polymer electrolytes[5]. Iodide salts have been used in electrolytes intendedfor DSSCs. The most commonly used liquid electrolyte in DSSCs is theiodide/triiodide redox couple in liquid organic solvents such asacetonitrile and propylene carbonate (PC), with this electrolyte ahigh overall energy conversion efficiency of more than 10%[6]. In order to develop quasi-solid or solid polymer electrolytesintended for PEC solar cells, various host polymers andplasticizers have been incorporated with different iodidesalts. The nature of the cation in the iodide saltincorporated with the host polymer matrix plays an importantrole in the ion transport mechanism in DSSCs[2]. The point of this work is to optimize the ionic conductivity efficiently by implies of shifting the KI and NaI salt composition in a PAN/PMMA based electrolyte and to explore the ionic conductivity and dielectric in arrange to optimize dependable and upgrade electrolytes.

MATERIALS AND METHODS

Experimental Part

PAN, PMMA, KI, NaI, (PC) and (EC) all purchased from Aldrich with purity greater than 98%. Iodine (I_2 – Breckland Scientific Supplies), were used as starting materials. The electrolyte samples were prepared with weight ratio of PAN (20%), PMMA (80%), EC and PC (1:1) the iodine (I_2=10%) weight ratio percentage were kept unchanged and the weight ratio of KI and NaI were varied as given in Table1.

Initially appropriate amount of EC, PC and salts were mixed in a closed glass bottle by continuous stirring at 50 °C for about 2 h. Then PAN was added to the mixture which was stirred further for about 4 h after that PMMA was added to the mixture with continues stirrer for 1 h. Finally, iodine was added to the mixture and heated to about 60 °C along with continuous stirring for a few more minutes until a homogeneous viscous solution was obtained. The complex impedance measurements were performed using LCR-8110G/8105G, impedance analyzer in the 50 Hz – 2 MHz frequency range to evaluate the ionic conductivity of the samples, The relationship of the specific ionic conductivity σ with the bulk resistance R_b can be represented by a simple form as shown in equation (1) for the measurement setup with polymer electrolytes film sandwiched between two electrodes [6]:

$$\sigma = \frac{l}{R_b A} \quad \text{..... (1)}$$

Where l (cm) represents the separation distance between the electrodes, A (cm^2) is the area of the electrode and σ ($S.cm^{-1}$) is the specific conductivity. The sample cell was prepared by sandwiching the electrolyte using two stainless steel electrodes. The temperature of the sample varied from 25 to 60 °C during the measurements. The real parts of dielectric constant (ε_r) values were calculated using the following equation [7]:

$$\varepsilon_r = \frac{C_t}{\omega C_o [Z_r^2 + Z_i^2]} \quad \text{..... (2)}$$

Where ω is the angular frequency ($\omega=2\pi f$), C_o is vacuum capacitance and Zr and Zi are real and imaginary parts of impedance. The Arrhenius law equation was used to fit the temperature conductivity dependency of gel polymer

electrolytes. Arrhenius law equation (3) is a basic relationship, which describes the linear relationship of log σ with 1/T as follows [7]:

$$\sigma = \sigma_0 \exp\left[\frac{-E_a}{K_B T}\right] \ldots\ldots\ldots\ldots \quad (3)$$

Where σ_0 is conductivity at an absolute temperature (T= 0 K), E_a is the apparent activation energy [J.mol^{-1}], and K_B is Boltzmann constant.

Assembly and Characterizing Cells

TiO_2colloidal suspension wasprepared by grinding 0.5 g powder of $TiO_2$with 2 mLof HNO, 0.1 g of Carbowax, and few drops of surfactantoctylphenol ethylene oxide condensate (Triton X-100) in anagate mortar. The TiO_2colloidal suspension was spread onthe clean (FTO) glass by applying the doctor blade technique and then sintered at 450 ºC for 30 minutes. The TiO_2 electrode was then soaked in a ruthenium (N3) dye solution diluted with ethanol to 5 mill mol for 24 hours for dye adsorption. The cells assembly was done by sandwiching GPEs between TiO_2/dye electrode and platinum (Pt) counter electrode in the configuration of FTO/TiO_2/Dye/GPE/Pt/FTO. TiO_2 functions as the base material for the photoanode. An advancepotentiostat (MLab 200, Bank Elek.GmBH) was used to measure the photocurrent density-voltage (*J*-*V*) characteristics of the DSSCs at room temperature under 1000 W·m^{-2} illumination. From the *J*-*V* plots, the current density, J_{max},and voltage, V_{max}at maximum power output were obtained and used in the equation (4) to calculate the fill factor, *FF*:

$$FF = \frac{J_m V_m}{J_{sc} V_{oc}} \ldots\ldots\ldots \quad (4)$$

In equation (2), $J_{sc}$is the short circuit current density and $V_{oc}$is the open-circuit voltage. The *FF* value was then used to calculate the overall energy conversion efficiency, η of the cell using the equation (5):

$$\eta(\%) = \frac{J_{sc} V_{oc} FF}{P_{in}} \times 100\% \ldots\ldots\ldots(5)$$

P_{in}in equation (5) is the total incident power density.

RESULTS AND DISCUSSION

Ionic Conductivity

Gel polymer electrolytes (GPEs) doped with different iodides (KI/ NaI) ratios were studied at a frequency range (50Hz – 2 MHz) and temperature range 298-373 K. The synergist effect of binary salts plays an important role in softening of polymer host. Thus, pre-determining the ratio of KI/NaI mixture is important to enhance the flexibility and performance of polymer electrolyte. The mixed of the two salts are helpful in improving the electrical conductivity. Fig, 1 describe the conductivity of electrolyte samples Ds that contain double iodides (KI/NaI) (0-35 wt.%). It shows that variation in the value of conductivity increase randomly, and the higher value of conductivity owned by sample D6 (2.53 mS.cm^{-1}) which contain KI/NaI (25/10) wt.% at a given salt concentration combination.

The dissociated K^+ and I^- ions from KI salt and I- ions from NaI salt will take part in the conduction process and contribute to the ionic conductivity of the gel electrolyte. The mass fraction can be attributed basically to an increase in both the number of charge carriers and their mobility with added KI. It has to be noted that salt separation, polymer crosslinking, the mobility of ions, ion consistency and shielding by polymer chains all are linked to the cation size and charge density.The electrolyte samples D1 and D8 that contain single iodide NaI and KI with (35 wt.%) have conductivity (2.33 and 3.11 mS.cm^{-1}) respectively. This can be due to the week contribution of Na^+ ions as a result of the small cation size of Na+. The Lewis acid-base interaction between the alkaline ion and the CN groups are weaker for Na^+. Thus iodide ions in Na^+ containing samples can also attain greater mobility when considering the polymer flexibility and the local viscosity. There are so many effects imposed by the nature of cations for the conductivity of solid or gel polymer electrolytes and some of the major effects are summarized with respect to the

cation radius as shown in Fig.2 [8]. The size of the cation K^+ is larger than Na^+, therefore, its mobility is expected to be lower **(Arof et al., 2014).**

The net ionic conductivity of the electrolyte series increases with increasing cation size and the iodide ion conductivity should also have a similar trend since some of the effects imposed by the increasing size of the cation are favorable also for iodide ion conductivity, as mentioned above. Re-dissociation of such ion pairs can occur due to long-range columbic forces giving rise to free ions, which contribute to conductance. At higher concentrations, short-range ion-solvent interactions take over and therefore, even though the number of ions dissolved in the electrolyte medium is higher, the effective number of charged species available for charge transport gets reduced[9].The higher salt dissociation with increasing amount of KI is evident from the increase in the pre-exponential factor, which correlates with the density of charge carriers, In addition, this bulky cation can impose more disorder on long polymer chains and it can make long polymer chains more separated increasing the flexibility of the material. Finally, the KI salt has given a significant ionic conductivity enhancement compared to NaI.Fig.3 illustrates the conductivity dependence on temperature for electrolytes D with double salts (KI/NaI) and concentration range (0-35 wt.%). It is obvious that conductivity increases with temperature, due to the fact that ions in the systems get more energy and hence their motion increase resulting conductivity increment [10].The ions get more kinetic energy due to the increase intemperature and become more mobile resulting a high ionic conductivity [11].

The ion transport and salt dissociation increase with increasing temperature besides the reduction of local viscosity. However, a conductivity reduction is shown with the increase in NaI salt composition. Therefore, increasing amounts of NaI may have reduced the polymer flexibility via strong cross-linking of long polymer chains reducing the mobility of ions, since the high charge density in the small Na+ cation assists the cross-linking of PAN/PMMA chains due to the presence of a CN group in the polymer. This cross-linking ability of Na+ was used to improve the iodide ion transport number in a PAN+PMMA based electrolyte system [8].As temperature increases, the hydrogen ions jump into neighboring vacant sites and, hence, ionic conductivity increases. The concentration dependence of the conductivity is a very complex function. High conductivity is achieved in polymer electrolytes by ensuring that the salt concentration is optimized to give sufficient charge carriers, without unduly immobilizing thepolymer [12].

Activation Energy

Activation Energy (Ea) is the required energy of an ion to detach from its initial site to become a free ion. The electrolytes conductivity is easily raised as temperature increases hence creating more free volume [13]. This phenomenon enhances ionic mobility and polymer segmental motion thus increasing the conductivity [14].Fig.3 can be best fitted by Arrhenius equation (Eq. 3), from Table 2 which tabulated the values of conductivity and E_a noting thatE_a decrease with increasing conductivityindicates that the ions in higher conducting electrolyte require lesser energy to migrate.From observation activation energy decreases as the iodide salts concentrations increases. The Ea of electrolyte samples (D1& D8) that contain single iodide (KI &NaI) with weight ratio (35%) have the values of (0.0725, 0.0628 and 0.0652 eV) respectively. The E_a of the sample D5 (0.0644 eV) owned the lowest values.The decrease in Ea values with increase single iodide weight ratio (35%) for the same iodide as a result of increase conductivity of the electrolyte samples. The variation in activation energy strongly supports the change in the electrical conductivity. It is observed that the minimum activation energy is the characteristics feature of the optimum conductivity value [15].

The dielectric constant

The dielectric constant of electrolytes Ds at room temperature

To further enhance the understanding in conductivity trend, Fig.4illustrates the dielectric constant corresponding to the frequency (50Hz - 4GHz), for electrolytes Ds, at room temperature, note that the dielectric constant values were calculated using (Eq. 2). It can be noticed that at low frequencies, the values of ε_r are higher compared to that at high frequency, the charge starts to accumulate at the surface of the electrode causing the electrode polarization to occur [16].

The dielectric constant of polymer electrolytes over a temperature range (298-333 K) at a frequency (50 Hz)

The variation of permittivity (ε_r) with respect to frequency (50 Hz) for electrolytes Ds over temperatures range (298-333 K) are depicted in Fig. 5. It can be seen that on assist increase of salts weight proportion, there's decrement of ε_r due to a lessening in chain segmental mobility. Carbonate esters play the role of ion dissociation enhancer and improve ion mobility because of their relatively high dielectric constants. Ethylene carbonate (ε_r = 89.78) and propylene carbonate (ε_r= 64.93) are among the most common carbonate esters used in lithium-ion polymer batteries. They both have excellent thermal stability and boiling point of above 240°C. That leads to enhance dielectric constants of the electrolytes.At higher temperature, the dipoles can situate effectively compared to exceedingly cross-linked fabric [17].

The higher values of dielectric consistent at higher temperature can be ascribed to the separation of particle totals and the next degree of salt separation. The crystallinity of the polymer electrolyte is reduced with an increment within the temperature. This, in turn, impacts the polymer elements and the dielectric behavior [18]. The increase in the dielectric constant with temperature can be attributed to the increase in charge carrier density due to the increase in dissociation of ion aggregates. The εr values increase with temperature, high temperature promotes more dissociation of ions thus enhances the value of εr[19].From Fig.5, one can notes that the higher values to the real dielectric constant for electrolyte samples that contain single salt D1 (9.19×10^7). However, the $\boldsymbol{\varepsilon}_r$ for the electrolytes with binary salts that owned the highest values was D3 (8.94×10^7). In reality, the addition of iodide salts to the polymer network makes amorphicity within the polymeric fabric and as a result increment in ε_r is observed [20].

Cells efficiency

The electrolyte used in dye-sensitized solar cells (DSSCs) plays a key role in the process of currentgeneration, and hence the analysis of charge-transfer mechanisms both in its bulk and at its interfaceswith other materials is of fundamental importance [21]. The nature and concentration of cationic species in the electrolyte exert a profound influence on the efficiency of nanocrystalline dye-sensitized solar cells (DSSCs). A series of DSSCs based onelectrolytes containing two alkali iodide salts (KI, and NaI) and PAN/PMMA withplasticizers were fabricated and studied[8].

The photocurrent density–photovoltage (*J–V*) characteristics of the DSSCs assembled using N3 dye in combination with the electrolytes containing the three different alkaline iodides are shown in Fig.6. These curves were used to calculate average solar cell parameters J_{sc}, V_{oc}, *FF*,and power-conversion efficiency (η), which are tabulated in Table 3. The highest efficiency (2.413%) was recorded for the cellwith electrolyte D7 contain KI 30%/NaI5%, mostly due to an improved photocurrent compared to all other metal salts, and the effectual combined of the two cations (K^+& Na^+). Therefore the using of a double mixture of two iodide salts consisting of a bulky cation (K^+) and a small cation (Na^+) with high charge density in the electrolyte. The performance of the cells with electrolytes D1 & D8which contain single iodide salts (Na^+& K^+) showefficiency of (1.072 & 1.525 %) respectively. The overall solar to energy conversion efficiency is hugely dependent on the mobility of the redox couple and consequently, on the ionic conductivity of the polymer electrolyte for gel electrolyte based dye-sensitized solar cell devices. Typically, electrolytes with smaller cations would have a higher drop in the V_{oc} due to a larger downward shift to the conduction band edge which induced by the adsorption of the smaller cations on the surface ofthe nano-sizedTiO_2grain.It was observed from Table 3, that the V_{oc}increases with the size of the cation in the electrolyte. The observed enhancement in $V_{oc}$with increasing size of the cation is now an established phenomenon[22],which can be attributed to the decrease of the recombination of electrons in the conduction bandof$TiO_2$with I_3^- in the electrolyte at the vicinity of the TiO_2electrode and to the relative shift of the conduction band edgeresultedby cation adsorption [8].The open circuit voltage $V_{oc}$of cells is dependent on the difference between redox potential in the electrolyte and Fermi level of TiO_2 electrode.

The photocurrent densityJ_{sc}values of solar cellsincrease with the cation size except for the cells with electrolytes D5 and D6. In general, the cation dependence of J_{sc}in a DSSCcan be attributed to the variation ofI^-/I_3^- conductivity and to the variation of charge injection rate from the dye to the TiO_2 influenced by the adsorbed cations[23].The conductivity of the electrolyte is not the only factor governing the solar cell performance and the short-circuit photocurrent (J_{sc}) in these DSSCs is mainly governed by the iodide/tri-iodide ion conductivity. The iodide and triode ion conductivity have profound influence on photocurrent density in a DSSC, since charge transport between photoanode and Pt counter electrode is carried by iodide/tri-iodide redox couple [22]. In addition to iodide/tri-iodide conductivity the charge transfer rate at the two interfaces, particularly at the TiO_2/electrolyte alsohasa major influence on photocurrent density as the electrontransferdynamics of photogenerated electrons are governed by theshiftedposition of the TiO_2conduction band edge due to cation adsorption by TiO_2 [24].The fill factor and the efficiency also increase with the size of the cation in the electrolyte as seen in Table 3.

CONCLUSION

Gel type polymer electrolyte based on PAN/PMMA have polymer was arranged by joining the salt, KI, NaI, and plasticizers EC and PC. The electrolyte B4 containing 15/20 wt.% salt have the higher conductivity (2.53 $mScm^{-1}$) at room temperature. The enactment vitality diminishes with expanding the conductivity of electrolyte whereas the dielectric increment when temperature expanded. The comes about demonstrated that the ionic conductivity values increment with expanding salts weight proportion up to (15%KI) and lower of NaI down to 20%. the conductivity watched to extend with expanding temperature. The electrolytes are effortlessly extended as temperature increments subsequently making more free volume, the activation energy E_a is a combination of the vitality of deformity arrangement and the vitality of imperfection relocation. At lower recurrence locale, εr is watched to diminish with expanding recurrence and level off at higher recurrence locale. The greatest dielectric steady esteem is gotten for polymer electrolyte D2 having one arrange increase in their sizes at room temperature. In reality, the expansion of iodide salts to the polymer lattice makes amorphicity within the polymeric fabric and as a result increment in εr is watched. The electrolyte with the highest conductivity showthe best energy conversion efficiency revealing that the effectof the cation on the efficiency of the DSSCs important, the best cell result in sample D4 was an energy conversion efficiency of 2.014 %.

REFERENCES

1. S. I. Jo,et., al, “Electrochemical studies of gel polymer electrolytes based on methyl methacrylate-styrene copolymers”, 2003, Journal of Power Sources 119–121, 478–481.
2. T. M. W. J. Bandara,et., al. “Efficiency enhancement in dye sensitized solar cells using gel polymerelectrolytes based on a tetrahexylammonium iodide and MgI2 binaryiodide system”, 2012, Phys. Chem. Chem. Phys.,14, 8620–8627.
3. M.S. Su’ait,et., al,“Review on polymer electrolyte in dye-sensitized solar cells (DSSCs)”,2015, Solar Energy 115, 452–470.
4. S. Ahmed,et, al., “Improving Microstructured TiO2 Photoanodes for Dye Sensitized Solar Cells by Simple Surface Treatment”, 2011, Adv.Energy Materials, 1, 879–887.
5. C. Sequeira and D. Santos , “Polymer electrolytes: fundamentals and applications ed.”, 2010, Elsevier.
6. Y. Chiba, et, al.,”Dye-Sensitized Solar Cells with Conversion Efficiency of 11.1%”, 2006, Appl. Phys., 45(25), L638–L640.
7. M.K.Jawad, “Synergistic effect of Metal- Phthalocyanine in Gelled Co-Polymer for Energy Conversion Device”,2015, Ph.D. Thesis, Baghdad University, Department of Physics, 87-88.
8. T. M. W. J. Bandara,et,al., “Effect of the alkaline cation size on the conductivity in gel polymer electrolytes and their influence on photo electrochemical solar cells”, 2016, Phys.Chem.Chem.Phys., 18, 10873.

9. R. Nimma Elizabeth et al., "Preparation and Characterization of PVC/PMMA Blend Polymer Electrolytes Complexed with LiN(C2F5SO2)2 ", 2004, Polímeros: Ciência e Tecnologia, vol. 14, No 1, pp. 1-7.
10. B. Cosar et al." Photovoltaic performance of bifacial dye-sensitized solar cell using chemically healed binary ionic liquid electrolyte solidified with SiO2 nanoparticles",2013,ElectrochimicaActa, Vol.87,425– 431.
11. W.V.T. Madhushani, et, al., "The effect of cation size of iodide salt in the electrolyte on the performance of dye-sensitized solar cells", 2016,Journal of the National Science Foundation of Sri Lanka 44(1).
12. M. K. Jawad, et, al., "Efficiency enhancement of photovoltaic performance of quasi-solid state dye-sensitized solar cell with TPAI and KI binary iodide salt mixture", 2014, Vol.34.
13. M.F. Shukur, et.al, "Proton conducting polymer electrolyte based on plasticized chitosan–PEO blend and application in electrochemical devices", 2013, Optical Materials, Vol. 35, pp.1834–1841.
14. D., Padalia, et, al., "Study of cerium doped magnetite (Fe3O4: Ce)/PMMA nanocomposites", 2012, Physica B, 407, 838–843.
15. M.S. Su'ait, et, al., "The potential of polyurethane bio-based solid polymer electrolyte for photoelectron- chemical cell application", 2014, International Journal of Hydrogen Energy, 39(6), pp. 3005–3017.
16. S.Selvasekarapandian and D.Chithra "Dielectric studies on a solid electrolyte AgI-PbBr2-Ag2O-B2O3 material", 1999, ChemPhys 58:90–93.
17. S. Jana, and W.H. Zhong, "Electrical conductivity enhancement of a polymer using butyl glycidyl ether (BGE)-lithium hexafluorophosphate (LiPF6) complex", Journal of Material Science, Vol.43, pp. 4607-4617, 2008.
18. A. Awadhi, et, al., "Dielectric investigations in PVA based gel electrolytes", 2006, Progress in Crystal Growth and Characterization of Materials, Vol.52, pp. 61-68.
19. R.Sengwaet, al.," Effects of plasticizer and nanofiller on the dielectric dispersion and relaxation behavior of polymer blend based solid polymer electrolytes", 2015, Curr App Phys 15(2):135–143.
20. O.A. Ileperuma, et, al."Photoelectrochemical solar cells with polyacrylonitrile-based and polyethylene oxide-based polymer electrolytes", 2004, Solar Energy Materials and Solar Cells, Vol. 84(1), pp.117-124.
21. O.Bettucci, et, al.,"Organic dye-sensitized solar cells containing alkaline iodide-based gel polymer electrolytes: influence of cation size", 2018,, Phys. Chem. Chem. Phys., 20, 1276—1285.
22. H. Wang and L.M. Peter, "Influence of electrolyte cations on electron transport,electron transfer in dye-sensitized solar cells", 2012, J Phys. Chem., 116 10468–10475.
23. M. Dissanayake, et, al., "Efficiency enhancement by mixedcation effect in dye-sensitized solar cells with PAN based gel polymerelectrolyte", 2012, J Photochemistry & Photobiology: A Chemistry 246 29–35.
24. T. Bandaraa, et, al., "Combined effect of alkaline cations and organic additives for iodide ionconducting gel polymer electrolytes to enhance efficiency in dyesensitized solar cells", 2017, ElectrochimicaActa 252, 208–214.

Table 1: Assigning and composition of [PAN-PMMA (20:80%)]-KI/NaI gel electrolytes system.

Electrolyte	KI wt.%	NaI wt.%
D0	0	0
D1	0	35
D2	5	30
D3	10	25
D4	15	20
D5	20	15
D6	25	10
D7	30	5
D8	35	0

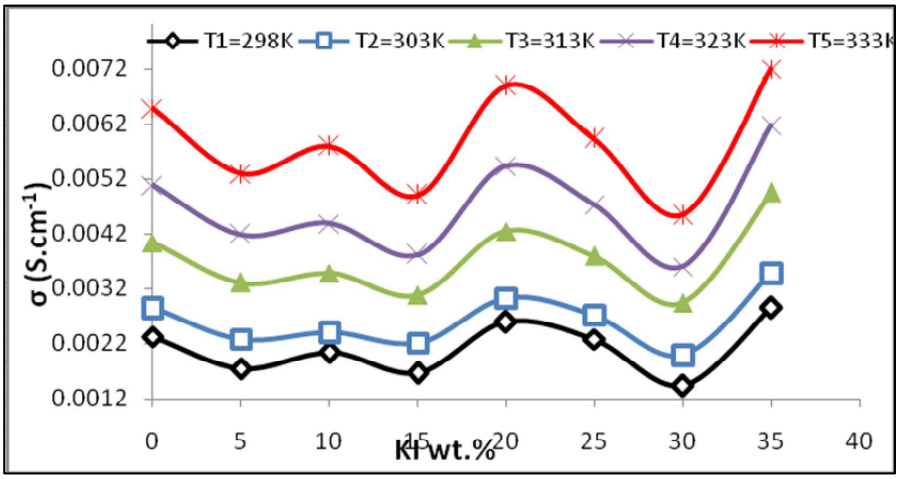

Fig. 1. Ionic conductivities dependence of temperature and KI/NaI wt.% of the electrolytes Ds.

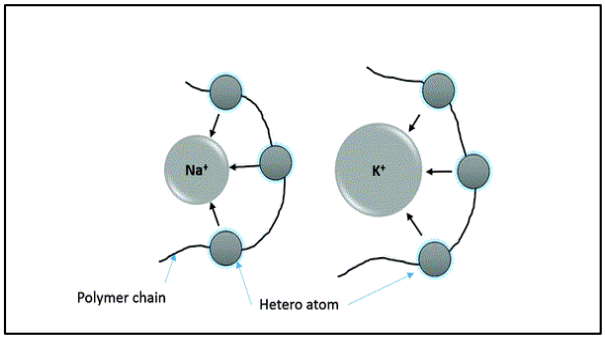

Fig. 2. Schematic illustration in 2 dimensions to show the increase in polymer chain flexibility due to the swelling effect of the electrolyte with increasing size of the cation.

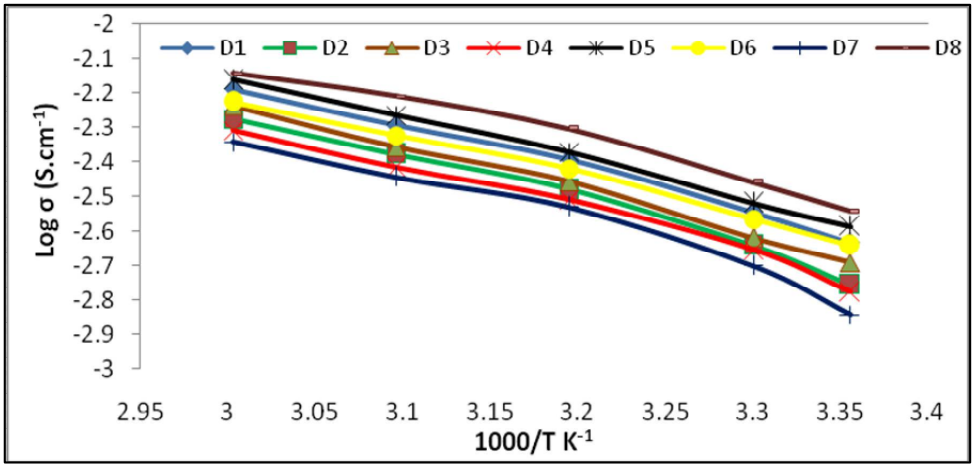

Fig.3.Temperature dependence of the ionic conductivity of electrolytes (Ds).

Table 2: The conductivity and activation energy values of electrolytes Ds at room temperature.

Electrolytes designation	σ(S.cm^{-1}) RT	Activation energy Ea (eV)
D1	0.00233	0.06522
D2	0.00175	0.06781
D3	0.00204	0.06688
D4	0.00167	0.06853
D5	0.0026	0.0644
D6	0.00228	0.06588
D7	0.00144	0.06958
D8	0.00311	0.06281

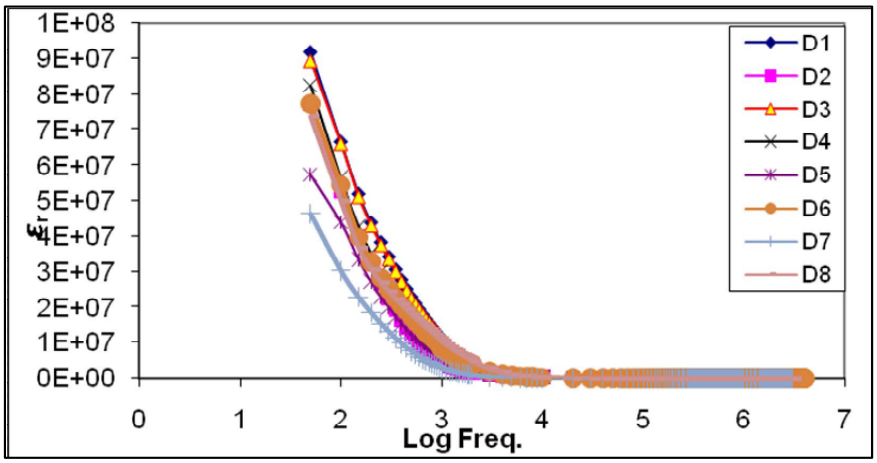

Fig.4:Real part of dielectric constant (εr) for electrolytes Ds at room temperature, corresponding to log frequency.

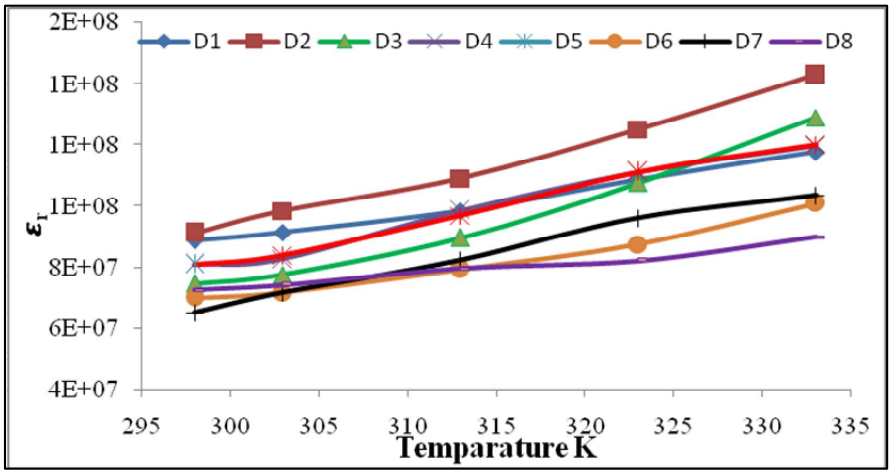

Fig.5.Real part of dielectric constant (εr) for electrolytes D corresponding to frequency over a temperature range (298-333K).

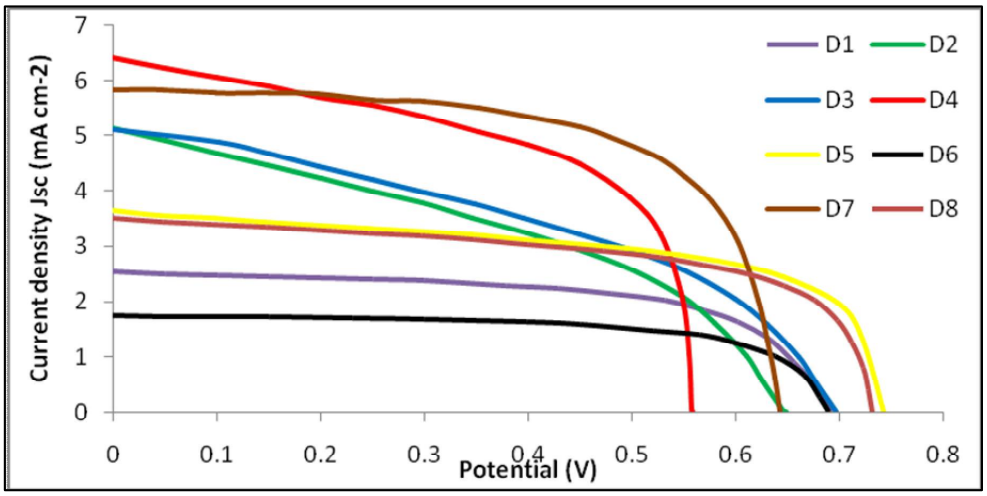

Fig. 6: Photocurrent density–photovoltage (*J–V*) of solar cells under illuminate 1000 W/m².

Table 3: J_{sc}, V_{oc}, *ff*,*and* η of solar cells using gel electrolyte witha different composition.

Electrolyte	KI %	NaI%	J_{sc}(mA/cm²)	V_{oc}(Volt)	*ff*	η, %
D1	0	35	2.531	0.692	0.612	1.072
D2	5	30	5.132	0.648	0.396	1.317
D3	10	25	5.11	0.696	0.407	1.456
D4	15	20	6.423	0.559	0.561	2.014
D5	20	15	3.64	0.742	0.592	1.598
D6	25	10	1.742	0.689	0.655	0.786
D7	30	5	5.841	0.642	0.643	2.412
D8	35	0	3.506	0.7314	0.595	1.525

Indian Journal of Natural Sciences www.tnsroindia.org.in ©IJONS

Vol.9 /Issue 52 / February / 2019 *International Bimonthly* *ISSN: 0976 – 0997*

RESEARCH ARTICLE

The Numerical and Experimental Work of Chaos System in Three Dimensions Phase Spaceusing Rossler Circuit

Dina A.Kafi[1], Raied K. Jamal[1]* , Kajeen I. Mosa[2] and Kais A. Alnaemme[1]

[1]Department of Physics, College of Science, University of Baghdad, Baghdad, Iraq.

[2]Department of Physics, College of Education (Ibn Al-Haitham), University of Baghdad, Baghdad, Iraq.

Received: 08 Nov 2018 Revised: 08 Dec 2018 Accepted: 10 Jan 2019

***Address for Correspondence**
Raied K. Jamal
Department of Physics,
College of Science, University of Baghdad, Baghdad, Iraq.
E-mail: raiedkamel@yahoo.com

ABSTRACT

In this paper, we deal with a dynamical system that can demonstrate a chaotic attractor of Rossleroscillator. We simulate the Rosslerequations numerically then we investigate the model experimentally. Numerically, the Rossler parameter *a* and *b* were fixed and *c* was changed.The evolution of the system exhibits period, period-doubling, second period doubling, and chaos when control parameters are changed. This evolution can be seen by analyze the time series, the bifurcation diagrams and phase space. Experimentally, the evolution of the system exhibited the same numerical behavior by changing the resistance (Rv) in Rossler circuit that represent as control parameter.

Keywords: Nonlinear dynamics, Chaos, Rossler circuit.

INTRODUCTION

Recently, chaos theory has attracted much interest in the academic and engineering study. Chaos is a phenomenon of irregular variations of systems' outputs derived from models that are described by a set of deterministic equations [1] or study of dynamical system (non-periodic system in motion) usually over time. Chaotic systems are known as nonlinear dissipative dynamical systems which state variables evolve with time, exhibiting complex dynamics that are highly sensitive on initial conditions. [2, 3].Chaotic behavior has been found in physics, chemistry, biology, robotics, bits generators, psychology, ecology, cryptography and economy [3].A nonlinear system includes various parameters and irregular oscillations of the output are generated under certain conditions in multi-dimensional parameter space [1].In a three-dimensional phase space thetrajectories can be wrapped or twisted around each other in quite intricate ways. Simple examples are provided by the Lorenzequationsand the Rossler equations [4]. In appropriate parameter ranges these systemspossess a strange attractor.The main reasons are that they (Lorenz & Rossler) arewell known but not completely understood, and as paradigmatic problems they have become test problems for almost all new analytical and numerical techniques in computational dynamics [5].Since 1976, the Rossler system is wellknown for its simplicity (three differential equations with only one nonlinear term) and its

dynamical richness producing chaos [6].The Rossler model is a three-dimensional problem with three dimensionless parameters. It is well known that for differentsetsof values of parameters the model exhibits a chaotic behavior, while for others a regular behavior. Therefore, a study of the different regions in the parameter space will give some interesting results. The attractor of the Rossler system belongs to the 1-scroll chaotic attractor family [7].Some tools for exploring time series data for Rossler model. Numerically the bifurcation diagram was used to study the effect of differentsetsof values of the parameterson a system. Experimentally, bifurcation diagram of the output voltage are constructed using a resistance as a control parameter. The phase space in two and three dimensions was studying of the different regions in the parameter space.

METHODOLOGY

Mathematical model of Rossler system

The Rosslersystem is described by three non-linear ordinary differential equations[8]:

$$\frac{dx}{dt} = -(y + z)$$

$$\frac{dy}{dt} = x + ay \qquad (1)$$

$$\frac{dz}{dt} = b + xz - cz$$

These differential equations define a continuous-time dynamical system that exhibits chaotic dynamics associated with fractal properties of the attractor. It have seven term, one quadratic nonlinearity and three parameter, where *a, b, c* ∈ R, and they are dimensionless parameters, and *x*, *y* and *z* are the three variables which evolves with continues time.The values of real parameters firstly are studied by Otto. E. Rossler were *a*and *b* =0.2 and *c*=5.7 the systemexhibits a chaotic behavior. The first two equations have linear terms that create oscillations in the variable *x* and y. The last equation has only one nonlinear term (*xz*) so the expected chaotic behavior is appeared from the system. The original Rossler paper says the Rossler attractor was intended to behave similarly to the Lorenz attractor, but also be easier to analyze qualitatively.By using MATLAB numerical simulation [with fourth-order Range Kutta method] of Rossler modelfor different values of *a*with fixed *b* and *c*values at 0.2 and 5.7 respectively with initial conditions[x_0, y_0, z_0] = [1,1, 0]obtain the figures (1) to (10).

The chaotic behavior in Rossler model can be described by the time series and the trajectories in the phase space (attractor). In figure (1), when the control parameter *a*=0 and keeping *b* and *c* fixed at *b*= 0.2 and *c* = 5.7, the time series is beginning to oscillate and the attractor is convergedas shown in figure (2). At a= 0.1 the time series fordynamics become periodic and the attractor convert to a limit cycle (one unique orbit) as shown infigure(3) and (4). When a=0.125, the Rossler system is changed to periodic doubling (two distinguish frequencies) and its attractor show two unique orbits, as shown in figure (5) and (6) respectively. By increasing more in a value to 0.1479 the Rossler system changed and the time series exhibit second periodic-doubling (four distinguish frequencies) and its attractor exhibit four unique orbit as shown in figures (7) and (8) respectively.When*a* =0.2 the time series shows different spikes with high and low amplitudes as shown in figure (9) and the chaotic attractorlooks very strange (strange attractor) that called hyper dense (the system displays a homoclinic orbit behavior), as shown in figure (10).In 3D phase space, an orbit within the attractor follows an outward spiral close to (*x*, *y*) plane around an unstable fixed point. Once the group spirals out enough, a second fixed point influences the graph, causing a rise and twist in the *z*-dimension.

In the time domain, it becomes apparent that although each variable is oscillating within a fixed range of values, the oscillations are chaotic. This attractor has some similarities to the Lorenz attractor, but is simpler and has only one manifold.Chaos is statically indistinguishable from randomness and yet it is deterministic and not random at all.

Chaotic system will produce the same result if given the same inputs, it is unpredictable in the sense that you cannot predict in what way the system's behavior will change for any change in the input to that system. A random system will produce different result when given the same inputs. The fast Fourier transformation spectra (FFT)of chaotic system is shown exponential decay behavior with frequencies range from 0 to 1 (a.u.) in *x* and *y* dynamics, while 0 to 3 (a.u.) in *z* dynamics, as shown in figure (11), while the FFT of random system is showing Gaussian spectrum.

The bifurcation in Rossler system occurs if any of the three parameters value is varied while other two parameters are fixed, as shown in figure (12). The data of Rossler system was analyzed using MATLAB program to obtain the bifurcation diagram, which has a period and period-doubling route to chaos. Firstly we will demonstrate the bifurcation diagram for Rossler system by changing the value of parameter *a* as a function of the orbit points y, here *b* and *c* are fixed at 0.2 and 5.7, respectively, where *a*value is changed (see figure 12a). We clearly see the system is changing from state to another one. The chaoticbehavior of attractor increases by increasing *a*value until *a*=0.187, where the system back to regular with three distinguish frequencies as shown in figure 12a, so we can conclude that not all *a*values gives chaotic behavior, where some ranges of the system may be back to regular state and this behavior is shown in *b* and *c* values. Secondly *a* and *c*values is fixed at 0.2 and 5.7 respectively and the parameter *b* is changed with local peaks of x, as shown in figure (12b). Varying *b* produces 3- period orbits and 6- period orbits accurse.Finally by fixing *a* and *b* at 0.2 the bifurcation diagram occurs when the parameter *c* increasing. The dynamic is periodic at$c \leq 2.7$, as *c* increases the period doubling behavior of the system is observed $2.7 \leq c \leq 4$. Second period doublingbehavior occurs at $4 < c < 4.2$.Higher order periodic orbits (chaotic system) obtained as *c* increases as shown in figure (12c). Through the above, we conclude the Rossler system presents stationary, periodic, quasi periodic and chaotic attractors depending on the value of the parameters (*a*, *b*, *c*).

RESULTS

The complete implementation of the Rossler chaotic circuitis shown in figure (13). The circuit employs simple electronic elements, such as resistors, capacitors, and operational amplifiers, where,one nonlinearity is a piecewise linear function made from op amp U4 with diode. The amplifier is switched on when the voltage exceed 3V. The output voltage x, y, and z are register with an oscilloscope (Tektronix, TD2024B).The variable resistor Rv(R14)is a control parameter, which varied from (0-200) kΩ, the system displays a period -doubling route to chaos. When the variable resister Rv equal 94.5 kΩ the dynamic system of Rossler shown periodic signal as shown in figure (14) and the attractor will be one orbit shape. With decreasing the Rv value to 77.7kΩ the dynamics exhibit period doubling (see figure (15)) and its attractor exhibit two orbits. The dynamics system is changing with many states with decreasing the Rv until 60.9 kΩ, as shown in figure (16), where system exhibit second periodic doubling with four orbits attractor. With decreasing the control parameter to Rv= 54.4kΩthe dynamic exhibit chaos and Rossler attractor obtained as shown in figure(17). The time series of z dynamic in chaotic state at Rv =54.4kΩ is illustrate in figure (18). It exhibit spikes shape where different of x and y dynamics behavior.

The real images of attractors that register from oscilloscope of experimental work are showing in the following figures (19-21). Again figure (19) presented chaotic homoclinic trajectory in phase space (x,y). A homoclinic chaotic orbit has the property that its phase trajectory fluctuates near a critical point in phase space.The FFT spectra that obtained from experimental work for x, y, and z dynamics is shown in figure (22), where these spectra also exhibit exponential decay behavior and the bandwidth ranging around( ). Again, through the above the numerical results match well with the experimental results.

CONCLUSION

In this paper the numerical and experimental of Rossler system has been presented. The resulting chaotic attractor has a single lobe and is referred to as spiral type chaos, which mainly manifests itself in irregular amplitude for the oscillations. Numerically the Rossler attractor at $a = 0$ converged. By Increasing in value of *a* from (0 – 0.2) we noticed

that the attractor change with itfrom periodic to chaotic behavior. The bifurcation diagram for Rossler system shows the period doubling rout for changing parameter*b* and*c*, also not all *a*, *b*, and *c* values in chaotic range can give chaotic behavior. Experimentally,the Rossler circuit described three-dimensional continuous autonomous chaotic system with nonlinearities involving piecewise linear functions often can be applied electronically using only diodes, capacitors, resistors, and op amps. The circuit displayed different states from behaviors by decreasing the control parameter (Rv). The system display chaotic behavior at Rv=54.5 kΩ. Finally the numerical results match well with the experimental results.

REFERENCES

[1] J. Ohtsubo, "Semiconductor Lasers Stability, Instability and Chaos", 3rd Edition. Springer, p. 1, 2013.
[2] Petros A. Daltzis, Christos K. Volos, Hector E. Nistazakis, Andreas D. Tsigopoulos and George S. Tombras, " Analysis, Synchronization and Circuit Design of a 4D Hyperchaotic Hyperjerk System", *Computation*, *6*, 14, 2018.
[3]A.Sambas, M. Sanjaya W. S., and M. Mamat," Design and Numerical Simulation of Unidirectional Chaotic Synchronization and its Application in Secure Communication System" Journal of Engineering Science and Technology Review 6 (4), 66-73, 2013.
[4] Rossler OE (1976),An equation for continuous chaos. Phy. Let. A57 (5):397-398.
[5] R.Barrio, M.A. Martinez, S. Serrano, D. Wilczak, "Qualitative analysis of the Rössler equations: Bifurcations of limit cycles and chaotic attractors",Physics Letters A 379(38), 2300-2305, 2015.
[6] Martin Rosalie, "Templates and subtemplates of R¨ossler attractors from a bifurcation diagram" Journal of Physics A, 49 (31), pp.315101, 2016.
[7] Abolhassan Razminia , Vahid Johari Majd and Dumitru Baleanu "Chaotic incommensurate fractional order Rössler system: active control and synchronization"Advances in Difference Equations 2011, 2011 :15.
[8]Otto E. Rossler, "Chaotic Behavior in Simple Reaction Systems", PHYSICS LETTERS, A 57,p.397, 1976.

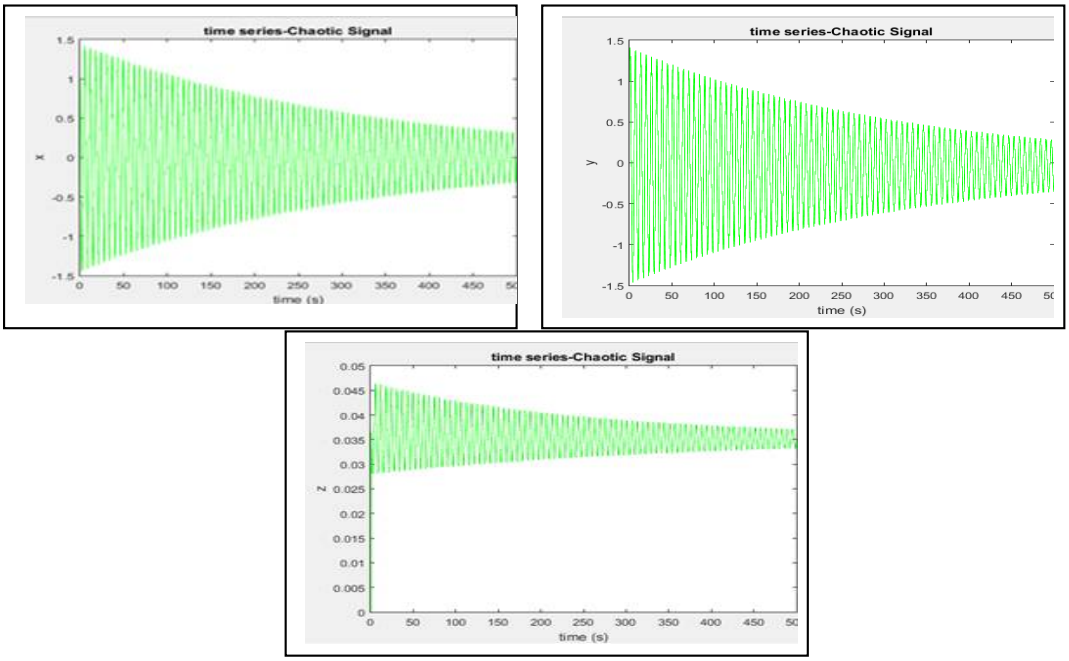

Fig.1.: Time series at x_0, y_0, and $z_0$equal 1, 1, 0 respectively and *a*, *b*, and *c* equal 0, 0.2, 5.7 respectively.

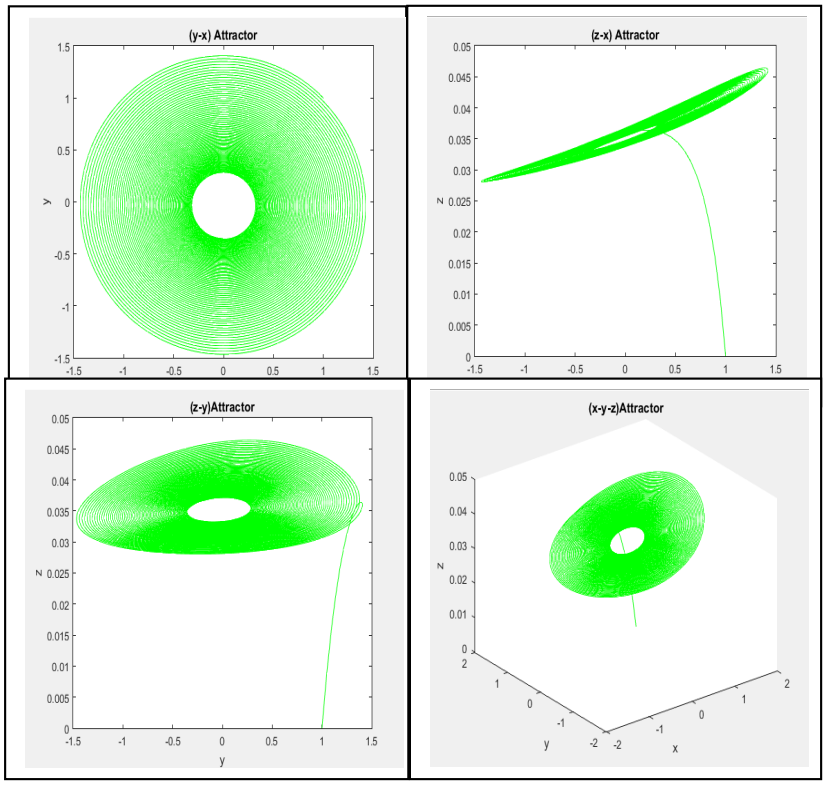

Fig.2: Rossler Attractors at x_0, y_0, and $z_0$equal 1, 1, 0 respectively and *a*, *b*, and *c* equal 0, 0.2, 5.7 respectively.

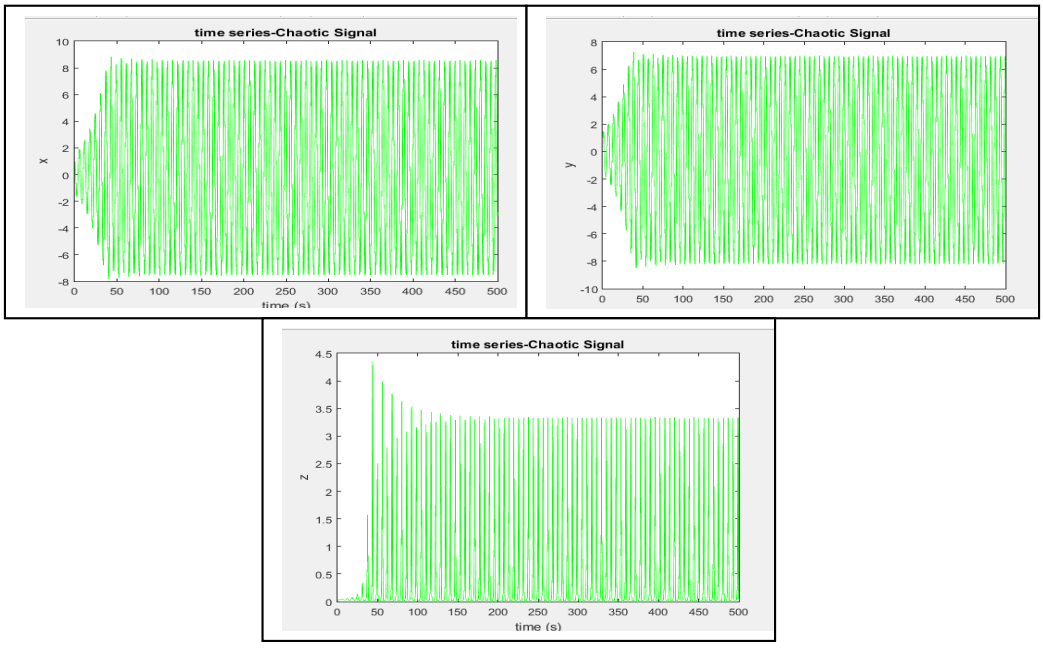

Fig.3.: Time series at x_0, y_0, and $z_0$equal 1, 1, 0 respectively and *a*, *b*, and *c* equal 0.1, 0.2, 5.7 respectively (parodic-one frequency).

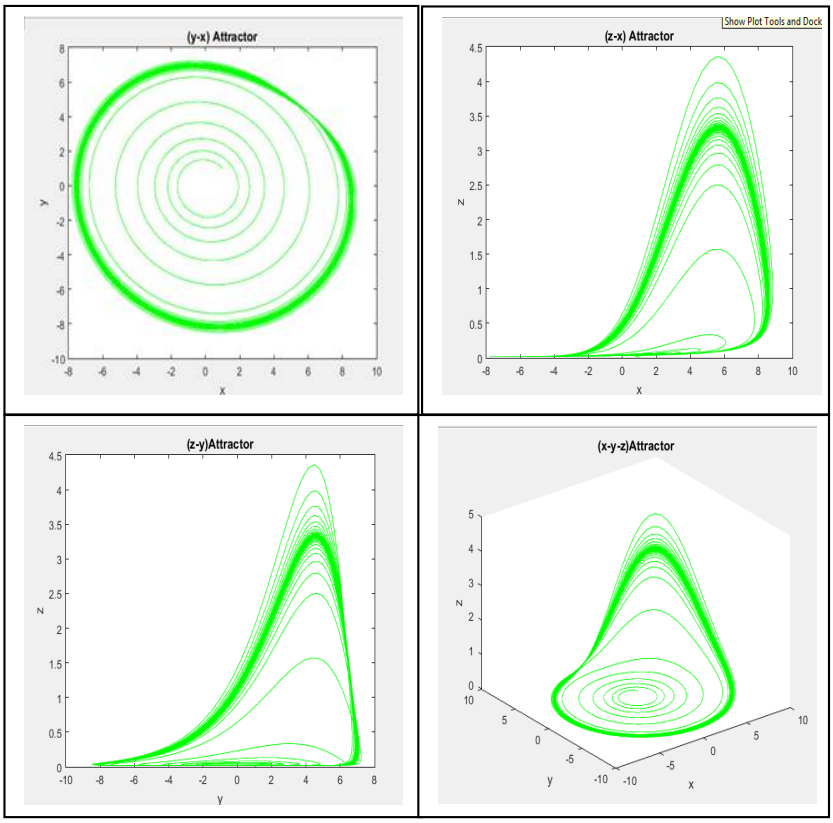

Fig.4: Rossler Attractors at x_0, y_0, and $z_0$equal 1, 1, 0 respectively and *a*, *b*, and *c* equal 0.1, 0.2, 5.7 respectively (one unique orbit).

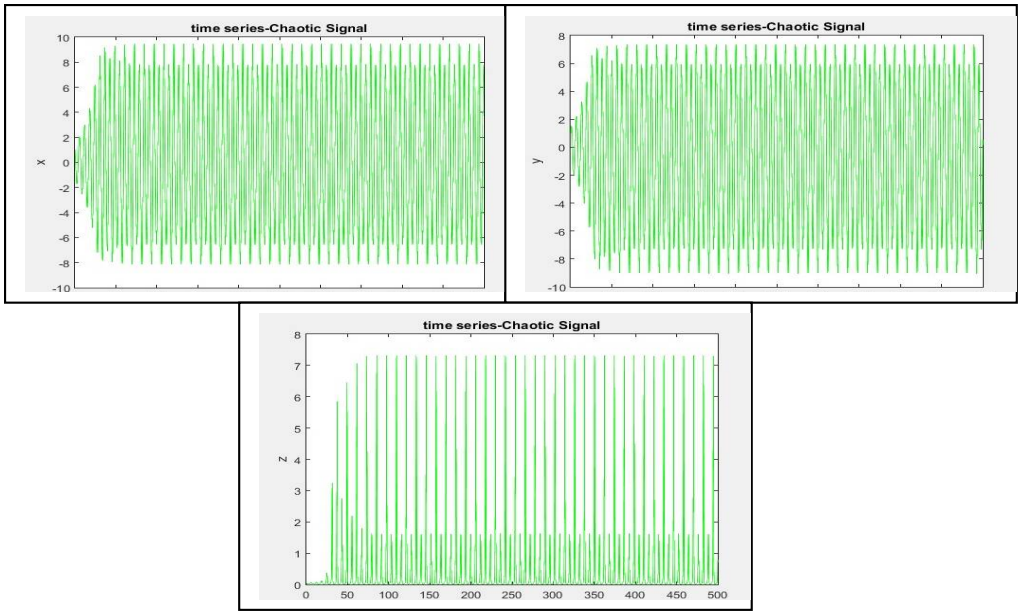

Fig.5: Time series at x_0, y_0, and $z_0$equal 1, 1, 0 respectively and *a*, *b*, and *c* equal 0.125, 0.2, 5.7 respectively (parodic-two frequency).

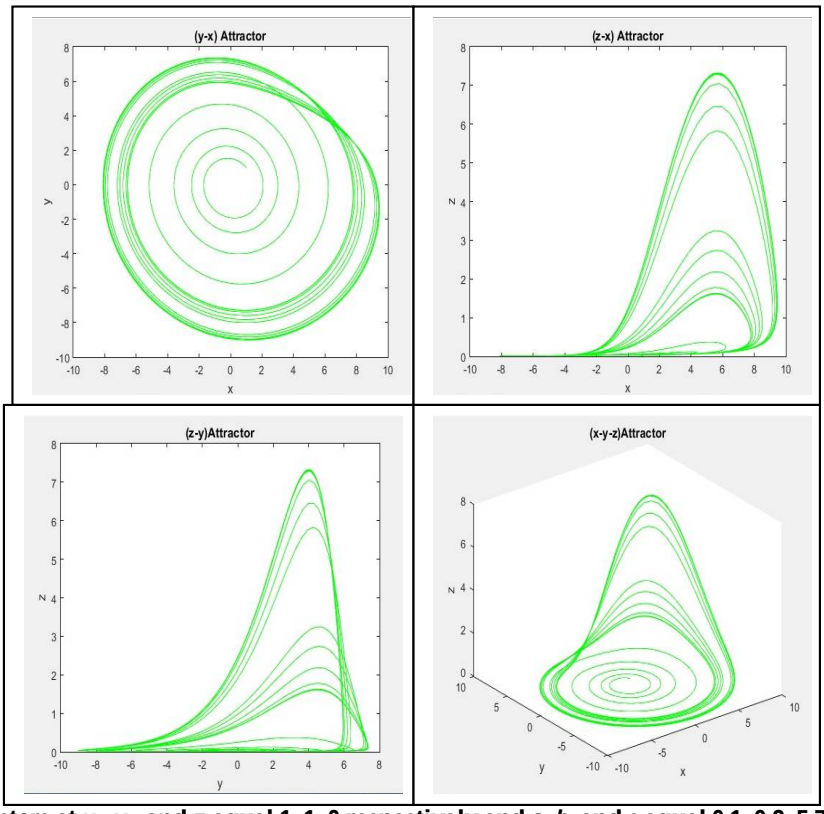

Fig.6: Rossler Attractors at x_0, y_0, and $z_0$equal 1, 1, 0 respectively and *a*, *b*, and *c* equal 0.1, 0.2, 5.7 respectively (two unique orbit).

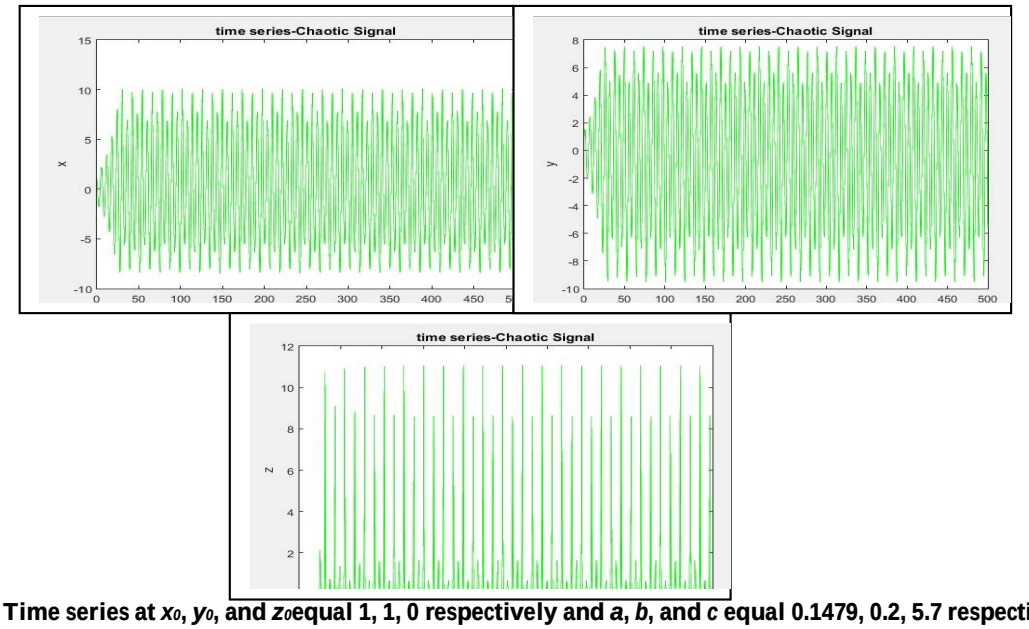

Fig.7): Time series at x_0, y_0, and $z_0$equal 1, 1, 0 respectively and *a*, *b*, and *c* equal 0.1479, 0.2, 5.7 respectively (parodic-four frequency).

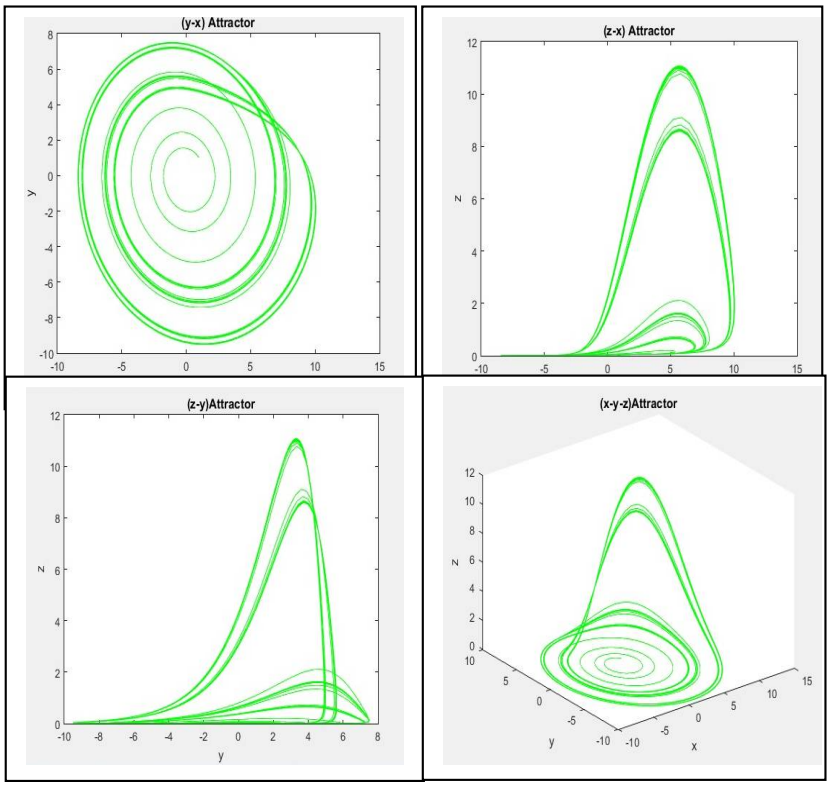

Fig.8: Rossler Attractors at x_0, y_0, and $z_0$equal 1, 1, 0 respectively and *a*, *b*, and *c* equal 0.1, 0.2, 5.7 respectively (four unique orbit).

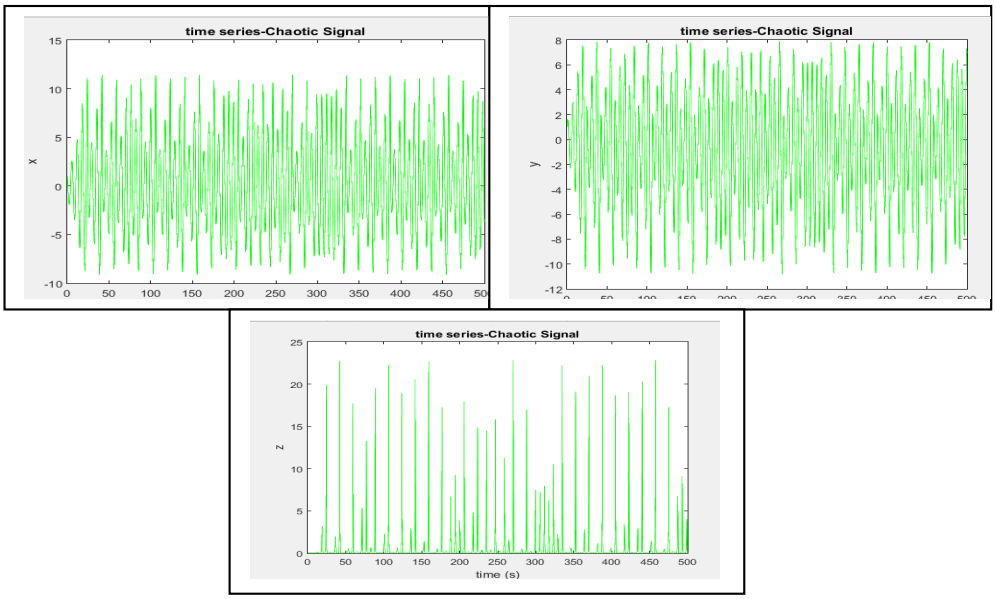

Fig.9: Time series at x_0, y_0, and $z_0$equal 1, 1, 0 respectively and *a*, *b*, and *c* equal 0.2, 0.2, 5.7 respectively (chaotic behavior).

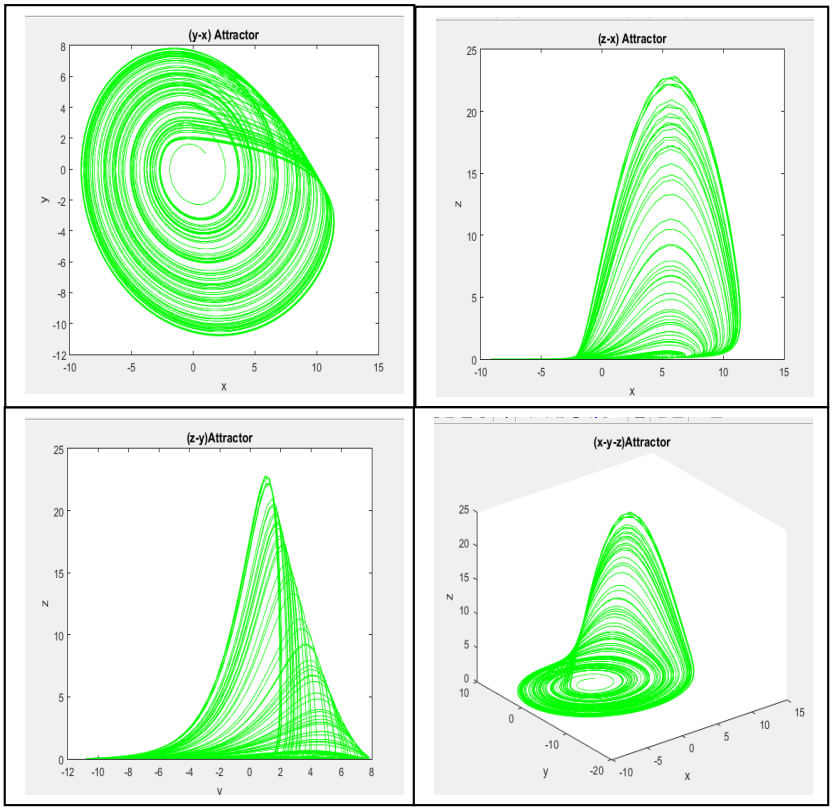

Fig.10: Rossler Attractors at x_0, y_0, and $z_0$equal 1, 1, 0 respectively and *a*, *b*, and *c* equal 0.2, 0.2, 5.7 respectively, where homoclinic orbits in (y-x) and hyper dines.

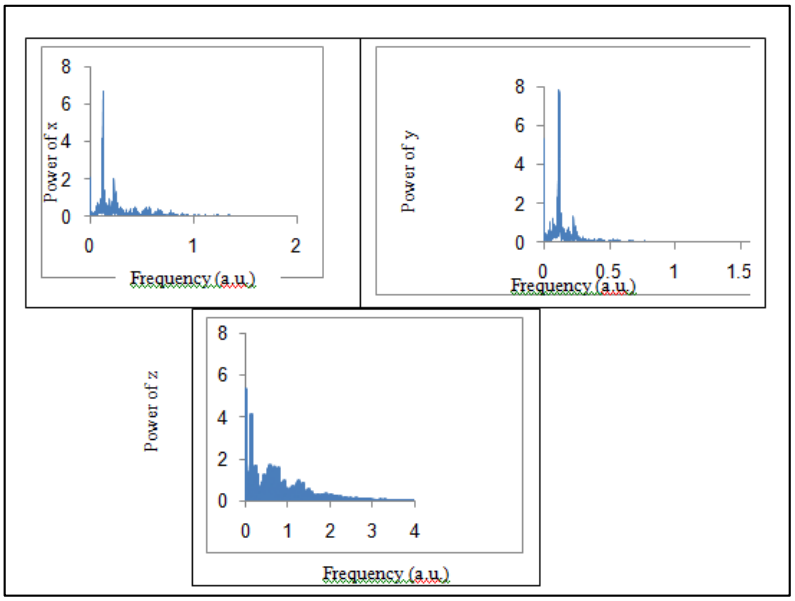

Fig.11: FFT spectra of x, y, and z dynamics.

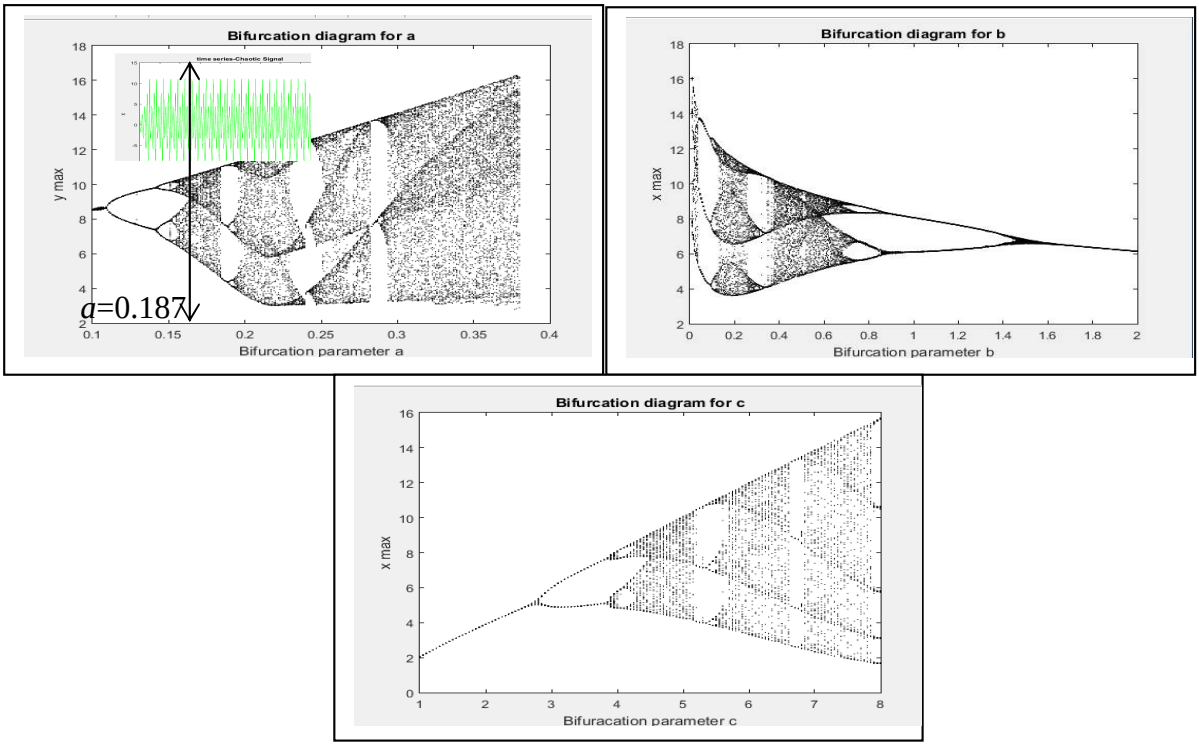

Fig.12: Bifurcations diagram for a, b, and c parameters.

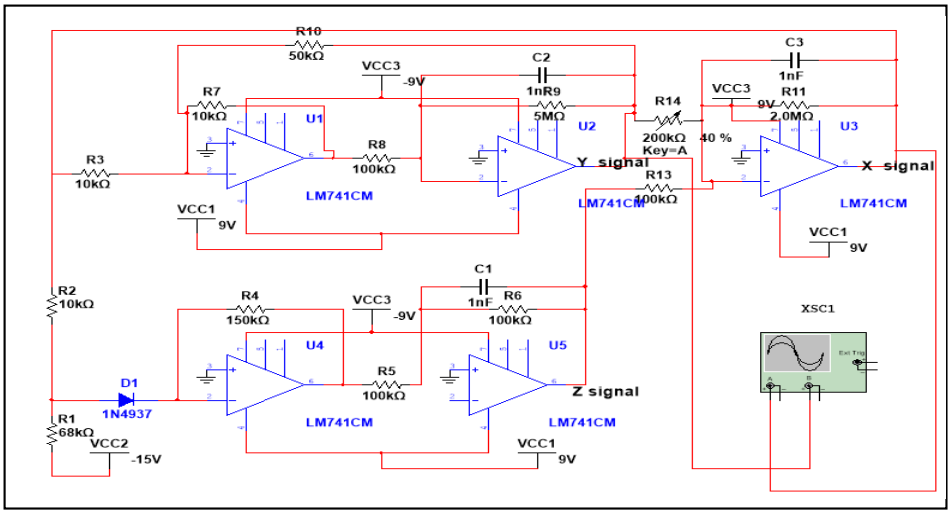

Fig.13: Schematic of the Rossler chaotic circuit

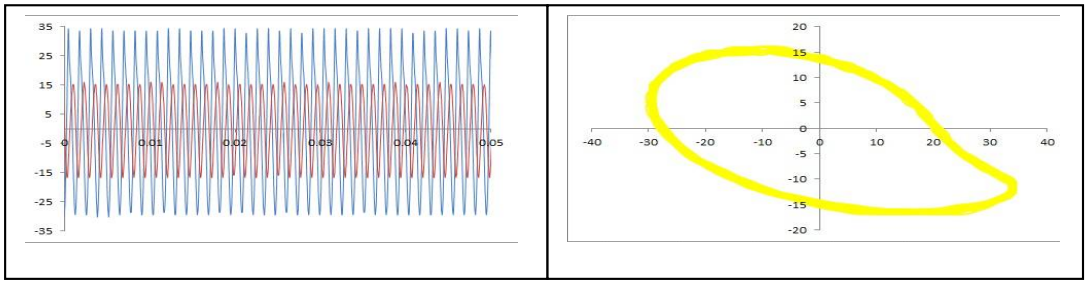

Fig.14.:(a) x and y vs. time at 94.5 kΩ (periodic signal), (b) attractor (one orbit).

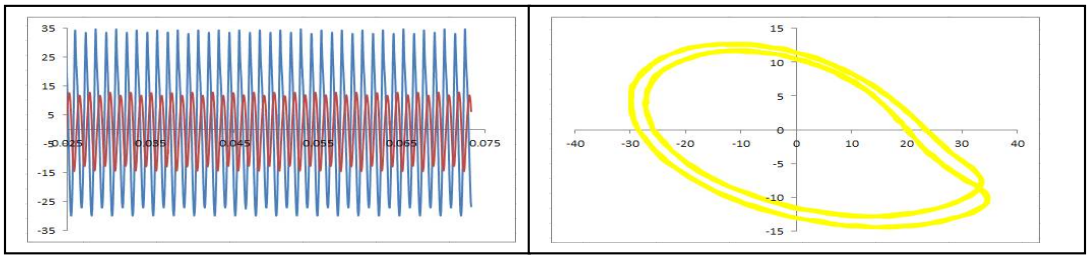

Fig.15:(a) x and y vs. time at 77.7 kΩ (periodic doubling), (b) attractor (two orbit).

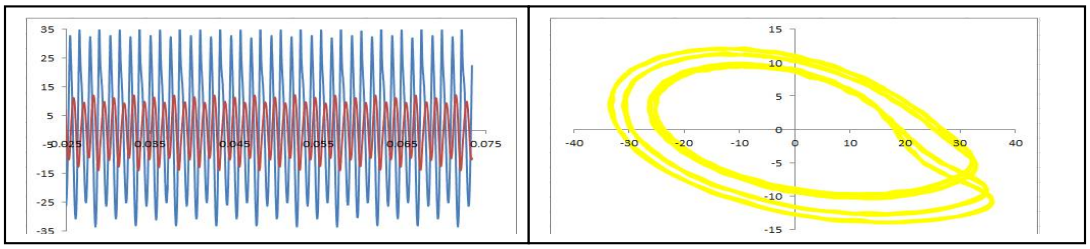

Fig.16:(a) x and y vs. time at 60.9 kΩ (second periodic doubling), (b) attractor (four orbit).

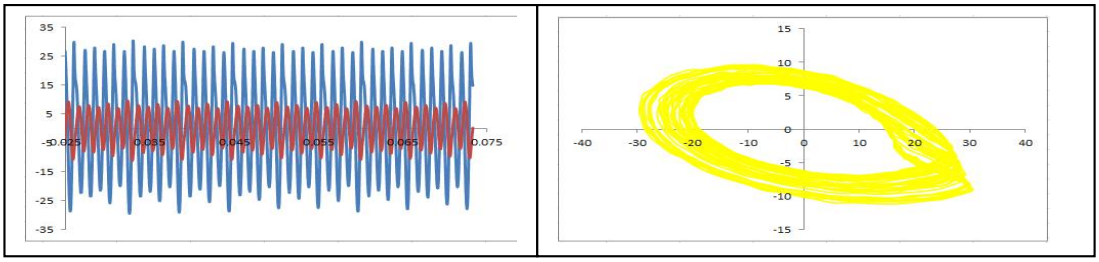

Fig.17:(a) x and y vs. time at 54.4 kΩ (chaotic system), (b) strange attractor.

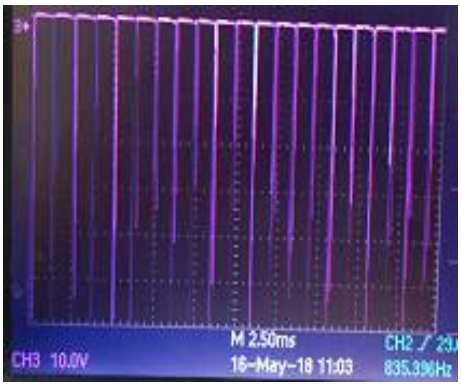

Fig .18.: Time series of z dynamic (chaotic signal) at Rv=54.4 kΩ.

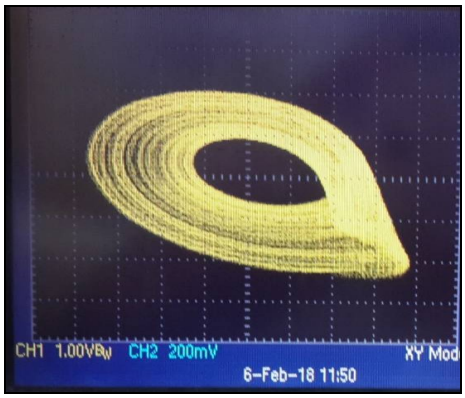

Fig.19: Chaotic homoclinic trajectory in phase space (x-y)

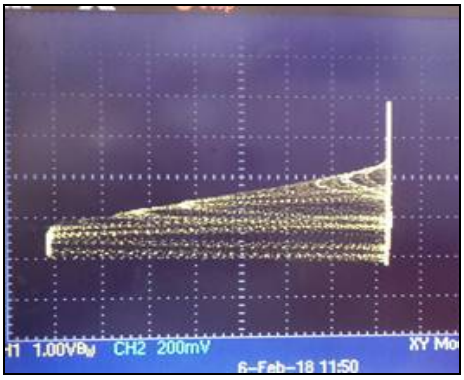

Fig .20:Chaotic homoclinic trajectory in phase space (y-z)

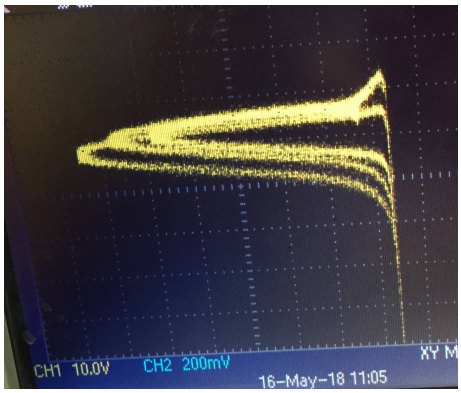

Fig.21.: Chaotic homoclinic trajectory in phase space (x-z)

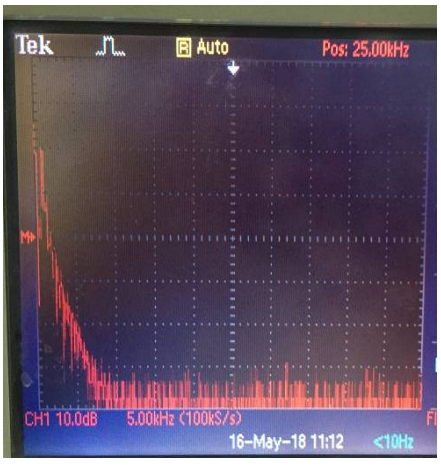

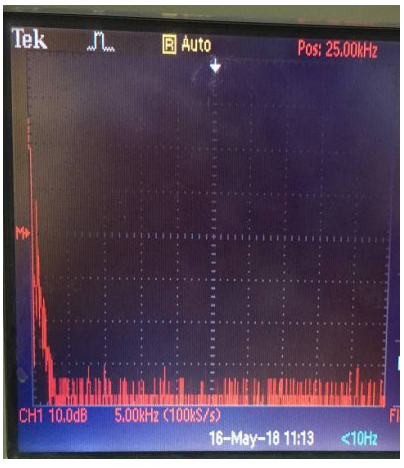

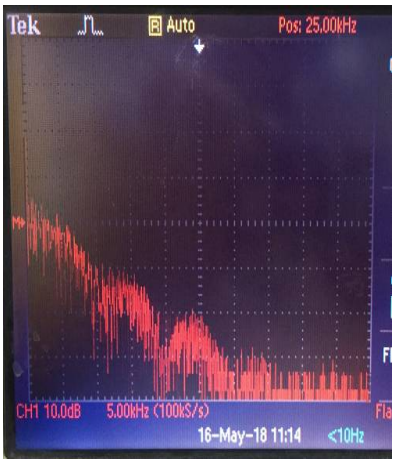

Fig.22: FFT spectra of x, y, and z dynamics respectively

Indian Journal of Natural Sciences www.tnsroindia.org.in ©IJONS

Vol.9 /Issue 52 / February / 2019 *International Bimonthly* *ISSN: 0976 – 0997*

RESEARCH ARTICLE

Surface Photometry and Morphology Properties of Spiral Galaxies: NGC4725, NGC4639 as Case Study

Huda Hardan and Abdullah. K. Ahmed*

Astronomy and Space Department, College of Science, University of Baghdad, Baghdad, Iraq.

Received: 18 Oct 2018 Revised: 20 Nov 2018 Accepted: 22 Dec 2018

***Address for Correspondence**
Abdullah. K. Ahmed
Astronomy and Space Department,
College of Science, University of Baghdad, Baghdad, Iraq.
E-mail: hudahardan1994@gmail.com / abdullahahmed1977@gmail.com

ABSTRACT

In this study, two active galaxies (NGC4725, NGC4639) have been chosen to study their morphological and photometric properties, by using the IRAF ISOPHOTE ELLIPS task with griz-filters. Observations are obtained from the Sloan Digital Sky Survey (SDSS) which reaches now to the DATA Release (DR14). The data reduction of all images (bias and flat field) has been done by SDSS Pipeline. The surface photometric investigation was performed like the magnitude. Together with isophotal contour maps, surface brightness profiles and a bulge/disk decomposition of the images of the galaxies, although the disk position angle, ellipticity, and inclination of the galaxies have been done. Also, the color of galaxies was studied, where chromatic distribution and extraction of chromatic processes were studied.

Keywords: Active Galactic Nuclei,Spiral Galaxy, Surface Photometry, and individuals: NGC4725, NGC4639.

INTRODUCTION

Surface photometry is a bidimensional broadband technique to quantitatively describe the light distribution of protracted objects like galaxies and HII regions. It is a technique rather than a distinct field of research [1].Was the first one to try applying surface photometry on galaxies so it is considered as one of the oldest techniques in modern astronomy Surface photometry is extremely important since it helps us to get information on galactic colors and its implied ages and metallicity gradients, stellar populations, dust content and its extinction, and structure, formation,and evolution of galaxies [2]According to Hubble, galaxies can be divided into the following types: elliptical(E), lenticular(S0), spiral or barred spiral(S, SB), and irregular(I).His original two-dimensional classification was known as the "tuning –fork" [3]. In this study, two active galaxies have been chosen, which is as follows:

NGC4725

The only barred spiral galaxy in our group of four is NGC4725. Shining at a dim magnitude of 9.2, this barred spiral is also a Seyfert galaxy as indicated by its bright nucleus. this galaxy is a distant 40 million light years and is a class SBa type galaxy-evident by the lightly wound spiral structure. What is fascinating about this galaxy is the determination of the distance to this galaxy was made possible by the use of 20 Cepheid variable stars [4].

Though most spiral galaxies, including our own Milky Way, have two or more spiral arms, NGC 4725 has only one. In this sharp color composite image, the solo Spiral mirabilis seems to wind from a prominent ring that kind of blue, newborn star clusters and red tinted star-forming regions. The odd galaxy also sports obscuring dust lanes a yellowish central bar structure composed of an older population of stars. NGC 4725 is over 100 thousand light-years across and lies 41 million light-years away in the well-groomed constellation Coma Berenices[5]**.** See Fig.1.

NGC4639

Is a barred spiral galaxy of some 45.000 light-years across that lies about 78 million light-years away from Earth in the constellation of Virgo, while it is moving away from us at roughly 1018 kilometers per second. It is a member of the Virgo Cluster of galaxies (also known as the Messier 87 Group), consisting of approximately 1300 (and possibly up to 2000) galaxies.NGC 4639 is a so-calledSeyfert 1 Galaxy, which are galaxies with extremely bright nuclei that produce spectral line emission from highly ionized gas. The centers of Seyfert galaxies have active galactic nuclei, and usually, contain supermassive black holes with masses between 10 and 100 million solar masses. Seyferts are classified as Type I or II, depending upon whether the spectra show both narrow and broad emission lines (Type I), or only narrow lines (Type II). The blue dots in the galaxy's outlying regions indicate the presence of young stars. Among them are older, bright stars called Cepheids, which are used as reliable milepost markers to obtain accurate distances to nearby galaxies. Astronomers measure the brightness of Cepheids to calculate the distance to a galaxy[6].

This barred galaxy exhibits a notable inner ring. The outer gaseous distribution is furthermore reminiscent of an outer pseudo-ring. This outer structure is visible in the B-band image but hardly in the NIR image, which principally shows the bar and the bulge. The velocity field is rather regular, consistent with a flat circular velocity pattern of the disc. It also shows streaming motions in the ring. A steep velocity rise is seen in the galaxy core[7]. See Fig.2.

METHODOLOGY

Basic Formulations

The datafor the two galaxies is obtained from the seventh Sloan Digital Sky Survey (SDSS) Data Release (DR7), which reaches now to (DR14)[8]. The bias and flat fieldwere corrected for all images by SDSS pipeline. The succeeding reduction of the data was carried out at National ResearchInstitute of Astronomy and Geophysics (NRIAG), using the standard procedures in the 1IRAF Package. All raw images were overscan modified, bias subtracted, and flat-fielded using the standard [1]IRAF tasks "quadprocess". The main reduction steps are as follows:

1.The sky contextualvalues arededucted by choosing empty regions in the image frame far from objects and measures its average intensity value.
2.Masking the superimposed and nearby objects, stars or galaxies as shown in Figure 3.
3-The IRAF ISOPHOTE ELLIPSE task is applied to obtain the intensity and structural profiles.
4.Transform pixel units into arcsec^2: by dividing on the scale (1 pixel = 0.396arcsec for Apache Point 2.5m Observatory (APO)).

5- Dividing frames by the exposure time value given in the header (the value is the same for all filters, it equals 53.907456 seconds).
6- Correct all frames for atmospheric extinction, galactic extinction, and transform to the standard system (using the zeropoint, atmospheric extinction and airmass of the SDSS photometric system at the time of observation) by multiplying the counts by the factor (***f)*** where:

$$f = 10^{(z_p + k*airmass)} \quad (1)$$

Where z_p and k are the zeropoint magnitude and the atmospheric extinction, respectively.Table 1 lists these values for the galaxy in each filter.

7- Convert to magnitude units by the formula[9]:

$$m = -2.5 \log (I) \quad (2)$$

Where m is the apparent magnitude and I is the intensity.Throughout this work Hubble constant was assumed to H0 = 73±4kms^{-1} Mpc^{-1}for NGC 4725 and 73kms^{-1} Mpc^{-1} for NGC 4369. Given the adopted distance to NGC 4725from the Tully et al. (2013), which is about 16.53 Mpc[9], and 13.34MpcwithTully-Fisher (1988) from NASA/IPAC EXTRAGALACTIC DATABASE (NED) to NGC 4369. The image scale for NGC4414was0.29pc/arcsec and 0.23pc/arcsecfor NGC 4369.

RESULTS AND DISCUSSION

Analysis Morphological

The ***griz***– image of NGC4725 barred galaxy where shown in Fig 1. The galaxy has a disky system with a bright bulge to about 20.4arcsec ,The neglect of the small bar in our fit resulted in a corresponding residual feature .this galaxy is like a ringed barred spiral galaxy because a prominent ring of stars encircles a bar of stars at its center .the brightness increase at the disk regions until it dissolves with the sky at end of disk to about 147.8arcsec.Fig.2. shows the ***griz***-images of barred galaxy NGC4639 exhibits a remarkable inner ring. The galaxy has a disky system with a bright bulge to about 8.27arcsec.the ends of the stellar bar and in a ring 30arcsec from the nucleus.The ***griz*** - isophotal contour maps of the NGC4725 active galaxy is shown in fig 4&5. The surface brightness levels are listed in table 2.

Analysis of Photometric Results
1-Position Angle, Ellipticity, and B4 Profiles

The position angle (PA), ellipticity (ε) and 4th harmonic deviations from ellipse (B4) of the two galaxies isophoteswere obtained as a function of the radius (***r)***, the distance from the center of the galaxy using the ellipse task of the STSDAS library in IRAF image-reduction system. The dependences of the position angle, ellipticity and B4 profiles on the distance from the center of the galaxy***r*** are shown in Figures 6, 7 and 8, respectively. It is noticed that the profiles show more or less similar behavior and consistency in the different bands.

For **NGC 4725**PA is Clearly fluctuated between the four filtersto about 26.9arcsec reaches to about 54º, then become constant at approximately 47º with some fluctuation at the end of the disk at about 200arcsec. the ellipticity profiles of NGC4725 increase from 0.06 in the center to about 0.62 at 58.9arcsec, decreases to 0.65 at the end of disk region (g=146.5arcsec).The B4(4th harmonic deviations from ellipse)profile illustrated in fig8a and presented in table 3 shows that the general trend of the galaxy is disky.
For **NGC 4639** the PA fluctuates, then decreases to about 102.3º, after this, it increases gradually, up to 156.4° at about 55.2", then became almost constant to the end of the disk. The ellipticity profile of NGC 4639 decreases from 17.3 at

0.5arcsec to about 43.9 at 0.2arcsec, then increases rapidly to 71.8 at 0.43 arcsec.The mean value of the B4 profiles is 0.0083, and illustrated in Fig8a and presented in Table 3 shows that the general trend of the galaxy is a disky system

Dissolution of Surface Brightness Profiles

The surface brightness profiles of the NGC 4414 and NGC 4369 galaxies have been decomposed to all ***griz-Filters***into a bulge which described by "$r^{1/4}$ law" proposed by de Vaucouleurs (1948)[10] to a good approximation (Eq.3) while the disk follows an exponential brightness profile (Eq.4).

$$\mu_{bulge}(r) = \mu_e + 8.3268\left[\left(\frac{r}{r_e}\right)^{1/4} - 1\right] \quad (3)$$

$$\mu_{disk}(r) = \mu_0 + 1.09\left(\frac{r}{r_0}\right) \quad (4)$$

Here, μ_e is the surface brightness at the effective radius r_e which is defined such that half of the brightness is emitted with inr_e. The central surface brightness and the scale-length of the disk are denoted by $\mu_0$and r_0, respectively.
The results of the decomposition, fitting and the residuals values from fittingwere shown in figure 9 andfigure 10 of ***griz-Filters*** from upper left to right. The resultswere also summarized in Tables 4, the surface brightness profiles of the two galaxies show that the outer disk of these galaxieswere of type II Freeman [11].

Color Profiles and metallicity gradients

Wirth (1981) and Wirth and Shaw (1983) obtained colors and color gradients for a moderate sample of spirals, using aperture photometry. They find that bulges show negative color gradients, which are small in earlier-type galaxies (E, S0, Sa) and several times larger in later types (Sb, Sc); Theyinterpret these gradients in terms of metallicitygradients [12].

For **NGC 4725:** Profiles of *g-r, r-i and i-z* color indices, along with the radius, were shown in figure 11. This galaxy has a star-burst galactic nucleus with (r = 13.6 arcsec); its effect is evident on the rest of the galaxy, where *g-r* = -0.454±0.259, *r-i*= -0.007±0.42and. *i-z* = 0.943±0.215.

And for **NGC 4369:** Profiles of *g-r, r-i,and i-z* color indices, along with the radius, were shown in figure 12. This galaxy has a star-burst galactic nucleus with (r = 5.7 arcsec); its effect is evident on the rest of the galaxy, where *g-r* = 0.183±0.18, *r-i*= -0.0014±0.14 and *i-z* = -1.52±0.16.

CONCLUSION

1-Data reduction was carried out using the procedures in the IRAF image-reduction Package, like sky subtracting,masking the superimposed and nearby objects, transform pixel units into arcsec^2, dividing frames by the exposure time value, correct all frames for (atmospheric extinction, galactic extinction, and transform to the standardsystem) and finally, convert to magnitude units by the formula 2.
2-The spiral galaxy NGC 4725 is a disky system with a very small, extremely bright nucleus in a faint,the galaxy has a symmetrical shape with the brightness increases at the disk, where the barred spiral galaxy NGC4639 is a disky system withbright regions of active star formation with non symmetrical bar shape and faint disc component.
3-from the photometric parameters, the spiral galaxy NGC 4725 tilted with approximately 46^o from the north, with semi-elliptical shape, with a disk inclined to about 54^o, while the barred spiral galaxy NGC 4639 is tilted with 112^o from the north, with semi-spherical shape, and the disc isinclined to about65^o.From the 4th harmonic of a Fourier expansion(B4), the general trend of the two galaxies is a disky system.

4-From the results of theDissolutionand fittingwas found that the type of the surface brightness profiles for the outer discs of the two galaxies is of type IIFreeman.
5-The color indices action in the inner and in the outer regions of these two galaxieswere showed anomaly for the color of normal spiral galaxies.

REFERENCES

1-Reynolds R.H,"The Light Curve of the Andromeda Nebula(NGC224),Monthly Notices of the Royal Astronomical Society,Vol. 74,1913,pp132-136.
2-OkamuraS., "Surface Photometry of Galaxies," Publications of the Astronomical Society of the Pacific, Vol. 100, No. 627, 1988, pp. 524-544.
3-Eskridge P. B., Frogel J. A., Pogge R. W., QuillenA. C., Berlind A. A., Davies R. L. et al. "Near-Infrared and Optical Morphology of Spiral Galaxies", ApJS. 2002 June; 143(1): 73-111.
4-Ricky Leon Murphy."Spiral galaxy Morphology and a Comparison of Four Spiral Galaxies". HET609 Semester 1-2005.
5-Robert Nemiroff (MTU) & Jerry Bonnell (UMCP)."Phillip Newman Specific rights apply", 2015.
6- SandageA..TammannG.A, and LabhardtL. (. Macchetto F.D and Panagia N. "(Space Telescope Science Institute and European Space Agency) "and NASA1992.
7-Cayatte, V.; Carignan, C; Amram A Virgo high-resolution Hα kinematical survey - II. The Atlas, AA, 03/2006.
8- Fix J D. Astronomy Journey to the cosmic frontier, 4th ed. New York: The McGraw Hill Companies; 2006.
9-Tully R. B.,Courtois H. M., Dolphin A. E., Fisher J.R. et. al. Cosmicflows-2: The Data. AJ. 2013 Oct; 146(4): 22.
10-Keel, W. C. "in The Road to Galaxy Formation", Springer & Praxis Publishing Ltd., p.21; 2007.
11-Freeman K C. "On the Disks of Spiral and S0 Galaxies". ApJ.1970 June; 160, 811.
12-Balcells M. and Peletier R. F."Colors and color gradients in bulges of galaxies". AJ. 1994 Jan; 107(1): 135-152.

Table 1 Correction Values: air masses, zero points, and atmospheric extinctions

Galaxy	Band	Air mass	Zero point	Atmospheric Extinction
NGC 4725	***g***	11.008	-24.350	0.1684
	r	1.0092	-24.0003	0.07035
	i	1.0089	-23.657	0.04544
	z	1.0086	-23.39	0.0487
NGC 4639	***g***	1.11307	-24.4	0.194
	r	1.11113	-24.06	0.095
	i	1.1183	-23.69	0.0567
	z	1.026	-21.965	0.0453

Table 2 Outer isophotal level and steps of the contours of NGC 4414 and NGC 4369galaxies.

Galaxy	Band	Outer isophot level (mag)	Outer isophot level (mag/arcsec²)	Steps
NGC4725	***g***	25.063	23.051	1.269
	r	24.812	22.801	1.117
	i	24.494	22.801	1.269
	z	24.485	22.474	1.458
NGC 4639	***g***	26.139	24.128	2.131
	r	25.354	23.343	1.938

	i	25.581	23.57	2.429
	z	23.814	21.802	1.549

Table 3 Isophotal position angle, Ellipticity,andInclination ofNGC 4414, NGC 4369.

Galaxy	Band	PA(°)	Ellipticity(ε)	Inclination(°)	B4
NGC 4725	***g***	48.7±4	0.32±0.09	65.8±6	0.00344
	r	44.6±6	0.28±0.1	44.8±9	0.01759
	i	33.5±0.1	41.2±9.3	44.7±9	0.00243
	z	40.6±0.15	50.5±4.3	61.04±7	0.00174
	global value	41.85±5.2	92.5±3.6	54.085±7.7	0.00630
NGC 4639	***G***	138.9±11	0.32±0.09	48.8±7	-0.03646
	r	142±12	0.32±0.08	48.5±7	1.79E-02
	i	142±8	0.32±0.09	48.8±8	0.02
	z	141±9	0.31±0.08	47.5±7	0.02199
	global value	140.9±10	0.32±0.08	48.4±7.25	0.001686

Table 4 Dissolution parameters of NGC 4725 and NGC 4639.

		Bulge				Disk				
	Band	range (arcsec)	μ_e (mag/arcsec^2)	r_e (arcsec)	Standared error	μ_o (mag/arcsec2)	r_o (arcsec)	Standared error	LB_T (mag)	B/D
NGC 5725	***g***	4.5-25.1	24.033	48.002	0.034	22.62	72.14	0.068	12.23	0.23
	r	4.59-24.6	21.3	44.8	0.03	19.5	44.2	0.104	9.698	0.386
	i	4.59-24.6	21.34	48.206	0.028	19.142	36.243	0.248	9.54	0.441
	z	4.59-24.3	23.938	44.359	0.028	22.48	52.2	0.048	12.314	0.559
NGC 4639	***g***	3.22-12.26	25.76	79.07	0.015	21.4	13.6	0.108	12.8	1.219
	r	4.61-14.05	23.92	95.9	0.013	19.9	17.174	0.097	10.62	1.54
	i	3.551-12.26	24.24	85.5	0.013	19.8	13.5	0.11	11.1	1.288
	z	4.53-13.98	26.30	86.85	0.013	22.98	22.58	0.153	13.22	1.311

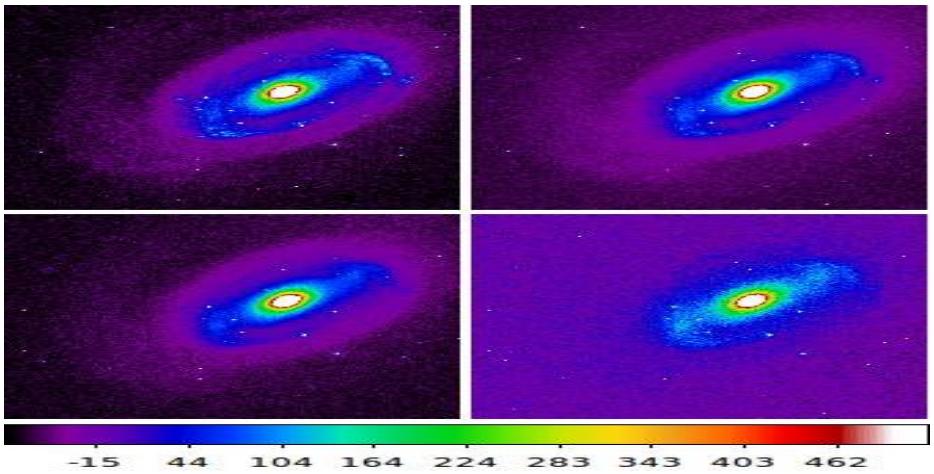

Figure 1 false-color image of NGC4725an intermediate barred spiral galaxy with griz-Filters, from left to right. North is up and East is at left.

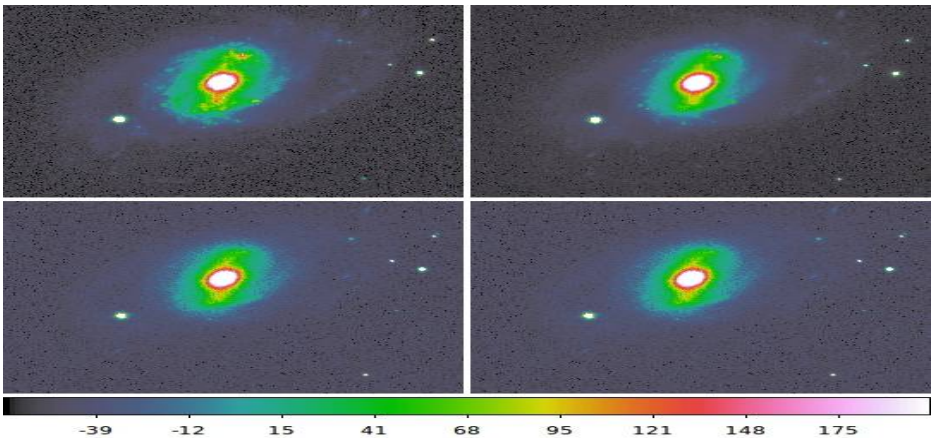

Figure 2.Fuzzycolor images of NGC 4369 active galaxy with griz-Filters, from left to right. North is up and East is at left.

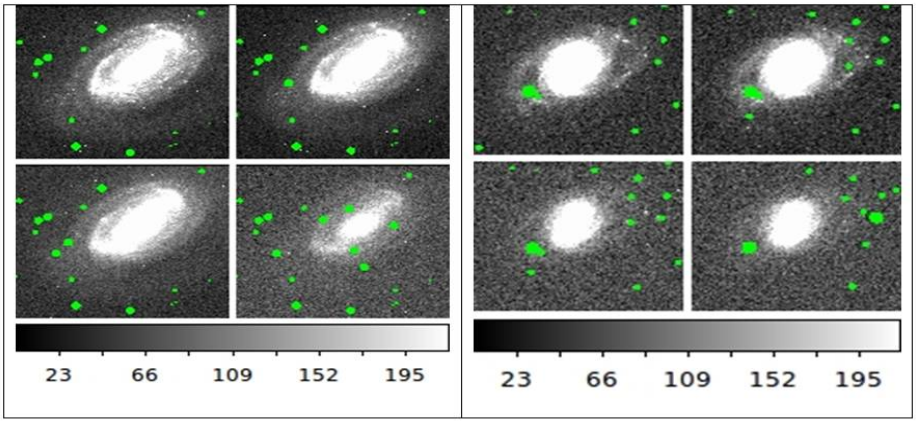

Figure 3.griz-Filters mask region, left NGC4725 and right NGC4639.

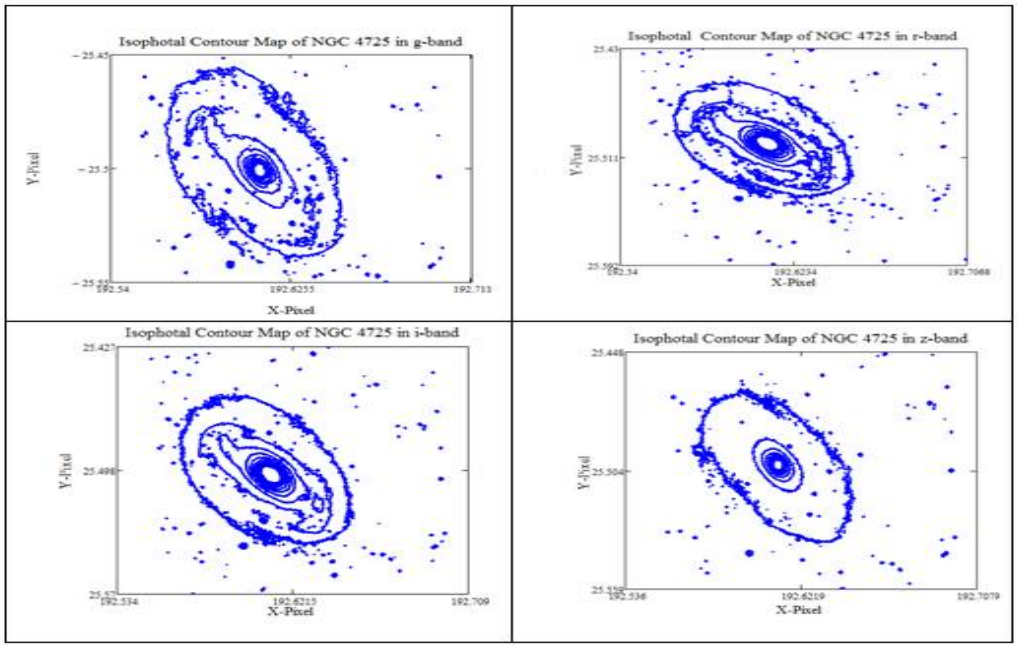

Figure 4 Isophotal Contour Maps of NGC 4725 Galaxy in gri and z-bands, North is up and East is at left.

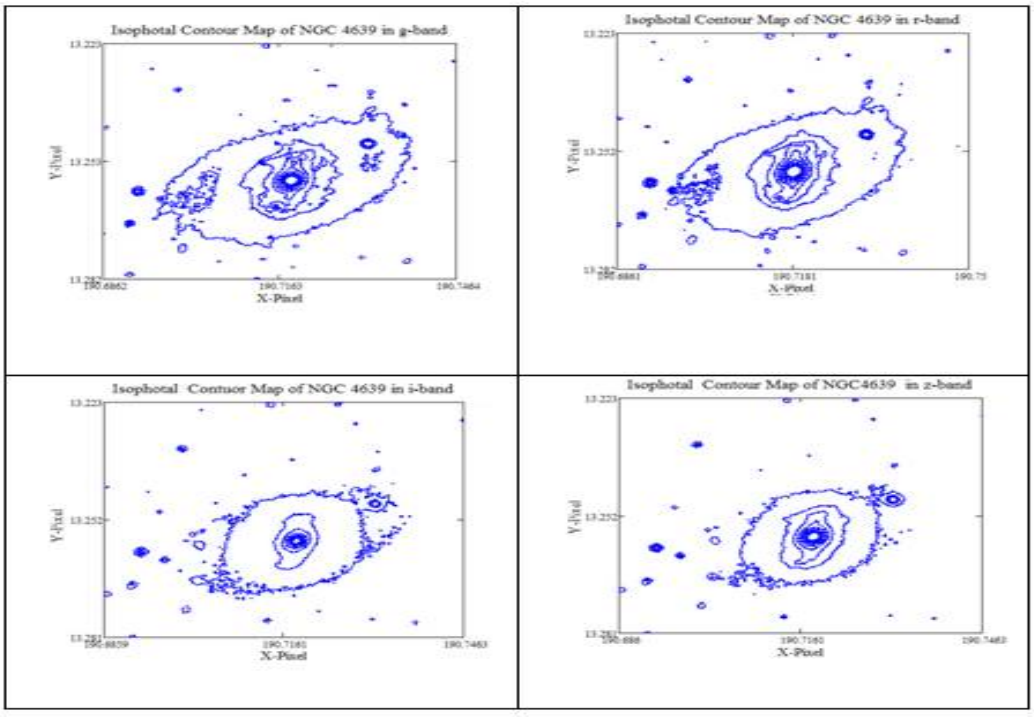

Figure 5 Contour Maps of NGC 4639 Galaxy in gri and z-bands, north is up and East is at left.

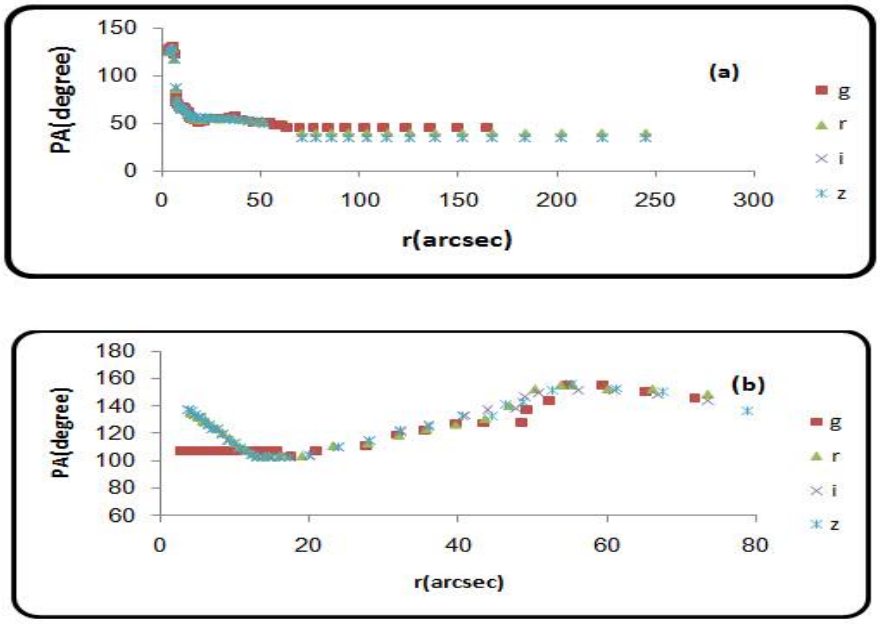

Figure 6 Position angle profiles of a-NGC 4725,b-NGC 4639 in griz-bands

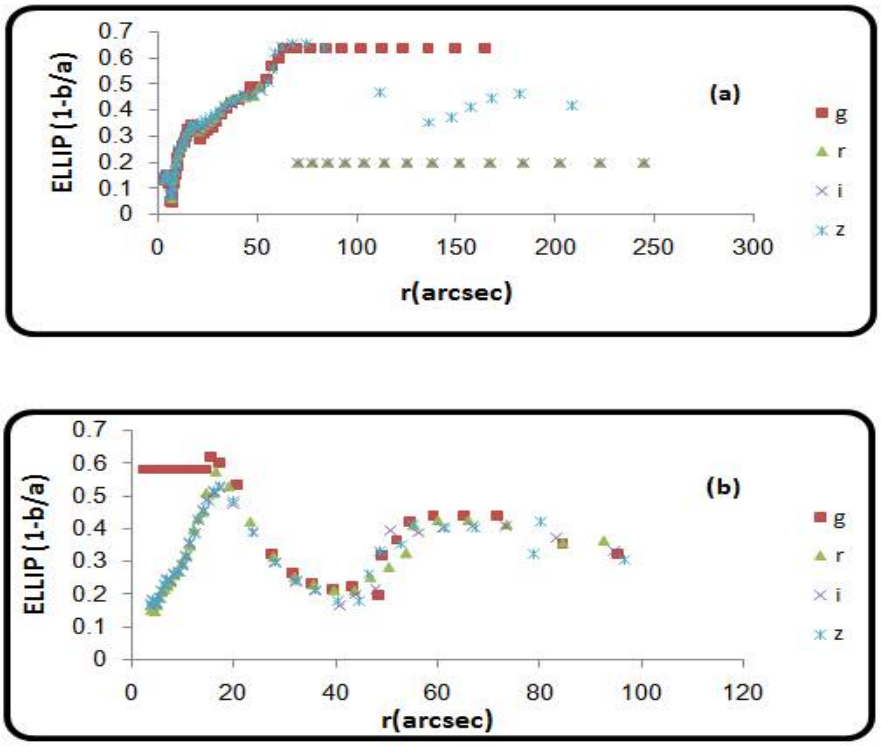

Figure 7. Ellipticity profiles of a-NGC 4725,b- NGC 4639 in griz-bands.

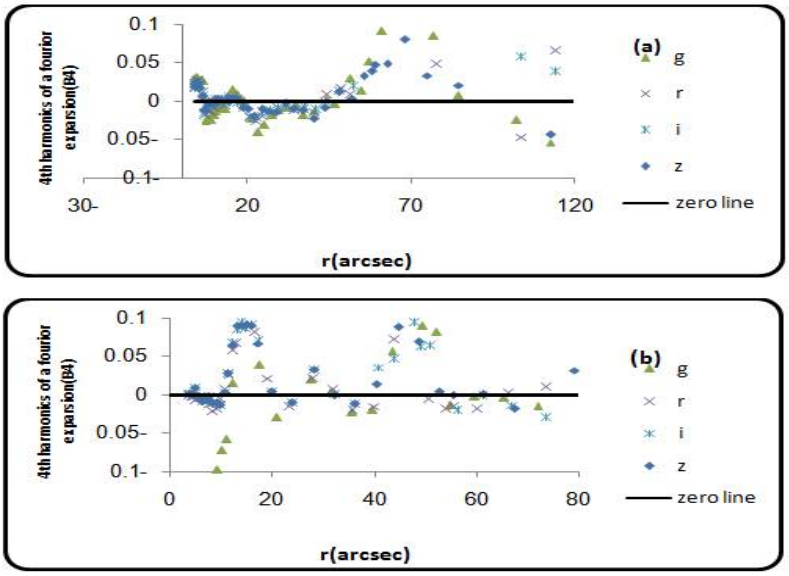

Figure 8. B4 profiles of a- NGC 4725,b- NGC 4639 in griz-bands.

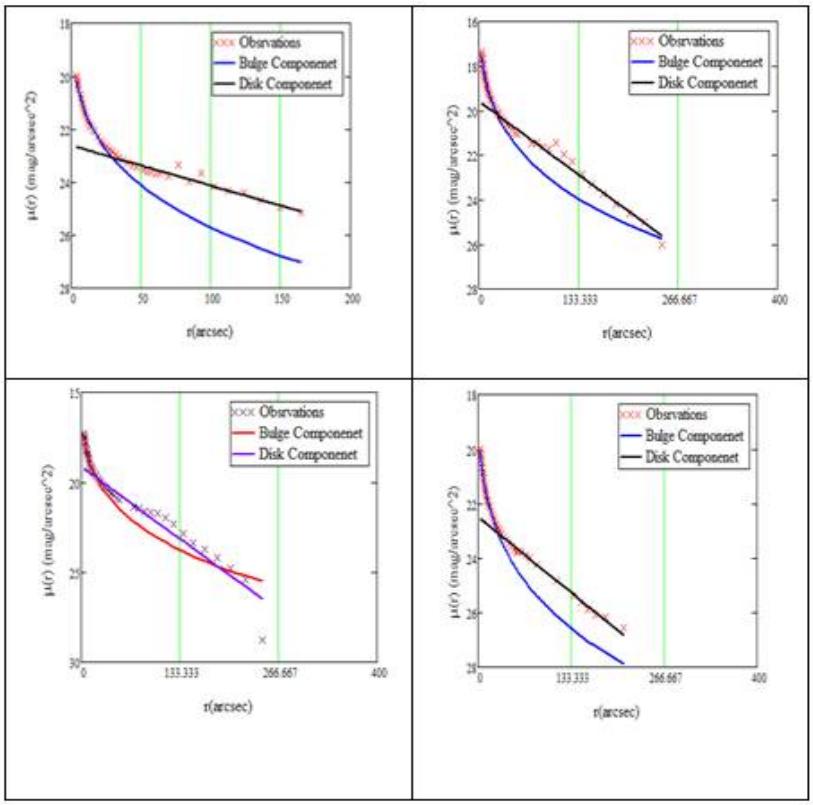

Figure 9. ProfilesDissolutionof *griz*-Filters and the observed data for NGC 4725.*griz*-Filters from upper left to right.

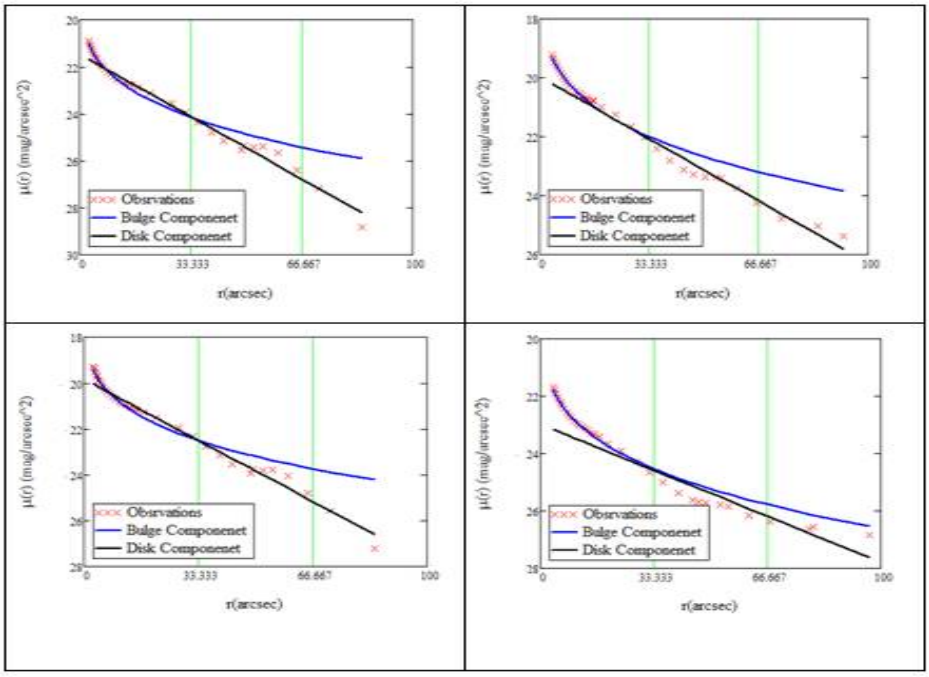

Figure 10. Profiles Dissolutionof *griz*-Filters and the observed data for NGC 4639.*griz*-Filters from upper left to right.

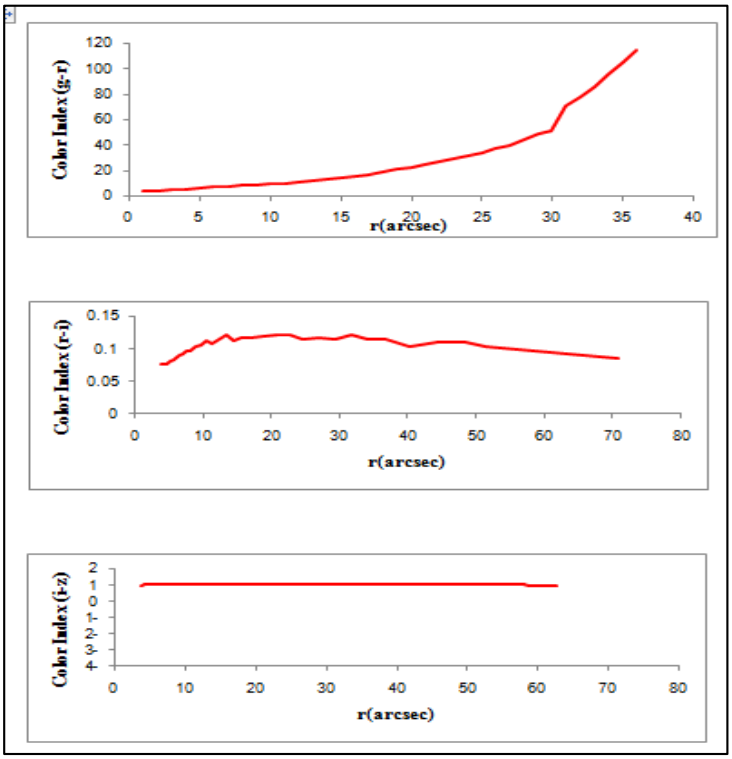

Figure 11.Color profiles of NGC 4725.

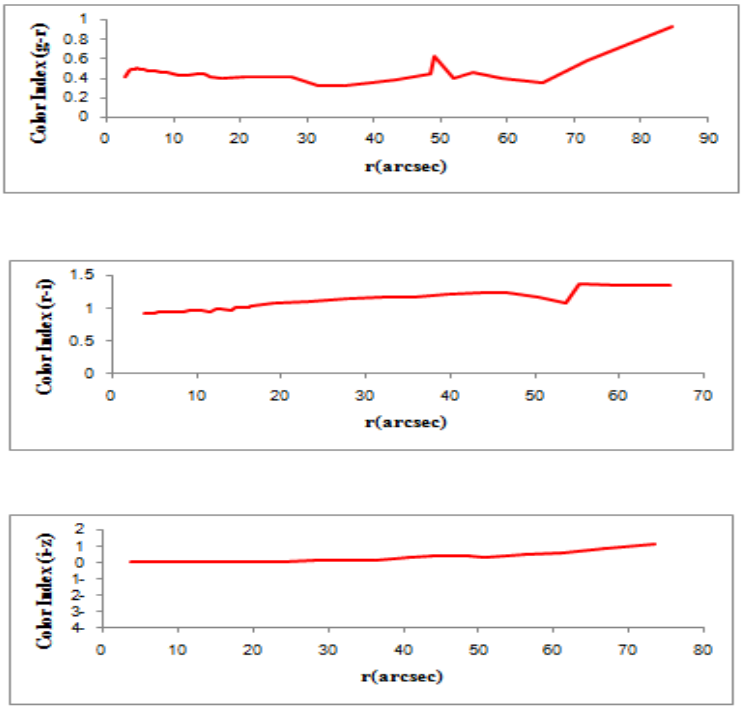

Figure 12. Color profiles of NGC 4639.

Indian Journal of Natural Sciences www.tnsroindia.org.in ©IJONS

Vol.9 /Issue 52 / February / 2019 *International Bimonthly* *ISSN: 0976 – 0997*

RESEARCH ARTICLE

Topical Effects of Metformin on Induced Ocular Hypertension in Rabbits

Ali Jasim[1], Haitham M Kadhim[2] and Ahmed Majeed Rasheed[3]

[1]MSc. Pharmacology Department, College of Medicine, Al-Nahrain University, Baghdad, Iraq
[2]Assist. Prof. Pharmacology Department, College of Pharmacy, Al-Nahrain University, Baghdad, Iraq
[3]FICMS.Ophthalmology, College of Medicine, Al-Nahrain University, Baghdad, Iraq.

Received: 18 Oct 2018 Revised: 21 Nov 2018 Accepted: 23 Dec 2018

*Address for Correspondence
Ali H. Jasim
Pharmacology Department,
College of Medicine,
Al-Nahrain University,
Baghdad, Iraq.

ABSTRACT

The present study was designed to evaluate the possible intraocular pressure lowering effect of corneal instillation of metformin in experimentally corticosteroid induced ocular hypertensive eyes of rabbits, and to explore the possible anti-oxidant and anti-inflammatory activities and the possible side effects of the tested drugs on eyes after instillation. Group of (40)adult male of New Zealand rabbits,were divided to 3 groups: isotonic buffer group (8 normotensive rabbits), this group was instilled with isotonic buffer solution in the right eye and DW in the left eye to show if there is any effect of the vehicle (isotonic solution) on the eye, latanoprost group(8 rabbits) were both eyes of this group have been induced for ocular hypertensive,the right eyes instilled with latanoprost (0.005%) drop once daily which considered as a positive control group, while the left eyes instilled with DW once daily which considered as a negative control group., metformin group (24 rabbits), divided in to (3) subgroups 8 rabbits in each to evaluate the effect of metformin (0.5%, 1%&2%) drop that instilled twice daily. The present day study demonstrated that metformin has a significant intraocular pressure lowering effect and a significant anti-oxidant and anti-inflammatory activities.

Keywords: intraocular pressure, metformin and latanoprost.

INTRODUCTION

Glaucoma defined as a group of optic neuropathies characterized by progressive retinal ganglion cells (RGCs) degeneration (weinreb*et al,2014*), resulted from fluid builds up in the front part of the eye. That extra fluid increases the pressure in the eye(keristan,2017). According to The World health Organization, glaucoma accounted for 2 percent of visual impairment and 8 percent of global blindness in 2010(WHO,*2017)*. It is a family of related diseases

frequently associated with elevated IOP which is exceeds 21 mmHg and may be as high as 70 or 80 mmHg during the attack(jay and Murdoch,1993).many factors lead to Retinal ganglion cell death (RGC death) include; elevated intraocular pressure , vascular dysregulationand oxidative stress(kaushik*et al,2003*)..the production and drainage of aqueous humor must be in Equilibrium to maintain the intraocular pressure within the normal range despite that disruption in aqueous inflow, outflow, or both, results in raise of intraocular pressure , which is a major risk factor in the pathogenesis of glaucoma(Goel*et al,2010*).·Open-angle glaucoma which is the most common form of glaucoma, accounting for at least 90% of all glaucoma cases(Glaucoma research foundation,2017).

Reduction of intraocular pressure is the primary goal in patients with glaucoma (Chang and Goldberg,*2012*). However, even with treatment to lower IOP and even in normal tension glaucoma optic nerve damage may progress(Mckinnon*et al,2008*) . There is an excessive formation of free radicals and oxidative stress is recognized as an etiopathogenetic factor and a significant depletion in antioxidant potential in glaucoma-affected patients (Ferriera et al,2004) .Neuroprotection in glaucoma is aimed at protecting those neurons that are damaged or likely to be damaged in glaucomatous optic neuropathy which consists of neurons along the entire visual pathway, chiefly the RGC axons. This strategy is an addition to that achieved by IOP lowering alone. Even though any treatment approach that preserves RGCs in glaucoma could be described as neuroprotective(Weinreb and Levin,*1999*).the intraocular pressure lowering effect of Metformin may be AMPK activationwhich in turn activates neuronal nitric oxide synthase (nNOS)and endothelial nitric oxide synthase eNOS(Fryer *et al,2000*), Enhanced NO levels facilitate outflow of aqueous humor in the TM to contribute to the normalization of the IOP accompanied by an up-regulation of iNOS gene expression(Lei,et al,*2015*)

Activation of AMPK leads to phosphorylation of Rho kinase(Gayard*et al ,2011*) which serine/threonine kinases that regulate smooth muscle contraction in which selective ROCK inhibitors could increase aqueous humor drainage through the TM, leading to a decrease in IOP(Rao and Epestin, 2007). Metformin decreased interaction with ROCK and subsequent decrease in ECM deposition. With decreased extracellular matrix (ECM) deposition in the TM and weaker intracellular actin stress fibers, aqueous humor outflow facility is enhanced and IOP is consequently reduced(Ayan*et al,2014*).the anti-oxidant effect of metformin may be via AMPK activation leading to reduce ROS production and then increase GSH levels(A.C *et al,2003*).Metformin also ameliorates ischemia-reperfusion injury by increasing the level of glutathione peroxidase (GPx), super oxide dismutase (SOD), catalase and MDA levels in cerebrum(Lukasz *et al,2016*) and the anti -inflammatory effect of metformin may be related to the inhibition of neuclear factor kappa b (NFκB) activation in macrophages so rducingpro-inflammatory cytokines (interleukin (IL)-1β, IL-6 and tumor necrosis factor (TNF)-α production (Hyun *et al,2013*)

MATERIALS AND METHODS

Group of (40) adult male of Zealandrabbits weighing 1.5 to 2 kg with no signs of ocular inflammation or gross abnormality were used in this study. Isotonic buffer group (8 normotensive rabbits),this group was instilled with isotonic buffer solution in the right eye and DW in the left eye to show if there is any effect of the vehicle (isotonic solution) on the eye. Latanoprost group(8 rabbits) both eyes of this group have been induced for ocular hypertensive ,the right eyes instilled with latanoprost0.005% drop (1-2drop) once daily which considered as a positive control group,While the left eyes instilled with DW which considered as a negative control group. Metformin group (24 rabbits), divided in to (3) subgroups. (8 rabbits): instilled with metformin 0.5% drop. (8 rabbits): instilled with metformin 1% drop. (8 rabbits): instilled with metformin 2% drop.

The right eyes of these groupswere induced for ocular hypertensive and instilled with (1drop) of metformin droptwice daily for 7 days. These concentrations were chosen after doing a pilot study on 6 animals using different

concentrations of the tested drugs and the used concentrations were chosen depend on the effect and adverse effect. Animals were housed individually in aplastic cages; all rabbits were maintained conventionally during the study with regulated air temperature (15-21 c), an artificial light cycle (12 hours light /12 hours darkness) and good ventilation. They fed a standard rabbit diet and had free access to drinking water(Mohammad *et al,2018*).

Induction of ocular hypertension

According to Melana((1998) and co-workers who found that this model of induction of Ocular hypertension is mimic human chronic open angle glaucoma(Melana*et al,1998*). the procedure as following: After proper anesthetization of eyes by local instillation of 2% lidocaine HCL , a subconjunctival injection (by using a micro-fine syringes, 30 gauge × 1/2 inches) of 0.7 ml of betamethasone suspension containing betamethasone sodium phosphate (3 mg/ml)and betamethasone acetate (3 mg/ml).using this formulation providesa readily accessible (sodium phosphate) and a sustained release(acetate) fraction of betamethasone. measures of IOP repeated twicea week to avoid corneal epithelium damage through too-frequent tonometry. the first measure being taken immediately beforethe weekly betamethasone subconjunctival injection and the secondtaken after 3 days. Three base-line IOP measures were recordedduring the week before betamethasone treatment. The valueobserved at zero time (first betamethasone injection) was consideredthe starting pressure. The animals received weekly subconjunctival injections of betamethasone over a period of 21 days (four doses given). The instillation of the tested drugs wasstarted at the 24th day of corticosteroid treatment (3 days afterthe fourth subconjunctival injection).. Tested drug was instilled in the right eyes as one drop (50µl) for 7 days twice formet form in (only after the ocular hypertension was definitely established) .

Preparation of Metformin ophthalmic solution

In the preparation of aqueous ophthalmic drops, a careful consideration of the need for isotonicity, a certain buffering capacity, the desired pH, the addition of antimicrobial agents and/or antioxidants, the use of viscosity-increasing agents, and the choice of appropriate packaging(The international pharmacopeia,2016). Ophthalmic solutions are isotonic, sterile, free from foreign particles, and specially prepared for instillation in the eye (Hecht,2000).

IOP measurement

After local anesthetization of the cornea with 1-2 drops of 2% lidocaine HCL ophthalmic solution, the animal was hold and Schiotz tonometer is placed on the cornea. A control or zero time value of IOP was taken 15 minutes (min) before the administration of tested drug . One drop of freshly prepared tested drug was instilled in the middle of inferior conjunctival sac followed by lid closure. Thereafter, IOP was measured after (1 hour) of topical application of tested drug. Metformin instilled as one drop (50µl) for 7 days twice daily and IOP measured daily at about the same time to avoid diurnal IOP fluctuation.cleansing the instrument with diethyl ether after each measurement properly to suppress growth of bacteria and other microorganism being introduced by the device or during drug administration, ophthalmic eye drop preparation containing a suitable antibacterial agent (chloramphenicol eye drop about 1-2 drops) were instilled in the eye rabbits at the end of each experiment(Mosses,1997).

Pupil diameter

Pupil diameter measurement was done by using the pupil gauge. The obtained results represented in millimeter unit (Ahuja,2003).

Light reflex

Pupillary response or the light reflex of both eyes was tested by swinging flashlight to detect a relative afferent papillary defect. The obtained results would be presented as either it was intact or absent (Jampel,2001).

Corneal reflex

Both eyes were tested by using wisp of cotton wool it applied from the side and award of its approach. The obtained results would be presented as either it was intact or absent (Ahuja, 2003).

Conjunctival redness

Both eyes was tested to detect by inspection of conjunctiva . The obtained results would be presented as either it was present or not (Macdonald,2000) .

Lacrimation

It could be detected by inspection of conjunctiva of both eyes. The obtained results would be presented as either it was present or not (Macdonald,2000).

Aqueous humor collection (AH):

This step will done for the measurement of the antioxidant and the anti-inflammatory effect of the tested drugs. aqueous humorwas collected carefully from the anterior chamber of rabbit's eye using 27-gauge needle after administration of diazepam 1 mg/kg i.v. and ketamine 25 mg/kg i.v. without causing any injury to the iris or lens throughout the procedure (Gupta *et al,2011*). the onset of anesthesia provided by ketamine begin after six minutes and the peak effect after ten minutes which persist about forty minutes (Green and Knight,1981), the combination of ketamine with diazepam produce surgical anesthesia in rabbit that continue for up to 30 minutes (Flecknell,2009). After collection, samples were immediately stored at temperature (−20°C) till the performance of various biochemical analysis from AH (Gupta *et al, 2001*).

Glutathione (GSH) determination in aqueous humor samples

This test was performed for the determination of the glutathione (GSH) levels in rabbit's aqueous humor.
Assay principle: The ELISA kit was used is a Competitive-ELISA.

Tumor necrosis factor alpha determination (TNF-α) in aqueous humor samples

This test was performed in mini market research and consumer center laboratories for the determination of the tumor necrosis factor alpha (TNF-α) levels in rabbits aqueous humor. Assay principle: The kit was used based on sandwich enzyme-linked immune-sorbent assay technology

Statistical analysis

The results were presented as means ± standard error of mean(SEM). One way analysis of variance (ANOVA) followed by Tukey test comparison was utilized to compare between groups. The differences between the means are studies as significant at the P< 0.05. This done by Microsoft excel 2016 and SPSS version 23. The concentration that

decreases 50% of the IOP this value was analyzed by linear regression equation and logarithmic equation. The level of significance was set at P<0.05 as significant (Daniel and Yu, 2008)

RESULTS

Effect of Isotonic buffer solution and DW on normotensive rabbits eyes

Response of mean IOP

The effect of isotonic phosphate buffer (vehicle) used for preparation of ophthalmic solution of the tested drugs on mean IOP of rabbits right eyes did not reach the level of statistical significant ($P \leq 0.05$) during the time course of the experiment (7 days).

Effect of Distilled Water

Response of mean IOP

Effect of DW on mean IOP of rabbits left eyes nearly remained constant during the time course of experiment (P = 0.949).Fig 1 Isotonic buffer solution and DW application in the present study had no effect on pupil diameter and no effect regarding other possible side effect (i.e. light reflex, corneal reflex, conjunctival redness and lacrimation).

Effect of latanoprost (0.005%) Drop

Response of mean IOP

Post induction of ocular hypertension , the mean IOP was (33.1 ± 2.88mmHg). After one hour of latanoprost 0.005% application the mean IOP decreased by (5.19mmHg) with significant effect compared to distilled water that the decrease started from the first day of treatment till the last 7th day with highly significant decrease (p<0.001).Fig 2 latanoprost drop application in the present study had no effect on pupil diameter and no effect regarding other possible side effect (i.e. light reflex, corneal reflex, conjunctival redness and lacrimation).

Effect of Metformin (0.5%, 1%,2%) Ophthalmic drop

Response of mean IOP

Mean IOP of Metformin(0.5%)

Post induction of ocular hypertension, the mean IOP was (32.05±1. 98mmHg),after one hour of metformin 0.5% instillation(twice daily), the mean IOP reduced by (0.5mmHg) which found non-significant (p>0.05). in the 3rd day the reduction of the mean IOP started (30.91±1.65 mmHg) with statistical significant (p<0.05)and reach maximum reduction in 7th day (25.4750±1.94) which consider highly significant (p<0.001)when compared with latanoprost and distilled water. Fig 3

Mean IOP of Metformin (1%)

In the 1st day, there was significant difference (p<0.05). whereas from the 2nd day to the 7th day a high significant decrease in the intraocular pressure noticed (p<0.001)when compared with DW, and there was no significant

differences in the reduction of the mean IOP between metformin 1% and latanoprost 0.005% from 2nd day to the 6th day (p>0.05).Fig 4

Mean IOP of Metformin (2%)

Post induction of ocular hypertension, the mean IOP was (32.06±1.97mmHg),after one hour of metformin 2% instillation the mean IOP reduced by (3.98mmHg) which found highly significant (p<0.001).maximum reduction achieved till the 7th day of treatment 15.50±2.72(p<0.001). Fig 5 in the present study,metformin (0.5%,1%,2%) had no effect on pupil diameter and no effect regarding other possible side effect (i.e. light reflex, corneal reflex, conjunctival redness and lacrimation).

Percent of intraocular pressure reduction

Comparing to latanoprost 0.005% IOP reducing effect ,metformin 2% , metformin 1% and metformin 0.5% showed the higher IOP reducing effect in the trial study . Fig 7

Determination of the antioxidant activity of metformin by measuring glutathione (GSH) levels in rabbit's aqueous humor

The result here indicated that there was a significant elevation in GSH levels among the metformin groups regardless the positive and the healthy group (p<0.008) .Maximum elevation of glutathione (GSH) levels was found in metformin 0.5% group (p=0.007).table 1, Fig 9

Determination of the anti -inflammatory activity of metformin by measuring tumor necrosis factor alpha (TNF-α) levels in rabbit's aqueous humor

There was a significant decrease in the TNF- α level in all metformin groups (p<0.05). Maximum reduction in TNF-α level accrued in group G(metformin 1%) group . Which was found to be highly significant (p<0.001).table 2, Fig 10

DISCUSSION

In the present study, the distilled water could not changed the mean of IOP in normotensive eyes of the rabbits after 7 days of instillation, and there was no significant effect (P > 0.05) when compared mean of IOP during trial period with pre-treatment mean of IOP.this agreed with (Heijl*et al,2002*). In the present study, the eye drops formulation of tested drugs (Metformin)were used inactive ingredients which include : sodium chloride, benzalkonium chloride, ethanol, phosphate buffer. Furthermore, these inactive ingredients did not changed the mean of IOP in normotensive eyes of the rabbits eyes after 7 days of inactive ingredients instillation and there was no significant effect (p>0.05) when compared mean of IOP during pre-treatment mean of IOP with trial period,this agreed with (Allen *et al,2005*). In present study , the effectiveness of betamethasone as an inducing agent for ocular hypertension could not counteracted by the distilled water.

Furthermore, distilled water had no effect on the tested parameters in this study thus; it could be accepted as a negative control group regards study of effect of tested drugs. This effect confirmed by(Urcola*et al,2002*). In present study, latanoprost had a noticeable ocular hypotensive effect on induced hypertensive eyes.Latanoprost (0.005%) eye drop was used as positive control to test the ocular hypotensive effect of most experimented drugs and its preferred in chronic open glaucoma(Achilles and pappano,2007).Latanoprost (0.005%) produced (45.23%) reduction in mean IOP at day 7, these results are strengthened by (Patelska*et al,1997*,Gupta and yucel ,2007.Perry *et*

al,2003)Latanoprost 0.005% drop application in the present study had no effect on pupil diameter and no effect regarding other possible side effect (i.e. light reflex, corneal reflex, conjunctival redness and lacrimation).the present study demonstrated that single drop of metformin 0.5% produce an obvious hypotensive effect and reduce the mean IOP by (19.26%) after 7 day treatment when compared with that of DW group, and there is a comparable hypotensive effect when we compared metformin(0.5%) to that of latanoprostgroup.Also the present study clearly demonstrated that metformin (1%) was able to decrease mean IOP in ocular hypertensive rabbits by (43.81%) after 7 day treatment. Also the present study demonstrated that metformin (2%) was able to reduce the IOP by (44.79%)after 7 days treatment . Metformin drop application in the present study had no effect on pupil diameter and no effect regarding other possible side effect (i.e. light reflex, corneal reflex, conjunctival redness and lacrimation). Regarding the anti-inflammatory and the anti-oxidant activities of metformin ,the present study demonstrated that topical instillation of metformin (0.5%,1%,2%) produce a significant elevation in glutathione (GSH) levels (p=0.008) and a significant reduction in tumor necrosis factor –alpha levels in rabbits aqueous humor via dose independent AMPK activation(Gao ,*et al,2013*).(p=0.028).

CONCLUSION

The topical instillation Metformin has a significant intraocular pressure lowering effect as compared with negative control group (DW group) and positive control group (Latanoprost group). and have a significant antioxidant activity 3)and anti-inflammatory activity also it was found to be Safe in their applied doses .

ACKNOWLEDGMENTS

We are grateful to all staff of the Department of Pharmacology in the College of Medicine ,Al-Nahrain University .

REFERENCES

1-Maritim, A. C. SandersR. A.and WatkinsJ. B. (2003) "Diabetes, oxidative stress, and antioxidants: a review," *Journal of Biochemical and Molecular Toxicology, vol. 17, no. 1, pp. 24–38.*

2-Achilles J. Pappano (2007): Cholinocepter-Activation & Cholinesterase-Inhibiting drugs: Katzung B.G. Basic and Clinical Pharmacology. 10th ed. McGraw Hill. Boston. Pp.103.

3-Ahuja M. (2003): Ophthalmology Handbook. 1st ed. India Binding House. Delhi. Pp. 6-24, 145-163.

4-Ahuja M. (2003): Ophthalmology Handbook. 1st ed. India Binding House. Delhi. Pp. 6-24, 145-163.

5-Allen LV, Popovich N.G. and Ansel H.C. (2005): Ansel's Pharmaceutical Dosage Forms and Drug Delivery Systems. 8th ed. Lippincott Williams and Wilkins. Philadelphia. Pp. 540-569.

6-AyanC G, Dong-Jin O K, Douglas J R. (2014); AMP-Activated Protein Kinase Regulates Intraocular Pressure, Extracellular Matrix, and Cytoskeleton in Trabecular Meshwork. *Invest Ophthalmol Vis Sci.* ; 55(5): 3127–3139.

7-Chang EE, Goldberg JL. (2012); Glaucoma 2.0: neuroprotection, neuroregeneration, neuroenhancement. *Ophthalmology*. 119(5): 979-86.

8-Daniel, A. and Yu, X. (2008) Statistical Methods for Categorical Data Analysis, 2nd edition, London.

9-Ferreira SM, Lerner SF, Brunzini R, Evelson PA, Llesuy SF,(2004); Oxidative stress markers in aqueous humor of glaucoma patients. *Am J Ophthalmol.*; 137(1):62-9.

10-Flecknell PA.(2009); laboratory animal anesthesia.Third edition. London: Academic press. p; 304.

11-Fryer LG, Hajduch E, Rencurel F, Salt IP, Hundal HS, Hardie DG, Carling D.(2000).Activation of glucose transport by AMP-activated protein kinase via stimulation of nitric oxide synthase.Diabetes ;49:1978–1985.

12-Gao Yi Zhimin He Xinke Zhou Lewu Xian Taize Yuan XiaotingJiaJian Hong Lu He Jifang Liu,(2013); Low concentration of metformin induces a p53-dependent senescence in hepatoma cells via activation of the AMPK pathway, *Journal of Oncology,* Volume 43 Issue 5, Pages: 1503-1510.

13-Gayard M, Guilluy C, Rousselle A, et al.(2011), AMPK alpha 1-induced RhoA phosphorylation mediates vasoprotective effect of estradiol. ArteriosclerThrombVasc Biol. ; 31: 2634–2642

14-Glaucoma research foundation ,(2017);types of glaucoma, https://www.glaucoma.org/glaucoma/types-of-glaucoma.php accessed .4.9.2018

15-Goel M., Picciani R. G., Lee R. K. and Bhattacharya S. K. (2010); Aqueous Humor Dynamics: A Review. *The Open Ophthalmology Journal, 4, 52-59.*

16-Green C. J , Knight J, Precious S &Simpkin S (1981); Ketamine alone and combined with diazepam or xylazine in laboratory animals: a 10 year experience. Laboratory Animals 15: 163-170.

17-Gupta N, Yucel YH.(2007), Should we treat the brain in glaucoma? Can J Ophthalmol. 2007;42:409–13.

18-Gupta S. K., Kalaiselvan V., Agrawal S. S., Srivastava S., Saxena R. (2011),Prevention of endotoxin-induced uveitis in rabbits by Triphala an Ayurvedic formulation. International *Journal of Current Pharmaceutical Research*;1(2):20–23.

19-Gupta S. K., Kalaiselvan V., Agrawal S. S., Srivastava S., Saxena R. (2011). Prevention of endotoxin-induced uveitis in rabbits by Triphala an Ayurvedic formulation. International Journal of Current Pharmaceutical Research;1(2):20–23.

20-Hecht G.(2000): Ophthalmic preparations .ch.89:1563-1573.

21-Heijl, A., Leske, M.C., Bengtsson, B., Hyman, L., and Hussein, M.(2002): Reduction of intraocular pressure and glaucoma progression: results from the Early Manifest Glaucoma Trial. Arch. Ophthalmol., 120:1268–1279.

22-Hyun B, Shin S, Lee A, (2013). Metformin down-regulates TNF-alpha secretion via suppression of scavenger receptors in macrophages. Immune Netw; 13: 123-132.

23-Jampel H. (2001): Intraocular pressure. In: Gross R.L. Clinical Glaucoma Management. W.B. Saunders Company. Philadelphia. Pp. 403-413.

24-Jay J. L. and Murdoch J.R. (1993):The rate of visual field loss in untreated primary open angle glaucoma .Br J Ophthalmol. 77:176.

25-Kaushik S, Pandav SS, Ram J.(2003); Neuroprotection in glaucoma. *J Postgrad Med*. ;49:90–5.

26-KierstanBoyd (2017), American Academy of Ophthalmology; Glaucoma treatment.

27-Lei Y, Zhang X, Song M, Wu J, Sun X. (2015); Aqueous Humor Outflow Physiology in NOS3 Knockout Mice*. Invest Ophthalmol Vis Sci. ;*56(8):4891–4898.

28-ŁukaszBułdak, Krzysztof Łabuzek, RafałJakubBułdak ,GrzegorzMachnik ,Aleksandra Bołdys, MarcinBasiak, OkopieńBogusław,(2016); Metformin reduces the expression of NADPH oxidase and increases the expression of antioxidative enzymes in human monocytes/macrophages cultured in vitro, Experimental and Therapeutic Medicine, Volume 11 Issue 3,*https://www.spandidos-publications.com/etm/11/3/1095.*

29-Macdonald M. (2000): The examination of the eye. In: Munro J. and Edwards C. Macleod's Clinical Examination. 10th .ed. Churchill Livingstone. Edinburgh. Pp. 257-271.

30-Macdonald M. (2000): The examination of the eye. In: Munro J. and Edwards C. Macleod's Clinical Examination. 10th .ed. Churchill Livingstone. Edinburgh. Pp. 257-271.

31-McKinnon SJ, Goldberg LD, Peeples P, Walt JG, Bramley TJ (2008) Curren management of glaucoma and the need for complete therapy. Am J Manag Care 14: S20–27.

32-Melena J, Santafé J, SegarraJ(1998): The effect of topical diltiazem on the intraocular pressure in betamethasone-induced ocular hypertensive rabbits. J PharmacolExpTher. 284(1):278-82.

33-Mohammad K.,Haitham M.,waleed K. Abdulsahib (2018);Effect of Telmisartan on Intra-Ocular Pressure in induced Open Angle Glaucoma in Rabbits , International Journal of Science and Research , 6(10) P:1656-1657.

34-Moses R.A. (1997): Intraocular pressure. In: Moses R.A. and Hart W.M. Alder's Physiology of the eye Clinical Application. 9th ed. Mosby Company. St. Louis. Pp. 223-245.

35-PATELSKA, B., GREENFIELD, D. S., LIEBMANN, J. M., WAND, M., KUSHNICK, H., & RITCH, R. (1997).Latanoprost for Uncontrolled Glaucoma in a Compassionate Case Protocol. American Journal of Ophthalmology, 124(3), 279–286.

36-Perry MP, McGavinJK ,Culy CR , Ibbotson T , (2003); latanoprost. An update of its use in glaucoma and ocular hypertension. Drug aging,28:183-98.

37-Rao VP, Epstein DL.(2007); Rho GTPase/Rho kinase inhibition as a novel target for the treatment of glaucoma. Bio Drugs.;21(3):167–177.

38-The International Pharmacopoeia - Sixth Edition, 2016 Ophthalmic preparations

39-UrcolaJ.H.. Hernandez M. and Vecino E. (2002): A study of experimental hydroxypropyl methylcellulose glaucoma and other experimental glaucoma in rabbits. *Exp. Eye Res*. 38: 172-175.

40-Weinreb R. N., Aung T., Medeiros F. A. (2014); The Pathophysiology and Treatment of Glaucoma A Review. *JAMA*. Volume 311, Number 18; 1901-1911.

41-Weinreb RN, Levin LA.(1999); Is neuroprotection a viable therapy for glaucoma? Arch Ophthalmol. ;117:1540–4.

42-WHO Word health organization (2017).Vision impairment and blindness.Available at ;http://www.who.int/mediacentre/factsheets/fs282/en/.

Table 1: Glutathione levelsoflatanoprost ,healthy group with metformin groups by unpaired t-test.

Glutathione (Mg/ml)	Control+ve (latanoprost0.005%) treated group	Control-ve(healthy untreated group)	Metformin 0.5%	Metformin 1%	Metformin 2%
Mean±SD	5.3±2.05	5.7±2.31	13.41±5.54	6.04 ±0.21	5.03 ±2.83
P value		0.755*	0.007*	0.633*	0.854*
			0.008**		

***** p value of comparison between control +ve and metformin groups by unpaired t- test,

** p value of comparison between metformin groups (apart from control) by ANOVA.

Table 2:tumor necrosis factor –alpha e levels of latanoprost ,healthy group with metformin groups by unpaired t-test

Tumor necrosis factor –alpha (Pg/ml)	Control + ve (latanoprost0.005%) treated group	Control -ve (healthy untreated group)	Metformin 0.5%	Metformin 1%	Metformin 2%
Mean± SD	15.1±3.46	13.3±0.49	11.6±4.52	5.83±1.96	10.45±4.53
P value		0.315*	0.162*	<0.001*	0.073*
			0.028**		

***** p value of comparison between control +ve and metformin groups by unpaired t- test,

** p value of comparison between metformin groups (apart from control) by ANOVA.

Fig. 1 Effect of Isotonic Buffer & Distilled water groups regarding the response of mean IOP in ocular normotensive rabbits

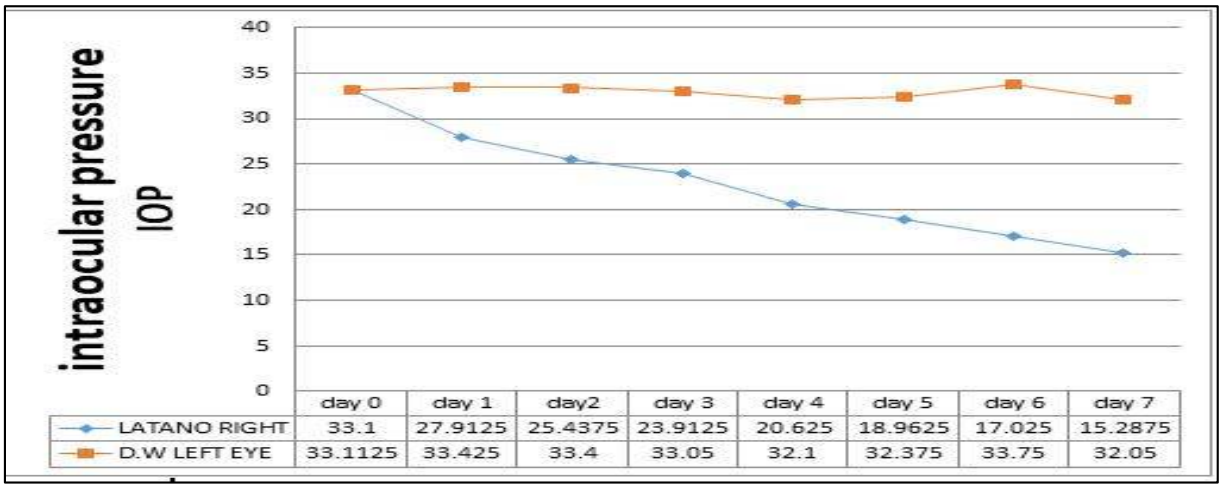

	day 0	day 1	day2	day 3	day 4	day 5	day 6	day 7
LATANO RIGHT	33.1	27.9125	25.4375	23.9125	20.625	18.9625	17.025	15.2875
D.W LEFT EYE	33.1125	33.425	33.4	33.05	32.1	32.375	33.75	32.05

Fig.2. Effect of latanoprost (0.005%) and DW on mean IOP of ocular hypertensive rabbits

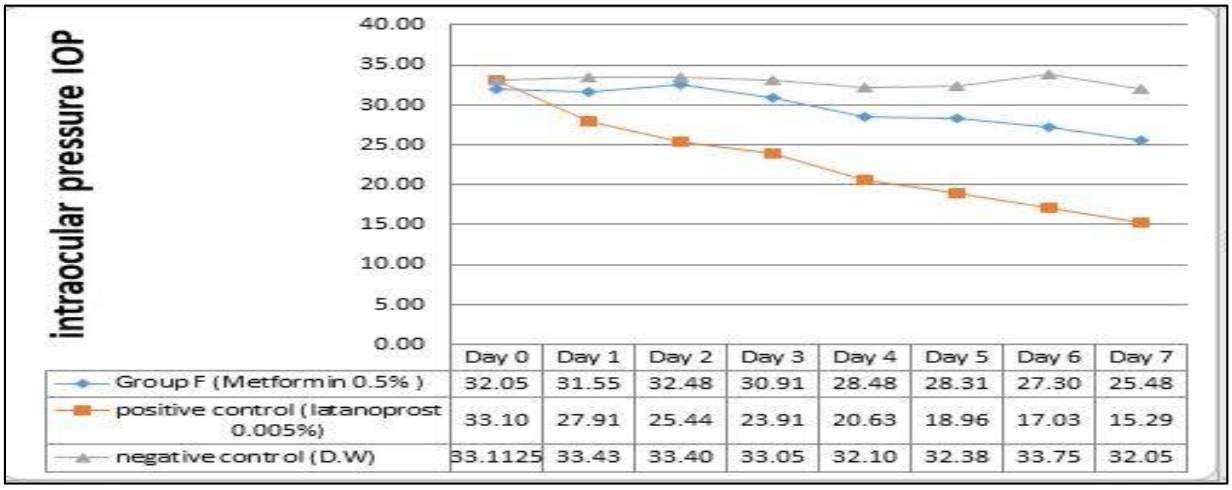

	Day 0	Day 1	Day 2	Day 3	Day 4	Day 5	Day 6	Day 7
Group F (Metformin 0.5%)	32.05	31.55	32.48	30.91	28.48	28.31	27.30	25.48
positive control (latanoprost 0.005%)	33.10	27.91	25.44	23.91	20.63	18.96	17.03	15.29
negative control (D.W)	33.1125	33.43	33.40	33.05	32.10	32.38	33.75	32.05

Fig. 3. Effect of metformin (0. 5%) ,latanoprost 0.005% and DW on mean IOP of ocular hypertensive rabbits .

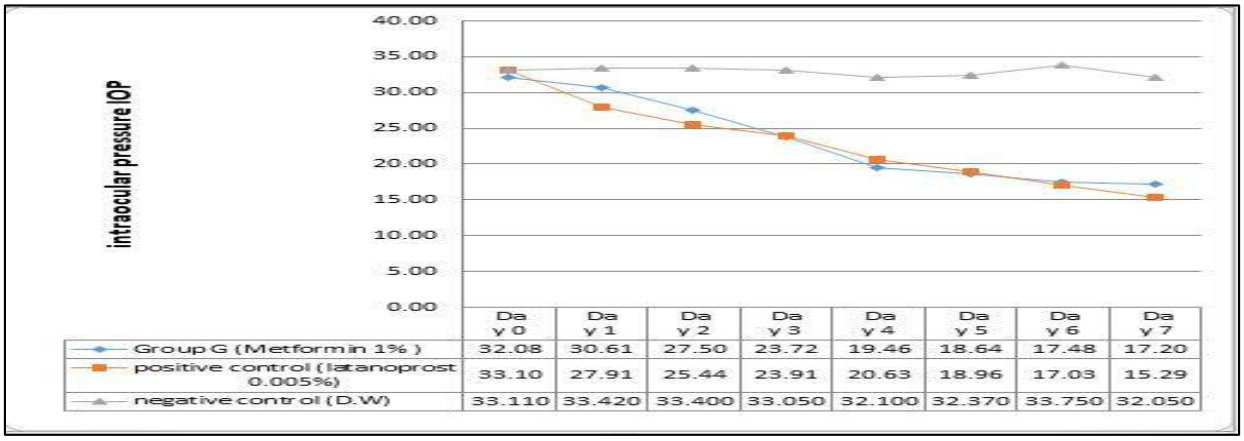

	Day 0	Day 1	Day 2	Day 3	Day 4	Day 5	Day 6	Day 7
Group G (Metformin 1%)	32.08	30.61	27.50	23.72	19.46	18.64	17.48	17.20
positive control (latanoprost 0.005%)	33.10	27.91	25.44	23.91	20.63	18.96	17.03	15.29
negative control (D.W)	33.110	33.420	33.400	33.050	32.100	32.370	33.750	32.050

Fig. 4. Effect of metformin (1%) ,latanoprost 0.005% and DW on mean IOP of ocular hypertensive rabbits n=8

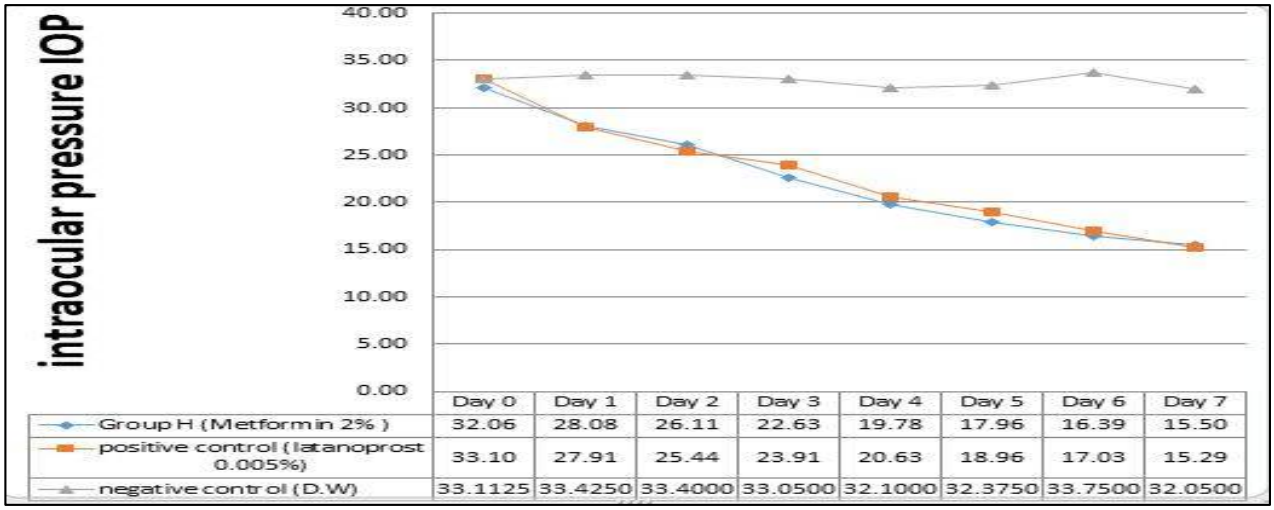

	Day 0	Day 1	Day 2	Day 3	Day 4	Day 5	Day 6	Day 7
Group H (Metformin 2%)	32.06	28.08	26.11	22.63	19.78	17.96	16.39	15.50
positive control (latanoprost 0.005%)	33.10	27.91	25.44	23.91	20.63	18.96	17.03	15.29
negative control (D.W)	33.1125	33.4250	33.4000	33.0500	32.1000	32.3750	33.7500	32.0500

Fig. 5. Effect of metformin (2%), latanoprost 0.005% and DW on mean IOP of ocular hypertensive rabbits n=8.

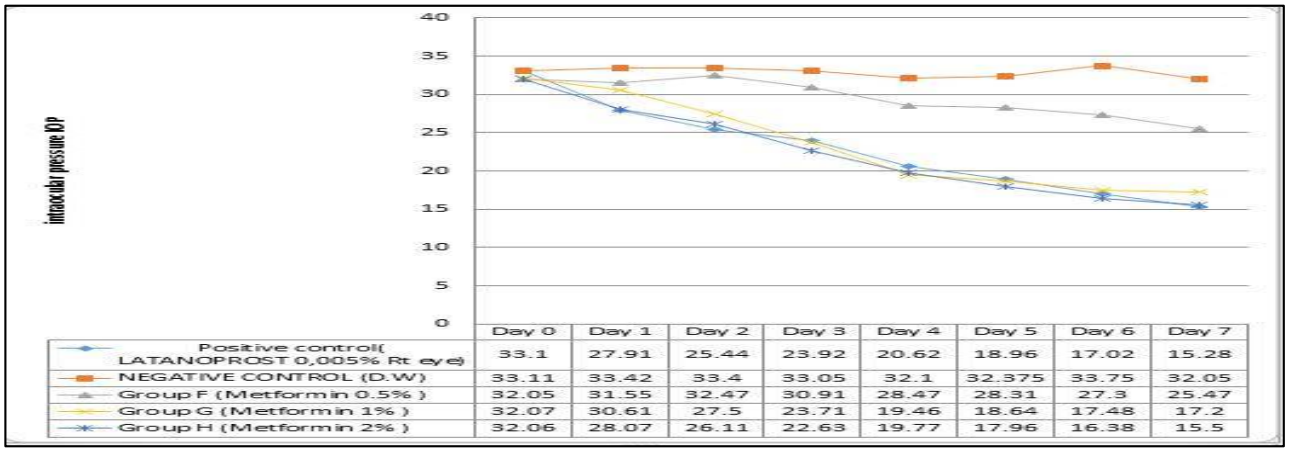

	Day 0	Day 1	Day 2	Day 3	Day 4	Day 5	Day 6	Day 7
Positive control(LATANOPROST 0,005% Rt eye)	33.1	27.91	25.44	23.92	20.62	18.96	17.02	15.28
NEGATIVE CONTROL (D.W)	33.11	33.42	33.4	33.05	32.1	32.375	33.75	32.05
Group F (Metformin 0.5%)	32.05	31.55	32.47	30.91	28.47	28.31	27.3	25.47
Group G (Metformin 1%)	32.07	30.61	27.5	23.71	19.46	18.64	17.48	17.2
Group H (Metformin 2%)	32.06	28.07	26.11	22.63	19.77	17.96	16.38	15.5

Fig. 6. Effect of different conc.ofmetformin and DW with latanoprost (0.5%) on mean IOP of ocular hypertensive rabbits n=8.

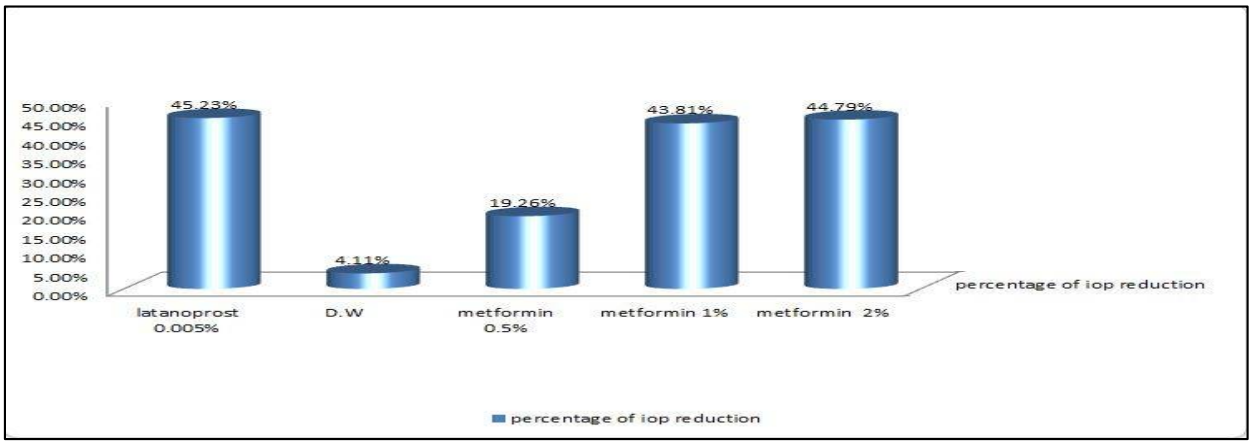

Fig.7.The percentage of IOP reduction of metformin

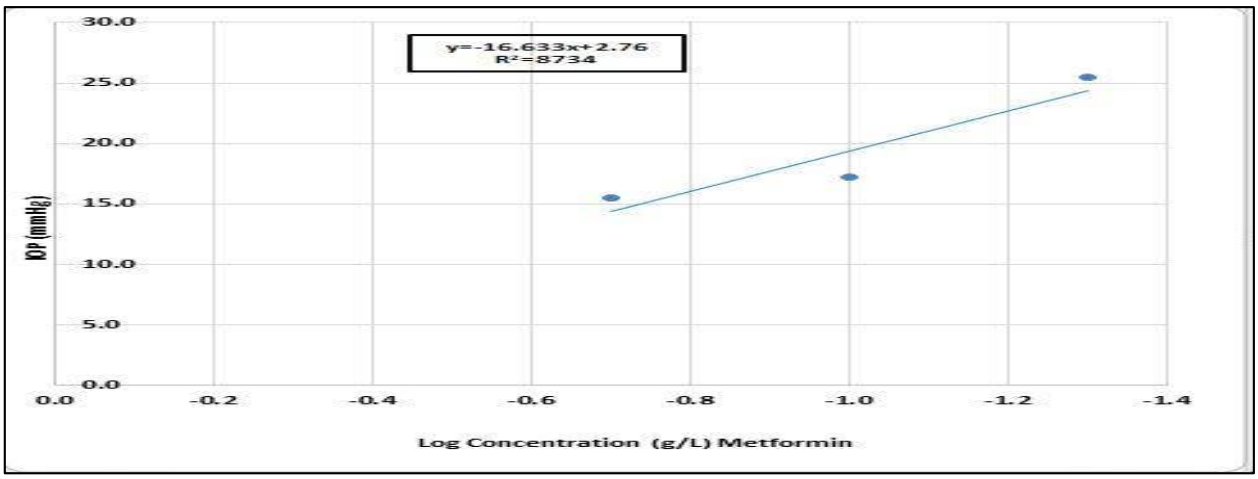

Fig. 8. Dose response curve of Metformin

this figure showed that 0.06 g/l of metformin to produce 50% decrease in IOP.

y=-16.663x+2.76 when y= 50 x= 0.06 g/L

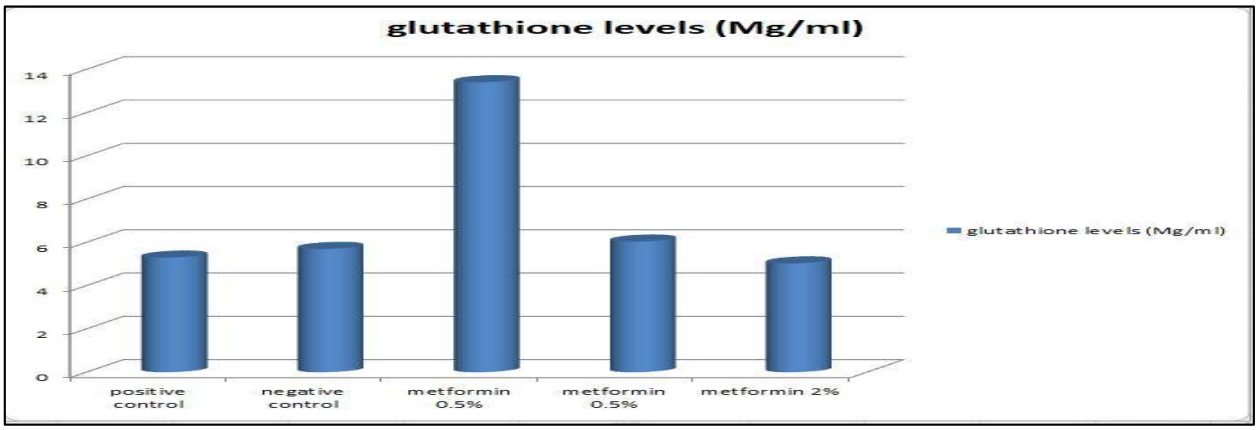

Fig. 9. The mean of glutathione levels after 7 days treatment metformin groups

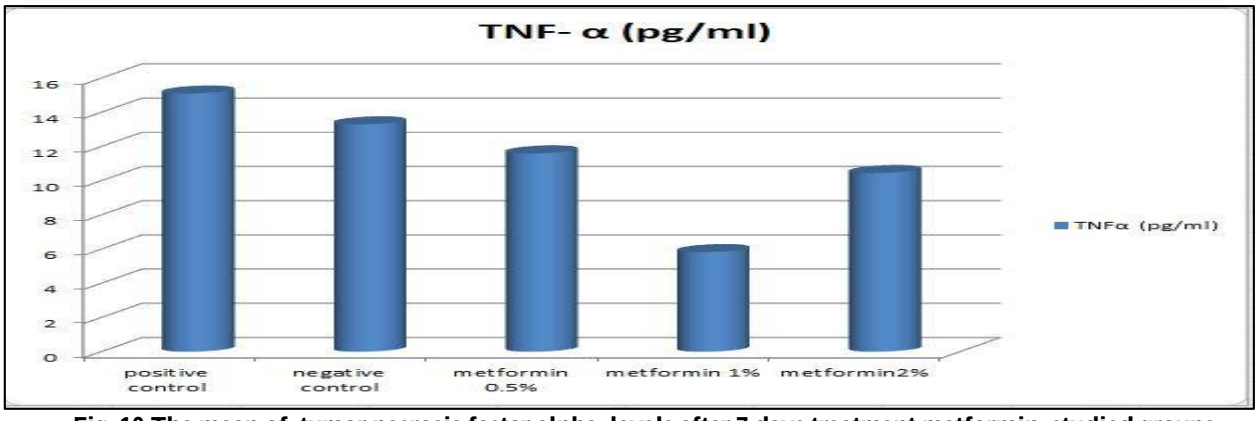

Fig. 10 The mean of tumor necrosis factor alpha levels after 7 days treatment metformin studied groups.

Indian Journal of Natural Sciences www.tnsroindia.org.in ©IJONS

Vol.9 /Issue 52 / February / 2019 *International Bimonthly* *ISSN: 0976 – 0997*

RESEARCH ARTICLE

Molecular Identification of Non-O157 Shiga Toxin-Producing *Escherichia coli* Isolated From Iraqi Patients

Sahar Kathem Khalaf Al-Qaisi[1]*, Nadirasalman Mohamed[1]and Ibrahim Abdul Hussain Al-Zubaidy[2]

[1]Forensic DNA Research and Training Center, AL-Naharian University, Iraq
[2]Zoonosis Unit, College of Veterinary Medicine, University of Baghdad, Iraq

Received: 14 Nov 2018 Revised: 16 Dec 2018 Accepted: 18 Jan 2019

*Address for Correspondence
Sahar Kathem Khalaf Al-Qaisi
Forensic DNA Research and Training Center,
AL-Naharian University, Iraq
Email: ibrahim_hussein2000@yahoo.com

ABSTRACT

The isolation and recovery of Shiga toxin-producing *Escherichia coli* (STEC) in human is very important due to the absence of sufficient molecular studies of non-O175 STEC in Iraq particularly and the world. The objective of the current study is to detect the prevalence of non-O157 STEC in Baghdad hospitals.The samples were collected from children and adults above 65 years in different hospitals of Baghdad during November 2017 to May 2018. The results of pathogenic isolates from CHROM agar was 21 out of 176 human diarrheal samples, followed by staining single colony from the growth by gram stain, biochemical tests were done to confirm the diagnosis of non-O157 STEC.Then they were processedby PCR for serotyping (wzxO26, *wzx*O45, *wzx*O103, *wzx*O111, *wzx*O121, and *wzx*O145) using targeting *wzx*(O *gene*).The positive results were furtheranalyzed to determine the prevalence of the main virulent *gene*s (stx1, *stx*2and *eae*). Theresults showed that the prevalence of non-O157 STEC was 20 out of 126(15.87 %) samples collected from children and 1out of 50 (2%) from adults.Furthermore, the serotyping showed that the serotype O26 wasdetect in (9.5%) of children samples and (2%) of the adults samples while the serotype O111 was (5.55%).The O145 was detected as (0.7%) in children samples. The O45 and O121 gave negative results in both. In conclusion, STEC O26 was the most frequent serotype among the other non-O157 STEC.Also *stx*2gene was higher in children with hemorrhagic diarrhea than others with watery diarrhea.

Keywords: Shiga toxin producing *E.coli (*STEC), O-serogroups (*wzx)*, *stx*,*eae gene*

INTRODUCTION

Shiga toxin-producing *E. coli* (STEC) is one of the eight important pathogens strains of *E. coli,* which are divided into two serogroups O-157, and nonOI-157 STEC. In recent years, numerous studies and investigations of STEC bacteria have been observed since it's one of the causes of food poisoning outbreaks that leads to serious diseases (Stromberg, 2015),such as Hemolytic uremic syndrome, hemorrhagic colitis, Thrombotic thrombocytopenic purpura) and renal injury. The STEC O157, O26, O103, O111, O145O and 121, named as a top six strains of non-O157 STEC .The pathogenicity of non-O157 serotype has been raised in worldwide (EFSA and ECDC, 2014) . Recently in Iraq, the infection has been reported in the calves and human (Jarad, 2016; Ramadhan, 2017), the reports were published the high infection rate in children for both genders (Rehman, 2014). The infection has been take place during the summer and winter months when the STEC shedding rate by cattle israised (Dewsbury *et al*., 2015). This severity associated with virulent factors especially shiga toxin *stx*, *eae*, and heamolysin *gene*s. Cattle have been recognized as the major reservoir for human infections (Wang, 2015).

The STEC isolates were frequently in the feces of animals, such as small ruminant, birds and swine. The transmission of STEC has been occurred through the consumption of contaminated food or water, person-to-person and animal-to-person (Conrad *et al* ., 2016). The most important feature of bacteria is its ability to survival outside of theintestines.In addition, STEC is tolerant to low acidic conditions and to undulating grade of heat. Nevertheless, a few numbers of bacteria after ingested could cause severe pathogenicity in humans (Dewsbury et al., 2015). The STEC strains are under the recognition in laboratory due to similarly of the nonpathogenic strains of *E .coli* by fermentation of sorbitol (Fruth et al., 2015). There is no gold based examination to STEC strains, in recent years a molecular methods such as the conventional or real-time PCR based protocols have been established t, to detected the *stx*1 *stx*2 *eae gene*s and other virulence factor successfully and sensitively

MATERIALS AND METHODS

Samples Collection

Hemorrhagic and watery diarrheal stool samples were collected of both sexes hospitalized in, Alawi children hospital, Ibn AL-Bladi hospital for children, Fatima EL-Zahraa hospital, AL-Sadar hospital, AL –Imam Ali Hospital, Child protection hospital and BaghdadGeneral Hospital. Samples were collected by sterile swabs with transport medium in soy broth and incubated at 42^{o} c for 18-24 hr.

Bacterial isolation and cultivation

The samples were cultivated on different selective media such as EMB agar , TC- SMAC agar ,TC-RMAC AGAR , SMAC –BCIG, chromogenic STEC and CHROM O175 agar. For identification STEC colonies, the samples were subjected to biochemical tests such as IVIMIC test, Urea, motility and Simmons citrate, colonies that gave mauve color on the CHROM O-157 agar were identified by PCR.

Molecular detection ofnon-157 STEC

DNA extraction

Genomic DNA of non-O157 STEC isolate was extracted using (Presto™ Mini g DNA Bacteria Kit*Gene*aid. USA) according to the manufacturer instruction. The amplified DNA products was done from isolated bacteria. The

conventional PCR technique was applied with electrophoresis on 1% agarose gels stained with2 µl red safe stain of 20000 u/ml and visualized by UV recommendation geldepending on DNA marker (100-10000 bp DNA ladder).

PCR Detection of O-serogroups (*wzx*)

The detection of O-serogroups associated with targeting the*wzx* O genes was done according to DebRoy *et al*. (2011), primers in Table (1).

Molecular Detection of virulence factors (stx1, *stx*2, and *eae*, *gene*s)

The *stx*1, *stx*2, and *eae* primers in this study was prepared according torelated researches (Paton *et al* ., 1998; ÇadIrc *et al*., 2010; Loo *et al*., 2013),while *eae* AFN primers wasredesigned to prevent the loop constriction by deletion one base pare (G, C) for both forward and reverse as shown in Table(1). For molecular detecting of *stx*1, *stx*2 and*eae*A *gene*s, the PCR amplification mixture 25µl includes green master mix5 µl(Invitogen, Germany), 3 µl of template DNA, 0.6 µl of each forwarded and reversed primers and 14.8µl of nuclease free water the thermocycler, program showed in the Tables (2, 3, 4) .

RESULTS

The pathogenic isolates from CHROM agar were 21 out of 176 human diarrheal samples. They cultivation results of pathogenic showed blue color colonies after incubation at 37°C for 24 hrsin CHROM O-157 media. The molecular results of*wzx*serogroubs and the percentage of virulent *gene*s (*stx1, stx2, eaeA*) among non-O157 STE serogroupare detailed in Tables (5, 6) and Figures (1, 2, 3, 4, 5).

DISCUSSION

The bacterial isolation approved that CHROM agar STEC showed a high sensitive and effective in detection and differentiation of top six STEC strains. These results agreed with Verhaegen(2015) and Ramadan (2017). The usage of CHROM agar O157 in thisstudy have amended the diagnostic efficacy of O157 STEC strains that is consistent with results obtained by Church (2007).This study provided useful information about the prevalence of STEC non-O157 serogroups which was greater in children under 5 years old who sufferings from bloody diarrhea than watery diarrhea. The results showed that *E. coli* O26 serotypes was the most strain followed by O111and O145. There was no singlesample was positive for serotypes; O103, O45 and O121 serotypes in children. The results of the present study agreed with other results obtained by some researches(Efsa and Ecdc, 2014; Jared, 2016; Ramadhan, 2017).The present study showed that in children the*stx*1 *gene* was detected in (40%), *Stx*2gen in(30%). Similar results were obtained byFriedrich (2002) Melton-Celsa, (2014), Fruth (2015) and Ramadan (2017). On the other hand, the results of this study disagreed with Bonyadian (2009), who found that all non-O157 STEC which were isolated from human stool did not carry *eae*.

CONCLUSION

Non-O157 STEC was an important cause of diarrhea in children, and *E coli* O26 was the most surveillance with childhood population in Baghdad hospitals. The isolated strain of non-O157 STEC carried various virulence factors. The *Stx*2 was more harboring *gene* than *stx*1 and showed most prevalence with hemorrhagic diarrhea than watery diarrhea.

Conflect of Interest

There is no conflict of interest.

Authors Contribution

All authors were participated to the doing research work as study protocol.

REFERENCES

1. ÇadIrc IO, SirIken B, Inat G, Kevenk TO (2010). The prevalence of *Escherichiacoli* O157 and O157:H7 in ground beef and raw meatball by immunomagneticseparation and the detection of virulence *gene*s using multiplex PCR. Meat Sci. (84): 553– 556.
2. Church DL, Emshey D, Semeniuk H, Lloyd T and Pitout JD (2007).Evaluation of BBL CHROM agar O157 versus sorbitol-MacConkey medium for routine detection of *Escherichia coli* O157 in a centralized regional clinical microbiology laboratory. J. Clin. Microbiol., (45): 3098 –3100.
3. Conrad K, Cheyenne C,Stanford C, Narvaez B, Todd y E and Tim M . (2016). Farm Fairs and Petting Zoos: A Review of Animal Contact as a Source of Zoonotic Enteric Disease Published Online : 1 Feb 2017https://doi.org/10.1089.
4. DebRoy C, Roberts E, Valadez AM, Dudley EG and Cutter CN. (2011).Detection of Shiga toxin-producing *Escherichia coliO26*.; O45.; O103.; O111.;O113.; O121.; O145.; and O157 serogroups by multiplex polymerase chainreaction of thewzxgene of the O-antigen *gene* cluster. Foodborne PathogDis., (8):651–2.
5. Dewsbury D M, Renter DG, Shridhar P B, Noll L W, Shi X, Nagaraja TG and Cernicchiaro N.(2015).Summer and winter prevalence of Shiga toxin-producing *Escherichia coli* (STEC): O26.; O45.; O103.;O111.; O121.; O145.; and O157 in feces of feedlot cattle. Foodborne Pathog. Dis. 12: 726-732.
6. European Food Safety Authority (EFSA) and European Centre For Disease Prevention And Control (ECDC): (2014): The European Union summary report on trends and sources of zoonoses.; zoonotic agents and food-borne outbreaks in(2012). EFSA Journal 12:3547-312.
7. Friedrich AW, Bielaszewska M, Zhang WL, Pulz M , Kuczius T, Ammon A, Karch H. (2002). *Escherichia coli* harboring Shiga toxin 2 *gene* variants: frequency and association with clinical symptoms. J. Infect. Dis. 185: 74–8410.
8. Fruth A, Prager R, Tietze E, Rabsch W, and Flieger A. (2015). Molecular epidemiological view on Shiga toxin-producing *Escherichia coli* causing human disease in Germany: Diversity, prevalence, and outbreaks. Int. J. Med. Microbiol., 305: 697–704.
9. Jarad A S. (2016). Bacteriological.; Immunological and Pathological Study on Mice Experimentally Infected with Non- O157 Shiga Toxin Producing *E.coli* Isolated from Children and Calves. PhD.; Dissertation. Collage of veterinary medicine / Baghdad University.
10. Loo YY, Puspanadan S, Goh SG, Kuan CH, ChangWS, LyeY L. (2013).Quantitative detection and characterization of Shiga toxin producing *Escherichia coli* O157 and non-O157 in raw vegetables by MPN-PCR in Malaysia. Int.Food Res. J. 20: 3313–3317.
11. Melton-CelsaA.R. (2014): Shiga Toxin(Stx): Classification. Structure And Function. Microbiol Spectr 2.;EHEC-0024-2013.; https://doi.org/10.1128/microbiolspec.EHEC-0024-.
12. Paton J C, Paton A W (1998). Pathogenesis and diagnosis of Shiga toxin- producing *Escherichia coli i*nfections.Clin.Microbiol. Rev., 11: 450-479.
13. Rahman M S, Huda S (2014). Antimicrobial resistance and related issues: An overview of Bangladesh situation. Bangladesh J Pharmacol. 9: 218-24.

14. Ramadhan MA (2017). Bacteriological.; Molecular and Immunopathological Study of O111 Shiga Toxin-Producing *Escherichia coli* Isolated from Human and Animal SourcesPhD.; Dissertation. Collage of veterinary medicine / Baghdad University.
15. Stromberg Z R, Baumann N W, Lewis GL, Sevart N J, CernicchiaroN,Renter, D G, Marx D B, Phebus RK, Moxle R A.(2015). Prevalence of Enterohemorrhagic*Escherichia coli*O26.; O45.;O103.; O111.; O121.; O145.; and O157 on Hides and Preintervention Carcass Surfaces of Feedlot Cattleat Harvest. Foodborne Pathog. Dis. 12: 631-638.
16. Verhaegen B, De Reu K, Heyndrickx M, De Zutter L. (2015). Comparison of six chromogenic agar media for the isolation of a broad variety of non-O157 Shiga toxin producing *Escherichia coli* (STEC): serogroups. Int. J. Environ. Res. Public Health 12:6965-6978.
17. Wang X, Wang J, Sun H, Xia S, Duan R, Liang J (2015). Etiology of Childhood Infectious Diarrhea in a Developed Region of China: Compared to Childhood Diarrhea in a Developing Region and Adult Diarrhea in a Developed Region. PLoS ONE 10: 0142136-10.

Indian Journal of Natural Sciences www.tnsroindia.org.in ©IJONS

Vol.9 /Issue 52 / February / 2019 *International Bimonthly* *ISSN: 0976 – 0997*

RESEARCH ARTICLE

Chaotic Dynamics of the Nuclear Energy Spectrum in ^{138}Ba Nucleus

Adel. K. Hamoudi[1]* and Shatha F. Murad[2]

[1]Department of Physics, College of Science, University of Baghdad, Baghdad, Iraq
[2]Physiology Department, Medicine College, Al-Muthanna University, Al-Muthanna, Iraq

Received: 22 Oct 2018 Revised: 24 Nov 2018 Accepted: 25 Dec 2018

*Address for Correspondence
Adel. K. Hamoudi
Department of Physics,
College of Science,
University of Baghdad,
Baghdad, Iraq.

ABSTRACT

Spectral fluctuations in ^{138}Ba nucleus are studied by the perspective of the shell model, using the isopspin-conserving N28K as an effective interaction for 6 particles in the N82-model space with a ^{132}Sn core. To examine the effect of the interaction strength (β) on the spectral fluctuations in ^{138}Ba, we perform shell model calculations using various strengths to the off-diagonal matrix elements of the N82K. The level density for considered class of states is found to have a Gaussian shape, which is in agreement with the prediction of other theoretical studies for a many-body system with two-body residual interaction. Both statistical measures of the nearest neighbor level spacing distribution $P(s)$ and the Dyson-Mehta statistics (Δ_3 statistics) are found to have a regular dynamic at $\beta = 0,$ a chaotic dynamic at $\beta \geq 0.3$ and an intermediate situation at $0 < \beta < 0.3.$

Keywords: Quantum chaos; Regular to chaos transition; Spectral fluctuations; Shell model calculations in the N82-model space .PACS number(s): 24.60.Lz, 21.60.Cs, 21.10.Ky

INTRODUCTION

Statistical fluctuations in many-body quantum system were examined extremely during the last three decades [1]. Bohigas et al. [2] suggested a relation between chaos in a classical system and the spectral fluctuations of the analogous quantum system, where an analytical proof of the Bohigas et al. conjecture is found in [3]. It is now typically known that quantum analogs of most classically chaotic systems demonstrate spectral fluctuations that agree with the random matrix theory (RMT) [4,5] while quantum analogs of classically regular systems reveal spectral fluctuations that agree with a Poisson distribution. For time-reversal-invariant systems, the suitable form of RMT is the Gaussian orthogonal ensemble (GOE). RMT was first used to describe the statistical fluctuations of neutron resonances in compound nuclei [6]. RMT has become a usual tool for studying the universal statistical

fluctuations in chaotic systems [7-10].Chaotic performance of the single particle dynamics in the nucleus may be examined through the mean field approximation. However, the nuclear residual interaction mixes different mean field configurations and affects the statistical fluctuations of the many particle spectrum and wave functions. These fluctuations may be investigated with different nuclear structure models. The statistics of the low-lying collective part of the nuclear spectrum were studied in the framework of the interacting boson model [11, 12], in which the nuclear fermionic space is mapped onto a much smaller space of bosonic degrees of freedom. Because of the relatively small number of degrees of freedom in this model, it was also possible to relate the statistics to the underlying mean field collective dynamic. At higher excitations, extra degrees of freedom (such as broken pair) come to be important [13], and the effects of interactions on the statistics should be examined in larger model spaces. The nuclear shell model offers an attractive context for such studies. In this model, realistic interactions are presented and the basis states are labeled by exact quantum numbers of angular momentum (J), isospin (T) and parity (π) [14].

The eigenvector components distribution [15-19] was studied by the context of the shell model. Brown and Bertsch [17] found that the basis vector amplitudes are consistent with Gaussian distribution (which is the GOE prediction) in regions of high level density but deviated from Gaussian behavior in other regions unless the calculation employs degenerate single particle energies. Later studies [19] also suggested that calculations with degenerate single particle energies are chaotic at lower energies than more realistic calculations.The intensities of electromagnetic transition in a nucleus are observables that are sensitive to the wave functions, and the study of their statistical distributions should complement [11, 12] the more common spectral analysis and serve as another signature of chaos in quantum systems. Hamoudi et al carried out [20] the fp-shell model calculations to study the statistical fluctuations of energy spectrum and electromagnetic transition intensities in A=60 nuclei using the F5P [21] interaction. The calculated results were in agreement with RMT and with the previous finding of a Gaussian distribution for the eigenvector components [15-19].

Hamoudi [22] analyzed the effect of the one-body hamiltonian on the fluctuation properties of energy spectrum and electromagnetic transition intensities in ^{136}Xe using a realistic effective interaction for the N82-model space. A clear quantum signature of breaking the chaoticity was observed as the values of the single particle energies are increased. Later, Hamoudi et al [23] achieved full fp-shell model calculations to investigate the regular to chaos transition of the energy spectrum and electromagnetic transition intensities in ^{44}V using the interaction of FPD6 [24] as a realistic interaction in the isospin formalism. The results exhibited that the transition from the regular to chaos can occur through applying different interaction strengths to the off-diagonal matrix elements of the considered interaction. Recently, Hamoudi et al [25] have performed sd-shell model calculations to examine the chaotic properties of energy spectra in ^{32}A (^{32}S, ^{32}P and ^{32}Si) nuclei adopting the interaction of W [26] as a realistic interaction in the isospin formalism. The results have been well described by the Gaussian orthogonal ensemble of random matrices. Besides, they show no dependency on the spin J and isospin T. Subsequently, Hamoudi et al [27] have accomplished shell model calculations adopting the realistic effective interaction of WPN [26] in the proton-neutron formalism to examine the statistical fluctuations of nuclear energy spectra in ^{32}A nuclei. The spectral fluctuations have been found to have an intermediate behavior between Wigner and Poisson limits. Moreover, they move gradually toward the GOE limit when going over ^{32}S, ^{32}P and ^{32}Si nuclei, correspondingly. Besides, they are independent of the spin J.

In present study, we examine the influence of the interaction strength (β) on the spectral fluctuations through doing shell model calculations for 6 protons in the N82-model space with a ^{132}Sn core using the effective interaction of N82K [28] together with realistic single-particle energies. The present statistical analysis is performed by applying different interaction strength to the off-diagonal matrix elements of the N82K. We find that the level density for the considered class of states have a Gaussian shape, which agrees the prediction of other theoretical studies for a many-body system with two-body residual interaction. We also find that both statistical measures of the nearest neighbor

level spacing distribution $P(s)$ and the Dyson-Mehta statistics (Δ_3 statistics) have a regular dynamic at $\beta = 0,$ a chaotic dynamic at $\beta \geq 0.3$ and an intermediate situation at $0 < \beta < 0.3.$

THEORY

The effective shell-model hamiltonian, which describes the many-body quantum system, is given by [14]

$$H = H_0 + H', \quad \textbf{(1)}$$

where H_0 and H' are the one-body part and the residual two-body interaction of $H.$ The unperturbed Hamiltonian

$$H_0 = \sum_{\lambda} e_\lambda a_\lambda^+ a_\lambda \quad (2)$$

describes non-interacting fermions in the mean field of the appropriate spherical core. The single-particle orbitals $|\lambda\rangle$ have quantum numbers $\lambda = (ljm\tau)$ of orbital (l) and total angular momentum (j), projection $j_z = m$ and isospin projection $\tau.$ The antisymmetrized two-body interaction H' of the valence particles is expressed as

$$H' = \frac{1}{4}\sum V_{\lambda\mu;\nu\rho} a_\lambda^+ a_\mu^+ a_\nu a_\rho. \quad (3)$$

The many-body wave functions with good spin J and isospin T quantum numbers are constructed via the $m-$ scheme determinants which have, for given J and $T,$ the maximum spin and isospin projection [14],

$$|M = J, T = T_3; m\rangle, \quad (4)$$

where m span the $m-$ scheme subspace of states with $M = J$ and $T_3 = T.$

The matrix of the many-body Hamiltonian

$$H_{kk'}^{JT} = \sum_k \langle JT; k|H|JT; k'\rangle \quad (5)$$

is eventually diagonalized to obtain the eigenvalues E_α and the eigenvectors

$$|JT; \alpha\rangle = \sum_k C_k^\alpha |JT; k\rangle \quad (6)$$

Here, the eigenvalues E_α are the main object of the present investigation.

The spectral fluctuations of nuclear energy spectrum are obtained via two statistical measures: the nearest-neighbors level spacing distribution $P(s)$ and the Dyson-Mehta or Δ_3 statistics [4, 29]. The staircase function of the nuclear shell model spectrum $N(E)$ is firstly build. Here, $N(E)$ is defined as the number of levels with excitation energies less than or equal to $E.$ In this study, a smooth fit to the staircase function is performed with polynomial fit. The unfolded spectrum is then defined by the mapping [12]

$$\tilde{E}_i = \tilde{N}(E_i). \quad (7)$$

The actual spacing reveal strong fluctuations whereas the unfolded levels $\tilde{E}_i$ have a constant average spacing.

The level spacing distribution (which exemplifies the fluctuations of the short-range correlations between energy levels) is defined as the probability of two neighboring levels to be a distance s apart. The spacing s_i are determined from the unfolded levels by $s_i = \tilde{E}_{i+1} - \tilde{E}_i$. A regular system is forecasted to perform by the Poisson statistics

$$P(s) = \exp(-s). \quad \textbf{(8)}$$

If the system is classically chaotic, we foresee to get the Wigner distribution

$$P(s) = (\pi/2)s\exp(-\pi s^2/4), \quad \textbf{(9)}$$

which is consistent with the GOE statistics. We have fitted the calculated $P(s)$ to a Brody distribution

$$P(s,\omega) = \alpha(\omega+1)s^{\omega}\exp(-\alpha s^{\omega+1}), \quad (10)$$

where

$$\alpha = \left(\Gamma\left[\frac{\omega+2}{\omega+1}\right]\right)^{\omega+1} \quad (11)$$

The Brody distribution interpolates between the Poisson distribution ($\omega = 0$) and the Wigner distribution ($\omega = 1$). The parameter ω can be used as a simple quantitative measure of the degree of chaoticity.

The Δ_3 statistic (which characterizes the fluctuations of the long-range correlations between energy levels) is utilized to measure the rigidity of the nuclear spectrum and defined by [4]

$$\Delta_3(\alpha, L) = \min_{A,B}\frac{1}{L}\int_{\alpha}^{\alpha+L}\left[N(\tilde{E}) - (A\tilde{E}+B)\right]^2 d\tilde{E}. \quad (12)$$

It measures the deviation of the staircase function (of the unfolded spectrum) from a straight line. A rigid spectrum corresponds to smaller values of Δ_3 whereas a soft spectrum has a larger Δ_3. To get a smoother function $\overline{\Delta}_3(L)$, we average $\Delta_3(L)$ over several n_α intervals ($\alpha, \alpha+L$)

$$\overline{\Delta}_3(L) = \frac{1}{n_\alpha}\sum_{\alpha}\Delta_3(\alpha, L). \quad (13)$$

The successive intervals are taken to overlap by $L/2$.

In the Poisson limit, $\Delta_3(L) = L/15$. In the GOE limit, $\Delta_3 \approx L/15$ for small L, while $\Delta_3 \approx \pi^{-2}\ln L$ for large L.

RESULTS AND DISCUSSION

Chaotic properties of the energy spectrum in ^{138}Ba nucleus are probed by the context of the nuclear shell model. This nucleus is considered to possess a ^{132}Sn core with 6 valence protons in the N82-model space defined by $2d_{5/2}$, $1g_{7/2}$, $1h_{11/2}$, $3s_{1/2}$ and $2d_{3/2}$ orbitals. The isospin-conserving N82K interaction [28] is chosen as an effective interaction together with realistic single particle energies. Shell model calculations for ^{138}Ba nucleus are performed by the code OXBASH [30] employing different strength (β) to the off-diagonal matrix elements of N82K interaction. The chaotic properties of the nuclear energy spectrum are investigated for states which have the same

spin (J), parity (π) and isospin (T). In this study, we commonly use the classes of states $J^{\pi}T = 1^{+}3,\ 3^{+}3$ and $5^{+}3,$ where the total numbers of states in these classes (included in the present analysis) are 1281, 2602 and 3110, respectively. Fig. 1 displays the calculated level density $\rho(E)$ (histograms) for the $1^{+}3$ class with different interaction strength (β). The dashed line which describes the Gaussian fit [31] is also presented for comparison. The histogram in Fig. 1(a) is related to the result when the off-diagonal residual interaction is not considered in the diagonalization (i.e., with $\beta = 0).$ The histogram in Fig. 1(b) is connected to the result obtained with the diagonalization of the full Hamiltonian (i.e., with $\beta = 1).$ It is clear that the histograms in Figs. 1(a) and 1(b) are identical, except for a shift in energy as a whole. This figure shows that the level density abruptly progresses along with excitation energy, reaches its maximum at the intermediate of the spectrum and then diminishes again for the highest energy. This presentation of the high energy, and the rough symmetry with respect to the middle of the spectrum, are non-natural features of models with restricted Hilbert space which is in contrast to real many-body systems. This figure also illustrates that the evaluated level density (histograms) $\rho(E)$ has a Gaussian shape, which is in agreement with what is predicted in the study [7] for a many body system with two-body residual interaction. In Figs. 2 and 3, we repeat the computations as in Fig. 1 but this time for the classes $3^{+}3$ and $5^{+}3.$ These figures provide similar argument as that obtained in Fig. 1.

Fig. 4 reveals the computed level spacing distributions $P(s)$ (histograms) for the unfolded $1^{+}3$ levels with different strengths $\beta.$ The GOE distribution (which describes chaotic systems) is shown in the above figure by the solid line. The Poisson distribution (which corresponds to a random sequence of levels and indicates regular systems) is shown by the dashed line. Fig. 4(a) displays the unperturbed hamiltonian result (the non-interacting particles case) for the $P(s)$ distribution evaluated with $\beta = 0.$ The computed histogram in Fig. 4(a) illustrates regular behavior (in accordance with the Poisson distribution) as a result of the nonexistence of mixing and repulsion between levels caused by the absence of the off-diagonal residual interaction whereas the histograms in Figs. 4(b)-4(i) (evaluated with $0 < \beta < 1$) transfer obviously away from the Poisson distribution. This figure shows that the level repulsion at small spacings (which is a distinctive feature of chaotic level statistics) progresses progressively with increasing the value of $\beta,$ as a consequence the computed histograms transfers commonly towards the GOE limit. To indicate the degree of chaoticity for the $P(s)$ by a parameter, we display in Figs. 4(b)-4(h) the fitted distributions of Brody (the red dash-dotted lines) with their fitted parameters $\omega.$ It is recognized from Fig. 2 that the transition from order to chaos happens at relatively weak interaction strength of about $\beta = 0.3.$ Nevertheless, the result of Fig. 4 approves the works done by Zelevinsky et al. [14] (for the $P(s)$ distribution of 12 particles in the $sd-$shell model) and Hamoudi et al. [23] (for the $P(s)$ distribution of 4 particles in the full $fp-$shell model). In Figs. 5 and 6, we replicate the calculations as in Fig. 4 but this time for the classes $3^{+}3$ and $5^{+}3.$ Here, the same argument is gained as that in Fig. 4. Fig. 7 demonstrates the influence of the strength β on the spectral rigidity [$\Delta_3(L)$ statistics]. Here, the computed distribution of the $\Delta_3(L)$ statistics (denoted by open circles) for the unfolded $1^{+}3$ levels is demonstrated with various strength $\beta.$ The Poisson distribution (denoted by the dashed line) and the GOE distribution (denoted by the solid line) are also demonstrated for comparison. It is clear that the computed distribution of $\Delta_3(L)$ statistics in Fig. 7(a) (which is evaluated with $\beta = 0)$ exhibits very well accordance with the Poisson limit while those in Figs. 7(b)-7(i) (which are evaluated with $0 < \beta < 1)$ reveal significant deviation from the Poisson distribution. Enlarging the strength β through Figs. 7(a)-7(h) leads to relocate the distribution of

$\Delta_3(L)$ statistics on the way to the GOE limit. Fig. 7 also exhibits that the $\Delta_3(L)$ statistics grows to the GOE limit at slight interaction strength of approximately $\beta = 0.3$. This as well confirms the outcome that we have gained in Fig. 4 from the study of the $P(s)$ distribution. On the other hand, the result of Fig. 7 also confirms the works achieved by Hamoudi et al. [23] for the distribution of $\Delta_3(L)$ statistics with 4 particles in the full $fp-$shell model). In Figs. 8 and 9, we do again the calculations as in Fig. 7 but this time for the classes 3^+3 and 5^+3. In these figures, we have obtained the same argument as that in Fig. 7.

CONCLUSIONS

The spectral fluctuations in ^{138}Ba nucleus are studied by the context of the nuclear shell model, using the isospin-conserving N82K as an effective interaction for 6 protons move in the N82 model space with a ^{132}Sn core. The transition from regular to chaos is searched by doing shell model calculations with various interaction strengths β to the off-diagonal matrix elements of the N82K. The level density for considered class of states is found to possess a Gaussian shape, which is in accordance with the prediction of the other studies for a many-body system with two-body residual interaction. The statistical measures, of the nearest neighbor level spacing distribution $P(s)$ and the Dyson-Mehta statistics (Δ_3 statistics), of considered classes of states are found to have a regular dynamic at $\beta = 0$, a chaotic dynamic at $\beta \geq 0.3$ and an intermediate limit at $0 < \beta < 0.3$.

ACKNOWLEDGMENTS

The authors would like to express their thanks to Professor B. A. Brown of the National Superconducting Cyclotron Laboratory, Micihigan State University, for providing the computer code OXBASH.

REFERENCES

[1] Haak, F. 2001. Quantum signature of chaos, 2nd enlarged ed. Springer-Verlag, Berlin.
[2] Bohigas.O, Giannoni M. J. and Schmit.C.1984.Characterization of Chaotic Quantum Syectra and Universality of Level Fluctuation Laws, Phys. Rev. Lett. 52, 1.
[3] Heusler. S, Muller. S, Altland. A, Braun. P, and Haak. F. 2007. Periodic-Orbit Theory of Level Correlations,Phys. Rev. Lett. 98,044103.
[4] Mehta, M. L. 2004. Random Matrices, 3nd ed. Academic, New York.
[5] Papenbrock. T, and Weidenmuller. H. A. 2007. Colloquium: Random matrices and chaos in nuclear spectra, Rev. Mod. Phys., Vol. 79, No. 3., 997.
[6] Porter, C. E. 1965. Statistical Theories of Spectra: Fluctuations .Academic, New York.
[7] Brody. T. A, Flores. J, French. J. B., Mello. P. A., Pandey. A and Wong. S. S. M. 1981. Random matrix physics, Rev. Mod. Phys. 53, 385.
[8] Guhr. T, M$\ddot{u}$ller-Groeling. A. and Weidenm$\ddot{u}$ller1. H. A. 1997. Random Matrix Theories in Quantum Physics: Common Concepts, Phys. Rep. 299, 189.
[9] Y. Alhassid. 2000. The statistical theory of quantum dots. Rev. Mod. Phys. 72, 895.
[10] Gutzwiller. M. C. 1990. Chaos in Classical and Quantum Mechanics. Springer-Verlag, New York.
[11] Alhassid. Y and Whelan. N. 1991. Chaos in the low-lying collective states of even-even nuclei: Classical limit, Phys. Rev. C 43, 2637.
[12] Alhassid. Y and Novoselsky. A. 1992. Chaos in the low-lying collective states of even-even nuclei: Quantal fluctuations, Phys. Rev. C 45, 1677.

[13] Alhassid. Y and Vretenar. D. 1992. Chaos in nuclei with broken pairs, Phys. Rev. C 46, 1334.
[14] Zelevinsky. V., Brown. B. A., N. frazier and Horoi. M.1996. The nuclear shell model as a testing ground for many-body quantum chaos, Phys. Rep. 276, 85.
[15] Whitehead. R. R. et al. 1978. On the distribution of shell-model eigenvector components, Phys. Lett. B 76, 149.
[16] Verbaarschot. J. J. M and Brussaard. P. J. 1979. A statistical study of shell-model eigenvectors, Phys. Lett. B 87, 155.
[17] Brown. B. A. and Bertsch. G. 1984. Gaussian distributions of shell-model eigenvector components, Phys. Lett. B 148, 5.
[18] Dias. H. et al., J. 1989. Chaotic behaviour of the nuclear shell-model Hamiltonian, Phys. G 15, L79.
[19] Zelevinsky. V, Horoi. M and Brown. B. A. 1995. Information entropy, chaos and complexity of the shell model eigenvectors, Phys. Lett. B 350, 141.
[20] Hamoudi. A, Nazmidinov. R. G, Shahaliev. E and Alhassid. Y. 2002. Statistical fluctuations of electromagnetic transition intensities and electromagnetic moments in pf-shell nuclei Phys. Rev. C65, 064311.
[21] Glaudemans. P. W. M, Brussaard. P. J and Wildenthal. R. H. 1967. Two-body matrix elements from a modified surface delta interaction, Nucl. Phys. A 102,593.
[22] Hamoudi.A. 2011. Spectral fluctuations and the statistics of electromagnetic transition intensities and electromagnetic moments in ^{136}Xe using the framework of the shell model, Nucl. Phys. A 849, 27.
[23] Hamoudi. A and Abdul Majeed Al-Rahmani. A. 2012. Regular–chaos transition of the energy spectrum and electromagnetic transition intensities in ^{44}V nucleus using the framework of the nuclear shell model, Nucl. Phys. A 892, 21.
[24] Richter. W. A, Van der Merwe. M. G., Julies. R. E., Brown. B. A. 1991. New effective interactions for the 0f1$_p$ shell, Nucl. Phys. A 523:325.
[25] Hamoudi. A and Abdul Hussein. Th. 2017. Spectral Fluctuations in A=32 Nuclei Using the Framework of the Nuclear Shell Model, Ammerican Journal of Physics and Applications, Vol. 5, No. 3, 35.
[26] Wildenthal. B. H, Prog. Part. 1984. Status of the Nuclear Shell Model, Nucl. Phys. 11, 5.
[27] Hamoudi. A and Abdul Hussein.Th. 2017. Statistical Fluctuations of Energy Spectra in ^{32}A Nuclei using the Proton-Neutron Formalism Interaction, International Journal of Science and Research (IJSR), Volume 6 Issue 9, September 2017.
[28] H.G. Kruse, B.H. Wildenthal., Bull. Am. Phys. Soc. 27 (1982) 533.
[29] Stephens F. S., Deleplanque. M. A., Lee. I.Y., Macchiavelli. A. O., Ward. D., Fallon. P., Cromaz. M., Clark. R. M., Descovich. M., Diamond. R. M., and Rodriguez-Vieitez. E. 2004. Searching for E(5) behavior in nuclei, Phys. Rev. Lett., 94, 042501.
[30] Brown B. A., Etchegoyen A., Godin N. S., Rae W. D. M., Richter W. A., Ormand W. E., Warburton E. K., Winfield J. S., Zhao L. and Zimmermam C. H. 1984. The computer code oxbash. MSU-NSCL Report Number 524.
[31] M. I. Ribeiro, Instituto Superior Tecnico, Av. Rovisco Pais. 2004. 1; 1049-0.001 Lisboa Portugal, Febreuary.

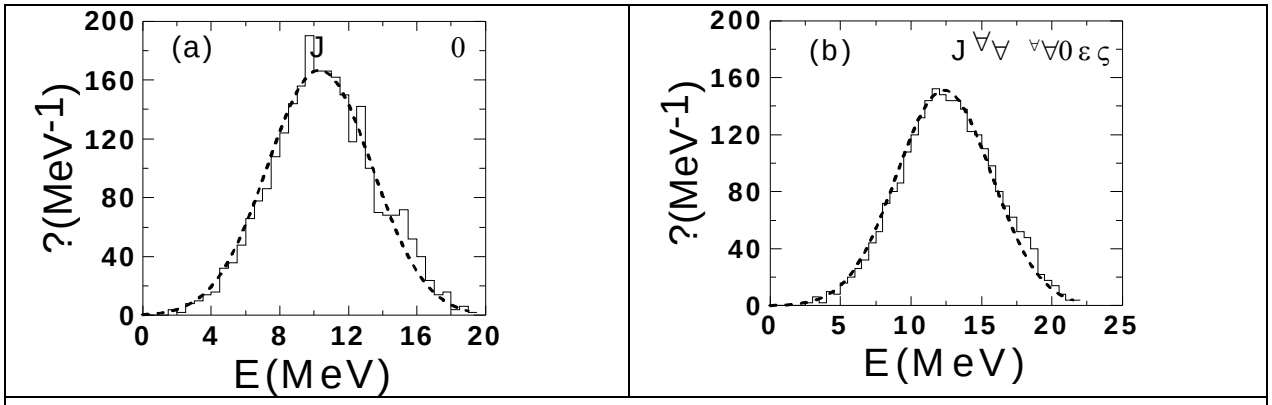

Fig. 1. The level density in ^{138}Ba nucleus for the $J^{\pi}T = 1^{+}3$ class of levels: (a) corresponds to the result with the absence of the off-diagonal interaction; (b) demonstrates the result with the full Hamiltonian.

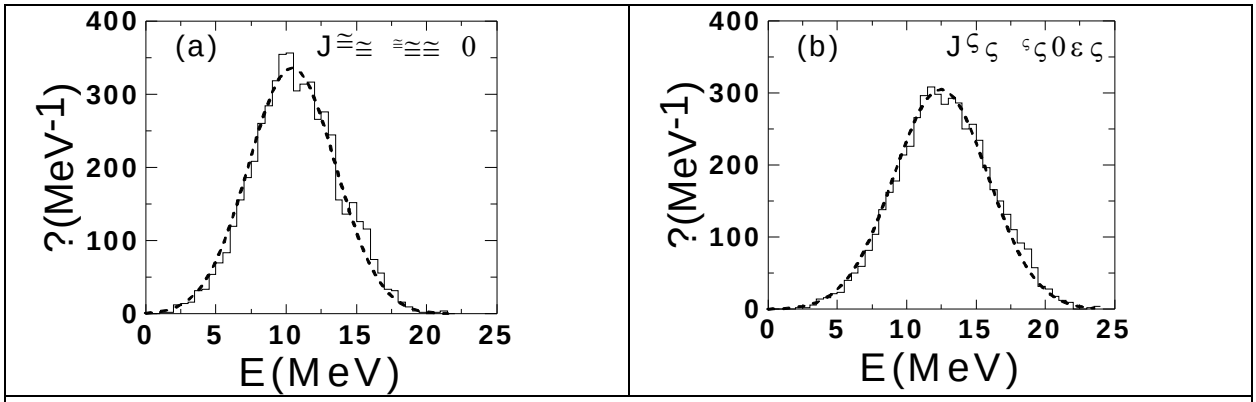

Fig. 2. Same as in Fig. 1 but for the $J^{\pi}T = 3^{+}3$ class of levels.

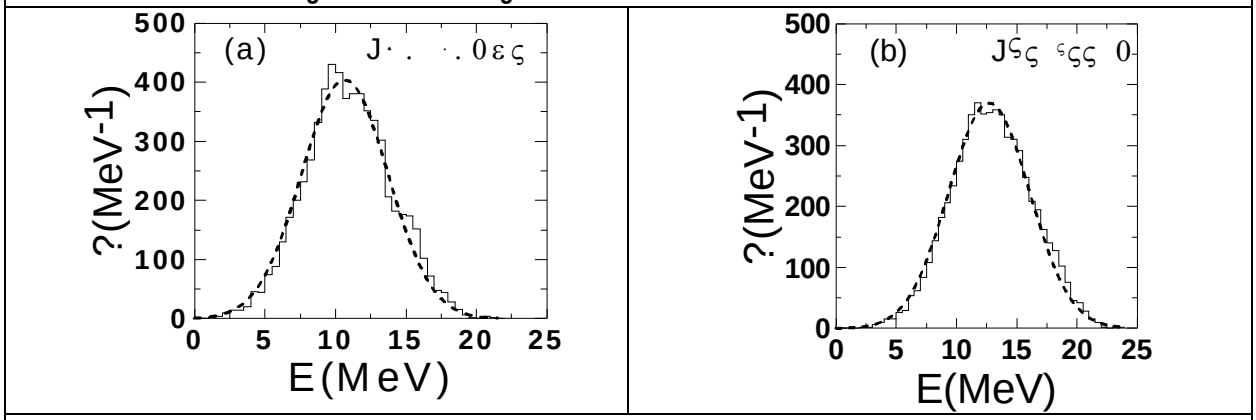

Fig. 3: Same as in Fig. 1 but for the $J^{\pi}T = 5^{+}3$ class of levels.

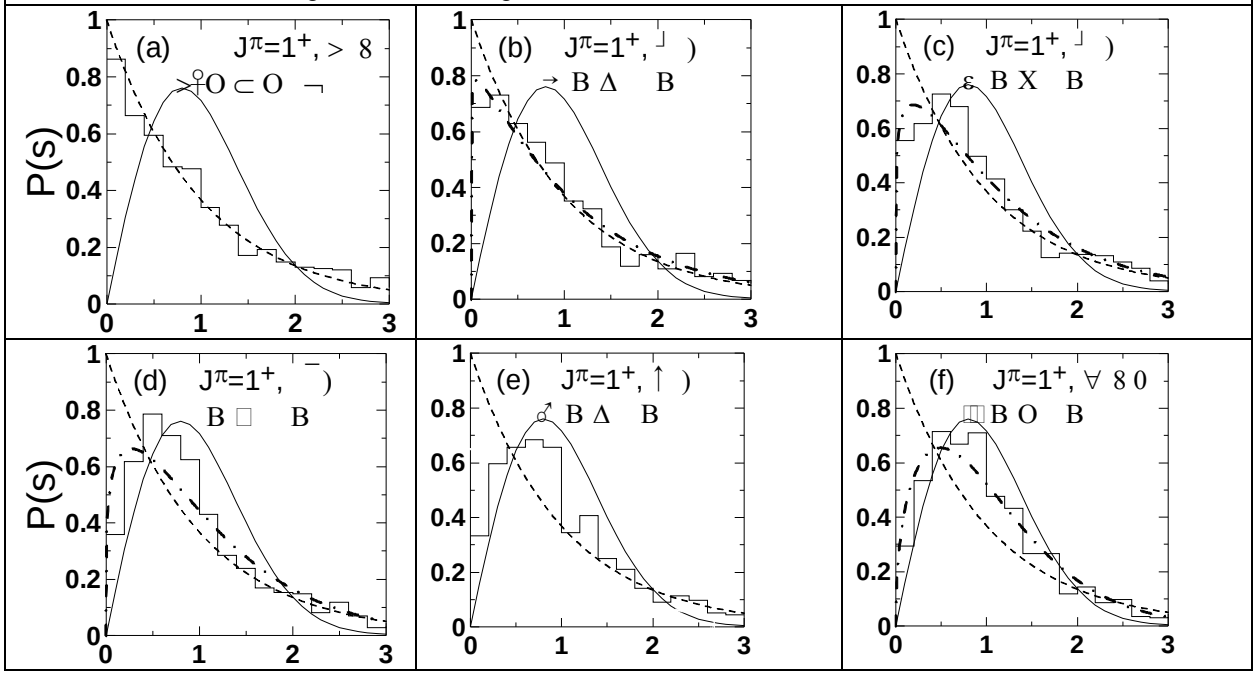

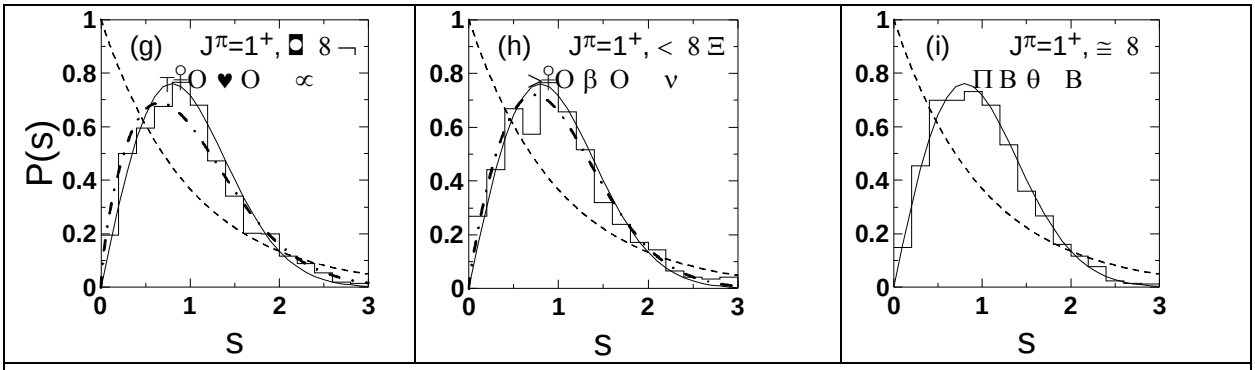

Fig. 4: The nearest neighbor level spacing $P(s)$ distributions in ^{138}Ba nucleus for the unfolded $J^{\pi}T = 1^{+}3$ states (histograms) calculated with interaction strength $\beta = 0$ (a), $\beta = 0.02$ (b), $\beta = 0.04$ (c), $\beta = 0.06$ (d), $\beta = 0.08$ (e), $\beta = 0.1$ (f), $\beta = 0.2$ (g), $\beta = 0.3$ (h), and $\beta = 1$ (i). The solid and dashed lines are the GOE and Poisson distributions, respectively. The dash-dotted line is the best-fitted Brody distribution with the quoted ω.

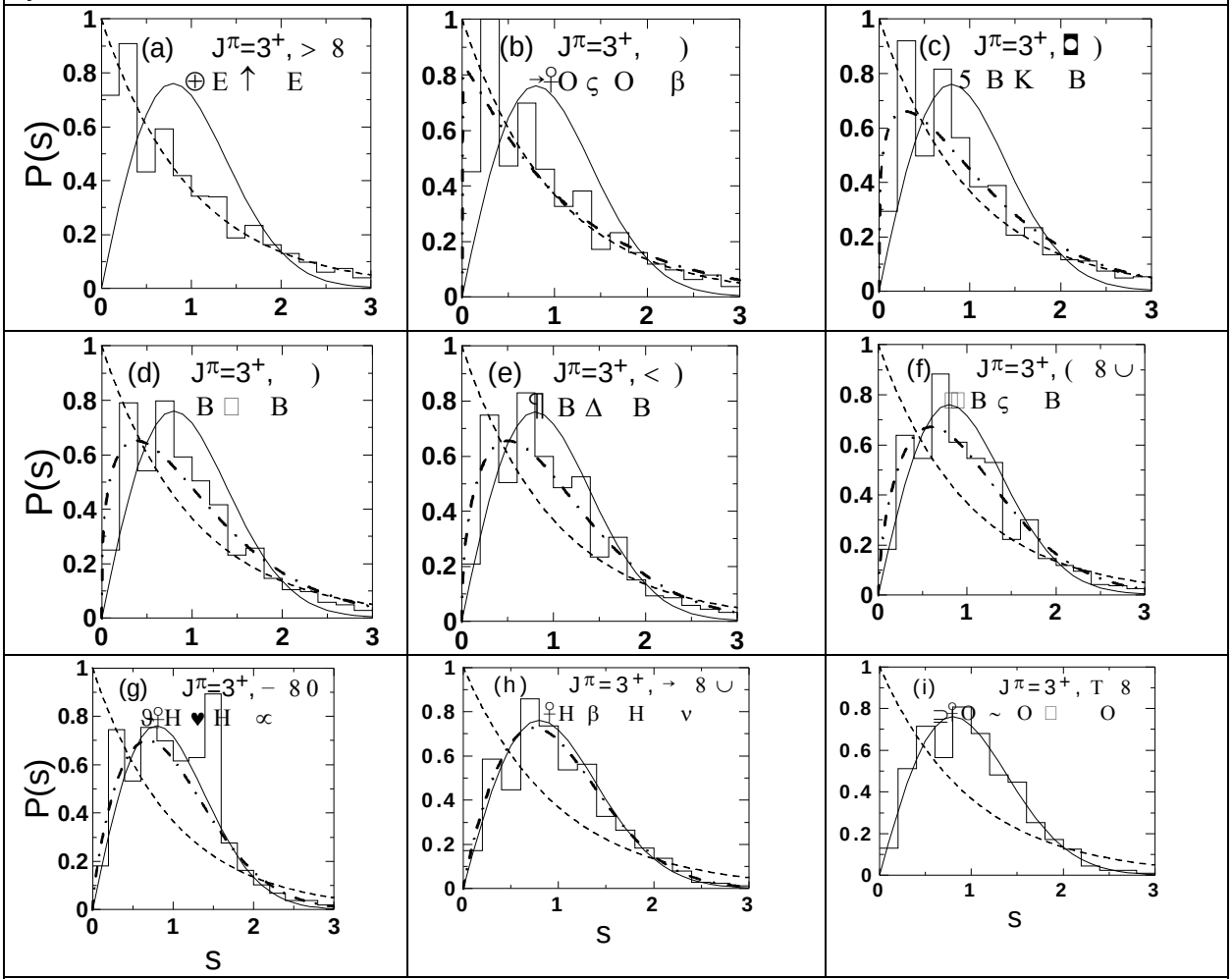

Fig. 5: Same as in Fig. 4 but for $J^{\pi}T = 3^{+}3$ states

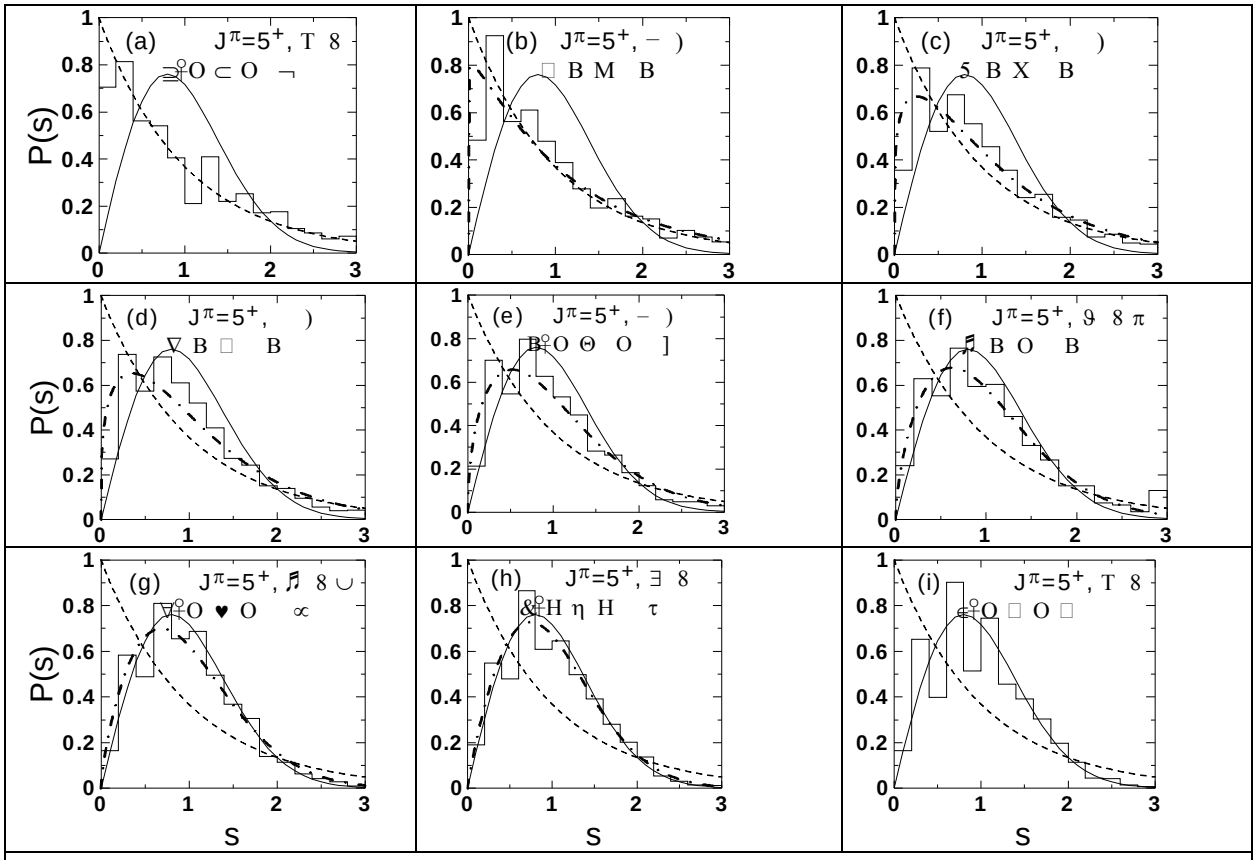

Fig. 6: Same as in Fig. 4 but for $J^{\pi}T = 5^{+}3$ states.

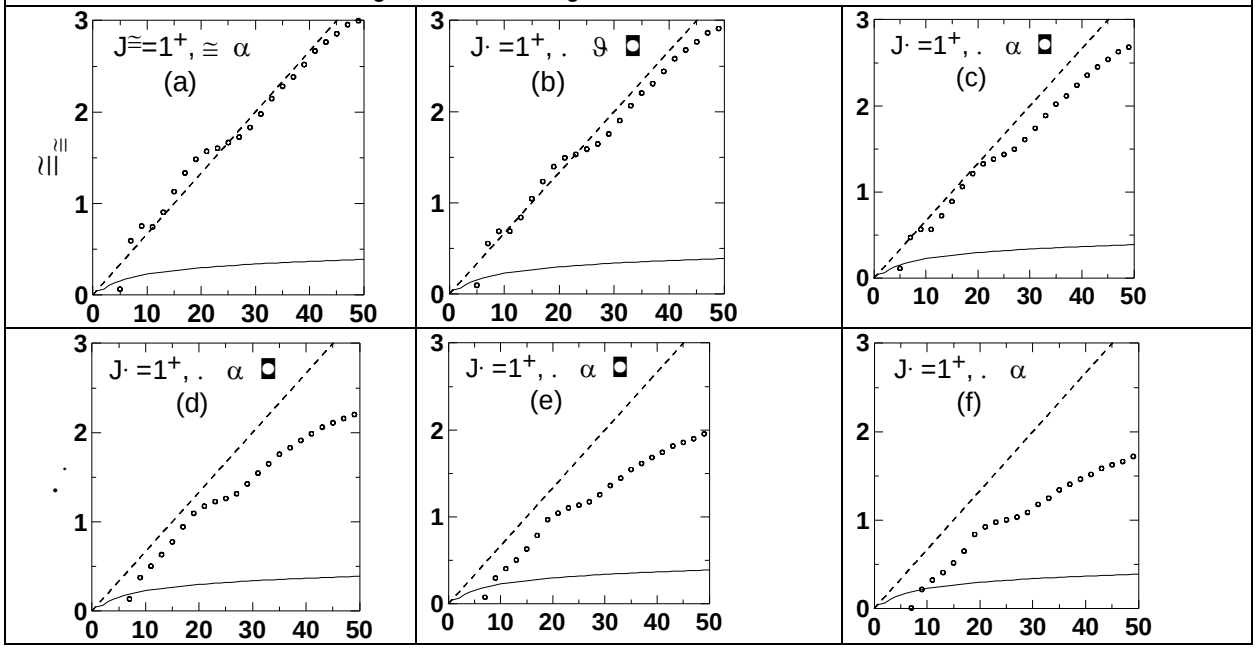

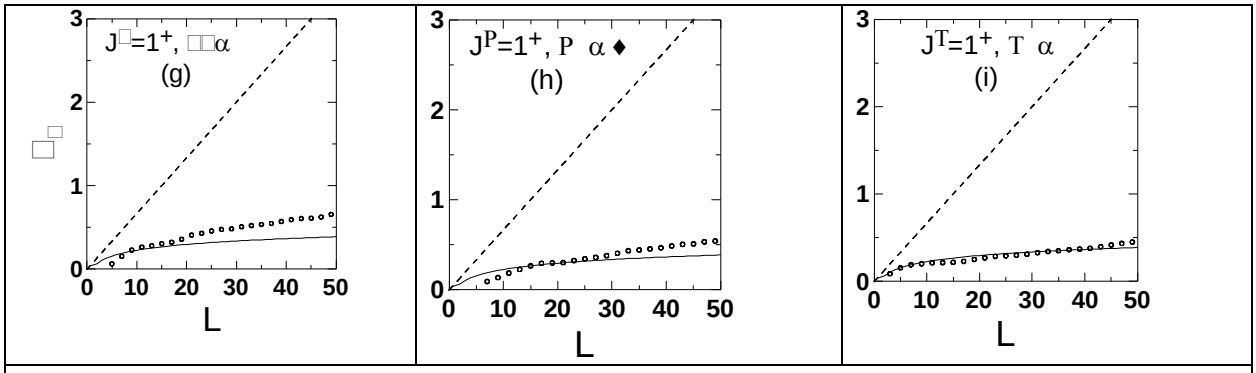

Fig. 7. The average Δ_3 statistic in ^{138}Ba nucleus for the unfolded $J^{\pi}T = 1^{+}3$ states (open circles) calculated with interaction strength $\beta = 0$ (a), $\beta = 0.02$ (b), $\beta = 0.04$ (c), $\beta = 0.06$ (d), $\beta = 0.08$ (e), $\beta = 0.1$ (f), $\beta = 0.2$ (g), $\beta = 0.3$ (h), and $\beta = 1$ (i). The solid and dashed lines are the GOE and Poisson distributions, respectively.

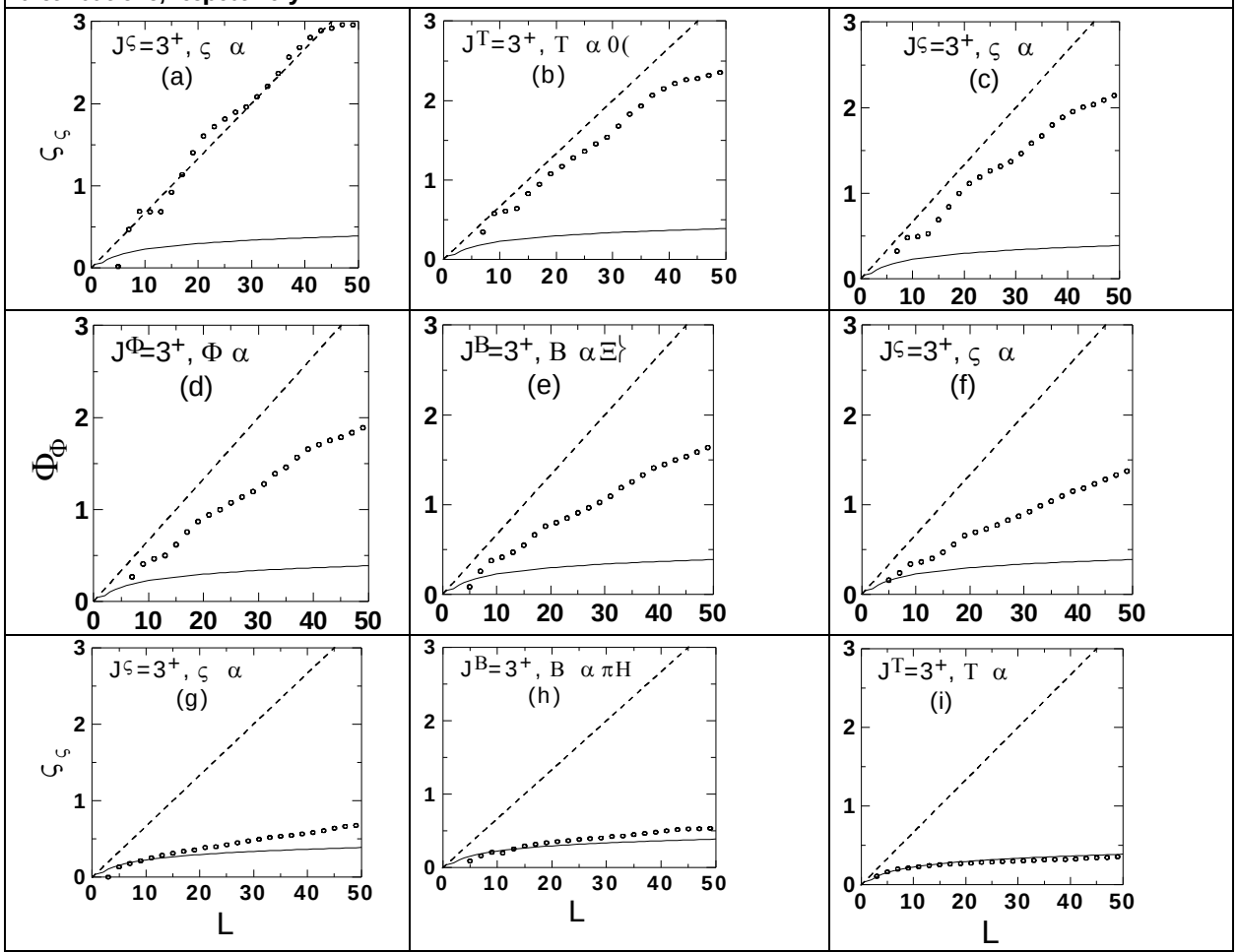

Fig. 8. Same as in Fig. 7 but for $J^{\pi}T = 3^{+}3$ states.

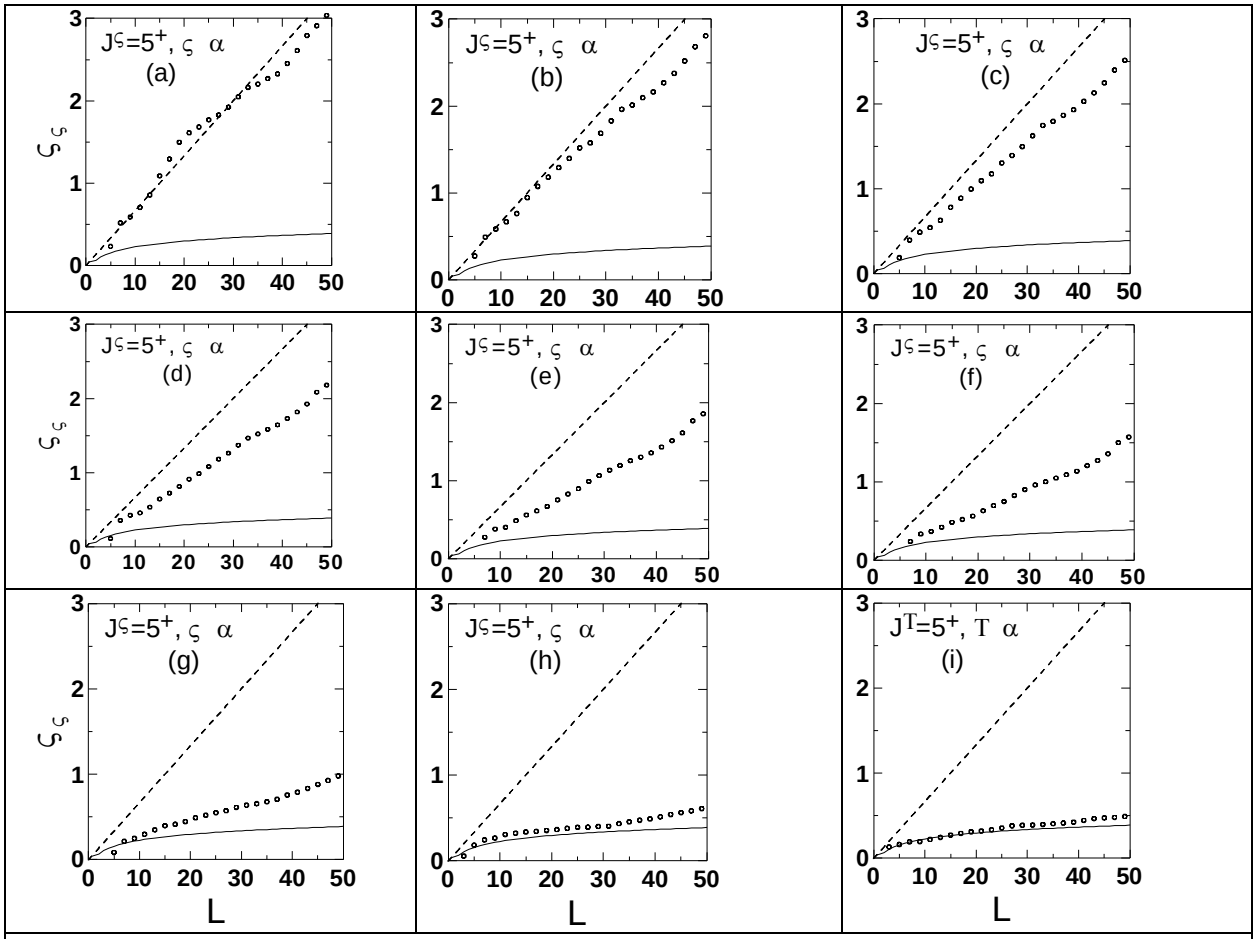

Fig. 9: Same as in Fig. 7 but for $J^{\pi}T = 5^{+}3$ states

Indian Journal of Natural Sciences www.tnsroindia.org.in ©IJONS

Vol.9 /Issue 52 / February / 2019 *International Bimonthly* *ISSN: 0976 – 0997*

RESEARCH ARTICLE

Using Exponential Weighted Moving Average EWMA Chart in Mixed Model ARMA

Halah Fadhil Hussein*

Post Graduate Institute for Accounting & Financial Studies, University of Baghdad, Iraq.

Received: 24 Oct 2018 Revised: 26 Nov 2018 Accepted: 28 Dec 2018

***Address for Correspondence**
Halah Fadhil Hussein
Post Graduate Institute for Accounting & Financial Studies,
University of Baghdad, Iraq.
Email: zain1alhak1@ gmail.com

ABSTRACT

The application of control charts in auto correlated processes is one of the important methods in controlling the statistical process, including time series models. When estimating these models for actual data, there are often errors in the estimation process. The design of the control charts by the presence of these errors leads to the average run length is much shorter than required in the statistical process.On the practical side, the ARMA models that were produced by Box – Jenkins were used for the sample representing the weekly sales of Apple Computers, and then the EWMA chart is used in three methods: the traditional chart (Roberts, 1959), the chart when the residuals are autocorrelated, and the modified charts to improve the quality of production processes and to detect changes of structural deviations in the process. It has been shown through the application that there is an effect of the parameter (λ) and the variance of the three using methods when calculating the average run length. It was found that there was an improvement in these averages when using the adjusted EWMA, followed by the EWMA when the residuals were correlated. In addition, the traditional EWMA was outside the statistical control limits at all values for (λ) and (L).

Keywords: Quality Control charts, EWMA chart, Residual chart, ARIMA Model, Average Run

INTRODUCTION

Control charts in time series are important methods of monitoring autocorrelated statistical processes. The techniques of these charts have been widely used to monitor and improve the quality of production processes. The main purpose of monitoring these processes is to detect changes or structural deviations in the process over time that may result from the inability to control the process. The Statistical Process Control (SPC) and in particular the traditional

process depends on the assumption that the observations of the process are independent, however, result in some cases where large amounts of highly autocorrelated in process data are available for process monitoring. Various research (see e.g., schewart [11], [12], page [8] and Goldsmith & Whitfield [5]) has investigated applying schewart, CUSUM, EWMA, and other type of control charts to the residuals of the models. Some of them using the Monte Carlo method in CUSUM chart.

At the end of the eighties, the problem of dependency became the subject of interest to most researcher. Alwan [2] analysed a large number of data and found that about 85% of control limits were inappropriate and did not match the dependency of statistical operations. Of the half of these cases, which neglect the correlation, the influential factor was within the control of those groups. Therefore, the impact of correlation in control charts should be reviewed as quality control tools. In 2014, Knoth and Schmind [6] studied autocorrelated statistical process charts of control charts for time series, also referred to as residual – based control charts. In addition, Siqueira [13] and others examined the application of control of the seasonal time series of the Nuclear acid (RNA) sample of children in Belem.

Search Problem

The application of control chart in the production processes and other assumes that the observations of the process are independent, and that the application of these charts in time series may lead to a violation within the control chart, because of the dependency of the time series observations, thus addressing the problem of dependency to obtain the limits of convincing control.

Objective of Research

The objective of research is to apply the EWMA chart based on the residuals of time series models described in the ARMA model for weekly sales of Apple computer for the period (1/9/2012 – 31/12/2015) by using three methods of control chart (EWMA) and the comparison between them to detect the structural deviations in estimated series of residuals.

Theoretical Side

The most widely method in the statistical process chart of autocorrelated processes is the control charts for time series, which also referred to as control charts based on residuals.
Assume that the process $\{X_t\}$ is subject to ARMA model as [4]:

$$X_t - \phi_1 X_{t-1} - \phi_2 X_{t-2} - \ldots - \phi_p X_{t-p} = \varepsilon_t - \theta_1 \varepsilon_{t-1} - \theta_2 \varepsilon_{t-2} - \ldots - \theta_q \varepsilon_{t-q} \qquad \ldots(1)$$

Where $\phi's$ and $\theta's$ are the parameters of autoregressive and moving average components respectively, (p) and (q) are the order of these components, and $\{\varepsilon_t\}$ is the random process which distributed independently with mean of zero and the variance of σ_ε^2 , i.e. $\varepsilon_t \sim N(0, \sigma_\varepsilon^2)$

Using the backshift operator (B) in eq. (1), it can be written:

$$X_t = \frac{\Theta(B)}{\Phi(B)} \varepsilon_t \qquad \ldots(2)$$

Whereas:

$$\Theta(B)=1-\theta_1 B-...-\theta_q B^q$$

$$\Phi(B)=1-\phi_1 B-...-\phi_p B^p$$

The basic idea of using the charts based on the residuals is to directly monitoring the series of residuals in the model of the time series generated by:

$$e_t=\Theta^{-1}(B)\phi(B)X_t \qquad ...(3)$$

In practice, the ARMA model evaluates of process observations. On the assumption that $\{\widehat{\theta}\}_1^q, \{\widehat{\phi}\}_1^p$ and σ_ε^2 represent the estimated parameters of the ARMA model and $\hat{\Phi}(B)$ and $\hat{\Theta}(B)$ are defined as the polynomials of the (AR) and (MA) respectively. To simplify, assume that p and q are known, then the residuals can be generated using the estimated model through:

$$e_t=\frac{\hat{\phi}(B)}{\hat{\Theta}(B)}X_t$$

$$=\frac{\hat{\phi}(B)\Theta(B)}{\hat{\Theta}(B)\phi(B)}\varepsilon_t \qquad ...(4)$$

With estimation error, the residuals follow the $\mathrm{ARMA}(p+q, p+q)$ model and no longer (iid) residual autocorrelation due to modelling errors can have a significant effect on the (ARL) [1], [7].

Traditional Ewma Chart

This chart was proposed by Robert [9], and its formula as follows:

$$Z_t=(1-\lambda)Z_{t-1}+\lambda X_t \qquad t>1 \qquad ...(5)$$

The initial value Z_0 is equal to (μ) , λ is the smoothing parameter and its value shall be within the period [0, 1]. In the EWMA chart, the averages of the subgroups are taken to form (Z_t) as follows:

$$Z_t=(1-\lambda)Z_{t-1}+\lambda\overline{X}_t \qquad ...(6)$$

And using the iterative replacement for (Z_t) when $t=1,2,...,n$ result that:

$$Z_t=\lambda\sum_{j=0}^{t-1}(1-\lambda)^j\,\overline{X}_{t-j}+(1-\lambda)^t Z_0 \qquad ...(7)$$

Thus, the variance formula is:

$$\mathrm{var}(Z_t)=\sigma_z^2=\frac{\sigma^2}{n}\left(\frac{\lambda}{2-\lambda}\right)\left[1-(1-\lambda)^{2t}\right] \qquad ...(8)$$

And when the eq. (5) is used to compute EWMA based on residuals, this is done as follows:

$$Z_t=(1-\lambda)Z_{t-1}+\lambda e_t \qquad ...(9)$$

For any specific value to (λ) ,the typical design of the (EWMA) when the model is optimal is to set the control limits as follows:

$$\pm L\sigma_{z,0} = \pm L\hat{\sigma}_{\varepsilon}\sqrt{\frac{1-v}{1+v}} \qquad ...(10)$$

Where λ is selected to determine the value of in-control (ARL) and $v = 1-\lambda$, as well as be:

$$\sigma^2_{z,0} = \hat{\sigma}^2_{\varepsilon}(1-v)/(1+v)$$

And it is a variance under the assumption that there are no errors for the model. It should be noted that there are special tables that give values of (L) which then produce different values to (ARL) and different values to (λ) .

Using the (Ewma) Variance in Case of Autocorrelated Residuals [3, 4]

Sometimes the residuals of model are autocorrelated, so the real variance of (Z_t) may be very different from $\sigma^2_{z,0}$. By combining equation (4) and (9), then Z_t is modelled as $\mathrm{ARMA}(p+q, p+q)$ with the following formula:

$$z_t = \frac{(1-v)\hat{\Phi}(B)\Theta(B)}{(1-vB)\hat{\Phi}(B)\Phi(B)}\varepsilon_t \qquad ...(11)$$

And when the estimates of the parameter are random estimates, the variance of the (EWMA) is itself random variable. And σ^2_z is the expected value of (EWMA) variance, which is related to the distribution of random estimates of the parameter, then σ^2_z will be a function of the common variance matrix of parameters $\{\hat{\phi}_i\}$ where $i = 1,...,p$ and $\{\hat{\theta}_i\}$ where $i = 1,...,q$. And according to equation (10), the basic idea would be to use the control limits of (EWMA) based on the residuals, where σ^2_z is always greater than $\sigma^2_{z,0}$ because of the uncertainly of the diagnosis and estimation of the ARMA model.

If assume that a time series $\{X_t\}$ is subject to $\mathrm{ARMA}(p,q)$ model, and that the parameters of model were estimated by using common estimation methods (non – linear least squares and approximate ML). The common variance matrix of the model is as follows:

$$\sum\nolimits_{\alpha} = \frac{\sigma^2_{\varepsilon}}{n}\sum\nolimits_{y}^{-1}$$

Where the $\sum_y$ the matrix of variance – covariance of the vector defined as:

$$y_t = \left[u_t u_{t-1}...u_{t-p+1} v_t v_{t-1}...v_{t-q+1}\right]$$

And

$v_t = -\Theta^{-1}(B)\varepsilon_t$, $u_t = -\Phi^{-1}(B)\varepsilon_t$

Thus, the matrix $\sum_{\alpha}$ in the case of ARMA (1,1) is as follows:

$$\sum_{\alpha} = \frac{(1-\phi_1\theta_1)}{n(\phi_1-\theta)_1}\begin{bmatrix}(1-\phi_1^2)(1-\phi_1\theta_1) & (1-\phi_1^2)(1-\theta_1^2)\\ (1-\phi_1^2)(1-\theta_1^2) & (1-\theta_1^2)(1-\phi_1\theta_1)\end{bmatrix} \qquad ...(12)$$

And from equation (11), it is clear that the variance of (Z_t) depends on $(\hat{\alpha})$ which

$$\sigma_z^2 = E\left[E(Z_t^2/\hat{\alpha})\right] = E\left[\sigma_{z/\hat{\alpha}}^2\right]$$

To find the variance of (σ_z^2) and $(\sigma_{z/\hat{\alpha}}^2)$, equation (11) should be linearized about $\hat{\phi}(B) = \phi(B)$ and $\hat{\Theta}(B) = \Theta(B)$,then, learizing gives:

$$\frac{(1-v)\hat{\phi}(B)\Theta(B)}{(1-vB)\hat{\Theta}(B)\phi(B)} = \left[\frac{(1-v)\Theta(B)}{(1-vB)\phi(B)}\right]\left[\frac{\hat{\phi}(B)}{\hat{\Theta}(B)}\right]$$

$$= \left[\frac{(1-v)\Theta(B)}{(1-vB)\,\hat{\phi}(B)}\right]\left[\frac{\phi(B)+\phi^*(B)}{\Theta(B)+\Theta^*(B)}\right]$$

Where:

$\phi^*(B) = \hat{\phi}(B) - \phi(B)$

$\Theta^*(B) = \hat{\Theta}(B) - \Theta(B)$

Represent the errors of estimation of the two parameters.

$$\therefore \frac{(1-v)\hat{\phi}(B)\Theta(B)}{(1-vB)\hat{\Theta}(B)\phi(B)} = \left[\frac{(1-v)\phi(B)}{(1-vB)\Theta(B)}\right]\left[\frac{\phi(B)}{\Theta(B)} + \frac{\phi^*(B)}{\Theta(B)} - \frac{\phi(B)\Theta^*(B)}{\Theta^2(B)}\right]$$

$$= (1-v)\left[\frac{1}{(1-vB)} + \frac{\phi^*(B)}{(1-vB)\phi(B)} - \frac{\Theta^*(B)}{(1-vB)\Theta(B)}\right] \qquad ...(13)$$

Assuming that the $wj = 0,1,2,...$, represent the coefficients of the impulse response function, then:

$$\frac{(1-v)\hat{\phi}(B)\Theta(B)}{(1-vB)\hat{\Theta}(B)\phi(B)} = (1-v)\sum_{j=0}^{\infty} wjB^j \qquad ...(14)$$

Thus:

$$Z_t = \left\{(1-v)\sum_{j=0}^{\infty} wjB^j\right\}\varepsilon_t$$

$$= (1-v)\sum_{j=0}^{\infty} wj\varepsilon_{t-j} \qquad ...(15)$$

The parameters of the response function depend on v, α, α^* when $\alpha^* = \hat{\alpha} - \alpha$. Then the conditional and unconditional variance of (Z_t) become:

$$\sigma^2_{z/\alpha} = (1-v)^2 \sigma^2_\varepsilon \sum_{j=0}^{\infty} w_j^2$$

$$\sigma^2_z = E\left[\sigma^2_{z/\alpha}\right] = (1-v)^2 \sigma^2_\varepsilon \sum_{j=0}^{\infty} E(w_j^2) \qquad ...(16)$$

To find an (EWMA) variance of ARMA (1,1) , it should be found $\sum_{j=0}^{\infty} E(w_j^2)$ as follows:

The impulse response in equation (13) represents the sum of responses to three transform functions:

$$W_j = W_{0j} - \phi^* W_{\phi, j-1} + \Theta^* W_{\theta, j-1} \qquad ...(17)$$

Whereas

$$\sum_{j=0}^{\infty} w_{0,j} B^j = \frac{1}{1-vB} = \sum_{j=0}^{\infty} v^j B^j \qquad ....(18)$$

$$\sum_{j=0}^{\infty} w_{\phi,j} B^j = \frac{1}{(1-vB)(1-\phi B)} = \frac{1}{v-\phi} \sum_{j=0}^{\infty} (v^{j+1} - \phi^{j+1}) B^j \qquad ....(19)$$

$$\sum_{j=0}^{\infty} w_{\theta,j} B^j = \frac{1}{(1-vB)(1-\theta B)} = \frac{1}{v-\theta} \sum_{j=0}^{\infty} (v^{j+1} - \theta^{j+1}) B^j \qquad ....(20)$$

And by equating the coefficients on the right and left sides of the equations (18, 19, 20) and substituting these into equation (17), gives:

$$w_j = v^j - \frac{\phi^*(v^j - \phi^j)}{v-\phi} + \frac{\theta^*(v^j - \phi^j)}{v-\theta}$$

$$\therefore E(w_j^2) = v^{2j} + \frac{\sum \phi}{(v-\phi)^2}(v^{2j} - 2v^j\phi^j + \phi^{2j}) + \frac{\sum \theta}{(v-\theta)^2}(v^{2j} - 2v^j\theta^j + \theta^{2j})$$

$$- 2\frac{\sum \phi\theta}{(v-\phi)(v-\theta)}(v^{2j} - 2v^j\phi^j - 2v^j\theta^j + \phi^j\theta^j) \quad ...(21)$$

Where $\sum \phi\theta, \sum \theta, \sum \theta$ represents the variance of ϕ and θ and the covariance of $\phi\theta$ respectively.

Summing equation (21) term by term for $j = 0,1,2,....$ gives:

$$\sum_{j=0}^{\infty} E(w_j^2) = \frac{1}{1-v^2} + \frac{\sum\phi}{(v-\phi)^2(1-v^2)}\left[1 - \frac{2(1-v^2)}{1-v\phi} + \frac{1-v^2}{1-\phi^2}\right]$$

$$+ \frac{\sum\theta}{(v-\theta)^2(1-v^2)}\left[1 - \frac{2(1-v^2)}{1-v\theta} + \frac{1-v^2}{1-\theta^2}\right]$$

$$- \frac{\sum\phi\theta}{(v-\phi)(v-\phi)(1-v^2)}\left[1 - \frac{1-v^2}{1-v\phi} - \frac{1-v^2}{1-v\theta} + \frac{1-v^2}{1-\phi\theta}\right]$$

$$= \frac{1}{1-v^2}\left[1 + \frac{\sum\phi}{1-\phi^2}\left(\frac{1+v\phi}{1-v\phi}\right) + \frac{\sum\theta}{1-\theta^2}\left(\frac{1+v\theta}{1-v\theta}\right) - \frac{\sum\phi\theta}{1-\phi\theta}\left(\frac{1-v^2\phi\theta}{(1-v\phi)(1-v\theta)}\right)\right] \quad ....(22)$$

And substituting equation (22) into equation (16) gives:

$$\sigma_z^2 = \sigma_\varepsilon^2 \frac{1-v}{1+v}.\left[1 + \frac{1+v\phi}{n(1-v\phi)} + \frac{1+v\theta}{n(1-v\theta)}\right] \quad ....(23)$$

Modified Ewma Chart

The idea of modifying this chart is to generalize the control of the traditional charts when the data is correlated. The modified EWMA chart presented by Schmid [10] and Knoth & Schhmid [6] and based on the formula:

$$Z_t = (1-\lambda) Z_{t-1} + \lambda X_t \qquad , t \geq 1$$

Assume that the process $\{Z_t\}$ is stationary on the mean (μ) , and the (γ_v) represents the autocovariance function, then:

$$\sigma_e^2 = \frac{\lambda}{2-\lambda} \sum_{j=-\infty}^{\infty} \gamma_j (1-\lambda)^{|j|} \qquad , t \to \infty$$

$$\operatorname{cov}(Z_t, Z_{t+h}) = \lambda^2 \sum_{t=-(t+h-1)}^{t-1} \gamma_i \sum_{r=\max(0,-h-i)}^{\min(t-1+i,\,t-1)} (1-\lambda)^{2r+i+h}$$

For example, for AR (1) model, the variance is:

$$\sigma_e^2 = \sigma_\varepsilon^2 \frac{\lambda}{2-\lambda}.\frac{1+\phi_1(1-\lambda)}{1+\theta_1(1-\lambda)} \qquad .....(24)$$

And when $\phi_1 = 0$, then the variance of independent variables will be obtained.

Applid Side

A sample of (171) observations representing the weekly sales of Apple Computers were used for the period (1/9/2012 – 31/12/2015) shown in Table (1) and then the time series as shown in Figure (1). The graph shows that the series is free of high fluctuations indicating that it is stationary in the variance, and in order to know its stationarity on mean, the coefficients of autocorrelation function (ACF) were calculated and therefore these coefficients were plotted in Figure (2). It is shown in Figure (2) that the ACF coefficients were significant at the lags (1, 2, 3, ……, 8). This indicates that the series is non – stationary on mean. Thus, the first difference of the series shown in Figure (3) was obtained and the coefficients of the partial autocorrelation function (PACF) of differencing series were determined as shown in Figures (4) and (5) respectively. As shown in Figure (4), the (ACF) coefficients decreases exponentially and decays to zero. And the (PACF) coefficients were irregular in their behaviour, but the first lag was significant differed from zero. Therefore, the initial diagnosis of the model is first order autoregressive model ARI (1,1). The maximum likelihood method (MLE) was used to estimate the parameters of the proposed model. The initial estimate of the model was as follows:

$$(1-B)(1-0.5227B)X_t = a_t$$

Where the mean square error (MSE) for the model was equal to (298.1). To examine the suitability of the model, the (ACF) coefficients of the residuals were calculated. Figure (6) shows the plot of these coefficients, and it is clear that all these coefficients fall within the confidence level (± 0.151) with significance level (0.05). In addition to the original series was plotted with the estimated values as shown in Figure (7). The value of the (Ljung – Box) statistic was calculated as equal to (29.3) and compared with the value of tabulated χ^2 with (48) degrees of freedom and (0.05) significance level, which is equal to (65.152), indicating that the calculated value was less than the table value. This means that the series of risduals being random and the proposed model was appropriate.

Application Control Charts

After calculating the residuals series as shown in Table (2), it was plotted as in Figure (8). Thus, the values of the smoothing parameter (λ) were selected as in Table (3). Therefore, the variance of the methods were calculated. The variance of the traditional (EWMA) $\sigma^2_{z,0}$, the variance of the (EWMA) when residuals were calculated σ^2_z and the variance of the modified (EWMA) σ^2_e were calculated according to equations (10, 23 and 24) respectively. As shown in Table (3), the values of these variance increase as the value of (λ) increases. It is noted that the values of variance σ^2_e were greater than the values of variances for other charts for different values of (λ) . The control limits of the three methods were also calculated. Table (4) shows the values of the control limits $(\pm L\sigma_e),(\pm L\sigma_z),(\pm L\sigma_{z,0})$ at (0.01) and (0.05) significance level, when the values of L equal to (2.616) and (2.814) respectively. It is also shown in Table (4) that the control limit of modified (EWMA) chart was greater than the control limit of the other methods with various value of (λ) . In addition to, the ARL has been calculated for the three methods as shown in Table (5) as follows: Six different cases were then selected to plot the control limits for the residual series of the estimated model when (L= ± 2.216) and $\lambda = 0.05, 0.25, 0.40$ as shown in Figures (9, 10, 11) and L= ± 2.814, $\lambda = 0.05, 0.25, 0.40$ as shown in Figures (12, 13, 14).

CONCLUSIONS

1. The studied time series was non – stationary in the mean and the first difference was taken. The optimal model for the series observation was ARI (1,1).
2. The variance of the modified EWMA was the largest compared to the variance values of traditional EWMA and EWMA in case the residuals were calculated to the different values of (λ) as in Table (4).
3. There was an effect of the (λ) values and variance of the used methods when calculated the (ARL). The use of modified EWMA chart gave the largest value of (λ), especially when L= $\pm$ 2.814 , and only one when L= $\pm$ 2.216 and $\lambda = 0.15$.
4. Through the figures of control charts for all methods, the values of residuals were found to be within the control limits of modified EWMA when L= $\pm$ 2.216, $\lambda = 0.40$ as shown in Figures 12 and 13 respectively. For the traditional EWMA, most of the residuals were out of the control limits for all (λ) and (L) values.

Recommendation

1. Using the modified control chart (EWMA) method for the residuals series of seasonal and non – seasonal models.
2. Making a theoretical comparison between the three control charts (EWMA).
3. Studying the effect of outliers in time series on the control charts (EWMA).

REFERENCES

1. Adams, B. M. and Tseng, L.T. (1998), "Robustness of Forecast – Based Monitoring Schemes", J-Quality Tech., 30(4), PP328 – 339.
2. Alwan, L.C. and Roberts, H. V. (1988). "Time – Series Modeling for Statistical Process Control", J.Bus. Econ. Stat., PP87 – 95.
3. Apley, D.W. (2002), "Time Series Control Charts in the Presence of Model Uncertainty", J. of Manuf. Science and Engi.,vol.124, 891-898
4. Box, G., Jenkins, G. and Reinsel, G. (1994). Time Series Analysis Forecasting and Control 3rd ed. Englewood cliffs, NJ.
5. Goldsmith, P.L. and Whitield (1961), "Average run Lengths in Cumulative Chart quality Control Schemes",Technometrics, 3,48 – 57.
6. Knoth, S. and Schmid, W. (2014). "Control Charts for time Series: A review", Statistical Papers, 38, PP 1 – 28.
7. Lu, C. W. and Reynolds, M. R. (1999), "EWMA Control Chart for monitoring the mean of Auto correlated Processes", J. Quality Tech, 31(2), PP 166 – 188.
8. Page, E. S. (1954). "Continuous inspection schemes", Biometrika 41, PP 100 – 115.
9. Roberts, S. W. (1959). "Control chart tests based on heometric moving Averages", Technometrics, 1, PP 239 – 250.
10. Schmid, W. (1997a). "on EWMA charts for time Series, in: H, J. lenz and P.Th. wilrich (EDS), Frontiers in Statistical Quality control, physica, Heidelberg, Germany, PP 115 – 137.
11. Shewhart, W. A. (1926), "Quality control charts", Bell system Technical Journal, PP 593 – 603.
12. Shewhart, W. A. (1931), "Economic control of Quality of manufactured product, D. van Nostrand company, Inc., Toronto, Canada. seasonality of norovirus ".Rev.Pan-Amaz saude , 6(2), pp 61-68 .
13. Siqueira , H.A.M., Nunes , A.A.G.C. and Ferreira , M.S.(2015). " Application of Time Series Control Charts to model and monitor the seasonality of norovirus ".Rev.Pan-Amaz saude , 6(2), pp 61-68 .

Table 1. Time series observations of Apple Computers sales

t	Z_t	t	Z_t	t	Z_t	t	Z_t	t	Z_t
1	1200.13	36	1241.68	71	1531.22	106	1432.89	141	1415.24
2	1202.78	37	1261.38	72	1532.90	107	1435.10	142	1404.25
3	1207.49	38	1246.87	73	1535.33	108	1430.72	143	1429.64
4	1215.75	39	1263.83	74	1537.93	109	1426.22	144	1423.65
5	1228.38	40	1311.19	75	1539.67	110	1423.72	145	1420.24
6	1227.63	41	1342.48	76	1539.86	111	1418.59	146	1427.29
7	1241.17	42	1386.09	77	1540.85	112	1419.11	147	1461.77
8	1263.46	43	1398.17	78	1541.35	113	1420.07	148	1492.04
9	1283.54	44	1426.83	79	1543.13	114	1421.13	149	1512.97
10	1307.67	45	1460.21	80	1539.56	115	1422.77	150	1504.67
11	1333.26	46	1499.73	81	1537.40	116	1424.39	151	1504.01
12	1361.92	47	1510.82	82	1535.12	117	1427.53	152	1512.23
13	1353.22	48	1522.61	83	1535.16	118	1430.85	153	1512.59
14	1332.85	49	1511.35	84	1533.35	119	1432.71	154	1487.52
15	1347.53	50	1521.90	85	1530.89	120	1434.77	155	1438.74
16	1346.33	51	1547.91	86	1529.94	121	1435.20	156	1443.35
17	1295.17	52	1587.26	87	1528.13	122	1434.23	157	1433.68
18	1287.76	53	1591.10	88	1523.46	123	1429.72	158	1409.35
19	1297.09	54	1589.64	89	1516.27	124	1428.69	159	1387.84
20	1299.59	55	1586.02	90	1516.09	125	1427.24	160	1350.91
21	1305.33	56	1577.74	91	1512.57	126	1428.76	161	1360.85
22	1327.88	57	1576.66	92	1510.46	127	1429.95	162	1386.82
23	1387.07	58	1578.39	93	1508.35	128	1433.41	163	1372.53
24	1374.05	59	1580.16	94	1506.21	129	1439.65	164	1349.23
25	1394.55	60	1577.79	95	1505.15	130	1440.55	165	1320.89
26	1407.62	61	1570.37	96	1504.73	131	1437.53	166	1289.56
27	1429.29	62	1561.17	97	1505.74	132	1439.84	167	1276.93
28	1424.20	63	1550.42	98	1508.03	133	1442.77	168	1269.77
29	1406.69	64	1548.84	99	1509.97	134	1444.31	169	1268.63
30	1392.74	65	1551.44	100	1512.77	135	1445.39	170	1276.03
31	1374.92	66	1549.85	101	1509.29	136	1446.31	171	1280.46
32	1356.01	67	1545.00	102	1496.06	137	1445.27		
33	1314.04	68	1538.87	103	1484.06	138	1439.11		
34	1261.74	69	1531.34	104	1456.30	139	1428.65		
35	1243.17	70	1528.85	105	1438.19	140	1411.73		

Table (2) Residuals series of ARI (1,1) model

t	$\hat{a}_t$	T	$\hat{a}_t$	t	$\hat{a}_t$	t	$\hat{a}_t$	t	$\hat{a}_t$
1	*	36	8.2158	71	3.6714	106	4.1664	141	12.3528
2	1.9261	37	20.4788	72	0.4413	107	4.9756	142	-12.8251
3	3.3249	38	-24.0164	73	1.5519	108	-5.5280	143	11.1340
4	5.7983	39	24.2438	74	1.3299	109	-2.2104	144	-19.2603
5	8.3128	40	18.4957	75	0.3811	110	-0.1566	145	-0.2793
6	-7.3512	41	6.5368	76	-0.7194	111	-3.8137	146	8.8323
7	13.9320	42	21.2560	77	0.8907	112	3.1921	147	20.7952

8	15.2132	43	-10.7132	78	-0.0174	113	0.6884	148	12.2487
9	8.4299	44	22.3463	79	1.5187	114	0.5638	149	5.1091
10	13.6350	45	18.4006	80	-4.5003	115	1.0819	150	-19.2393
11	12.9782	46	22.0736	81	-0.2941	116	0.7709	151	3.6781
12	15.2851	47	-9.5655	82	-1.1511	117	2.2856	152	8.5650
13	-23.6794	48	5.9937	83	1.2317	118	1.6779	153	-3.9363
14	-15.8229	49	-17.4222	84	-1.8309	119	0.1293	154	-21.3582
15	24.3259	50	16.4352	85	-1.5140	120	1.0863	155	-23.6769
16	-8.8727	51	20.4959	86	0.3357	121	-0.6427	156	20.1054
17	-20.5328	52	18.7556	87	-1.3135	122	-1.1998	157	-12.0795
18	19.3293	53	-16.7267	88	-3.7240	123	-3.9985	158	-19.2759
19	13.2029	54	-3.4670	89	-4.7492	124	1.3206	159	-8.7937
20	-2.3764	55	-2.8569	90	3.5779	125	-0.9120	160	-25.6876
21	4.4333	56	-6.3880	91	-3.4259	126	2.2874	161	20.2419
22	19.5499	57	3.2476	92	-0.2702	127	0.3894	162	20.7748
23	17.4040	58	2.2945	93	-1.0072	128	2.8331	163	-22.8635
24	-18.9563	59	0.8658	94	-1.0372	129	4.4417	164	-15.8312
25	17.3050	60	-3.2951	95	0.0585	130	-2.3681	165	-16.1620
26	2.3555	61	-6.1813	96	0.1340	131	-3.4898	166	-16.5178
27	14.8388	62	-5.3219	97	1.2295	132	3.8870	167	3.7450
28	-16.4161	63	-5.9415	98	1.7621	133	1.7217	168	-0.5588
29	-14.8497	64	4.0386	99	0.7431	134	0.0137	169	2.6022
30	-4.7982	65	3.4258	100	1.7860	135	0.2780	170	7.9958
31	-10.5289	66	-2.9489	101	-4.9434	136	0.3469	171	0.5623
32	-9.5962	67	-4.0190	102	-11.4111	137	-1.5127		
33	-16.0865	68	-3.5951	103	-5.0852	138	-5.6220		
34	-14.3639	69	-4.3261	104	-21.4881	139	-7.2428		
35	8.7651	70	1.4456	105	-3.6009	140	-11.4479		

Table.3. The variance of methods used

λ	$\sigma^2_{Z,0}$	σ^2_Z	σ^2_e
0.05	7.644	7.777	22.722
0.10	15.689	15.946	43.564
0.15	24.170	24.540	**62.819**
0.20	33.122	33.593	**80.731**
0.25	42.586	43.159	**97.505**
0.30	52.606	53.272	**113.314**
0.35	63.233	63.988	**128.312**
0.40	74.525	75.364	**142.629**

Table.4. Control limits of methods used

λ	$L\sigma_{z,0}\pm$		$L\sigma_{z}\pm$		$L\sigma_{e}\pm$	
	L=2.216	L=2.814	L=2.216	L=2.814	L=2.216	L=2.814
0.05	± 6.127	± 7.780	± 6.180	± 7.847	± 10.563	± 13.414
0.10	± 8.778	± 11.146	± 8.849	± 11.237	± 14.626	± 18.573
0.15	± 10.895	± 13.835	± 10.978	± 13.941	± 17.564	± 22.303
0.20	± 12.754	± 16.195	± 12.845	± 16.311	± 19.911	± 25.284
0.25	± 14.461	± 18.364	±14.558	± 18.850	± 21.882	± 27.787
0.30	± 16.076	± 20.410	± 16.174	± 20.534	± 23.589	± 29.955
0.35	± 17.621	± 22.377	± 17.726	± 22.510	± 25.102	± 31.876
0.40	± 19.130	± 23.293	± 19.238	± 24.439	± 26.465	± 33.607

Table 5. ARL comparison of the standard EWMA, dependent EWMA, and modified EWMA for the ARI (1,1) model

λ	$L\sigma_{z,0}\pm$		$L\sigma_{z}\pm$		$L\sigma_{e}\pm$	
	L=2.216	L=2.814	L=2.216	L=2.814	L=2.216	L=2.814
0.05	90	94	90	94	111	113
0.10	107	109	108	109	128	129
0.15	110	115	112	116	130	128
0.20	118	123	120	124	140	146
0.25	125	128	126	128	147	148
0.30	129	130	130	131	148	151
0.35	130	138	132	139	151	153
0.40	139	143	139	143	153	158

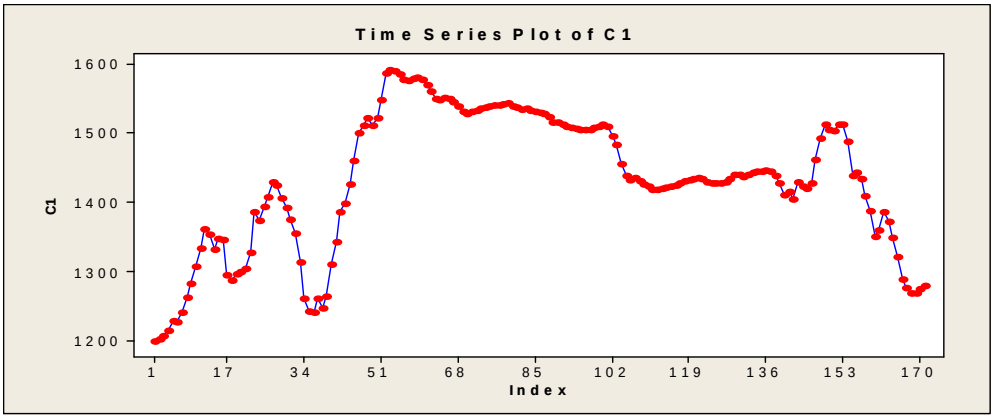

Figure.1. Original time series of Apple Computers sales

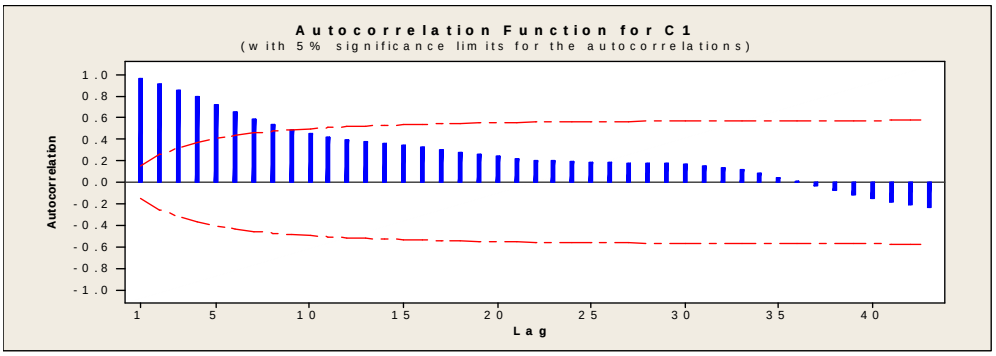

Figure 2. ACF of original time series

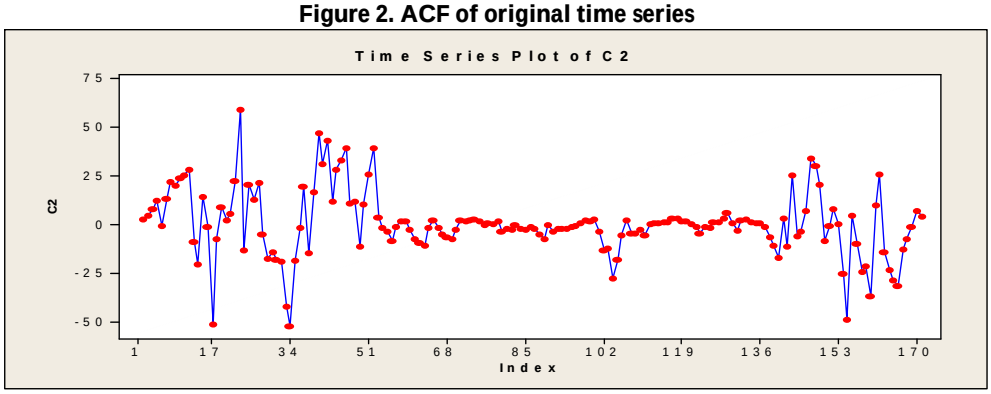

Figure 3. Time series of Apple Computers sales after 1st difference

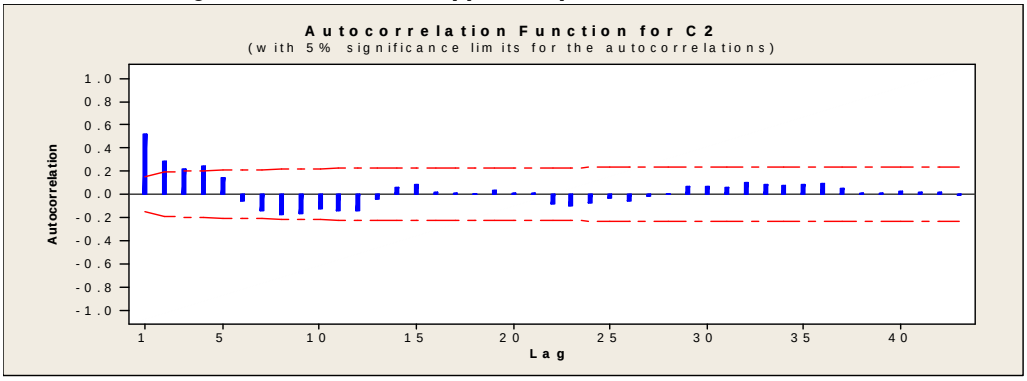

Figure 4. ACF of time series after 1st difference

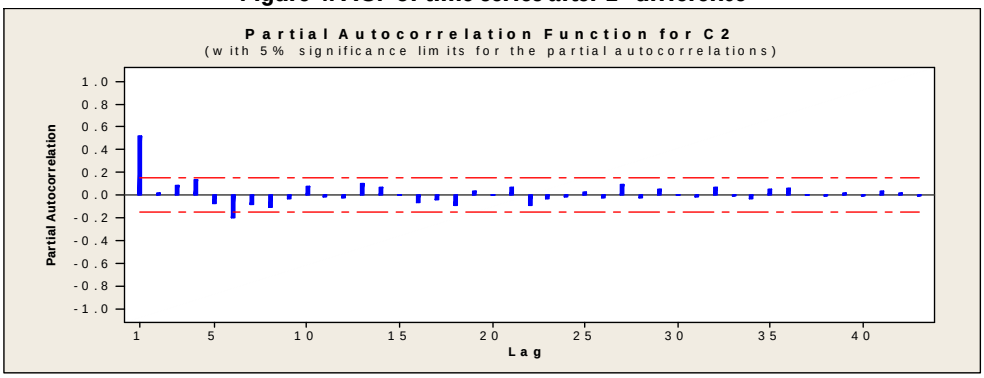

Figure 5. PACF of time series after 1st difference

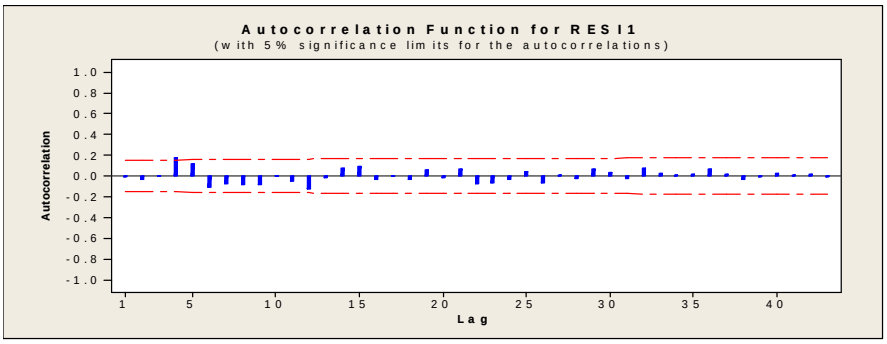

Figure 6. ACF of residuals series of ARI (1,1) model

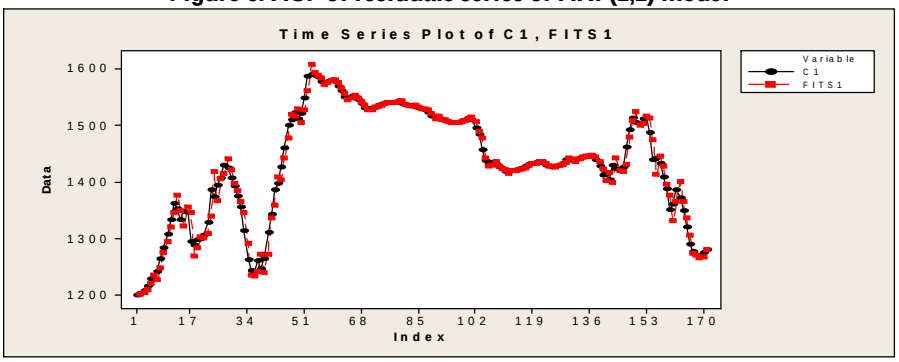

Figure 7. Original and estimated observations of time series Apple Computers sales according to ARI (1,1) model

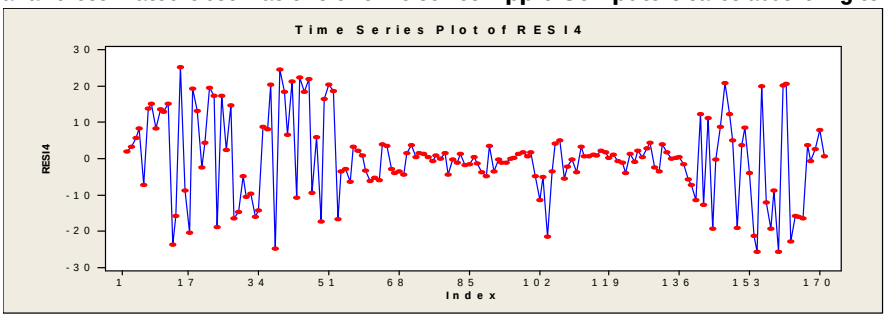

Figure 8. Residuals series of ARI (1,1) model

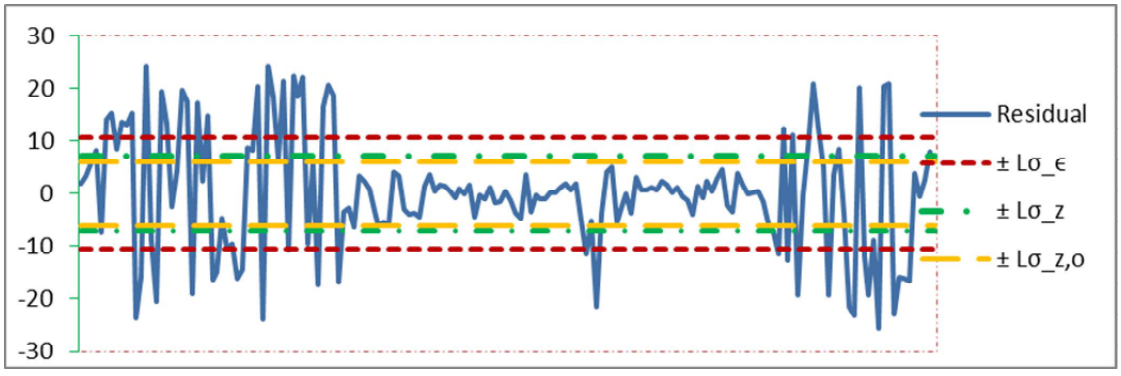

Figure 9. Residuals series and EWMA statistics (Z_t) for ARI (1,1) model with $\lambda = 0.05$ and L= ± 2.216

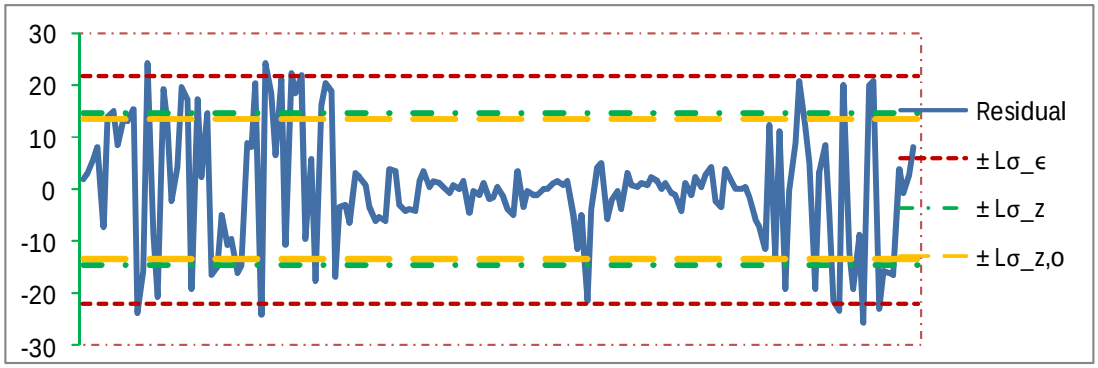

Figure 10. Residuals series and EWMA statistics (Z_t) for ARI (1,1) model with $\lambda = 0.25$ and L= ± 2.216

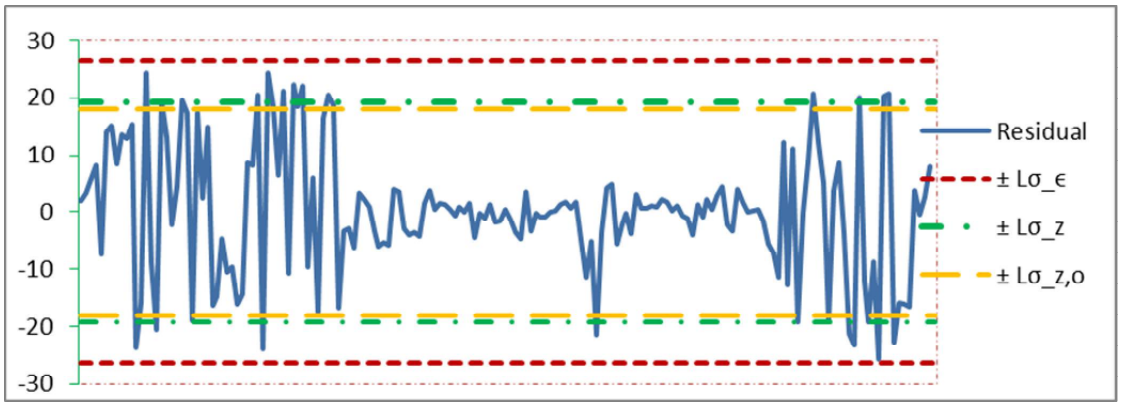

Figure 11. Residuals series and EWMA statistics (Z_t) for ARI (1,1) model with $\lambda = 0.40$ and L= ± 2.216

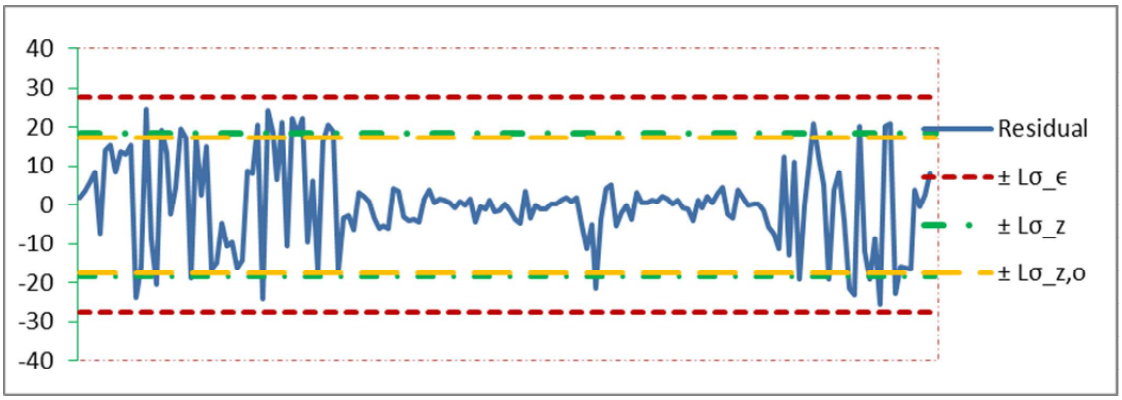

Figure 12. Residuals series and EWMA statistics (Z_t) for ARI (1,1) model with $\lambda = 0.05$ and L= ± 2.814

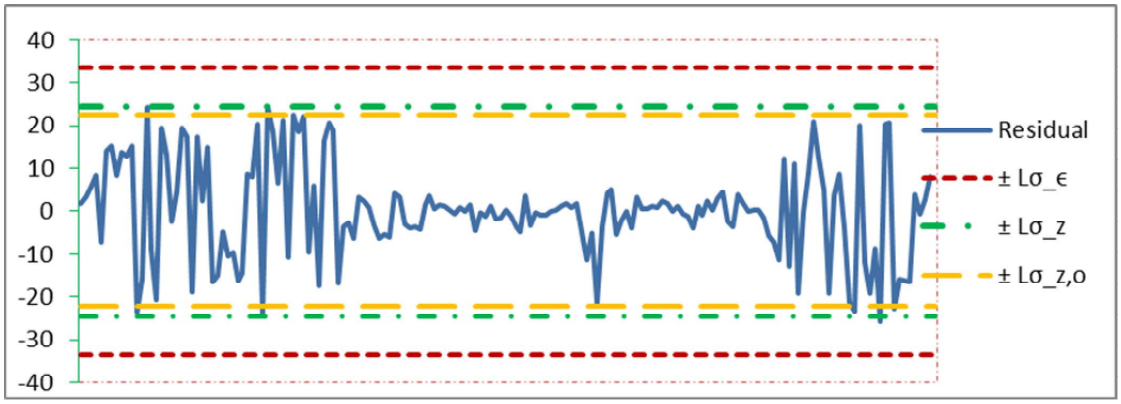

Figure 13. Residuals series and EWMA statistics (Z_t) for ARI (1,1) model with $\lambda = 0.25$ and L= ± 2.814

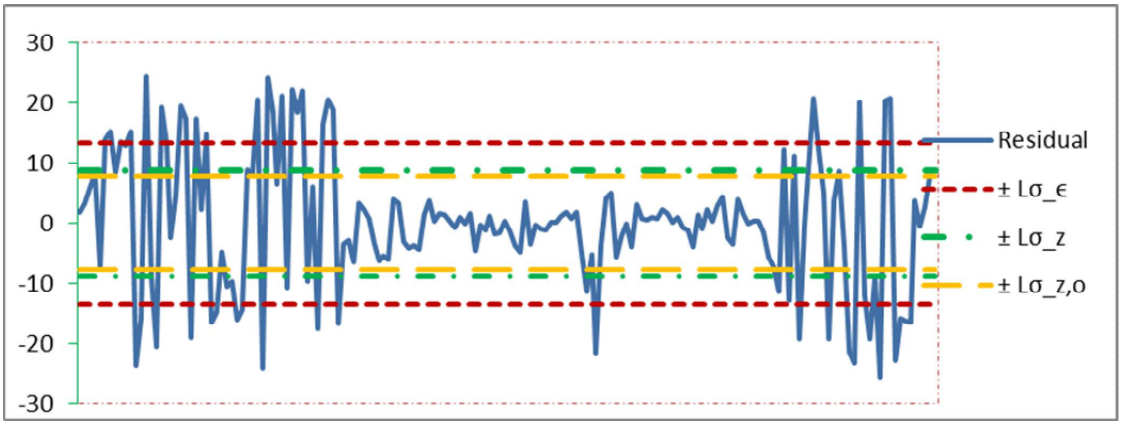

Figure 14. Residuals series and EWMA statistics (Z_t) for ARI (1,1) model with $\lambda = 0.40$ and L= ± 2.814

Indian Journal of Natural Sciences www.tnsroindia.org.in ©IJONS

Vol.9 /Issue 52 / February / 2019 *International Bimonthly* *ISSN: 0976 – 0997*

RESEARCH ARTICLE

Calculating the Time and Cost of Completing a Construction Project using PERT Network Optimization

Hamza Barakat Habib[1]*, Wadhah Abdulellah Hussein[1] and Ali Al-dulaimi1[2]

[1]Assistant Lecturer, Department of Mathematics, Science College, University of Diyala, Iraq.
[2]Assistant Lecturer, Department of Physics, Science College, University of Diyala, Iraq.

Received: 26 Oct 2018 Revised: 28 Nov 2018 Accepted: 30 Dec 2018

***Address for Correspondence**
Hamza Barakat Habib
Assistant Lecturer,
Department of Mathematics,
Science College,
University of Diyala, Iraq.
Email: halsaadi18@yahoo.com

ABSTRACT

Planning for the activities and estimating and evaluating the time of a project can be done by Pert network method. In this paper, we calculate the time and cost of completing a construction of the College of Basic Education at Diyala University using Pert network in the Operations Research. Also, determining the critical path for the construction project network is done in this paper.

Keywords: Pert: Network Pert, QSB: Quantitive System for Business, Critical Path Method: CPM

INTRODUCTION

The network is used in programmingthe constructional and industrial projects, such that, programming the projects includes planning and inspection that consider as of the main jobs for the management office.[1]Hence, there is an urgent need to follow the models of network analysis, for example, Pert network is the method for evaluation and reviewing the projects and the critical path method, CPM, which used in making the decisions process such as planning and inspection of the engineering projects.[2]. In this paper,we discussed the cost and time of construction the College of Basic Education at Diyala University, which is located in Baqubah city the capital of Iraq's Diyala Governorate, about 50 km to the northeastto the northeast of the capital Baghdad.

Basic Concepts for the represented project

An activity [2]:It is part of the project and is expressed as an arrow $\longrightarrow$that is the necessary work to accomplish a certain task. That task requires human and financial resources and durationof time (a beginning time and an end) to

be accomplished, such as constructing the base of the buildings, passing the students for the course and so on. An event [3]: It is a moment of time, and it is a node is expressed as(○). Also, it does not require time or resources and appears at the beginning and end of each activity. The event that requires an activity (an arrow) is called the start or previous event, while the event that the arrow ends to is called the end event or the subsequent event. Any diagram must begin with a node taking number one and ending with another node taking the largest number in that diagrams shown in the diagrams.

A path[4]: It is a set of interrelated and differentiated activities connects the events starting with the start event and ending with the end event. The paths are divided into two types, the first one is called the Critical Path and the rest arecalled the non-critical paths or the Slack paths. The identification of these two paths is the most important goals of network analysis. A project[5]: It is a set of activities and processes characterized by having a specific starting point and a specific ending point, for example, obtaining a bachelor's degree, doing a scientific research, participating in the preparation of a training program, building a bridge and so on. A network[4]: It is a graphical representation of a set of related and sequential activities that a particular project is consisting of, such as, the sequence of activities and events to complete the project is shown according to their logical technical sequence. In order for the network to be built, it is necessary for the technical authorities to identify all the activities that comprise the project, indicating which activities should be started first then moving to the next activity and so on.

Optimal Costs[6]: One of the most important factors that identify the effectiveness of a project's performance is the amount of costs that affords by management when each project activity is completed to achieve the final goal. Thus, entering the cost element into project planning helps the management to monitor the costs accurately and effectively in a unified framework that combines time and costs.Entering the cost element into project scheduling provides the basis for determining the type of exchange relationships that can occur between the time on one hand and the costs on the other. Thus, the administration can compare the different alternatives for the time and cost relationship that is related to each activity according to the situations and circumstances. Then, determining the possibility of reducing the duration of implementing the project in return for the administration to bear some of the additional costs that result from an increase of the required materials in order to accelerate the implementation of some activities. To study the relationship between the time and cost, it is necessary to identify the different types of the costs, so the costs of implementing the project can be divided into:

Direct Costs of the Activity [7]

The direct costs of the activity include the required costs to implement the activity directly, such as the equipment, work, etc. These costs change depending on the period of time taken to implement the project, for example, when the activity is to be implemented for a shorter period, then the equipment, work and so on are required to be increased resulting an increase in the direct cost. Thus, these costs are assumed to be inversely proportional to the time required to carry out the activity.

Indirect costs [7]

They include the fixed costs associated with the project as a whole and are realized regardless of the work's progress of the project, for example, administrative costs (Rent or insurance) etc. These costs are general so it is difficult to allocate them to the activities, and these costs are assumed to increase directly with the completion time of the project.

Estimating the activity completion time and its cost

Since the cost of completing each activity is affected by the time of its completion, then there are several estimates of the cost as follow:

1. Normal time: The time required to implement the activity under the normal (natural) circumstances.
2. Normal cost: It represents the direct costs required to implement the activity under the normal time.
3. Crash time: It is the least possible time for the activity to be completed in the case of additional materials is used at the implementation.
4. Crash cost: It is the direct cost associated with the achievement of the activity under the crash time.

Through these points, we can get that point of time that we achieve at it the optimal situation in terms of the total cost of the project and these points achieve a balance between:

i. Increasing the direct costs as a result of accelerating some activities.
ii. Reducing the indirect costs as a result of reducing the overall project completion time.

Critical Activity

Is the activity or all of the activities that fall on the critical path that starts from the first event and ends with the last event, and the total completion time of the project depends on it. The feature of this activity (critical) is that the delay in its implementation affects the total time of completion of the project. The critical path is represented by double lines or a zigzag line. There are two methods to identify the Critical Path:

Graphical Method (Paths)

In this method, we find the possible paths for the network from the start event to the end event. The required time for each path is calculated by summing the times of the activities in that path. Thus, the longest path (in time), which represents the completion of accomplishing all activities, is called the critical path. Also, the duration of this path is considered as the lowest expected time to complete the project.The features of this method are it is easy to be used, and it is usually applied in simple networks with few activities, while in the large networks, it may be difficult to find all the possible paths of the network; therefore, the second method (Float Time) is used.

The mathematical method (Float Time)

The first method to calculate the critical path may be impossible to be applied, only in the case of small projects with no more than 10 paths. Therefore, a more efficient and easy method to identify the path (or critical paths) must be used, and then to identify the required time to complete the project on time.To identify the critical path according to this method, we must calculate the earliest possible start time (**Earliest Start Time**) and the allowed delaying time (**Latest Finish Time**) to accomplish each activity in the Project.The Early Start time, of an activity$K$, which is the time that an activity, say, K cannot begin before due to specific considerations of the predecessor activities.For example, suppose that the required time to complete the activities X and Y are 12 and 18 days respectively, and if both of them can be started immediately, then the activity K cannot be started unless Y is completed (i.e. the activity that requires longer time). That is,K will be started after18 days.The Latest Finish Time, on the other hand, is the time that the finishing time of the activity cannot be delayed after it (by delaying the starting time). Thus, the activity time itself is constant at this stage without affecting the total time required to complete the project.
Now, we give below the definitions that can be used to calculate the early and latest time for an activity and also, and to determine the float time. .

Definition 1: Early Start Time (ES). It is the earliest time for a certain event to be started, and it is the total time required to complete the previous activities of this event.
Definition 2: Latest Finish Time (LF).It is the latest time that the work leading up to a certain event can be completed without affecting the total time of the critical path.
Also, there are other two definitions that we give below.

Definition 3: Latest Start Time (LS).It is the latest time allowed for the activity to be started, in which the activity cannot be delayed anymore. It is given as $LS = LF - D$,where, D is the previous activity time.

Definition 4: Earliest Finish Time (EF)

It is the earliest time for the entire project to be completed, and it can be calculated as follow $EF = ES + D$,where, D is the previous activity time.

PERT Method [2]

Bert method was reached in 1958 and through the research that carried out by the staff to schedule various events for the purpose of finding a way to plan, review and evaluate the Polaris missiles program for the US Navy. The staff has achieved a great success in applying the new method (PERT) to complete the new activities of that program by giving estimates of the expected time and to estimate the completion time of each activity on which the network worked (Network Diagram) and write it on the arrow that represents the activity.There may be only one completing time of the activity called the exact time, but if the expected time to complete the activity is an estimated time (i.e. the completion time of each activity is a random variable), then the best way to determine the completion time of the activities is to express them through probability distribution. Regarding this, Beta Distribution is the best distribution for this purpose and therefore instead of expressing the time required to complete the activity in an only one single time, we have three estimates:

The Optimistic Estimate

Under this estimate, the completion time of the activity is the time that can be the shortest of times, such that, the actual time is less than the time of optimism by (1%) of the time.This means that under this estimate, the best conditions that allow the implementation to happen are assumed.

The Most Likely Estimate

It is the expected time that the activity takes under normal circumstances, and it is the most realistic and probable time to complete the activity. It is usually determined technically or by the experience in estimating the most likely to achieve.

The Pessimistic Estimate

Under this estimate, the completion time of the activity is the time that can be the longest, such that, the actual completion time is greater than this time by (1%) of the time.This means that under this estimate, the worst conditions that allow the implementation to happen are assumed.

In order to calculate the scheduling of a least cost to complete the project, the following steps must be taken:

1. The network diagram must be drawn
2. The critical path must be identified, and set the duration value above each activity.

Practical Part

We provide the tableof working stages of building the project, College of Basic Education at Diyala University taken from the engineering department at the university. The table includes the working stage of each activity, the cost in Iraqidinar, the duration in days and the weight in ton, see Table 1 below. Also, we provide a table includes the duration with the normal time and cost and the crash time and cost for each activity, see Table 2 below Moreover, we

provide network diagrams for normal time and costs and crash time and cost for the construction of the project. These figures show the critical paths for the normal and crash (time and cost) and they are 1, 2, 5, 6 and 7.

CONCLUSION

The calculation of the least cost of completing the construction of the College of Basic Education at Diyala University has been calculated, and it has been found that it was less than the cost approved by the engineering department at the University. The duration of time for completing the project was also calculated and equals to 470 day, and it was less than the duration approved by the engineering department where it was done by using the programs (Microsoft Word and Qsb program). However, the issue of reducing the cost of constructing the project in order to achieve the desired revenue is considered as the main problem in the project because the reasons for high construction cost are several and overlapped, for example, the constant rise in the prices of the various essential materials or supplementary required for construction in addition to the high cost of shipping and transportation of imported construction materials such as reinforcing steel. Also, there is no realistic connection between the wages and salaries paid and the real value of efforts in the work, and also there is lack of the necessary laborers for various construction processes.

Moreover, there is lack of the attention to the quality control imposed on the essential materials,and weak of supervision of construction with poorof planning and proper organizing at the administrative and engineering levels cause high construction cost.Finally, the critical path is calculated and it is possible to notice that it is 1, 2, 3, 5 ,6 and 7 as shown in the network diagrams. In order to reduce the completion time and cost we recommend that several matters need to be done. Firstly, improving the work conditions in terms of heat, humidity and lighting and paying attention to the safety of laborers by providing them working clothes to keep them safe can help to raise the performance of work and laborers. Secondly, specifying the standard time required to complete the project and simplifying the work by excluding unnecessary work and applying more efficient methods can reduce the lost time and effort.Thirdly, as a result of the continuous evaluation of work and laborers, training the laborers on the correct scientific working methods, providing counseling sessions for the employees and setting a correct system of financial incentives help to increase the laborers' efforts and then increase the work's production. Finally, controlling the cost of construction materials by the regular and accurate studies that help to get rid of the unnecessary high-cost ones, and also inspecting the construction quality regularly in order to record the notes and analyzing them to determine their differences from the required specifications.

REFERENCES

1. Bazaraa, M. and J. Jarvis,(2004), "Linear Programming and Network Flows", Wiley, New York.
2. Hamdy A.Taha, (2006),"Introduction to Operations Research ", 4th ed.
3. K. V. Mital and C.,(2005),Mohan, "Optimization Method in operations Research and Systems Analysis", Willy Eastern Limited.
4. Hamed Sa'ad Noor Al Shamerty, (2010), "Introduction to Operation Research ".
5. Bazaraa, M. S., Hanifd Sherali and C. M. Shetty,(2006), "Nonlinear Programming, Theory and Algorithms", Wiley New.
6. Prem Kumar Gupta and D. S. Hira, (2007), "Operation Research an Introduction", S. Chand and company (PVT) LTD.
7. Paul A. Tensen, Jonathan F. Bard,(2008), "Operation Research, Models and Methods", Wiley, New York.

Table 1: Table shows the working stages of the project

No.	Project's Stage	The cost Iraqi dinar	Duration Days	The weight Ton
1	Brick construction above the base with the cost of designs and drawings	166000000	365	
2	Concrete slab (ceiling)	48000000	21	9
3	covering the exterior of the walls with cement 1	1840000	42	4.8
4	covering the exterior of the walls with cement 2	800000	14	1.7
5	Gypsum Plaster	66000000	49	15
6	Stonework	60800000	56	17
7	Painting works	23100000	14	5
8	Ceramic tiles works	7000000	28	5
9	Floor tiles works	83900000	35	17
10	Restrooms works	34000000	14	7
11	Electrical works	80000000	56	18
12	Total	571440000	329	99.5

Table 2: The table shows the way of finding the critical path by the mathematical method

An Activity	Normal Time Days	Crash Time Days	Normal Cost Iraqi dinar	Crash Cost Iraqi dinar
1 – 2	365	320	166000000	166000005
1 – 3	21	19	48000000	48000003
1 – 4	42	40	1840000	18400002
2 – 5	14	12	800000	800002
3 – 4	49	45	66000000	66000004
3 – 7	56	54	60800000	60800002
4 – 5	14	12	23100000	23100002
4 – 6	28	25	7000000	7000003
5 – 6	35	30	83900000	83900005
5 – 7	14	12	34000000	34000002
6 – 7	56	54	80000000	80000002
Total	694	623	571440000	588000032

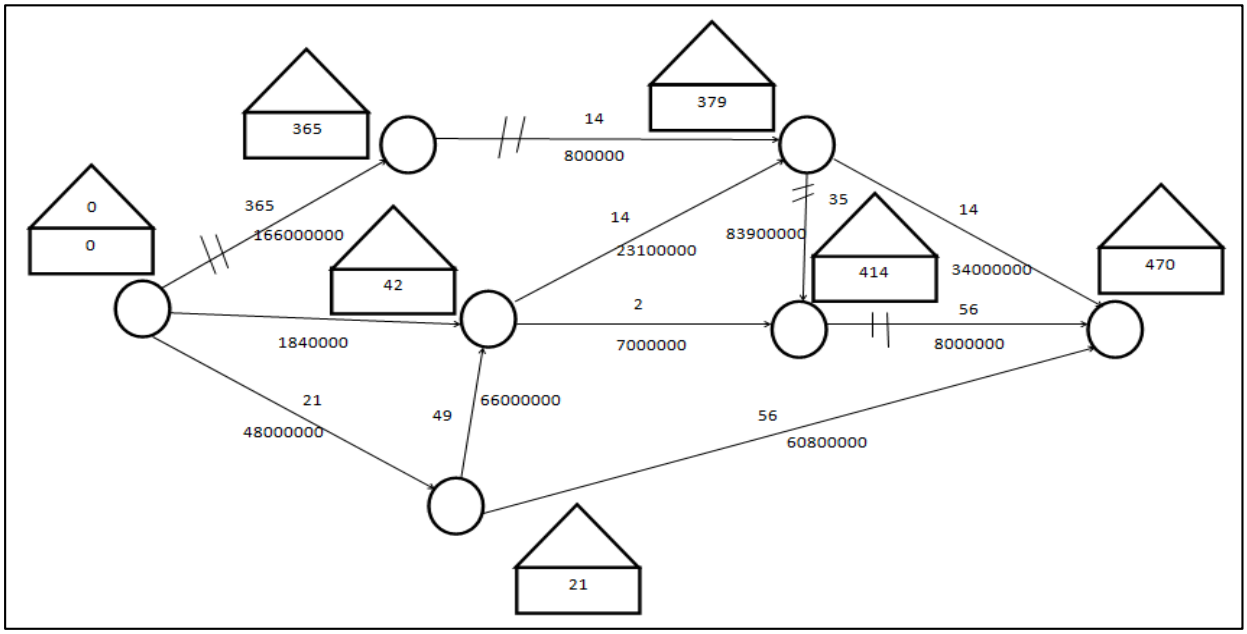

Figure 1. The figure shows the network diagram (the normal time and cost time) of the College of Basic Education at University of Diyala.

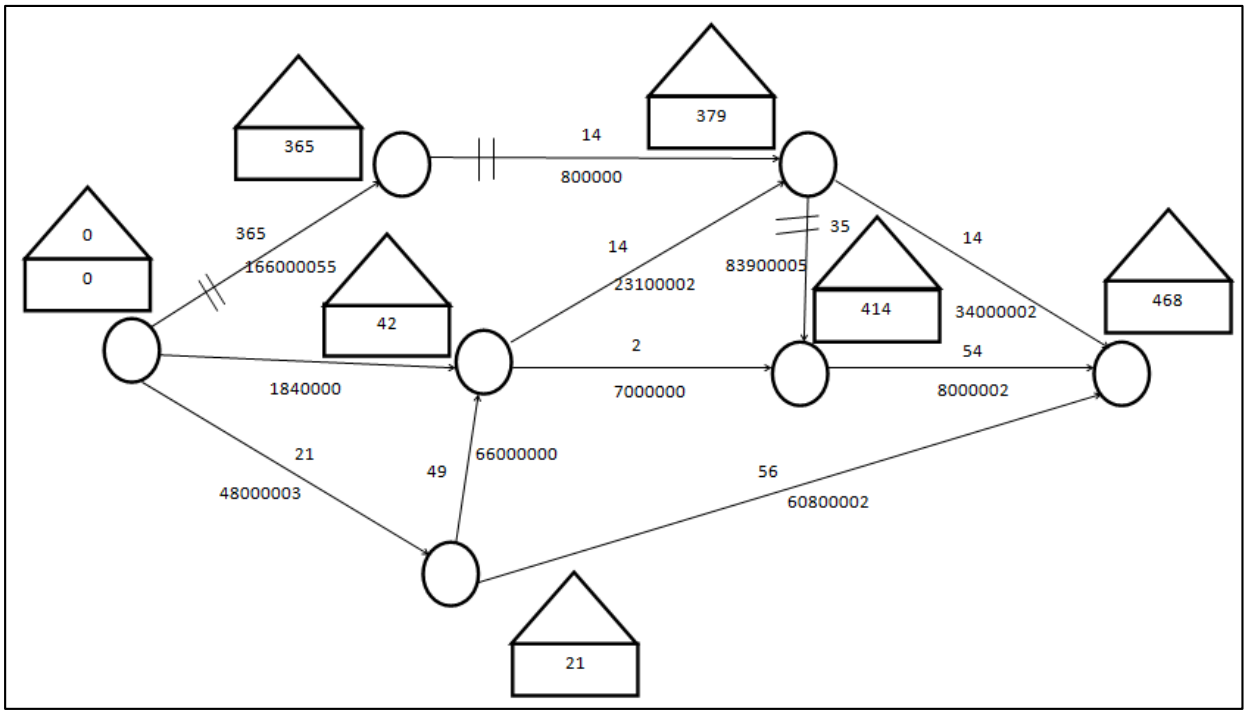

Figure 2. The figure shows the network diagram (the crash time and cost) of the College of Basic Education at University of Diyala.

Indian Journal of Natural Sciences www.tnsroindia.org.in ©IJONS

Vol.9 /Issue 52 / February / 2019 *International Bimonthly* *ISSN: 0976 – 0997*

RESEARCH ARTICLE

Flexural Properties of Functionally Graded Nanocomposites

Ali A. Abbas* and Zainab R. Muslim

Physics Department, College of Science, University of Baghdad, Iraq.

Received: 20 Nov 2018 Revised: 24 Dec 2018 Accepted: 26 Jan 2019

***Address for Correspondence**
Ali A. Abbas
Physics Department,
College of Science,
University of Baghdad, Iraq.
Email: aliadilabbas@yahoo.com

ABSTRACT

Functionally graded polymer nanocomposites were prepared by Hand lay–up technique by addition graphene and carbon nanotubes particles with different weight fraction (1 and3) wt.% to epoxy.flexural properties of functionally graded polymer nanocomposite for each weight fraction were determined the by three-point bending test, withloading from pure and composite side. The results show that flexural strength and Young's modulus loaded from pure epoxy side was higher than when samples loaded from composites side.

Keywords: polymer, grapheme, weight, modulus, samples.

INTRODUCTION

The term “functionally graded materials” contains two important words: “functionally” and “graded.” The word “functionally” modifies “graded.” These refer to not only simple functional materials but also to graded materials. The general concept of functionally graded materials is materials with graded functions inside them. Functionally graded materials are abbreviated as FGMs hereafter [1]. Functionally Graded Material (FGM), a revolutionary material, belongs to a class of advanced materials with varying properties over a changing dimension [2].Functionally graded material eliminates the sharp interfaces existing in composite material which is where failure is initiated. It replaces this sharp interface with agradient interface which produces smooth transition fromone material to the next. One unique characteristics of FGM is the ability to tailor a material for specific application [3]..number of studies have been undertaken about graded nanocomposites

Tsotra and Friedrich investigated flexural properties of functionally graded epoxy-resin/carbon fiber composites, the centrifugation technique was used to create a graded distribution of carbon fibers in an epoxy resin matrix Flexural strength and modulus of the FGM were affected by graded structure[4]. Wang et.al studied the distribution, mechanical properties, electrical properties and microwave shielding properties of functionally graded multiwalled

carbon nanotube (MWCNT) reinforced epoxy matrix composites are fabricated using a centrifugal method. they successfully modified the surface of MWCNTs and produced s-MWCNT polymer based FGMs using a centrifugal method. The gradual incorporation of the s MWCNTs in the epoxy resin resulted in the formation of deep-penetrating gradients in all properties that studied. The promising grading capabilities of the s- MWCNTs indicated that it is possible to tailor the gradient of nanofillers by carefully modifying their surfaces, thus enabling grading of the properties and microstructure of the final composite material using a simple centrifugal method. The present results strongly suggest that treated nanomaterials should be considered as novel high-performance filler candidates for the design and preparation of graded functionalities and properties compared with those used in conventional polymer composites [5]. Rihan and El-Bary studied graded silica/epoxycomposites and homogenous compositesthat prepared by gravity molding processto investigate the effect of silica content on the wear characteristics. wear resistance and electrical conductivity increased by increasing the wt % content of silica compared with the pure epoxy[6].

MATERIALS AND METHODS

Materials Used

1- Epoxy and hardener type (HT 2000 were provided by Renksan Group, turkey) were in the ratio of 3:1 for curing as a matrix.

2- The materials used as filler like Multi-wall carbon nanotubes(CNTs) (Cheap Tubes Inc., USA) purity 90% with particle size < 10 nm, graphene (GR) (sky spring nanomaterials, Inc., USA) purity 99%with particle size 40-60 nm.

Preparation of Nanocomposites

The mixing process consisted of three steps. Firstly, graphene and carbon nanotubes were stirrer mixed with the epoxy resin, with different weight ratios (1and 3) wt. %, the mixing was done at 40 ^{o}C with a magnetic stirrer for 45 min to have good distribution and the mixture left to cool then hardener was added to the mixture then the sample were kept in container under vacuum to remove the bubbles before cast the composites.

Preparation of Graded Nanocomposites

Hand lay–up technique was used to prepare graded nanocomposites, subsequently the first layer which was poured into mould. Then succeeding layers with different content were poured into the mould. Before pouring succeeding layers,the gelation time were one hours were made to allow pre-curing of previous layer.

The list ofsamples prepared with different composition are shown in Tables (1) and (2).

Flexural Strength Test

In engineering mechanics, flexure (or bending) characterizes the behavior of a structural element subjected to an external load applied perpendicular to the axis of the element [7]. Flexural strength represents the strength at the fracture of the beam section when tested. The flexural strength can be calculated by “Three- Point Test”,this test is performed according to (ASTM D790) at room temperature. The flexural strength in this test can be calculated by the following equation[8]:

$$\text{Flexural strength (N/m}^2\text{)} = \frac{3PL}{2bd^2} \quad \ldots\ldots\ldots\ldots\ldots\ldots\ldots\ldots (1)$$

Where:

P: the load at fracture (N).

L: Length of sample (m).

d: Thickness of sample (m). b: Width of sample (m).

The support span (distance between the support) was depending on the sample thickness, the load was applied on a sample at the middle of support span.Two cases were compared in which the samples were center loaded during three-point bending, i.e. either at the composites side (a) or at the pure side (b)

RESULTS AND DISCUSSION

The properties of bending usually depend on the nature of the bonding between the filler and the matrix materials **.**The figure (4) illustrates that theflexural strength increases with increasing weight fraction of nanoparticles, maximum increment at 3% wt. fraction ([CNT3%]1 and [GR3%]1) ,this behavior in nanocomposites is due to the role of nanoparticles, the particle size is very small, resulting in larger surface area and high interaction between particles and polymer matrix also which decreasing in space distance between chains crosslink caused by adding nanoparticles which createVan der-waals bonding between chains and particles lead to increase constrained between particles/ polymer chains, and polymer chains itself [9]. There is similar trend for the Young's modulus of nanocomposite, as shown in figure (5),polymer matrix composites filled with organic particles shows improvement in Young's modulus,this is because of particles agglomeration where it leads to increasing the constrained between polymer chains [10]. This improvement of mechanical properties is resulted by change in the morphology of polymer matrix due to the combination of organic components on nanometer level[11]. In this case, improvement in Young's modulusis due to the high quality of interfacial interaction between epoxy resin and nanoparticles. [CNT3%]1 has highest value was due to higher fillers content of CNTs which resistant the crack movement and give high toughness to nanocomposites.

The highest value recorded for CNTs composites to the presence of a weak van der Waals force between individual graphene shells causes easy slip between the shells. Therefore, by the application of load, the CNTs in the polymer matrix can be drawn layer by layer providing toughness tothe samples suggesting that the small agglomerates are behaving as rigid particles in their interactions with the advancing crack [12]. Figure (6), shows a higher force were required for nanocomposites compared to epoxy and reduction in the elongation at break of nanocomposites for pure epoxy with increasing the filler loading because the formation of Vander-Waals bonding, the nanoparticles with chains leads to increase restriction between chains of epoxy and chains of nanoparticles/epoxy, will decrease free volume space and decreases the length of epoxy chains [13].

From figures (7) , (8) (9) and (10), the flexural strength and Young's modulus of the graded nanocomposites are higher when loaded from the pure epoxy side due to the lowest layer i.e. composite layer that has highYoung's modulusas compared to pure epoxy, it was observed that flexural strength and Young's modulus for non-graded nanocomposites was higher than pure epoxy, due to presence of nanoparticles. On the other hand, flexural strength and modulus is lower when graded nanocomposites was loaded from composites side. In this case, lowest layer pure epoxy layer has the lowest flexural strength and modulus that causing reduction in the strength and modulus of graded nanocomposites [14].

Thus, the stiffer and stronger layersin non-graded nanocomposites in the three-point bending test contribute in enhancing the flexural properties of graded nanocomposites. Higher flexural strength was for [CNT1%,3%]3 pure side due to elongation in samples in lower part (i.e. tensile mode), because high modulus means a material require higher stress to stretch. Higher Young's modulus was observed for [CNT1%,3%]3 as compared to [GR1%,3%]3 , which means as a stiff material while flexible material have a low Young's modulus. Figures(11)and **(**12**)** show elongation at break for nanocomposites which is considerably decreased with increasing of fillers loading as it is shown, as the elongation is reciprocal of the stiffness of a material, the result shows that the fillers impartin a higher stiffness,graded nanocomposites loaded from pure side have high stiffness than from composites side[15].

CONCLUSIONS

Flexural strength and Young's modulus of non- graded nanocomposites increase with increase weight fraction of nanoparticles, highest value was for carbon nanotubes. In graded nanocomposites, flexural strength and Young's modulus increase with number of layers of composites and with weight fraction.

REFERENCES

1. Y. Shinohara "Handbook of Advanced Ceramics", second Edition, Elsevier Inc.,2013.
2. H. Sai B.V,"A Review on Functionally Gradient Materials (FGMs) and TheirApplications",8(1),79-83(2018).
3. K. Gupta, H. Saini and M. A.Zaidi," Synthesis of Functionally Graded Material byPowder Metallurgy", 4(3),163-165(2017).
4. P .TsotraandK.Friedrich"Electrical and Mechanical Properties of Functionally Graded Epoxy-Resin/Carbon Fibre Composites ",Composites Part A Applied Science and Manufacturing,34(1),75-82(2003).
5. Y.Wang,Q. Ni ,Y. Zhuand T.Natsuki ,"Functionally Graded Epoxy Composites Using Silane Coupling Agent Functionalized Multiwalled Carbon Nanotubes", Nano brief reports and reviews ,9(1) ,1450011 (2014).
6. Y. Rihan and B. Abd El-Bary"Wear Resistance And Electrical Properties Functionally Graded Epoxy-Resin/SilicaComposites", ,"EArab Conference the Peaceful uses of Atomic energy,2012.
7. D. Rees ,"Basic Engineering Plasticity:An Introduction with Engineering and ManufacturingApplications",1st edition, CTI Reviews,2017.
8. D. Sarkar"Nanostructured Ceramics: Characterization and Analysis" CRC Press,2019.
9. M. M. Abd, H. Jaffer and E. A. Al-Ajaj, "Comparison Study of Some Mechanical Properties of Micro and Nano Silica EP Composites", Iraqi Journal of Physics,10(18), 62-68 (2012).
10. S. K. Singh, A. Kumar and A. Jain,"Improving Tensile and Flexural Properties of SiO_2-Epoxy Polymer Nanocomposite", Materials Today: Proceedings, 5 ,6339–6344 (2018).
11. J. K. Nelson,"Dielectric Polymer Nanocomposites" ,Springer Science & Business Media,2010.
12. B. S. Hadavand , K. M. Javid , M.Gharagozlou" ,Mechanical Properties of Multi-Walled Carbon Nanotube/Epoxy Polysulfide", Materials and Design ,50, 62–67(2013).
13. R. M. Hussein "The Effect of Walled Nano-Carbon on the Physical, Thermal and Mechanical Properties of Epoxy", Al-Khwarizmi Engineering Journal, 13(4), 69- 79 (2017).
14. S. K. Mishra, D. K. Shuklaand R. K. Patel "Flexural Properties of Functionally Graded Epoxy-Alumina PolymerNanocomposite"Materials Today: Proceedings ,5, 8431-8435(2018).
15. F. Mirjalili, L. Chuah and E. Salahi "Mechanical and Morphological Properties of Polypropylene/Nano α-Al_2O_3 Composite",The Scientific World Journal,2014.

Table 1. non-graded composites.

Sample no.	Sample ID	Composition
1	Ep	Epoxy
2	[CNT1%]1	Epoxy+1%wt. CNTs
3	[CNT3%]1	Epoxy+**3**%wt. CNTs
4	[GR1%]1	Epoxy + **1**% wt. GR
5	[GR3%]1	Epoxy + 3% wt. GR

Table 2. functionally graded nanocomposites.

SampleNo.	Samples ID	Composition		
		1st layer	2nd layer	3rd layer
1	[CNT1%]2	Epoxy	Epoxy+1%wt. CNTs	/
2	[CNT3%]2	Epoxy	Epoxy+3%wt. CNTs	/
3	[CNT1%,3%]3	Epoxy	Epoxy+1%wt. CNTs	Epoxy+3%wt. CNTs
4	[GR1%]2	Epoxy	Epoxy + 1% wt. GR	/
5	[GR3%]2	Epoxy	Epoxy + 3% wt. GR	/
6	[GR1%,3%]3	Epoxy	Epoxy + 1% wt. GR	Epoxy + 3%wt. GR

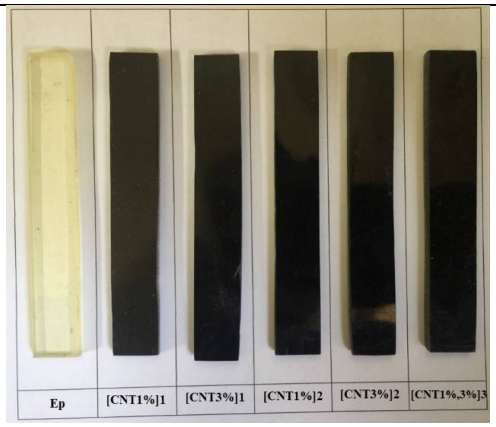

(a)

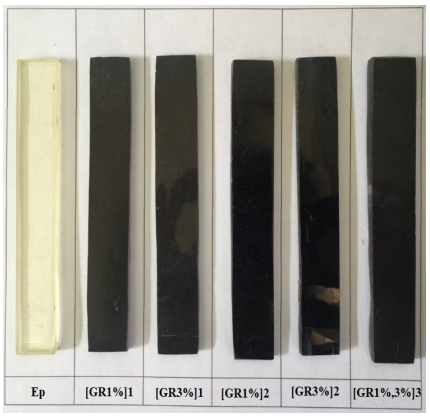

(b)

Figure 1. (a) and(b) Functionally graded and non graded graphene and carbon nanotubes composites samples respectively for bending test.

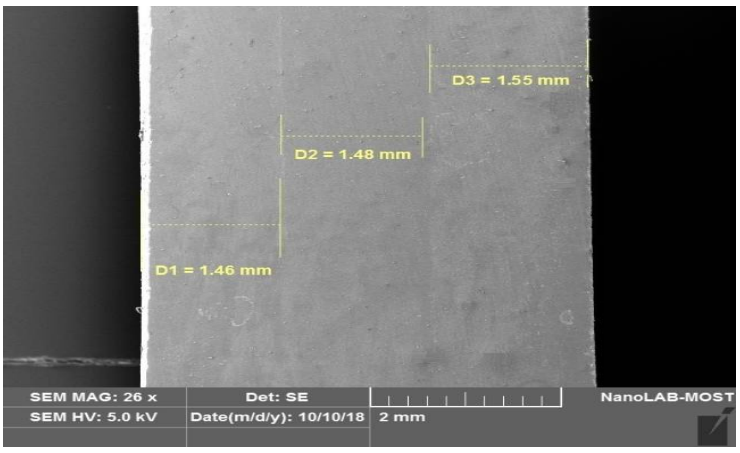

Figure 2. SEM photo to cross section of functionally graded nanocomposites sampleto show the layers.

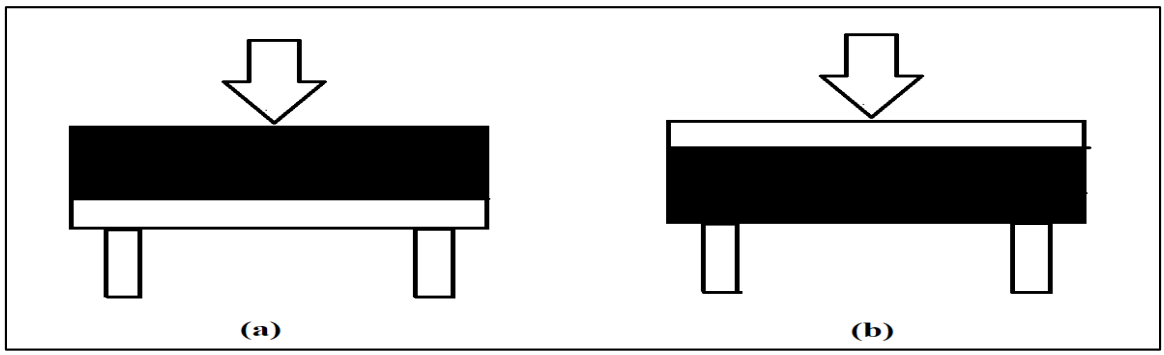

Figure 3. Flexural test of the functionally graded nanocomposites.

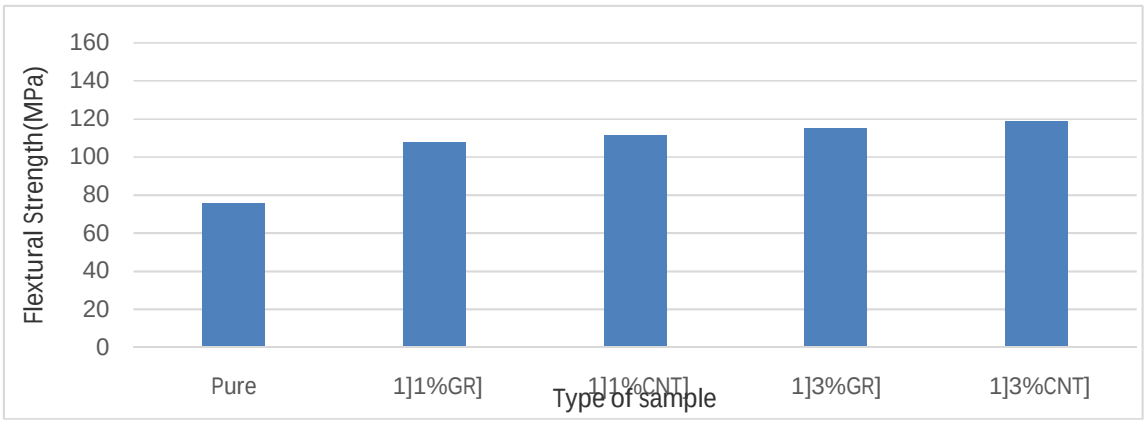

Figure 4. Flexural strength of non-graded graphene, carbon nanotubes composites.

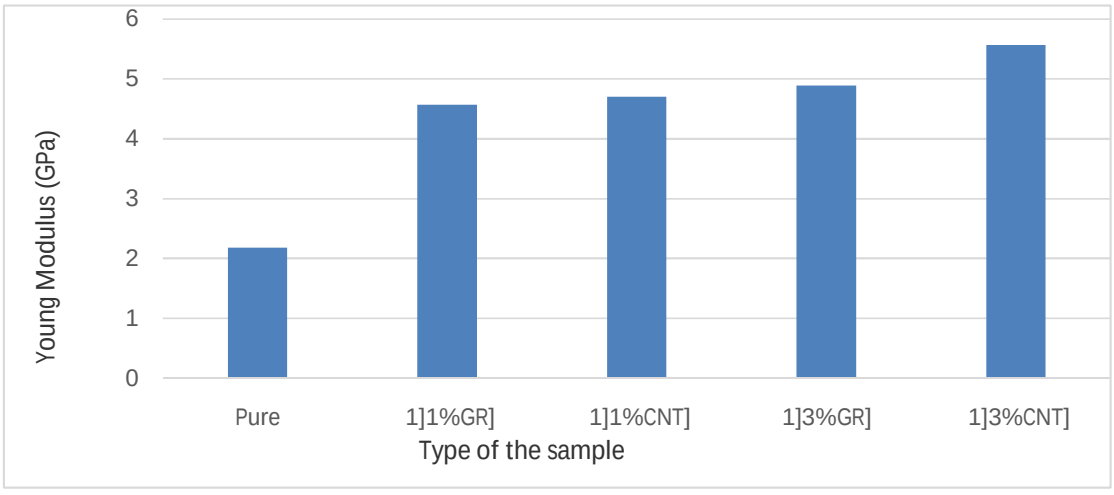

Figure 5. Young's modulus of non- graded graphene and carbon nanotubes composites

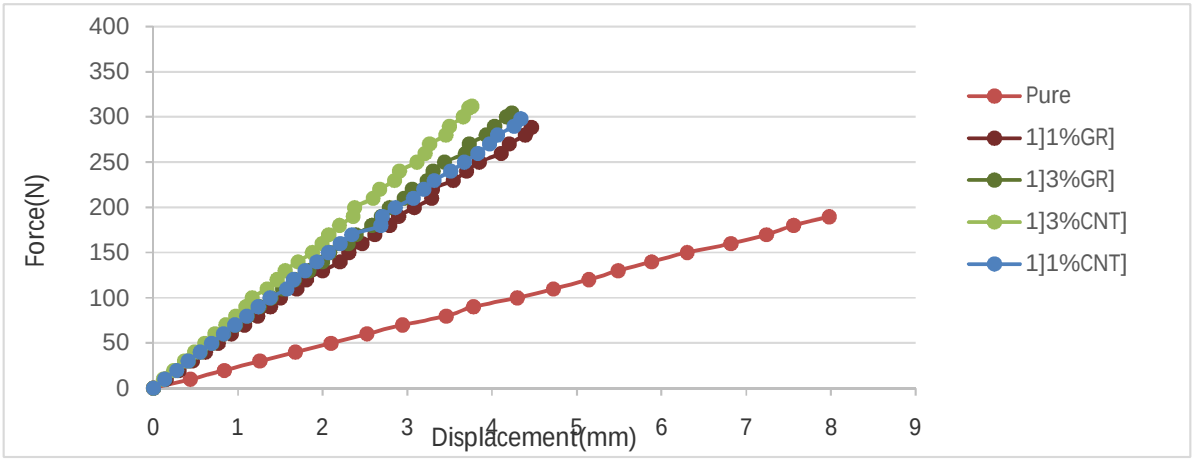

Figure 6. Force – Displacement of non-graded carbon nanotubes composites

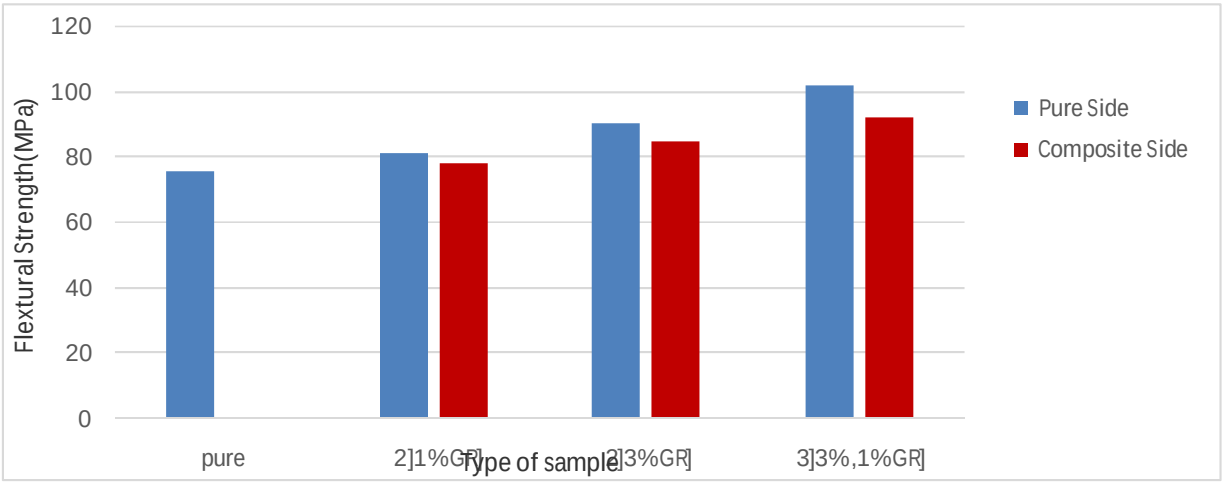

Figure 7. Flexural strength of functionally graded graphene composites.

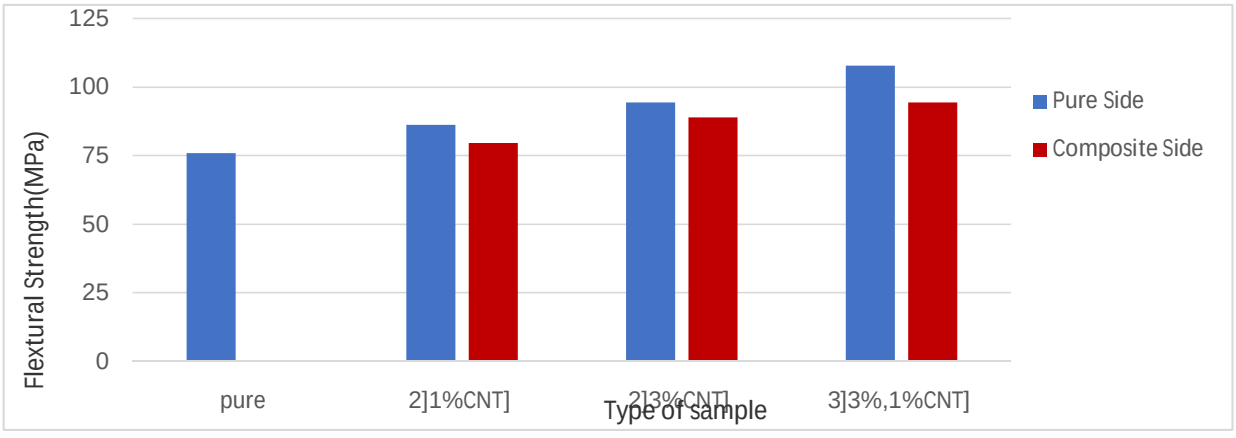

Figure 8. Flexural strength of functionally graded carbon nanotubes composites.

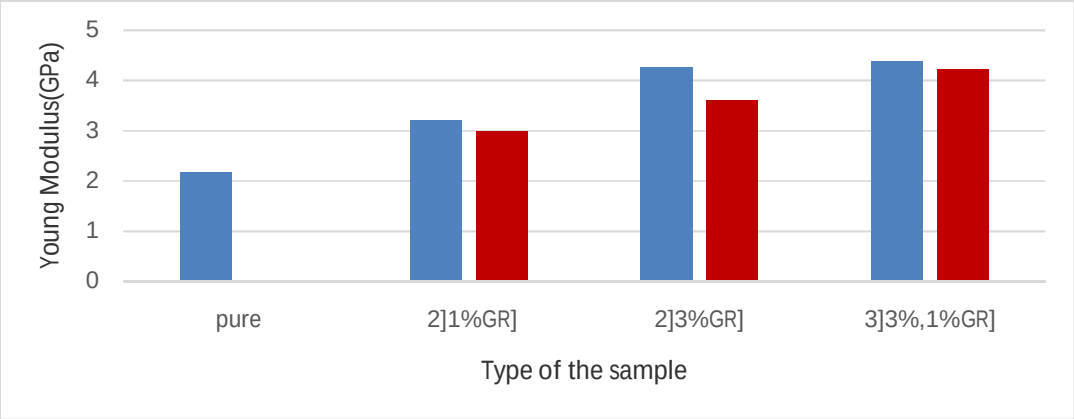

Figure 9.Young's modulus of functionally graded graphene composites.

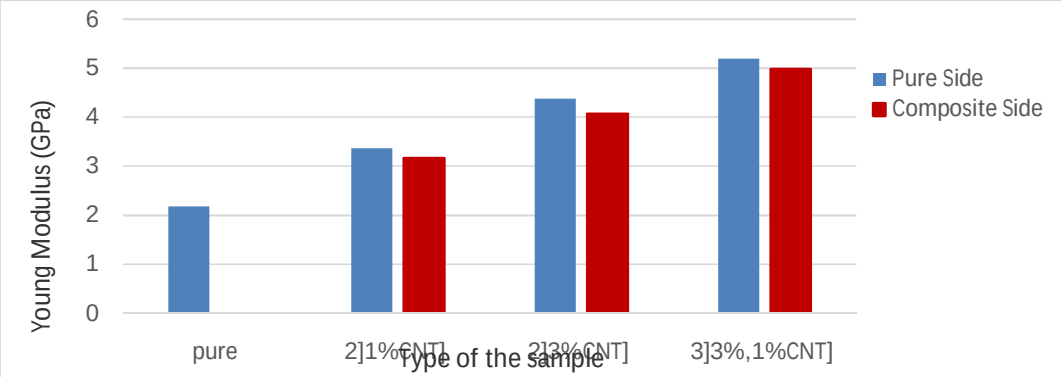

Figure 10. Young's modulus of functionally graded carbon nanotubes composites

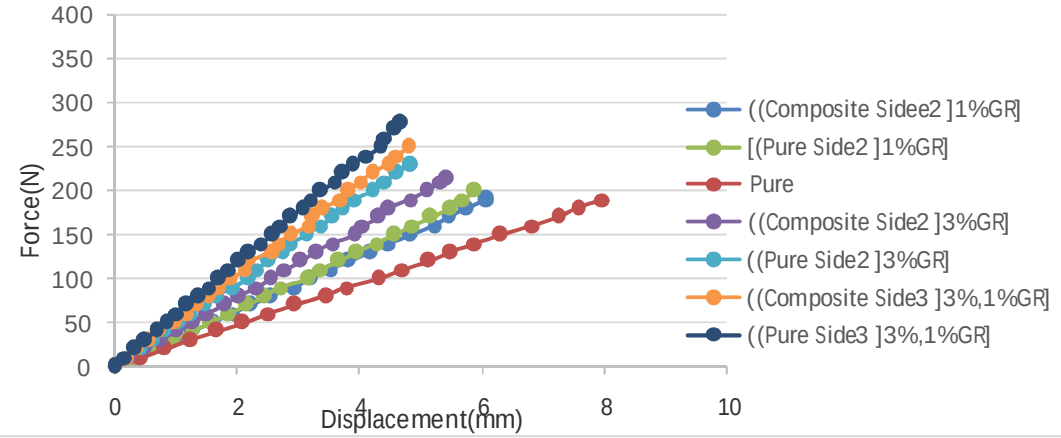

Figure 11. Force – Displacement of functionally graded graphene composites.

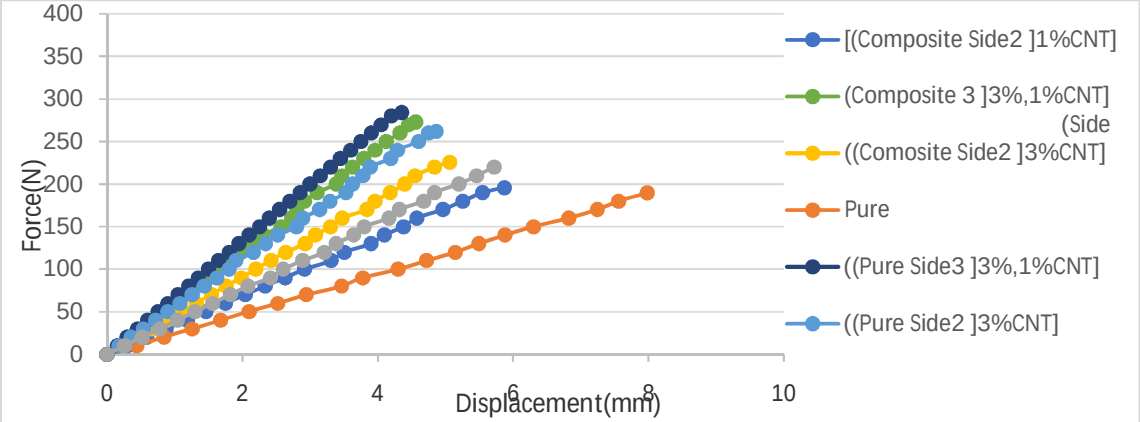

Figure 12. Force – Displacement of functionally graded carbon nanotubes composites.

Indian Journal of Natural Sciences www.tnsroindia.org.in ©IJONS

Vol.9 /Issue 52 / February / 2019 *International Bimonthly* *ISSN: 0976 – 0997*

RESEARCH ARTICLE

Characterization of Al - Doped CdO Thin Films Prepared by Pulsed Laser Deposition Technique

Omar Sh. Shafeeq*

Department of Physics, College of Science, University of Baghdad, Iraq.

Received: 21 Nov 2018 Revised: 23 Dec 2018 Accepted: 26 Jan 2019

***Address for Correspondence**
Omar Sh. Shafeeq
Department of Physics,
College of Science,
University of Baghdad, Iraq.
Email: almola.omar82@gmail.com

ABSTRACT

In this work, cadmium oxide (CdO) thin films doped with 0.1% Al were deposited onto glass substrates using alow-cost and simple pulsed-laser deposition (PLD) technique. The structural characteristics of these films wereintroduced by the x-ray diffraction (XRD).The optical and electrical parameters were also studied. Further, the surface morphology of the deposited films was determined by the atomic force microscopy (AFM). The optical absorbance spectra for samples showed a good value of thin film. Moreover, the optical energy gap, refractive index, extinction coefficient and absorption coefficient of CdO thin films are determined.

Keywords: Cadmium oxide; Pulsed-laser deposition; Thin films; Al-doped CdO.

INTRODUCTION

Cadmium oxide CdO is considered as a compound semiconductor including cadmium and oxygen [1]. CdO is generally used extensively as TCOs in different physical applications, especially in the production of opto-electronic devices as in n-type window layer in thin films for solar cell as well as a result of its high transparency in the visible region of the solar spectrum. CdO has a high electrical conductivity (low resistivity), that is resulted as an effect of moderate electron mobility and higher Carrier concentration arising from native defects of oxygen anionic vacancies and cadmium interstitials [2], in addition CdO includes an intermediate direct band gap ranging from 2.2 - 2.5 eV as thin films, and 2.5 eV as bulk [3]. Pulsed-laser deposition (PLD) is a very important and powerful technique for the growth of thin films of complex materials. It consists of three major parts, laser, vacuum system and chamber [4]. PLD setup is simple and economical compared to other thin film deposition techniques [5]. Most of the applications of PLD do not require ultra-high vacuum (UHV) deposition conditions (<10^{-7} Torr) [6 -7].

The main advantages of PLD are [7]: As the laser source is outside the deposition chamber, it introduces minimal contamination to the grown film. With high power densities obtained by focusing the laser beams, high melting point materials can be vaporized at high deposition rates. Independent control of deposition parameters such as target to substrate distance, substrate temperature, deposition gas pressure, laser energy etc. Stoichiometry of target is maintained in thin films. Small Target Size the PLD technique is also flexible, because the spot size of the focused laser beam is small and, therefore, the target area may even be less than $1cm^2$. Thin film formation process in PLD can be divided into the following four stages [1, 4]:

1. Laser radiation interaction with the target.
2. Dynamics of the ablated materials.
3. Deposition of the ablation materials on the substrate.
4. Nucleation and growth of a thin film on the substrate surface.

Target preparation

Thin films of CdO can be grown either through the ablation of pure Cd targets in an oxygen environment, or through the ablation of pure Al targets, For the present study, sintered polycrystalline CdO targets was used . According to standard Sieve charts the small particles mean that there is more surface area, and that means there are more opportunities for atoms to diffuse out to neighboring particles, which is how the sintering process works. Pure CdO and powder with high purity (99.999%) pressing it under 6.5 ton to form a target of 3 cm diameter and 0.4 cm thickness. It should be as dense and homogenous as possible to ensure a good quality of the deposit. The substrate used to deposits of CdO: Al thin films in this work are microscope glass slides (boro-silicate glass) with dimensions $(3\times2)\ cm^2$. The substrates are first cleaned in distilled water in order to remove the impurities and residuals from there surface.

Then cleaned in alcohol ultrasonically for 15 min and subsequently dried by blowing air prior to film deposition experiment.The most important features of a substrate holder are its movement relative to the target and plasma plume and ability to heat the substrate up to 400°C. The adjustment of the target-substrate-distance provides an opportunity to control the deposition rate, as well as the energy of the particles hitting the substrate. In this system, the arrangement is placed parallel to the target surface at a suitable distance. In this system we used to connect to the deposition chamber to get a vacuum up to 10^{-3} Torr and monitoring the pressure inside the chamber by using the pirani gauge. Nd: YAG laser, with wavelength of 1064 nm, and pulse energy of 100-1000 mJ. (Huafei Tongda Technology-DIAMOND-288 pattern EPLS) is used for the deposition of CdO: Al on substrate. X-ray diffraction measurements were performed according to the ASTM cards using Philips PW 1050 X-ray diffractometerof 1.54 Å from Cu-kα.

Pulsed Laser Deposition (PLD) Technique

The pulsed laser deposition experiment is carried out inside a vacuum chamber generally at (10^{-2} Torr) vacuum conditions and Kept at low pressure of a background gas for specific cases of oxides and nitrides.Photograph of the set-up of laser deposition chamber, is shown in figure (1), which shows the arrangement of the target and substrate holders inside the chamber with respect to the laser beam. The focused Nd: YAGSHG Q-switching laser beam coming through a window is incident on the target surface making an angle of 45° with respect to the normal to the target. The substrate is placed in front of the target with its surface parallel to that of the target. Sufficient gap is kept between the target and the substrate so that the substrate holder does not obstruct the incident laser beam. Optimization of the deposition technique was done by many investigators from time to time with the aim of obtaining optimum quality films by this process. These included rotation of the target, heating the substrate, positioning of the substrate with respect to target.

EXPERIMENTAL PART

The X-ray Diffraction (XRD) investigation has been carried out for the prepared films of CdO doped Al. The results are illustrated in figure (2). According to (ASTM) cards, the structure of these films showed a polycrystalline, and exhibited tetragonal structure. The majority of the thin films are oriented in the (110), (211) and (200) were also exhibited. The XRD shows peaks whose position was shifted slightly form the data of (ASTM) card. The inter planner spacing (d_{hk1}) was determined using Bragg relationship. The (ASTM) values of inter-planner spacing and the miller indices (hkl) were tabulated in table. Also evaluated are the grain sizes using the well-known Scherer's equation given below [8]:

$$D = 0.94\,\lambda/\beta\cos\theta$$

where D is the grain crystallite diameter (average crystalline grain size), λ is the wavelength (1.5406 Å), θ is the Bragg's diffraction angle of the XRD peak in degree and β is the half-width of the diffraction peak at half height (FWHM) in radian.The doping of CdO seems to have no effect on position of the characteristic peaks. The observed effect of doping CdO is the change of peak broadening which increases slightly with the increase of doping ratio. For the purpose of examining the CdO: Al thin film, Atomic Force Microscope (AFM) figure (3) tests were devoted to examine the deposited film homogeneity, surface roughness, and morphology. For many studies, AFM was applied together with another optical characterization or morphological technique. The surface roughness of the thin films is an important parameter which besides describing the light scattering at the surface gives a significant indication about the quality of the surface under investigation. The increase in surface roughness of the films leads to increase in efficiency for sensing properties; therefore, it is very important to investigate the surface morphology of the films. The absorption coefficient is defined as the ability of a material to absorb the light of a given wave length, and is measured quantitatively by the absorption coefficient presented in units of reciprocal distance [9-10].

$$\alpha = \frac{2.303\ (A - \acute{A})}{d}$$

Where A is the absorption at certain were length, $\acute{A}$ is the correction factor, and d is the thickness of the film. The absorption coefficient was calculated using the above equation. Figure (4) shows the relation between absorption coefficient and photon energy for all undoped and doped samples under Investigation. It is clearly seen that the absorption edge is not sharp and this may be related to the polycrystalline structure of thin films. The extinction coefficient was figure (5) shows that the variation of extinction coefficient as function of photon energy for all the undoped and doped CdO samples. It is obviously seen that k0 for undoped sample increase approximately exponentially with photon energy and then increases rapidly in the high photon energy. The data of (k0) for the doping samples shows that the value decreases as the doping percentage increases. The refractive index versus photon energy is plotted as function of doping percentage in figure (6). This figure illustrates the decrease of refractive index when increasing Al concentration. The same behaviors were reported by illustrating the refractive index decreases by doping An approximate expression was reported by Freeman and Paul relating the refractive index and electronic band stricture [11]:

$$n_0^2 - 1 = \frac{4\pi N e \hbar^2}{m E g^2}$$

where N is the density of the valence band per unit volume and m is their mass. From the above expression, it could be seen that there is an inverse relation between the refractive index and the band gap. Our result is good agreement with the above expression. Real and imaginary part of dielectric constant sowed in figures (7, 8). The plots of real and

imaginary part of undoped and doped samples were illustrated in figures. The optical conductivity was also determined, and we notice that the variation of optical conductivity varies in a similar way as the variation of the imaginary part of dielectric constant, because it depends on it. This might be due to the improvement of crystallinity which laid to the increase in the concentration of charge carriers. Figure (9) illustrate conductivity versus photon energy for all undoped and doped samples.

REFERENCES

1. Eckertova, L., (2012). Physics of thin films. Springer Science and Business Media.
2. Medvedeva, J. E., (2010). Combining Optical Transparency with Electrical Conductivity: Challenges and Prospects. Transparent Electronics: From Synthesis to Applications, 29.
3. Chauhan, R., Garg, U., and Tak, R. K., (2011). Corrosion Inhibition of Aluminium in Acid Media by Citrullus Colocyn this Extract. Journalof Chemistry, 8 (1), 85-90.
4. Gosling, K., Jackson, N. L., Leon, N. H., Mulley, V. J., and Baldock, M. J., (1982). U.S. Patent No. 4,359,456. Washington, DC: U.S.Patent and Trademark Office.
5. Frumar, M., Frumarova, B., Nemec, P., Wagner, T., Jedelsky, J., and Hrdlicka, M., (2006). Thin chalcogenide films prepared by pulsedlaser deposition–new amorphous materials applicable in optoelectronics and chemical sensors. Journal of non-crystalline solids, 352(6), 544-561.
6. Scriven, L. E., (1988). Physics and applications of dip coating andspin coating. In MRS proceedings (Vol. 121, p. 717). Cambridge University Press.
7. Zeng, X., Pogrebnyakov, A. V., Kotcharov, A., Jones, J. E., Xi, X. X., Lysczek, E. M., and Schlom, D. G., (2002). In situ epitaxial MgB2 thin films for superconducting electronics. Nature materials, 1(1), 35-38.
8. Kachhava, C. M., (2003). Solid State Physics, Solid State Device AndElectronics. New Age International.
9. Valeur, B., Berberan-Santos, M. N., (2012). Molecular fluorescence: principles and applications. John Wiley & Sons.
10. Schubert, M., Tiwald, T. E., and Herzinger, C. M., (2000). Infrared dielectric anisotropy and phonon modes of sapphire. Physical Review B, 61 (12), 8187.
11. Freeman EC, Paul W, (1979). Optical constants of sputtered hydrogenated amorphous Si. Phys. Rev. B 20: 716-728.

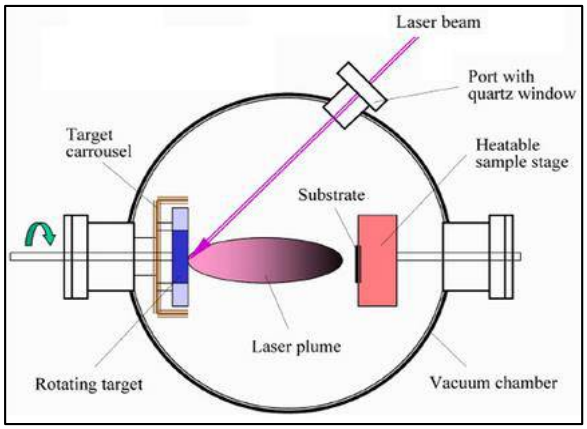

Figure 1: Pulsed Laser Deposition (PLD) system set-up.

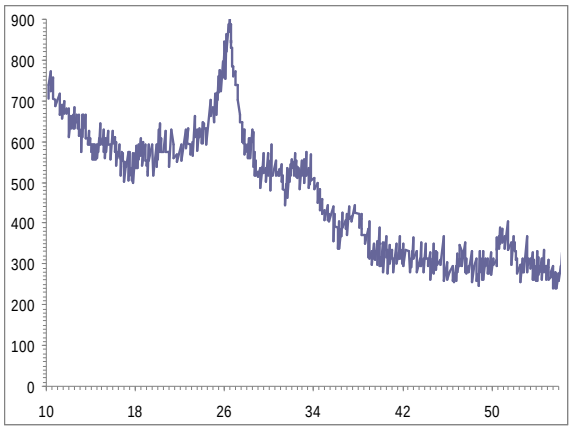

Figure 2: XRD for CdO: Al.

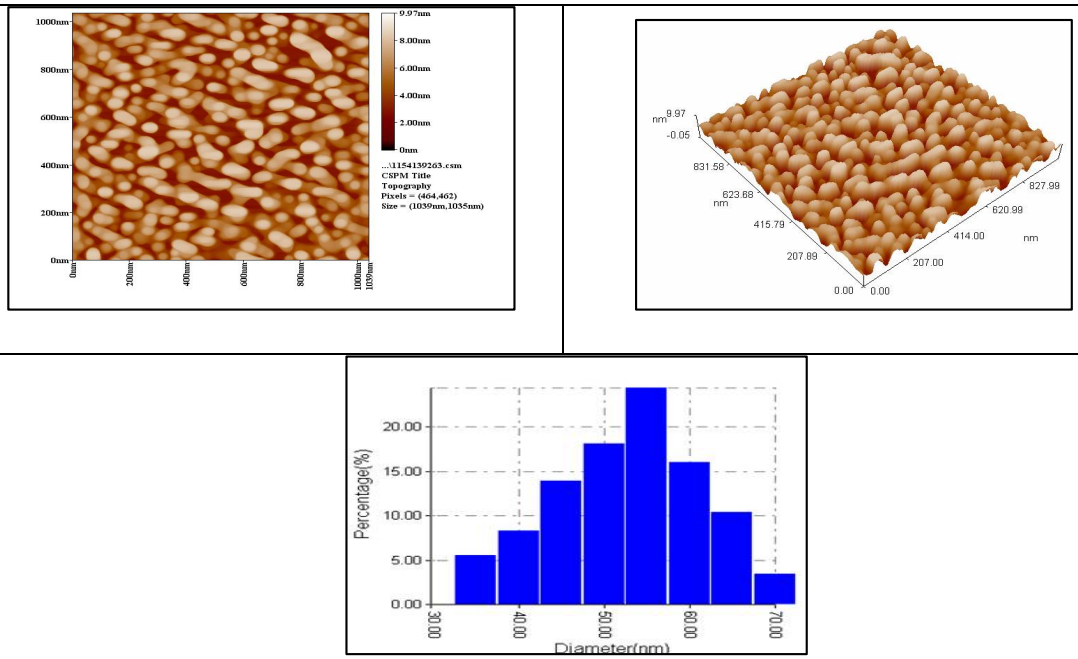

Figure 3. 2D, 3D AFM topography images, and Granularity cumulating distribution of CdO: Al.

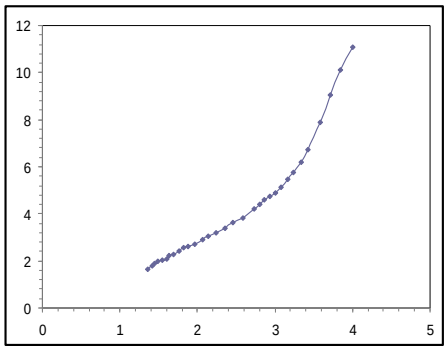

Figure 4. Absorption Coefficient versus photon energy for CdO: Al.

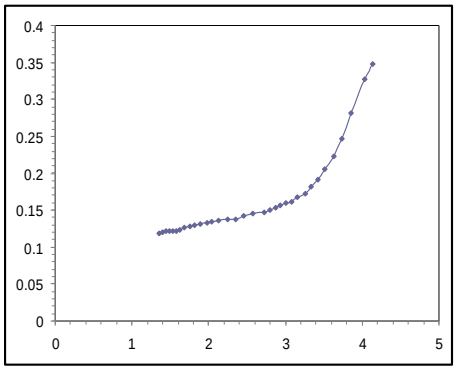

Figure 5. Extinction coefficient versus photon energy for CdO: Al

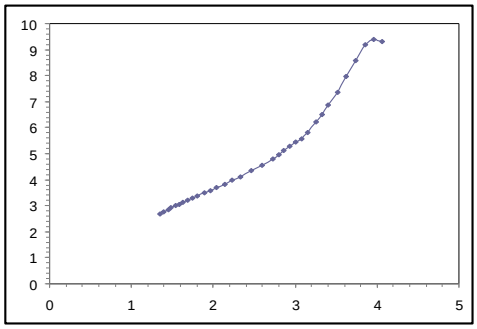

Figure 6. Refractive index versus photon energy for CdO: Al.

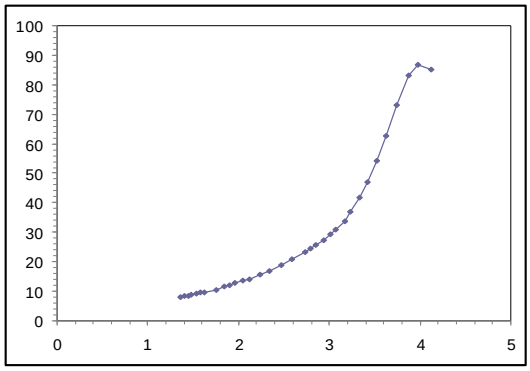

Figure 7. Real part of dielectric constant versus photon energy for CdO: Al.

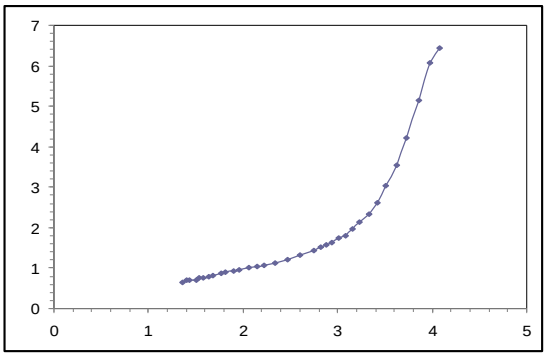

Figure 8. Imaginary part of dielectric constant versus photon energy for CdO: Al

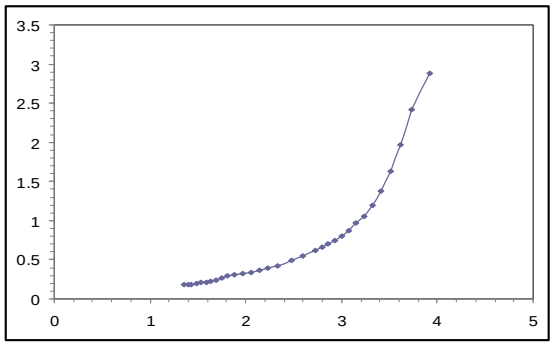

Figure 9. Optical conductivity versus photon energy for CdO: Al.

Indian Journal of Natural Sciences www.tnsroindia.org.in ©IJONS

Vol.9 /Issue 52 / February / 2019 *International Bimonthly* *ISSN: 0976 – 0997*

RESEARCH ARTICLE

Immune Thrombocytopenia Purpura, Experience of Single Institute, Wasit, Iraq

Safa A. Faraj[1*] and Hasanein H. Ghali[2]

[1]MD Oncology Unit, Children's Welfare Teaching Hospital, Wasit University College of Medicine, Wasit, Iraq.

[2]MD Oncology Unit, Children's Welfare Teaching Hospital, University of Baghdad, College of Medicine, Baghdad, Iraq.

Received: 28 Nov 2018 Revised: 20 Dec 2018 Accepted: 26 Jan 2019

[*]**Address for Correspondence**
Safa A. Faraj
MD Oncology Unit,
Children's Welfare Teaching Hospital,
Wasit University College of Medicine,
Wasit, Iraq.
Email: almola.omar82@gmail.com

ABSTRACT

Idiopathic or immune thrombocytopenia purpura (ITP) is a common hematologic disease in children. ITP is subdivided into an acute, persist and chronic forms based solely on the duration of thrombocytopenia. This retrospective study was conducted on 118 patients with ITP, who were treated in the Hematology and Oncology center in Al kut for a period of 9 years from 2008 to 2017. Data including: name, age, sex, address, blood group, weight, height, date of birth, chief complaint, presenting signs, place of diagnosis, mode of diagnosis, mode of treatment, platelet count at time of diagnosis, platelet count in the last visit, family history, consanguinity, outcome. For both data entry and data analysis Statistical package for social science version 24 (SPSS24) was used. Out of the 118 patients with ITP there were 60 males (50.8%) and 58 females (49.2%) aged from 2 months to 321 months. Good response to treatment was found in 45 (38.1%) patients while 47 (39.8%) has not responded to treatment and 23 (28.7%) patients has unknown response. 41 (34.7%) patients developed chronic ITP. Out of 3 patients had splenectomy 1 with good result and 2 are not improved. The benefits of splenectomy in markedly symptomatic chronic ITP far outweigh the risks. The majority of patients with acute ITP had good response after corticosteroids therapy. Bone marrow was done in 53 (44.9%) patients. Immune thrombocytopenia purpura is one of main clinical problem which need more attention and to put under focus in developing countries

Keywords: Platelet, bleeding, steroid.

INTRODUCTION

The most common cause of acute onset of thrombocytopenia in an otherwise well child is immune thrombocytopenic purpura (ITP).ITP seems to occur more often in late winter and spring after the peak season of viral respiratory illness.[9]Immune thrombocytopenic purpura (ITP) is an autoimmune bleeding disorder in children, presenting itself with petechiae, easy bruising, and mucosal bleeding [1]. ITP is characterized by isolated thrombocytopenia (platelet count of <100,000/ul with normal white blood cell count and hemoglobin[1-2]. While the acute form of ITP often follows an infection and usually resolves spontaneously within 12 months, chronic ITP persists longer than 12 months without a specific cause. The cause of ITP is still unknown in most cases, but it can be triggered by vaccines or exposure to viral antigens via respiratory or gastrointestinal infections [1, 3, 4]. Although the disease is more common in children aged 1 to 4 years old , it occurs in other age groups as well . In children with ITP, the risk of serious bleeding and intracranial hemorrhage (ICH) is about 3 and 0.5 percent, respectively. [5] It remains unproven that pharmacologic therapy reduces the risk of ICH and other life-threatening complications of ITP. Approximately 20 percent of affected children will develop chronic ITP, defined as ongoing thrombocytopenia, lasting more than 12 months from presentation [6-7]. As the disease resolves spontaneously in many cases, treatment is rather of a more prophylactic type, with medical intervention necessary only in cases where dangerously low platelet counts increase the risk of life-threatening spontaneous bleeding. Standardized treating options include corticosteroids, immunoglobulins and anti-D antibodies in various regimens [8].

Why some children develop the acute presentation of an ITP is unknown. Although in chronic ITP, many patients demonstrate antibodies against the platelet glycoprotein complexes, αIIb-β3 and GPIb. Afer binding of the antibody to the platelet surface, circulating antibody-coated platelets are recognized by the Fc receptor on splenic macrophages, ingested, and destroyed. [9] Infantile ITP is reported to be characterized by different clinical features including: higher prevalence in male patients, lower rate of chronicity, less frequently preceded by infection, more severe clinical course and less favorable response to treatment[4,8].Despite the importance of ITP in children under 2-years old, a few publications are available in the literatures.

Aim of the study

To evaluate the effects of various treatment modalities on the clinical course, and long term outcome in children with ITP.

Patients and methods

The current study sought to undertake a retrospective study to investigate the clinical symptoms, laboratory findings, history of viral infections, vaccination history, and treatment efficacy in children under 2-years old with ITP.

ITP Diagnosis

The diagnosis of ITP was determined by the physicians based on history and physical examination; complete blood count presented isolated thrombocytopenia (platelet count <100,000), normal hemoglobin, white blood cell count, peripheral blood smear, absence of underlying conditions such as familial thrombocytopenia, HIV, systemic lupus erythematosus, or malignancy. Bone marrow aspirate and serological studies were used to rule out infectious and rheumatic diseases. Coagulation studies were also performed as clinically indicated. Eventually, the diagnosis was confirmed by bone marrow aspiration (BMA)

ITP Classification

Chronic ITP was defined as cases with platelet count of less than 100,000/µl for more than 12 months despite treatment. Newly diagnosed (Acute) ITP was defined as thrombocytopenia within 3 months from diagnosis. Persistent ITP was defined in patients with duration of thrombocytopenia between 3 to 12 months from diagnosis. Chronic ITP was defined in patients with duration of thrombocytopenia more than 12 months from diagnosis Active mucosal bleeding was defined as bleeding from the nose and gums, gross hematuria, gastrointestinal bleeding, and brain hemorrhage. Response to therapy was defined as platelet count of $\geq 30 \times 10^9$/L and at least 2-fold increase in the baseline platelet count and absence of bleeding. Complete response (CR) to treatment was reported when platelet count was $\geq 100 \times 10^9$/L and absence of bleeding [1, 4]. An easy to use classification system has been proposed from the United Kingdom to characterize the severity of bleeding in ITP on the basis of symptoms and signs, but not platelet count:

1. No symptoms
2. Mild symptoms: bruising and petechiae, occasional minor epistaxis, very little interference with daily living
3. Moderate: more severe skin and mucosal lesions, more troublesome epistaxis and menorrhagia
4. Severe: bleeding episodes—menorrhagia, epistaxis, melena— requiring transfusion or hospitalization, symptoms interfering seriously with the quality of life

The presence of abnormal findings such as hepatosplenomegaly, bone or joint pain, remarkable lymphadenopathy other cytopenia, or congenital anomalies suggests other diagnoses (leukemia, syndromes). [9]

Statistics

Calculations of means, medians and routine statistical measureswere performed by the mathematical component of the MicrosoftExcel spreadsheet program.

RESULTS

In our study data was collected from 118 patients as shown in Table (1), 60(50.8%) of them were males and 58 (49.2%) of them were females. Regarding age 23 (19.5%) patients were less than two years, 41 (34.7%) patients were from two to five years, 40 (33.9%) patients were from five to ten years, 8 (6.8%) patients were from ten to fifteen years and 4 (3.4%) patients were above 15 years, 2 (1.7%) were unknown age at diagnosis. Regarding consanguinity 59 (50%) patients their parents were positive consanguinity state, 34 (28.8%) patients their parents were negative consanguinity state and 25 (21.2%) patients their parents were unknown consanguinity state. Regarding family history 85 (72%) patients were negative family history of any bleeding, 8 (6.8%) patients were positive bleeding family history and 25 (21.2%) patients were unknown family history of bleeding. Regarding ITP type there were 39 (33.1%) patients had acute ITP, 10 (8.5%) patients had persistent ITP, 41 (34.7%) had chronic ITP and 28 (23.7%) patients had unknown ITP type.

Sixty patients (50.8%) were males, there were 18(30%) had acute ITP, 4(6.7%) had persistent ITP and 20(33.3%) had chronic ITP and 18(30%) had unknown data. While there were 58(49.2%) females, 21(36.2%) of them had acute ITP, while 6(10.3%) of them had persistent ITP , while 21(36.2%) of them had chronic ITP and 10(17.2%) of them had unknown state, as shown in Table no. (2).Table (3) shows that 82 (69.5%) were treated with only steroids,10 (8.5%) were treated with steroids and Anti-D, 6 (5.1%) were treated with steroids and immunoglobulin, 4 (3.4%) were treated with steroids, immunoglobulin and Anti-D, 3 (2.5%) with immunoglobulin only, 2 (1.7%) were treated with steroids, Anti-D and splenectomy, 1 (0.8%) was treated with steroids and splenectomy, 1 (0.8%) was treated with steroids, rituximab and Anti-D, 1 (0.8%) was treated with steroids, blood transfusion and Anti-D, 1 (0.8%) was treated

with steroids, immunoglobulin, rituximab, blood transfusion and Anti-D, 7 (5.9%) patients were on no treatment and 21 (17.8%) patients unknown data. Table (4) shows that from the 39 patients with acute ITP there were 8 (20.5%) patients aged less than two years old, 16 (41%) patients aged from two to five years old, 12 (30.8%) patients aged from five to ten years old, 1 (2.6%) patients aged from ten to fifteen years old, 2 (5.1%) patients aged above fifteen years old. Ten patients with persistent ITP no one of them aged less than two years old, 5 (50%) patients aged from two to five years old , 3 (30%) patients aged from five to ten years old , no patients from ten to fifteen, 2 (20%) patients aged above fifteen years old Fourteen patients with chronic ITP 8 (20%) patients were less than two years old , 12 (30%) patients were from two to five years old , 15 (37.5%) patients were from five to ten years, 5 (12.5%) patients were from ten to fifteen years old , no patients above fifteen.

Table (5) shows that there were 85 (72%) patients with negative family history, 26 (30.6%) of them had acute ITP , 6 (7.1%) of them had persistent ITP , while 32 (37.6%) had chronic ITP and 21 (24.7%) of unknown ITP type. Also there were 8 (6.77%) with positive family history, 1 (12.5%) had acute ITP , 3 (37.5%) had chronic ITP and the remaining 4(50%) had unknown ITP type. Also there were 22 (18.6%) patients of unknown family history , 11 (50%) of them had acute ITP , 4 (18.2%) had persistent ITP , 4 (18.2%) had chronic ITP and 3 (13.6%) of unknown About one third of the thrombocytopenic patients 39 (33.1%) presented with multiple ecchymosis, 38 (32.2%) patients was presented with ecchymosis, 11 (9.3%) was a known case of ITP diagnosed outside the hematology center, 5 (4.2%) was presented with epistaxis, 4 (3.4%) was presented with pallor, 2 (1.6%) presented with conjunctival hemorrhage, , 2 (1.6%) presented with petechia, 1 (0.8%) was presented with gum bleeding, 1 (0.8%) was presented with bluish discoloration, 8 (6.7%) was presented with mixed symptoms, 7 (5.9%) patients with unknown presentation, as shown in table no (6). Table (7) shows the response to treatment by each type of ITP 24 (61.5%) patients with acute ITP, 5 (50%) patients with persistent ITP, 16 (39%) patients with chronic ITP has responded to treatment but 15 (38.5%) patients with acute ITP, 5 (50%) patients with persistent ITP, 25 (61%) patients with chronic ITP, 2 (7.1%) patients with unknown ITP type has not responded to treatment, 26 (92.9%) patients with unknown ITP type has unknown response to treatment.

DISCUSSION

The study was made to analyze all available data (which was taken from Hematology center at Al-karama teaching hospital, in Al-Wasit, Iraq. This retrospective study was conducted on 118 patients with ITP for a period of 9 years from 2008 to 2017. Data that was analyzed in relation to our study including: age, sex, chief complaint, Type of ITP, mode of diagnosis, mode of treatment, response to treatment, family history on Statistical package for social science version 24 (SPSS24) to be categorized in tables and charts for comparing with other studies and textbooks.As a result of our study in Iraq sampling (Al-Kut) the range of age was from 2 months to 26 years with peak of age below 5 years in comparison with Nelson Textbook [9] in which the and peak was 1-4 years but peak was 2-5 years in Lanzkowsky's Manual of Pediatric Hematology and Oncology[13]. Male to female ratio in Iraq according to our study is nearly 1:1 and also it was equally in [9,11] and in Lanzkowsky's Manual of Pediatric Hematology and Oncology [13] there was no sex predilection.

Regarding the chief complaint the most presenting symptom in our study is multiple ecchymosis (33.1%) and single ecchymosis (32.2%) while petechia , gum bleeding and epistaxis is less common while in Nelson Textbook [9] is bruising and petechiae is the main presenting chief complaints and Often there is bleeding from the gums and mucous membranes but in Manual of Pediatric Hematology and Oncology[13] is petechiae, purpura and nonpalpable ecchymoses, and less commonly hematuria, hematochezia, menometrorrhagia, or epistaxis, and in Fleisher et al, & Ludwig et al Textbook of Pediatric [10] the main chief complaint is ecchymoses and petechiae that may be accompanied by gingival bleeding, epistaxis, and hematuria, In comparison with Turkish study [12] The most frequent chief complaint were petechia and ecchymosis (71%). Regarding Type of ITP most of our patients were chronic ITP 34.7% while acute ITP 33.1% persistent 8.5% which was in Nelson Textbook [9] acute 70-80% chronic 20% , and in

comparison with Turkish study [12] acute and persistent ITP was 69.2% and chronic ITP was 29.8% And most of our ITP patients was diagnosed by bone marrow examination in addition to complete blood count which was 54.6% and complete blood count only 45.4% due to family refusal to do bone marrow examination which is compared with Iranian study [11] 60.6% of their patients done bone marrow examination Regarding treatments)69.5) of our patients was treated with steroids only comparison with Iranian study [11] which was (16.2%), and in Turkish study [12] study (35%),(2.5%) of our patients treated with IVIG only in comparison with Iranian study [11] it was (3.2%),and in Turkish study [12] study it was (65%), (5.1%) of our patients received both steroid and IVIG in comparison with Iranian study [11] which was (78.4%), (5.9%) of our patients received no medications only follow up in comparison with Iranian study [11] which was (2.3%) while in Turkish study [12] study (49%), (2.5%) of our patients needed splenectomy in comparison with Turkish study [12] (3%) of their patients needed splenectomy and according to Iranian study [11] rarely (0.9%) splenectomy are used to treat ITP Among our patients (50%%) were born from consanguineous marriages in comparison with Iraniain study [11] it was (9.9%).

CONCLUSION

Immune thrombocytopenia purpura is one of main clinical problem which need more attention and to put under focus in developing countries. More developed referral system required to achieve real statistical view to put local applicable guidelines

REFERENCES

1. Sandoval C, Visintainer P, Ozkaynak MF, Tugal O, Jayabose S. Clinical features and treatment outcomes of 79 infants with immune thrombocytopenic purpura. Pediatric Blood & Cancer. 2004;42(1):109–12.
2. Bolton-Maggs P, Moon I. Assessment of UK practice for management of acute childhood idiopathic thrombocytopenic purpura against published guidelines. The Lancet. 1997;350(9078):620–3.
3. Watts RG. Idiopathic thrombocytopenic purpura: a 10-year natural history study at the Children's Hospital of Alabama. Clinical pediatrics. 2004;43(8):691–702.
4. Kühne T, Buchanan GR, Zimmerman S, Michaels LA, Kohan R, Berchtold W, et al. A prospective comparative study of 2540 infants and children with newly diagnosed idiopathic thrombocytopenic purpura (ITP) from the Intercontinental Childhood ITP Study Group. The Journal of pediatrics. 2003;143(5):605–8.
5. Kühne T. Idiopathic thrombocytopenic purpura of childhood: A problem-oriented review of the management. Transfusion and apheresis science. 2003;28(3):243–8.
6. Rodeghiero F, Stasi R, Gernsheimer T. Standardization of terminology, definitions and outcome criteria in immune thrombocytopenic purpura of adults and children: report from an international working group. Blood. 2009;113(11):2386–93.
7. Boruchov DM, Gururangan S, Driscoll MC, Bussel JB. Multiagent induction and maintenance therapy for patients with refractory immune thrombocytopenic purpura (ITP) Blood. 2007;110(10):3526–31.
8. Kalyoncu D, Yildirmak Y, Cetinkaya F. Comparison of idiopathic thrombocytopenic purpura in children between 3 months and 2 years versus 2–5 years. Pediatric blood & cancer. 2009;52(5):656–8.
9. Robert M. Kliegman, MD , Bonita F. Stanton, MD Joseph W. St Geme III, MD,Nina F. Schor, MD, PhD, Richard E. Behrman, MD NELSON TEXTBOOK OF PEDIATRICS, 20ed , 2016 :2402-4.
10. Fleisher et al, & Ludwig et al Textbook of Pediatric Emergency Medicine 7ed :824.
11. SajedehSaeidi, Kaveh Jaseb, Ali Amin Asnafi, Fakher Rahim, Fatemeh Pourmotahari, Samira Mardaniyan,HomayonYousefi,ArashAlghasi, Mohammad Shahjahani and Najmaldin Saki: Immune Thrombocytopenic Purpura in Children and Adults: A Comparative Retrospective Study in IRAN. 2014 Jul 1; 8(3): 30–36.

12. MelikeSezginEvim, BirolBaytan, and AdaletMeralGüneş: Childhood Immune Thrombocytopenia: Long-term Follow-up Data Evaluated by the Criteria of the International Working Group on Immune Thrombocytopenic Purpura .2014 Mar; 31(1): 32–39
13. James B, Thomas R, platelet disorders. In: Lanzkowsky P, editor. Manual of Pediatric Hematology and Oncology. 5th ed. Elsevier Academic press; 2011. p.321-377

Indian Journal of Natural Sciences www.tnsroindia.org.in ©IJONS

Vol.9 /Issue 52 / February / 2019 *International Bimonthly* *ISSN: 0976 – 0997*

RESEARCH ARTICLE

Investigation the Role of HOXB13 in Benign and Malignancy Prostatic Cancer Patients Using IHC Technique

Asyad Abdul-Abbas Hussein[1], Kareem Hamed Ghali[1]*, Mahdi Saber Al-Deresawi[1] and HameedNaeem Mousa[2]

[1]Department of Biology, College of Science, University of Wasit, Iraq.
[2]Department of Pathology and Forensic Medicine, College of Medicine, Thi Qar University, Iraq.

Received: 21 Nov 2018 Revised: 23 Dec 2018 Accepted: 26 Jan 2019

***Address for Correspondence**
Kareem Hamed Ghali
Department of Biology,
College of Science,
University of Wasit, Iraq.
Email: Kareem_958@yahoo.com

ABSTRACT

Prostate cancer (Pca) is the third most common cancer with 1.3 million diagnosed cases worldwide in 2018. HOXB13 is localized exclusively in prostate luminal epithelial cell and also acts as a tumor suppressor. This study was designed to investigation the role and expression of HOXB13 protein in initiation and development of PCa as well as in benign hyperplasia. The study included sixty tissue were collected from samples of prostate tumors patients, twenty nine of them were diagnosed as PCa and thirty one were recorded as a benign.Thosepatients samples then compared with twelve non-tumors prostate tissues as control group. This study was carried out in Laboratories of the College of Science/ Department of Biology, Wasit University, during period between October 2017 and May 2018. The study of HOXB13 expression was done by immunohistochemistry staining technique. Results showed HOXB13 expression significant ($p \leq 0.05$) increasing in cancer patients comparing with control group and benign. While ,no significant ($p \geq 0.05$) different between benign patients and control in the expression and staining intensity of HOXB13, also showed significant ($p \leq 0.05$) correlation between HOXB13 expression with overlapping effects of histopathological variables (age and grade) in prostatic cancer patients.

Keywords: Prostate, Cancer, Benign, HOXB13, Expression, IHC.

INTRODUCTION

Prostate cancer (Pca) is the third most common cancer with 1.3 million diagnosed cases worldwide in 2018 after breast and lung cancers and it's the second most common cancer in men after lung canceraccounting for 13.5 % of the cancers diagnosed in men during that year with 6.7% mortality rate [1]. It is the fifth cause of death from cancer in

men worldwide with estimated 307000 deaths representing 6.6% of the total male cancer mortality and it's more common in men above 50 years of age [2]. However, prostate cancer incidence is increased and it's estimated that new cases will be 78,468 in 2020 [3]. Prostate cancer is an adenocarcinoma that may be slow growing, aggressively evolving and metastising predominantly in the bones and lymph nodes [4]. Also prostate cancer has a multifactorial origin with environmental as well as genetic factors[5]. Aging increases prostate cancer risk in different ways [6]. As with almost all cancers, aging allows for more time for accumulation of DNA damage in the prostate both due to internal and external carcinogens, Inflammation processes have been linked to initiation and progression of prostate cancer, and immune system function is altered with aging [7]. Additionally, there is evidence to support an increased risk of prostate cancer among men whose biological mother had breast cancer [8].

Multiple molecular events control PCa initiation, growth, invasion and metastasis, therefore, some genes are considered as biologic markers to diagnose and develop prostate cancer,*Homeobox (HOX)* family genes encode key transcription factors for embryogenesis and may be correlated with carcinogenesis [9]. The HOXB13 protein has characteristic homeobox region called the homeodomain locate in chromosome 17 at position 21.32 and play a role in the development and maintenance of the skin [10]. HOXB13 gene is unique in the prostate because it's highly expressed into adulthood in multiple species, within the normal adult human prostate, HOXB13 is localized exclusively in prostate luminal epithelial cell [11]. It also acts as a tumor suppressor, which means that it keeps cells from growing and dividing too fast or in an uncontrolled way [12]. HOXB13 G84E variant is associated with a significantly increased risk of hereditary prostate cancer[13]. HOXB13 G84E mutation also confers 3.4 times higher risk of developing prostate cancer, but other mutations conferring similar risk increases haven't been detected [14].Recent studies showed over expression of HOXB13 was correlated high grade of prostate cancer in compared with benign hyperplasia [15].

MATERIALS AND METHODS

Patients and tissue samples

All specimens of patients were collected from Al-Zahraa and AL-Karama Teaching Hospitals in Wasit Province, and form Ibn Al-BitarPrivate Laboratory in ThiQarProvince.Fixed paraffin embedded tissue blocks were cut into 4-5μm thickness from each tissue block.

Immunohistochemistry (IHC)

HOXB13 antibody and ABC staining system (rabbit monoclonal antibody) were provided by AbcamBiotech. Inc. Serial tissue sections were cut 4- 5μm thick and positioned on positive charged slides. The slides were baked in 60-65°C oven overnight.The tissue sections were deparaffinizedby xylene(100%); then the slides were rehydrated by graded ethanol concentration (100%, 95%,70% and 50%) and distal water.The slides were treated withTris/EDTA buffer (PH=9 for 30 minutes, and then washed twice in distal water for 2 minutes. After preparation of tissue sections, slides were incubated in 3% hydrogen peroxide (H2O2) diluted in D.W. for 10 minutes.Each slide was washed in PBS twice for 3 minutes. The slides were incubated in 3% hydrogen peroxide (H_2O_2) for 10 minute. Then, the slides were washed in 2x PBS, for 3 minute. The tissue sections were incubated in protein block serum solution for 10 minutes at room temperature in humidity chamber. Then, the slides were washed in 2x PBS, for 3 minute Incubating the section with primary antibody for 60 minutes. Or Overnight at 4°C in humidity chamber, slides were in PBS for 3 minutesfor three times. The slides were incubated in biotinylated secondary antibody for 10 min, and washed in PBS for 3 minutes 3 times. Applied Streptavidin Peroxidase and incubated for 10 minutes at room temperature. The slides were rinsed 4 times in buffer. Add 30 μl (1 drop) DAB Chromogen to 1.5 ml (50 drops) of DAB Substrate, mix by swirling and apply to tissue. Incubate for 1-10 minutes. Rinse 4 times in buffer. Applied counterstainHematoxylin on slides for

1minutes, washed slides in running tap water for 2 minutes. The cover slips were located on slides utilize DPX solution, slides were observed by light microscope.

Ethical consent

The study was submitted and approved by the College of Science, University of Wasit in collaboration with AL-Karama and AL-Zahraa Teaching Hospitals, Wasit – Iraq.

Statistical analysis

For all statistical analyses, the SPSS system for personal computer was used, and p values of 0.05 or less were regarded as statistically significant. Sensitivity and specificity of the tests (with 95% exact confidence intervals) were determined in studied group. Comparison between groups was carried out using Chi-square test.

Scoring system

Based on the percentage of stained cells and the intensity of nuclear stain.The staining of HOXB13 were scored as follows: The percentage of positive staining (P) was scored as 0 for negative, 1 for 1-25%, 2 for 26-50%, and 3 for 51-100% staining, and the levels of intensity of staining (I) were scored as 0, negative; 1, weak staining; 2, moderate staining; and 3, strong staining.

RESULTS AND DISCUSSION

HOXB13 expression and intensity in prostatic cancer and control group

Table (3.1) explains the expression of HOXB13 in prostatic cancer patients in comparison with control group.Expression of HOXB13 was reported positive in 21 (72.4%) of prostate cancer patients out of 29 casesand the rest 8 (27.6%) cases were showed negative staining, while in control group 3 (25%) out of 12 cases were showed positive staining for HOXB13 and the rest 9 (75%) cases were showed negative staining. There was significant ($P \leq 0.05$) difference between patients of prostate cancer and control group in relation to HOXB13 expression. Intensity assessment of HOXB13 expression inprostate cancer patients showed that 9 (42.9%) cases with score +1,7 (33.3%)cases with score +2 , 5 (23.8%) cases were scored +3. While in control group 1 (33.3) case with score +1, 1(33.3%) case with score+2 , 1 (33.3%)case with score +3.There was no significantdifference ($p>0.05$) between prostate cancer and control group in the staining intensity of HOXB13 expression (Table 3.1) and (Fig 1).

Result of Cristina *et al*., (2015) found HOXB13 immunostaining was seen in 5,278 out of 10,216 (51.7%) interpretable prostate tumors 22.3% of them were scored weak, 19.7% were moderate and 9.6% of them were strong, while normal prostatic glands showed weak nuclear staining, positive staining was limited to theepithelial secretory cells, while basal cells were consistently negative [16]. Also Varinot*et al.* (2013) described strong HOXB13 immunostaining in all 400 analyzed prostate cancers and in secretory cells from all analyzed 120 normal prostates. Another study of Kim *et al.,* (2010) indicates moderate to strong HOXB13 expression was found in only 30% of 44 prostate cancers [17,18]. However, Kim *et al.,* (2010), attributed this overexpression of HOXB13 in prostate cancer for its role as a cell growth suppresser, by inhibition the activation of androgen mediated signals [18]. Also HOXB13 expression was seen in 64.4%in prostate cancer metastases patients [19]. Most studies showed that the HOXB13 overexpression in prostate cancer becaue of this gene displays a cancer predisposing mutation (G48E) in some males [16,15]. Moreover, Miller *et al.* (2012) founed that mutation in G48E was frequent 1.3% vs 0.4% in control group [20]. Jianfeng*et al.* (2012) reported when evaluating gremlin mutations of the HOXB13 gene in 2,433 prostate cancer families from the international consortium for prostate cancer genetics (ICPCG), that study confirmed the notice that the G84E mutation is

significantly associated with prostate cancer in subjects of European descent with family history of the disease [21]. Jeong*et al,* (2012) showed HOXB13 expression in 57 from 57 tumors and showed HOXB13 was mildly expressed in normal prostatic epithelial cells, while in cancer HOXB13 appeared to be overexpressed in more invasive tumor cells [22]. Finding of Barresi *et al.* (2016) showed that HOXB13 is very sensitive (sensitivity: 100%) marker for prostatic derivation in metastatic carcinoma [23]. The same study showed strong staining in ≥ 75 % of neoplastic cells, finally previous study noted that HOXB13 is expressed in normal prostate but it is overexpression in prostate cancer [16].

HOXB13 expression and intensity in prostatic cancer and benign patients

Expression of HOXB13 was reported positive in 21 (72.4%) of prostatic cancer patients out of 29 cases and the rest 8 (27.6%) cases were showed negative staining for HOXB13, while in benign patients 12 (38.7%) out of 31 cases was showed positive staining for HOXB13 and the rest 19 (61.3%) cases were showed negative staining for HOXB13. There was significant ($p \leq 0.05$) difference between prostatic cancer patients and benign group in relation to HOXB13 expression. Intensity assessment of HOXB13 expression in prostatic cancer patients showed that 9 (42.9%) cases with score +1 , 7 (33.3%) cases with score +2 , 5 (23.8 %) cases were score +3. While in benign patients 4(33.3%)cases with score +1 , +2 and +3. There were no significant ($p>0.05$) differences between patients of prostatic cancer and benign in relation to intensity of HOXB13 expression (Table 3.2).

Kim *et al.*(2010) observed by using total RNA there was no differential expression of HOXB13 between the benign and malignant tumors of prostate and they explained it due to the multifocal nature of Prostate cancer [18]. Also Jung *et al.* (2004) findings showed that HOXB13 expression level was not altered in patient samples of prostate cancer compared with matching benign tissues due to the well-known heterogeneous population of prostate cancer [24]. WhileLiesel*et al.* (2017) reported increase in HOXB13 expression in malignant compared to benign cells ($P=0.01$) and there was no significant difference in HOXB13 expression was observed between the prostate tumors (malignant and benign) of G84E variant carriers and non-carriers ($P = 0.21$) [15].

HoxB13 expression and intensity in benign patients and control group

Expression of HOXB13 was reported positive in 12 (38.7%) out of 31 cases and the rest 19 (61.3%) cases were showed negative staining for HOXB13 in the benign patients, while in control group 3 (25%) out of 12 cases were showed positive staining for HOXB13 and the rest 9 (75%) cases were showed negative.There was no significant ($p>0.05$) between benign patients and control group in the HOXB13 expression. Staining intensity assessment of HOXB13 expression in benign patientsshowed that 4 (33.3) case with score +1, +2 and +3.While in control group,1 (33.3%) case with score +1, +2 and +3.There were no significant ($p>0.05$) differences between benign patients and control group in relation to intensity of HOXB13 expression (Table 3.3) and (Fig 2). The results Economides *et al.,* (2003) suggested a specific role for Hoxb13 in a differentiation pathway that gives the ventral prostate epithelium a unique identity, as well as a more general role in ventral prostate morphogenesis that is redundant with other Hoxb13 paralogs [25]. Despite the high expression of HOXB13 in the normal prostate, alteration of HOXB13 expression during the transformation process remains controversial [26]. Studies of Jung *et al.* (2004) suggest overexpression of HOXB13 in prostate tumors, while others reported no such change [24,27].

Correlation between HOXB13 expression and overlapping effects of clinic pathological variables in prostatic cancer patients

The statistical analysis between HOXB13 expression with age and grade of prostatic cancer using correlation coefficient (Person and Spearman's rho) ,showed highly significant correlation coefficient in HOXB13 expression withoverlapping of age groups ($p \leq 0.001$) ($p \leq 0.001$), and significant with tumor grade($p \leq 0.05$) ($p \leq 0.05$),as shown in (Table 3.4). Joeng*et al.* (2012) result reported that no correlation between HOXB13 expression age ($r = -0.086$, $P=0.299$), while there were correlation between HOXB13 expression and grade ($r = 0.286$, $P=0.031$) [22]. Athor study done

byCristina *et al.,*(2015), found that HOXB13 were linked to high grade, but indepat from parameter [16]. On the other hand , our study found highly correlation between HOXB13expression and age of prostate cancer patients, this result confirms that the aging may increase the HOXB13 expression in prostate cancer patients .

CONCLUSIONS

HOXB13 was showed over expression in prostate cancer compared with benign and control group. This may be because it's tumor suppressor gene and mutations such as (G48E) which increased risk and aggressive of prostate cancer. Also

REFERENCES

1. Bray, F., Ferlay, J., Soerjomataram, I., Siegel, R. L., Torre, L. A., and Jemal, A. (2018). Global cancer statistics 2018.Cancer Journal for Clinicians. doi:10.3322/caac.21492
2. Ferlay, J., I. Soerjomataram, R. Dikshit, S. Eser, C. Mathers, M. Rebelo, D. M. Parkin, D. Forman, and F. Bray. (2015). 'Cancer incidence and mortality worldwide: sources, methods and major patterns in GLOBOCAN 2012', Int J Cancer, 136: E359-86.doi:10.1002/ijc.29210.
3. Harutake S, Atsushi S and Masaaki I. (2014). Feedback on baseline use of staging images is important to improve image overuse with newly diagnosed prostate cancer patients. Asian Pac J Cancer Prev, 15, 1707-10
4. Lozano R., Naghavi M., Foreman K., Lim S., Shibuya K., Aboyans V., Abraham J., Adair T., Aggarwal R. and Ahn S.Y. (2013). Global and regional mortality from 235 causes of death for 20 age groups in 1990 and 2010: a systematic analysis for the Global Burden of Disease Study 2010. The Lancet 380(9859), 2095-2128.
5. Finnish Cancer Registry. (2017).(Referred 9.10.).
6. De Angulo A, Faris R, Daniel B, Jolly C., and deGraffenried L.(2015). Age-related increase in IL-17 activates pro-inflammatory signaling in prostate cells. Prostate 2015;75: 449-462.
7. Sfanos KS and De Marzo AM.(2012). Prostate cancer and inflammation: the evidence. Histopathology 2012;60: 199-215
8. Cordella, Uleta, Fiona, Kelly Hill. (2015). Thesis; Identification of potential mechanisms of action of 3',4',5'- -trimethoxyflavonol in the inhibition of prostate cancer. Department of Cancer Studies University of Leicester.
9. Bambury RM, Gallagher DJ.(2012).Prostate cancer: germline prediction for a commonly variable malignancy. BJU Int. 2012 Dec;110(11 Pt C):E809-18. doi: 10.1111/j.1464-410X.2012.11450.x. Epub 2012 Sep 14. Review
10. Ko SY, Ladanyi A, Lengyel E and Naora H.(2014). Expression of the homeobox gene HOXA9 in ovarian cancer induces peritoneal macrophages to acquire an M2 tumor-promoting phenotype. Am J Pathol;184:271–81
11. Cerdá-Esteban, N., &Spagnoli, F. M. (2013). Glimpse into Hox and tale regulation of cell differentiation and reprogramming. Developmental Dynamics, 243(1), 76–87. doi:10.1002/dvdy.24075
12. Smith SC, Palanisamy N, Zuhlke KA, Johnson AM, Siddiqui J, Chinnaiyan AM, Kunju LP, Cooney KA. and Tomlins SA.(2014). HOXB13 G84E-related familial prostate cancers: a clinical, histologic, and molecular survey. Am J Surg Pathol.38(5):615-26
13. Ewing C.M., Ray A.M., Lange E.M.(2012)Germline mutations in HOXB13 and prostate-cancer risk. N Engl J Med. ;366:141–14.
14. Cuzick J, Thorat MA, Andriole G, Brawley OW, Brown PH, Culig Z,Eeles RA, Ford LG, Hamdy FC, Holmberg L, Ilic D, Key TJ, La Vecchia C, Lilja H, Marberger M, Meyskens FL, Minasian LM, Parker C, Parnes HL, Perner S, Rittenhouse H, Schalken J, Schmid HP, Schmitz-Dräger BJ, Schröder FH, Stenzl A, Tombal B, Wilt TJ and Wolk A.(2014). Prevention and early detection of prostate cancer. The Lancet Oncology, 15(11), e484–e492. doi:10.1016/s1470-2045(14)70211-6
15. Liesel M. FitzGerald, KelsieRaspin, James R. Marthick, Matt A. Field, Roslyn C. Malley, Russell J. Thomson, Nicholas B. Blackburn, Annette Banks, Jac C. Charlesworth, Shaun Donovan, and Joanne L. Dickinson. (2017). Impact

of the G84E variant on HOXB13 gene and protein expression in formalin-fixed, paraffin-embedded prostate tumours. Scientific Reports, 7(1). doi:10.1038/s41598-017-18217-w

16. Cristina VillaresZabalza, Meike Adam, ChristophBurdelski, WaldemarWilczak, CorinaWittmer, Stefan Kraft, Till Krech, Stefan Steurer, Christina Koop, Claudia Hube-Magg, Markus Graefen, Hans Heinzer, Sarah Minner, Ronald Simon, Guido Sauter, Thorsten Schlomm and Maria Christina Tsourlakis.(2015). HOXB13 overexpression is an independent predictor of early PSA recurrence in prostate cancer treated by radical prostatectomy. Institute of Pathology, University Medical Center Hamburg-Eppendorf, Germany. Oncotarget journals. Vol.6, N14.

17. Varinot J, Cussenot O, Roupret M, Conort P, Bitker MO, Chartier-Kastler E, Cheng L and Comperat E.(3013). HOXB13 is a sensitive and specific marker of prostate cells, useful in distinguishing between carcinomas of prostatic and urothelial origin. Virchows Arch; 463:803–809.

18. Kim, Y.-R., Oh, K.-J., Park, R.-Y., Xuan, N., Kang, T.-W., Kwon, Dong-Deuk Kwon, Chan Choi, Min Soo Kim, Kwang Il Nam, KyuYounAhn, and Chaeyong Jung. (2010). HOXB13 promotes androgen independent growth of LNCaP prostate cancer cells by the activation of E2F signaling. Molecular Cancer, 9(1), 124. doi:10.1186/1476-4598-9-124

19. Kristiansen, I., Stephan, C., Jung, K., Dietel, M., Rieger, A., Tolkach, Y., & Kristiansen, G. (2017). Sensitivity of HOXB13 as a Diagnostic Immunohistochemical Marker of Prostatic Origin in Prostate Cancer Metastases: Comparison to PSA, Prostein, Androgen Receptor, ERG, NKX3.1, PSAP, and PSMA. International Journal of Molecular Sciences, 18(6), 1151. doi:10.3390/ijms18061151

20. Miller,S. M., Karyadi, D. M., Smith, T., Kwon, E. M., Kolb, S., Stanford, J. L., & Ostrander, E. A. (2012). HOXB13mutations in a population-based, case-control study of prostate cancer. The Prostate, 73(6), 634–641. doi:10.1002/pros.22604

21. JianfengXu, Ethan M. Lange, Lingyi Lu, Siqun L. Zheng, Zhong Wang, Stephen N. Thibodeau, Lisa A. Cannon-Albright,Craig C. Teerlink, Nicola J. Camp, Anna M. Johnson, Kimberly A. Zuhlke, Janet L. Stanford, Elaine A. Ostrander,Kathleen E. Wiley, Sarah D. Isaacs, Patrick C. Walsh, Christiane Maier, Manuel Luedeke, Walther Vogel,JohannaSchleutker, TiinaWahlfors, TeuvoTammela, Daniel Schaid, Shannon K. McDonnell, Melissa S. DeRycke,Geraldine Cancel-Tassin, Olivier Cussenot, Fredrik Wiklund, HenrikGrönberg, RosEeles, Doug Easton,ZsofiaKote-Jarai, Alice S. Whittemore, Chih-Lin Hsieh, Graham G. Giles, John L. Hopper, GianlucaSeveri,William J. Catalona, DiptasriMandal, Elisa Ledet, William D. Foulkes, Nancy Hamel, LoviseMahle, Pal Moller,Isaac Powell, Joan E. Bailey-Wilson, John D. Carpten, Daniela Seminara, Kathleen A. Cooney, William B. Isaacs and International Consortium for Prostate Cancer Genetics.(2012).HOXB13 is a susceptibility gene for prostate cancer: results from the International Consortium for Prostate Cancer Genetics (ICPCG).Data Coordinating Center for the ICPCG, Wake Forest University School of Medicine, Winston-Salem, NC, USA. doi:10.1007/s00439-012-1229-4.

22. Jeong, T.-O., OH, K.-J., Nguyen, N. T. X., Kim, Y.-R., Kim, M. S., Lee, S. D., Ryu,S.B., and Jung, C. (2012). Evaluation of HOXB13 as a molecular marker of recurrent prostate cancer. Molecular Medicine Reports, 5(4), 901–904. doi:10.3892/mmr.2012.769

23. Barresi, V., Ieni, A., Cardia, R., Licata, L., Vitarelli, E., ReggianiBonetti, L., &Tuccari, G. (2016). HOXB13 as an immunohistochemical marker of prostatic origin in metastatic tumors. APMIS, 124(3), 188–193. doi:10.1111/apm.12483

24. Jung, C., Kim, R.-S., Zhang, H.-J., Lee, S.-J., &Jeng, M.-H. (2004). HOXB13 Induces Growth Suppression of Prostate Cancer Cells as a Repressor of Hormone-Activated Androgen Receptor Signaling. Cancer Research, 64(24), 9185–9192. doi:10.1158/0008-5472.can-04-1330

25. Economides K.D., Capecchi M.R.(2003). Hoxb13 is required for normal differentiation and secretory function of the ventral prostate. Development. 130:2061–2069.

26. Feber A, Clark J, Goodwin G, Dodson AR, Smith PH, Fletcher A, Edwards S, Flohr P, Falconer A, Roe T, Kovacs G, Dennis N, Fisher C, Wooster R, Huddart R, Foster CS, Cooper CS.(2004). Amplification and overexpression of E2F3 in human bladder cancer. Oncogene.23:1627–1630

27. Fromont G, Chene L, Latil A, Bieche I, Vidaud M, Vallancien G, Mangin P, Fournier G, Validire P, Cussenot O.(2004).Molecular profiling of benign prostatic hyperplasia using a large scale real-time reverse transcriptase-polymerase chain reaction

Table 1.HOXB13 expression and intensity in prostatic cancer and control group

Case	Expression + No %	No%	Total	P value	Intensity 3 No%	2 No%	1 No%	Total	P Value
Prostatic cancer patients	21 72.4%	8 27.6%	29	P≤0.05 *	9 42.9%	7 33.3%	5 23.8%	21	P≥0.05
Control group	3 25%	9 75%	12		1 33.3%	1 33.3%	1 33.3%	3	
Total	24	17	41		10	8	6	24	

P>0.05,non-significant))(P ≤0.05, significant*(

Table 2. HOXB13 expression and intensity in prostatic cancer and benign patients

Case	Expression + No %	No%	Total	P value	Intensity 3 No%	2 No%	1 No%	Total	P value
Prostatic cancer patients	21 72.4%	8 27.6%	29	P≤0.05 *	9 42.9%	7 33.3%	5 23.8%	21	P≥0.05 *
Benign patients	12 38.7%	19 61.3%	31		4 33.3%	4 33.3%	4 33.3%	12	
Total	33	27	60		13	11	9	33	

* (p≤0.05, significant) (p>0.05,non-significant)

Table 3 .HoxB13 expression and intensity in benign patients and control group

Case	Expression + No %	No%	Total	P value	Intensity 3 No%	2 No%	1 No%	Total	P value
Benign patients	12 38.7%	19 61.3%	31	P≥0.05 *	4 33.3%	4 33.3%	4 33.3%	12	P≥0.05 *
Control group	3 25%	9 75%	12		1 33.3%	1 33.3%	1 33.3%	3	
Total	15	28	43		5	5	5	15	

* (P≥0.05,non-significant)

Table 4.Correlation between HOXB13 expression and overlapping effects of clinic pathological variables in prostatic cancer patients

Gene	Variables	Person factor		Spearman's factor (Rho)	
		R	P	R	P
HOXB13	Age	-0.874	p≤0.001	-0.910	p≤0.001
	Grade	-0.416	p≤0.05	-0.444	p≤0.05

(P≤0.001, highly significant) (p≤0.05, significant)

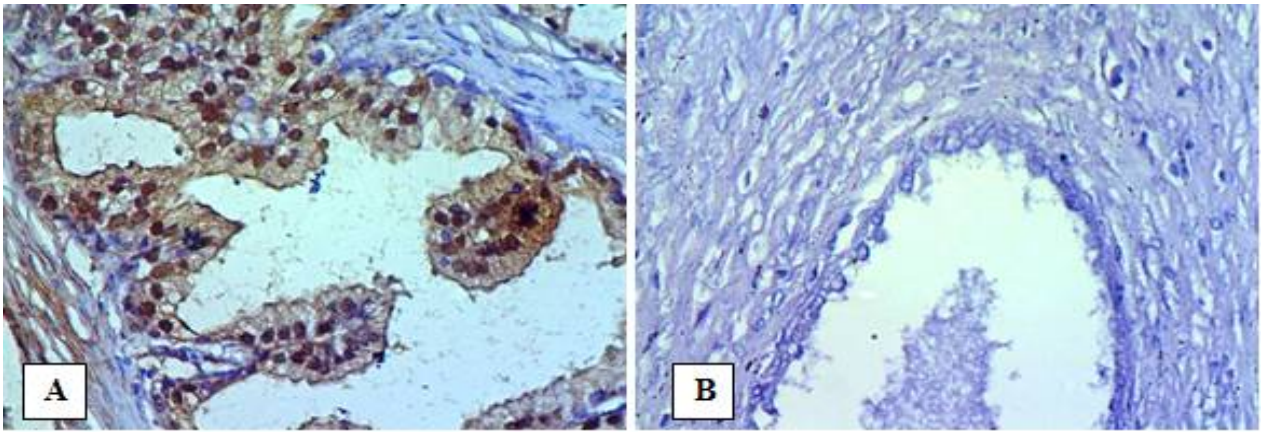

Fig 1.HOXB13 IHC staining in prostate patients. A: Cancer (positive) B: Cancer (negative) (40X).

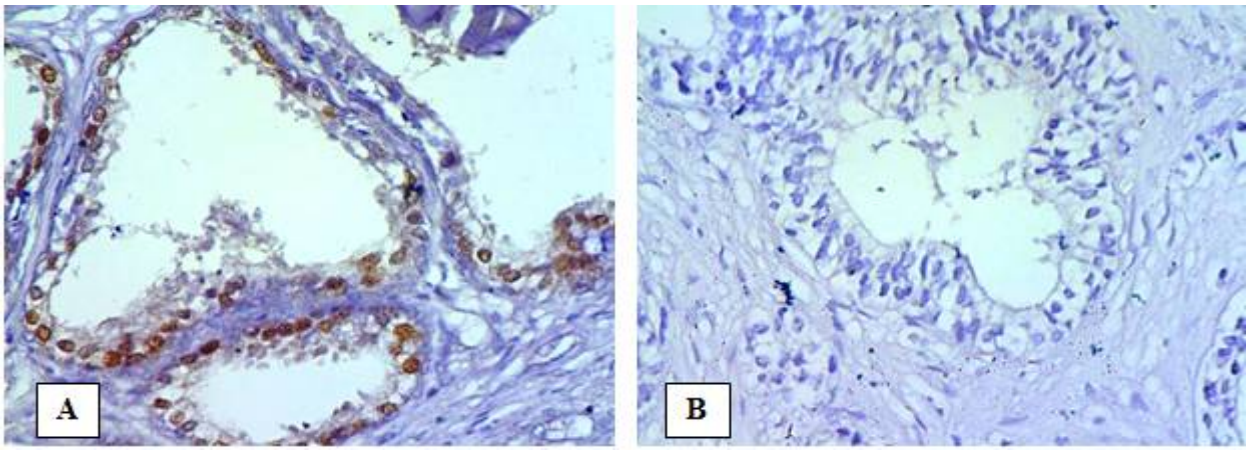

Fig 2. Nkx3-1 IHC staining in prostate patients. A: Benign (positive) B: Benign (negative) (40 X).

Indian Journal of Natural Sciences www.tnsroindia.org.in ©IJONS

Vol.9 /Issue 52 / February / 2019 *International Bimonthly* *ISSN: 0976 – 0997*

RESEARCH ARTICLE

Crude Oil Characterization and Affinity of Ahdab, East Baghdad and Badra Oil Fields, Eastern and Central Iraq

Ali Kh. Al-Temimi*

Department of Geology, College of Science, University of Baghdad, Iraq.

Received: 18 Nov 2018 Revised: 21 Dec 2018 Accepted: 26 Jan 2019

***Address for Correspondence**
Ali Kh. Al-Temimi
Department of Geology,
College of Science,
University of Baghdad, Iraq.
Email: asdtmim@yahoo.com

ABSTRACT

The study will be emphasized on the exploration study and development of Ahab, Badrea, and East Baghdad oil fields in East and Middle of Iraq.This study will be based on total petroleum system, essential elements and processes and all genetically related accumulation sites and seeps, as well as finding their origination (oil families) from an active source rocks, as well reservoirs properties for Zubair, Tanuma, Khasib, Mishrif, Rumaila, Ahmadi, and Mauddud formations in Ahdab, Badra, and East Baghdad oil fields.Gas Chromatography GC, Gas Chromatography–Mass spectrometry GC/MS techniques used for analysis of the crude oil that taken from (3) producing wells these (EB21, EB68, and EB92) from Zubair, Khasib, and Tanuma formations. The analysis shows that all oil samples are from one family, non-biodegraded, marine, and non-waxy deposits, derived from carbonate source rocks deposited in anoxic marine environment. All oil samples of East Baghdad oil field is from Late-Middle Jurassic to Early Cretaceous source rocks with similar level of maturity. Hence the most appropriate source for these crudes oils may be Chiagara and Zubair Formations.This study discusses how to apply the Jurassic – Cretaceous petroleum system concept to petroleum exploration in the area study. It defines petroleum province, basin, system, play, and prospect and it shows how the system relates to the complementary play. It also explains how to use this petroleum system study to reduce exploration risk in the area study.

Keywords: Crude Oil, Total Petroleum System, Gas Chromatography GC, Gas Chromatography–Mass spectrometry GC/MS.

INTRODUCTION

This study will be based on total petroleum system, essential elements and processes and all genetically related accumulation sites and seeps, as well as finding their origination (oil families) from an active source rocks, as well

reservoirs properties for Zubair, Tanuma , Khasib, Mishrif, Rumaila, Ahmadi, and Mauddud formations in Ahdab, Badra, and East Baghdad oil fields.Assessment for the best oil accumulation sites will be done on this scenario in the reservoir rocks as well as finding genetic relations with the disseminated organic matters (kerogen) of the source rocks. This study discusses how to apply the Jurassic –Cretaceous petroleum system concept to petroleum exploration in the area study. It defines petroleum province, basin, system, play, and prospect and it shows how the system relates to the complementary play. It also explains how to use this petroleum system study to reduce exploration risk in the area study.

The Study Area

Badra oil field is located in the Zagros fold belt province basin, neighboring Iraqi-Iranian border. Badra oil field is situated in Wasit Governorate, 160 km South – East Baghdad, and extends across the border with Iran.While East Baghdad and Ahdab oil fields are located between longitude (44.5) latitude (33.2) to longitude (44.5) latitude (32.6), Baghdad government, central Iraq and detailed map of field is showing in (figure 1).

METHODOLOGY

Sampling

Seventy core samples are collected from wells EB-92 of East Baghdad oil field for Zubair, Tnuma, and khasib Formations and it is showing in (table 1) as well as six oil samples from the same formations (EB – 01, EB- 10, EB – 21, EB -25, EB – 58, EB – 68, EB – 81, EB – 82, EB – 92, AD-2, AD-13, AD-15, BD-4, BD-5, and BD-15) wells.(Table 1) Shows the analyzed rock samples:
(1) Petrographic analysis.
(2) Geochemical analyses and crude oil samples for gas chromotography mass spectrometer shows in (table 2), at GeoMark Research Inc., Houston in Texas, U.S.A. Appendix I.

Geochemical Organic analysis

Geochemical Organic analysis includes the following parts:
A. Total organic carbon (TOC).
B. Pyrolysis. Because the instruments and the materials used in performing different analysis arenot available in Iraq, The analysis of crude oil and some of the source rock sample were analyzed in the GeoMark Research Inc., Texas, U.S.A (Tables 1) and (Table 2) in addition to making use of information from ministry of oil reports of the field.

Crude oil analysis

Crude oil analyses of this study have been performed according to the aims of study which include the correlation between crude oil with rock kerogen using geochemical analysis, (see Table 2). The geochemical analysis were performed on six samples of crude oil taken directly from the wells shown in (Table 2) they are done at GeoMark Research Inc., in Texas - U.S.A.(Table 2): shows the analyzed crude oil samples.
1) Gas Chromatography (GC.)
2) Gas Chromatography - Mass spectrometry (GC/ MS.)
3)Carbon Isotopes.

Petroleum Geochemistry

Crude oils are technically separated to saturate HC (hydrocarbon), aromatic HC with benzothiophenes and then analyzed using GC (Gas-chromatography) and GC/MS (Gaschromatography/mass spectrometry) techniques [1].

Bulk properties and petroleum composition

The crude oils are analyzed in this study and hence characterized by the followings:

API degrees: Crude oils and hydrocarbon compositions relations Sulfur content

of the oil fields in East Baghdad oil field are varying in their API (American Petroleum Institute scale) that is related inversely to the density of liquid hydrocarbon and wt% sulfur depending on the depth of the reservoir (Figure 2), the oils of Zubair reservoir Formation, with depths more than 3000 meters, are of above and slightly below than 30 API with 3.2- 4.0 wt% sulfur and hence could be considered medium to light oil. The oils in the Khasib and Tannuma Reservoir Formations, with depths 2060-2179 meters, are ranged between 20-16 with 3-3.5 wt% sulfur and hence could be considered heavy oil with increased aromatic (40- 40%), %NSO (13- 22%) relative to paraffin and saturate hydrocarbons (Figure 3).

Asphalts

Petroleum asphalt is either straight- run residues from distilling crude oil or blown asphalt produced by air oxidation of crude residues. Asphalt contains heavy oils, resin, asphaltenes, and high molecular weight waxes. Asphaltenes are agglomeration of molecules with condensed aromatic and naphthenic rings connected by paraffin chains. High variations of asphalt percentage between reservoirs of oil fields might be due to heat increase on the oil within a reservoir and hence separated oil into light oil migrated to special reservoirs and asphalt that make heavy oil that may stay nearby due to large size of the asphalt or may block the permeability necks in some migration pathways.

Porpherin content

They are complex biomarkers characterized by a tetrapyrole ring, usually containing vanadium or nickels, which originate from various sources including chlorophyll and heme [2]that indicate by their presence of marine anoxic source according [3]. Plots of these variables on vanadium- nickel diagram (Figure 4) could show facies gathering of oil families in the studied fields, with two sub-zones. The first sub-zone represent gathering of the main oil family (A) contain 109-117 ppm vanadium with 34-35 ppm of nickel which include oil accumulations in Khasib and Tannuma reservoir oil while the second subzone represent gathering of the oil family (A-B) contain 68-97 ppm vanadium with 1624 ppm of nickel which include oil accumulations in Zubair reservoir oil.

Biodegradation

All the studied oil fields are characterized by Non-Biodegraded oil based on anoxic environment of deposition by comparison with [4], greater depth of reservoir (Table 2) with 2060 -3099 meters according [2], temperature of more than 80^{o}C according [4], [1] as well as strait line of alkanes of the GC (Figure 5) according [5], medium API, and could be considered of light biodegradation (Rank 1) of no destruction by comparison with [6]based on presence of n-alkanes and n-paraffins (comparison with [2]) as well as other compounds that indicate no microbial attack.

Crude oil composition and products

Both crude oils of Khasib and Tannuma Formations reservoirs are non-biodegraded, evidenced by correlating shapes of the whole crude gas chromatography with [2]. The bulk properties of the accumulated crude oil in the Khasib Formation reservoir [7] indicated from C15+ composition and whole crude gas chromatography (Figure 6) of the oils of well EB-51 from depths 2,395–2,410 m areheavy oil of 17.4 API and mainly C12–C23 with abundant aromatic materials (44.6%) and less saturates (22.0%) of mainly paraffinic and naphthenic hydrocarbons with ratio of n _ Paraffin=Naphthene ¼ 0:69.The heavy compounds are of 15.8% NSO and 17.6% asphaltenes with wax. Hence, the main distillated hydrocarbons from this crude oil, accordingly correlating our analysis with [1], are kerosen (C11–C13), diesel fuel (C14–C18), heavy gas oil (C19–C25), and subsidiary lubricating oil (C25–C40). On the other hand, the oil dissipated and accumulated in Tannuma Formation reservoir immediately above the Khasib Formation is lighter oil than the Khasib's crude oil. The whole crude gas chromatography (Figure 6) of the oil of well EB-31 from depths 2,325-2,325 m is of 18.8 API which contain light alkanes of C4–C12 as well as the ordinary alkanes of C12–C23 which overwhelmed the Khasib's crude oil. This Tanuma's crude oil is higher aromatic (49.3%) and less saturates (21.4%) withn _ Paraffin=Naphthene ¼ 0:46. The heavy compounds are less than Khasib's crude oil; they are 13.1% NSO and 16.2% asphaltenes. This last oil could distillate gasoline (C4–C11) as well as the other constituents of kerosin, diesel fuel, and heavy gas oil.

Crude Oil Affinity

Source environment and lithology

Plots of tricyclic terpane ratios of C22/C21 versus C24/C23 documented in (table 3) on tricyclic terpane diagram. The analyzed data indicate marine carbonate source for all the studied oils by comparison with global standard environments of [8]and [9]. These source lithology assumptions are confirmed by plots of hopane C35S/C34S versus hopane C29/C30 in the hopane diagram (Figure 7) and hopane C31R/C30 versus tricyclic terpane C26/C25 in the hopoterpane diagram (Figure 8) as well as Pristane/Phytane ratios versus Canonical variable (Figure 9). Eh effect in the basin of the source rocks could be indicated by trisnorhopane [10]and[2] based on Ts (18 (H)-22, 29, 30-trisnorneohopane) is more stable than Tm (17 (H)-22, 29, 30-trisnorhopane), and degrades less during diagensis and catagensis . Accordingly, Plotting Ts/(Ts+Tm) versus Pr/(Pr+Ph) values from (tables 5and 6) for oils of the studied wells of East Baghdad field on Trisnorhopane diagram (Figure 10) indicate mature oils of Anoxic carbonate source.

Source maturation

Plots of Pristane n/C17 versus Phytane n/C18 on the [1] global diagram (Figure 11) indicate sources of mixed kerogen of types II& III of algal marine and strongly reducing environments with some influence of Terrestrial. The plots show mature organic matters of low degradation for all the samples in all the studied oil fields. Analysis of the aromatics have proved valuable tool for determining comparable numerical Tmax or vitrinite values [11], [12], [4], [2]. Accordingly, plots of the values of the East Baghdad field oils as well as source rock Zubair Formation extracts of Methyldibenzothiophe ratio (MDR) and Methylphenothrene (MPI) from (Table 6) are plotted on MDR diagram (Figure 12) of [12]and MPI diagram (Figure 13) of [11]. They have showed Tmax= 430-435^{o}C or the source of the studied oils with Ro= 0.6- 0.7 & 0.7-0.9 for Zubair Formation extracts, 0.65-0.85 for Zubair Formation oil that indicate early maturation for the hydrocarbon generated from the Zubair Formation and early to late maturation for the oil sources in Zubair oils. Khasib and Tannuma oil are of Ro= 0.75-0.95 that indicate late maturation of the source rocks.

Source age

The ranges of all the studied oil samples values are; C28/C29 Sterane = 0.65 and 0.52 and in between, the stable carbon isotopes of $\delta^{13}C$ (‰) of C15+Saturate = - 28.03- 27.50, C15+Aromatic= -28.27- 27.56 (Table 5) and Oleanane /(Oleanane +Hopane) (equivalent to OL/H) = 0.0- 0.02 (Table 6). They are used to determine the age of the kerogen that formed this oil. Plotting of δ13C (‰)on stable carbon isotope age assignment diagram (Figure 14) and the calculated average C28/ C29 sterane ratio on [13]source age assignment diagram (Figure 15) of Geomark Research OIL™ database have suggesting oil source ages in East Baghdad oil field to be ranged from Middle Jurassic to Lower Cretaceous in general which indicate mixed oil within this petroleum system. This assumption could be confirmed by the correlation with ages of biomarker ratios of the specific indicators of angiosperm plants to prokaryotic organism (Figure 16) based on first appearance and ranges of the prokaryote (Precambrian – Recent) and the angiosperm (Lower Cretaceous – Recent) and the studies of [14] and hence pre-Cretaceous strata of the Jurassic time should have no angiosperm with no Oleanane biomarkers with their first appearance is early Cretaceous and increased diversity in the late Cretaceous and Tertiary (Figure 16). Detailed age assignment could be obtained from plots of (Figure 15) and hence East Baghdad oil field of the Mesopotamian Basin could have their oil sourced from early Cretaceous Chia Gara and Zubair Formations and this assumption confirmed by same age of the extracts of the Zubair Formation (Figures 13&15). For comparison of oil of this study as well as oils of South Iraq with global petroleum system; the stable carbon isotopes of this oil (-27.56 to -28.27) could be about Upper Jurassic- Lower Cretaceous in its generation time, younger than Ordovician Texas, Mississippian North Dakota , Permian Wyoming's and Upper Jurassic North Sea oil that have lower value of the stable carbon isotope ratios from South Iraq, and older than Cretaceous West African and Miocene California oils that have higher value of stable carbon isotope ratios (Figure 17).

The Characters Used for Oil- Source Correlation are the Followings

Age similarity assignment

The age assessment diagram of δC13(%) and C28/C29 ratios of (Figures 14&15) have showed three values for age assignment; the first of Zubair Formation extract from depth 3364 meters is showing Lower Cretaceous assessment that could be comparable with the Zubair Formation itself according comparison with [16]and [15]. The second from depths 3342-3319 and 3068-3099 meters is showing Upper Jurassic Lower Cretaceous assessments that are comparable with the Chia Gara Formation according comparison with [17] and [15], and the third with C28/C29 from depth 3190-3106 meters is showing Jurassic assessment comparable with the Sargelu Formation according comparison with [17]and [15]. Accordingly the first value assessment could indigenous and would be used for oil-source rock correlation while the other two values are belonging to contaminant from the migrated and settle in the Zubair Formation. No age correlation matched between the oil source and the extracts of the Zubair Formations on isotopic and biomarker bases discussed above under oil source affinity and organic matter extracts paragraphs. On the other hand, oil generated from Upper Jurassic- Lower Cretaceous Chia Gara and Jurassic Sargelu source rocks have charged the Zubair Formation reservoirs.

Environmental similarity assignment

Based on gas chromatography/mass spectrometry, the data of the Steranes C27 ,C28 ,and C from crude oils are almost have similarity to the source extracts indicating same depositional conditions as evident by [18]. Plotting of these data on two sterane triangles of C27-C28-C29 that belonging to the oil for the top triangle and to the bitumen extracts for the underlying triangle (Figure 18) has showed comparable locations of Zubair Formation Extract with oil source of the Khasib and Tannuma Reservoirs to indicate that oil generated from the Zubair Formation had contributed to the Khasib and Tannumah reservoirs.

Maturation assessment for the correlation

Aromatic hydrocarbon analysis of the Zubair extracted organic matters of this study of Methyldibenzothiophene ratios (Figure 12) and Methylphenothrene (Figure 13) showed mature organic matters that had generated hydrocarbons with Tmax 433؛C and mean Ro=0.6-0.7 and charged some hydrocarbons to the Zubair and the overlying formations. In these figures, values of extracted organic matters are close to the values of the Zubair oil as well as Khasib and Tannuma oils to confirm charging of these reservoirs by the oil generated from the Zubair Formation.

Isotopic diagram

Of carbon isotope ratios δC13 saturates and δC13 aromatic [19]shows that source rock extract of hydrocarbon organic matters deposited in marine under sub-oxic environment. Plot locations of sources from oils biomarkers (Figure 19) close to extractable organic matters of Zubair Formation could indicate same genetic sources for the oil and the source rocks and hence the reservoir rocks could have been partly charged by the oil generated from the Zubair Formation.

Resins and Asphaltenes:

Resins and Asphaltenes Compounds: are not discrete compounds but high -molecular-weight heteroaromatic molecules that are poorly defined. The difference between Resins and Asphaltenes is defined by their relative solubility in hydrocarbons, which roughly corresponds to size [9]. NSO Compounds (resins) molecules are usually with less than 40 carbon atoms. Asphaltenes are not soluble complex molecules with more than 40 carbon atoms. The amounts of asphaltenes plus resins generally less than 10% in paraffinic oils and less than 20% in paraffinic - naphthenic oils; they may reach (10 to 40%) in aromatic-intermediate [4]. Zubair, Khasib, and Tanuma crude oils is mainly aromatic (Figure 2), where saturated hydrocarbon percentage is ranging from(21.5%to 32.2%), while aromatic is ranging from(39.8% to 47.4%), and NSO and resin compound is between (16.9% to 22.5 %) (Table 3), and by plotting these data on ternary hydrocarbon plot of Aromatic HC, Saturated HC, and NSO compounds could assess a normal crude oil of Zubair, Khasib, and Tanuma with no degradation with abundant aromatic compounds (Figure 2).

Oil Source for Mishrif and Mauddud Formationsbasic Biomarkers

1. Pristane/phytane (The Pr/Ph ratio is partially controlled by the oxygen exposure of the chlorophyll phytol side chain during Burial/transport.);
2. C24 Tetracyclic Terpane % relative to C30 Hopane (A high content of the C24 Tetracyclic Terpane (17, 21-Secohopane) is empirically associated with carbonate/evaporite source rocks and is believed to be from microbial alteration of pentacyclic hopanes.).
3. Hopanes C35/(C34+C35)(The predominance of C35 over C34 Hopanes is associated with highly reducing environments (e.g. Carbonate/evaporite) where the C35 Bacteriohopanetetrol precursor is reduced intact rather than in less reductive environments where Processes cause chain shortening.).
4. R22 index (Index of middle parity and odd n-alkanes 2 * C22 / (C21 + C23), or equal to the odd - marine origin).
5. CPI (the ratio of n-alkanes with an odd number of carbon atoms in the molecule to the amount of n-alkanes with an even number of Carbon atoms in the molecule in different ranges of molecular weight)
6. In carbonate environments, the relative abundance is believed to be controlled by the balance of green (C29 sterols) vs. Red (C27 Sterols) algae. In clear deep water carbonate environments, red algae (C27) dominate, but shallow systems favor green algae (C29).
7. Source rock is the same for oil in Mishrif and Mauddud formations the original organic matter - algae, bacteria that have accumulated, probably in upwelling conditions.

Maturity of Mishrif and Mauddud Oil Basic Biomarkers

1. Ts/(Ts+Tm) (The ratio of 18α(H)-trisnorneohopane (Ts) to 17α(H) trisnorhopane (Tm) increases with maturity due to the greater thermal Stability of Ts. Starting at low values parameter H6 generally reaches 0.5 at OGT and 0.9 at late maturity. Variation in the catalytic effects of the source rock type will effects the absolute ratios between facies for the same level of maturity);
2. 4-METHYLDIBENZOTHIOPHENE/1-METHYLDIBENZOTHIOPHENE (With increasing thermal stress, the 1-isomer decreases relative to the 4-methyldibenzothiophene isomer. The ratio varies from 1 in immature sediments to above 300 in thermally mature condensates. It is Highly organofacies dependent and this has to be taken into account in its interpretation);
3. MPI [(3ME+2ME)/(PHENANTHRENE+9ME+1ME)]* 1.5 (As maturation progresses there is an increase in the relative amount of the 3- and 2- ethylphenanthrenes due to rearrangement to more stable forms. Emperical correlations to vitrinite reflectance (Ro)have been Published for MPI-1);
4. C29 STERANES αββ/(αββ+ααα) (Steranes derived from biological sources inherit a 5α(H), 14α(H),17α(H) ring configuration. With Increasing thermal stress the αββ forms predominate either due to isomerisation from ααα, greater stability of the αββ forms or later Liberation of αββ's from the kerogen);
5. C29 ααα STERANES 20S/(20S+20R) (Steranes derived from biological sources inherit a 20R side chain configuration. With increasing Thermal stress 20S forms occur either due to isomerisation of 20R, greater stability of the 20S or later liberation from the kerogen of the 20S isomer);
6. Pr/n-C17 и Pp/n-C18 (ratio isoalkanes and corresponding normal alkanes);
7. Generation of Mishrif and Mauddud oil happened on different stage of catagenesis. Mishrif - early stage MC1, Mauddud - later MC2-3.

RESULTS AND CONCLUSION

- The geochemical analyses of Zubair, Khasib, Maudud, Ahmadi, Rumaila, Mishrif, and Tanuma reservoir crude oils of East Baghdad, Ahdab, and Badra Oil Fields show that oil samples could be related to one family and this oil are non-biodegraded, marine, and non-waxy derived from carbonate deposited in anoxic marine environment.
- The oil samples analysis shows the Muddud crude oil in Badra oil field is light (32-34 API). While the medium crude oil from Zubair and Mishrif in East Baghdad, Badra oil fields respectably (28-31 API). The heavy crude oil (10-28API) for Tanuma and Khasib formation in East Baghdad, either Khasib Formation only in Ahdab oil field. As well as Mishrif Formation in Badra oil field.
- The source of all oil samples of studied formations from late Middle Jurassic-late Cretaceous source rocks. Hence the most appropriate source for this crude oil mainly Sargelu Formation.

REFERENCES

1. Hunt, J. M. (1996) Petroleum geochemistry and geology, 2nd edn, Freeman, New York, 743P.
2. Peters, K.E., Walters, C.C., and Moldowan, J.M. (2005b) The biomarker guide. Vol. 2: Biomarkers and isotopes in petroleum exploration and earth history. The press syndicate of the University of Cambridge, pp.475 -1155.
3. Moldowan, J.M., P. Sundararaman, and M. Schoel 1986: Sensitivity of biomarker properties to depositional environment and/or source input in the Lower Toarcian of S.W. Germany. Organic Geochemistry, 10: pp 915- 926.
4. Tissot, B. P. and Welte, D.H. (1984) Petroleum Formation and Occurrence. Springer-Verlag, New York .699 P.
5. Bastow, T.P., R. Alexander, R.I. Kagi, I,B, Sosrovidjojo 1998: The effect of maturity and biodegradation on the enantiometric of sedimentary dihydro-*ar*-curcumene and related compounds. Organic Geochemistry, 29: pp 1297-1304.

6. Wegner. L.M., Davis, C.L. and Isaksen, G.L. 2002: Multiple controls on petroleumbiodegradation and impact on oil quality. SPE Reservoir Evaluation and Engineering,3, pp. 375-383.
7. Al-Ameri, Thamer K. and Al-Obaidi, R.Y., 2011: Cretaceous Petroleum system of theKhasib and Tannuma oil reservoir, East Baghdad oil field, Iraq. Arabian Journal of Geoscience, Springer, 4: 915-932.
8. Zumberge, J. E., Russell, J. A., and Reid, S. A. (2005) Changing of Elk Hills reservoirs as determined by oil geochemistry, Bulletin of AAPG, v.89, pp.1347-1371.
9. Peters, K.E., Walter, C.C., and Moldowan, J.M. (2005a) The biomarker guide. Vol.1: Biomarkers and isotopes in the environment and human history. The press syndicate of the University of Cambridge, pp. 471.
10. Isaksen, G.H. 2004: Central North Sea hydrocarbon systems generation, migration, entrapment and thermal degradation of oil and gas. AAPG Bulletin, vol. 8, No. 11, pp.1545-1572.
11. Peters K. E. and Moldowan, J. M. (1993) The biomarker guide, interpreting molecular fossils in petroleum and ancient sediments. Prentice – Hall, Englewood Cliffs, N.J, pp.863-87.
12. Radke, M. (1988) Application of aromatic compounds as maturity indicators in source rocks and crude oils, Marine and Petroleum Geology, Vol. 5(3), pp. 224-236.
13. Grantham, P.J. and L.L. Wakefield 1988: Variations in th sterane carbon number distribution of matine source rock derived crude oils through geological time. Organic Geochemistry, volume 12, pp 293-304.
14. Moldowan J.M., Dahl, J., Huizinga, B.J. et.al., 1994: The molecular fossils record of Oleanane and its relation to angiosperm. Science, 265, pp 768- 771.
15. Bellen, R. C. Van, Dunnington, H.V., Wetzel, R. and Morton, D.(1959) *Lexique stratigraphique Internal Asie. Iraq.* Intern. Geol .Conger. Comm. Stratigr, 3, Fasc. 10 a, 333 P.
16. Al-Ameri, T. K. (2011) Khasib and Tanuma oil sources, East Baghdad oil field, Marine and Petroleum Geology v.28, and pp.880-894.
17. Al-Ameri, Thamer K. and Srood. F. Al-Nagshbandi 2015: Age assessments andpalynofacies of the Jurassic oil source rocks succession of North Iraq. Arabian Journal of Geoscience. Volume 8 (2), pages 759-771.
18. Peters, K. E. and Cassa, M.R. (1994) Applied Source rock geochemistry .In: The petroleum system – from source to Trap (L.B.Magoon and W.G.Dow, eds).AAPG, Tulsa, OK, pp. 93-117.
19. Sofer, Z. (1984) Stable carbon isotope compositions of crude oil: application to source depositional environments and petroleum alteration. AAPG Bulletin, Vol.68, pp. 31-49.

Table 1. Core sample and kind of analysis.

S. No.	Well No.	Formation	Depth (m)	Oil field	Sample Type	Kind of analysis
1	EB92	Tanuma	2029	East Baghdad	core	1
2	EB92	Tanuma	2034	East Baghdad	core	1
3	EB92	Tanuma	2043.5	East Baghdad	core	1
4	EB92	Tanuma	2053.5	East Baghdad	core	1
5	EB92	Tanuma	2059	East Baghdad	core	1
6	EB92	Tanuma	2064	East Baghdad	core	1
7	EB92	Tanuma	2071	East Baghdad	core	1
8	EB92	Tanuma	2094	East Baghdad	core	1
9	EB92	Tanuma	2098	East Baghdad	core	1
10	EB92	Khasib	2146	East Baghdad	core	1
11	EB92	Khasib	2157	East Baghdad	core	1
12	EB92	Khasib	2161	East Baghdad	core	1
13	EB92	Khasib	2170	East Baghdad	core	1
14	EB92	Khasib	2175	East Baghdad	core	1

15	EB92	Khasib	2178	East Baghdad	core	1
16	EB92	Khasib	2182	East Baghdad	core	1
17	EB92	Khasib	2188	East Baghdad	core	1
18	EB92	Khasib	2193.5	East Baghdad	core	1
S. No.	Well No.	Formation	Depth (m)	Oil field	Sample Type	Kind of analysis
19	EB92	Zubair	3045	East Baghdad	core	1
20	EB92	Zubair	3062	East Baghdad	core	1,2
21	EB92	Zubair	3066	East Baghdad	core	1,2
22	EB92	Zubair	3099	East Baghdad	core	1,2
23	EB92	Zubair	3106	East Baghdad	core	1,2
24	EB92	Zubair	3110	East Baghdad	core	1,2
25	EB92	Zubair	3174	East Baghdad	core	1
26	EB92	Zubair	3181	East Baghdad	core	1
27	EB92	Zubair	3190	East Baghdad	core	1,2
28	EB92	Zubair	3199.5	East Baghdad	core	1,2
29	EB92	Zubair	3205	East Baghdad	core	1,2
30	EB92	Zubair	3209	East Baghdad	core	1
31	EB92	Zubair	3263	East Baghdad	core	1
32	EB92	Zubair	3270	East Baghdad	core	1
33	EB92	Zubair	3277	East Baghdad	core	1
34	EB92	Zubair	3306	East Baghdad	core	1,2
35	EB92	Zubair	3331	East Baghdad	core	1,2
36	EB92	Zubair	3342	East Baghdad	core	1,2
37	EB92	Zubair	3347	East Baghdad	core	1
38	EB92	Zubair	3355	East Baghdad	core	1
39	EB92	Zubair	3364	East Baghdad	core	1,2
40	BD-4	Maudud-A	4486.25	Badra	core	1,2
41	BD-4	Maudud-B	4520.31	Badra	core	1,2
42	BD-4	Maudud-B	4520.71	Badra	core	1,2
43	BD-4	Maudud-B	4523.59	Badra	core	1,2
44	BD-4	Maudud-B	4526.57	Badra	core	1,2
45	BD-4	Maudud-B	4532.44	Badra	core	1,2
46	BD-4	Maudud-B	4535.18	Badra	core	1,2
47	BD-4	Maudud-D	4590.4	Badra	core	1,2
48	BD-4	Maudud-D	4615.64	Badra	core	1,2
49	BD-4	Maudud-D	4619.93	Badra	core	1,2
50	BD-5	Maudud-D	4581.32	Badra	core	1,2
51	BD-5	Maudud-D	4589.40	Badra	core	1,2
52	BD-5	Maudud-D	4595.23	Badra	core	1,2
53	BD-5	Maudud-D	4583.20	Badra	core	1,2
54	BD-5	Maudud-D	4586.14	Badra	core	1,2

55	BD-5	Maudud-D	4590.85	Badra	core	1,2
56	BD-5	Maudud-D	4591.67	Badra	core	1,2
57	BD-5	Maudud-D	4593.08	Badra	core	1,2
58	BD-5	Maudud-D	4598.18	Badra	core	1,2
59	BD-5	Maudud-G	4725.55	Badra	core	1,2
60	BD-5	Maudud-B	4514.12	Badra	core	1,2
61	BD-5	Maudud-D	4596.79	Badra	core	1,2
62	BD-5	Maudud-D	4597.53	Badra	core	1,2
63	BD-5	Maudud-D	4600.08	Badra	core	1,2
64	BD-5	Maudud-D	4600.95	Badra	core	1,2
65	BD-5	Maudud-D	4602.62	Badra	core	1,2
66	BD-5	Maudud-D	4603.25	Badra	core	1,2
67	BD-5	Maudud-D	4603.56	Badra	core	1,2
68	BD-5	Maudud-E	4627.04	Badra	core	1,2
69	BD-5	Maudud-E	4627.18	Badra	core	1,2
70	BD-5	Maudud-E	4622	Badra	core	1,2

Table 3. The geochemical analysis of crude oil samples

Sample no.	Field name	Well No.	Formation	Depth (m)	Latittude and longitude	
1	East Baghdad	EB-92	Zubair	3099.5	E 437618.55	N 3705066.48
2	East Baghdad	Eb-92	Zubair	3433	E 437618.55	N 3705066.48
3	East Baghdad	EB-21	Zubair	3042.5	E 441996.4	N 3700559.4
4	East Baghdad	EB-68	Khasib	2161	E 439484	N 3705159
5	East Baghdad	EB-68	Khasib	2179	E 439484	N 3705159
6	East Baghdad	Eb-68	Tanuma	2060	E 439484	N 3705159
7	Badra	BD-5	Mishrif	4252		
8	Badra	BD-5	Maudud	4589.2		

Table 3. Selected source lithology biomarkers for crude oil in East Baghdad oil field

No	Well	Formation	Depth (m)	Tr. C22/21	Tr. C24/23	Hopane C35S/C34S	Hopane C29/C30	Tr. C26/C25	Hopane C31R/C30	0L/H	MPI	MD R
1	EB92	Zubair	3099	0.99	0.31	0.92	1.29	0.79	0.31	0.00	0.68	1.76
2	EB21	Zubair	3042	0.94	0.30	0.97	1.35	0,81	0.33	0.00	0.56	1.82
3	EB68	Khasib	2161	0.93	0.31	1.05	1.47	0.80	0.32	0.00	0.77	1.61
4	EB68	Khasib	2179	0.93	0.31	1.02	1.51	0.80	0.33	0.00	0.78	1.63
5	EB68	Tannuma	2060	0.88	0.32	1.03	1.51	0.78	0.32	0.00	0.74	1.65
6	EB5	Khasib	2508	0.90	0.31	1.06	1.41	0.78	0.36	0.01	-	-
7	EB31	Tannuma	2441	0.91	0.30	1.02	1.39	0.77	0.31	0.02	-	-

Table 4. The geochemical analysis of crude oil samples

Sample No.	Well No.	formation	Depth (m)	Saturated HC	Aromatic HC	NSO
1	EB92	Zubair	3099.5	32.3	39.8	16.9
2	EB21	Zubair	3042.5	29.5	37.6	17.5
3	EB68	Khasib	2161	22.5	41.2	22.5
4	EB68	Khasib	2179	22.7	46.2	17.8
5	EB68	Tanuma	2060	21.5	47.4	17.6
6	BD-5	Maudud	4593	34.8	42.6	15.7
7	BD-5	Maudud	4581	33.4	45.3	17.2
8	BD-4	Mishrif		22.4	27.6	27.5

Table 5. Organic geochemical analysis for rock samples of this study in EB01

Sample No.	***Well No.***	***Formation***	***Depth***	**TOC %**	***S_1 Mg/g***	***S_2 Mg/g***	***HI***	***PI***	***PP***	***S1/TOC***	***T_{max}***
			(M)				***S_2/TOC***	***$S_1/(S_1+S_2)$***	***S_1+S_2***		
1	EB01	Shuaiba	3325	0.14	-	-	-	-	-		-
2	EB01	Shuaiba	3406	0.21	-	-	-	-	-		-
3	EB01	Zubair	3433	0.74	0.78	1.45	196	0.35	2.23	1.05	431
4	EB01	Zubair	3450	0.54	0.27	0.45	83	0.83	0.72	0.5	429
5	EB01	Zubair	3475	2.05	0.48	2.01	98	0.19	2.49	0.23	433
6	EB01	Zubair	3505	0.88	0.28	1.76	200	0.14	2.04	0.31	429
7	EB01	Zubair	3540	4.47	0.86	12.37	261	0.07	13.23	0.19	419
8	EB01	Zubair	3575	1.06	0.07	71.62	153	0.3	2.32	0.06	427
9	EB01	Zubair	3596	0.67	0.2	0.72	109	0.22	0.92	0.29	418
10	EB01	Zubair	3605	0.7	0.09	0.93	133	0.09	1.02	0.12	437
11	EB01	Zubair	3653	0.8	0.22	0.78	98	0.22	1.0	0.27	431
12	EB01	Zubair	3667.2	0.5	-	-	-	-	-	-	-
13	EB01	Zubair	3710	0.96	0.15	1.36	142	0.1	1.51	0.15	429
14	EB01	Zubair	3763	0.92	0.48	1.54	167	0.24	2.02	0.52	431
15	EB01	Zubair	3809	0.70	0.45	1.56	233	0.22	2.01	0.46	427
16	EB01	Zubair	3832	0.99	0.27	1.38	138	0.17	1.65	0.27	431

Table 6. Organic geochemical analysis for rock samples of this study in EB01

Sample No.	*Well No.*	*Formation*	*Depth*	*TOC (Wt) %*	*S1 Mg/g*	*S2 Mg/g*	*HI*	*PI*	*PP*	*S1/TOC*	*Tmax*
			(M)				*S2/TOC*	*S1/(S1+S2)*	*S1+S2*		*(ºC)*
17	EB01	Zubair	3837	0.84	0.32	0.97	116	0.25	1.29	0.38	431
18	EB01	Ratawi	38833	0.31	0.08	0.28	94	0.22	0.36	0.25	439
19	EB01	Ratawi	3920	0.52	0.13	0.5	96	0.21	0.63	0.25	431
20	EB01	Ratawi	4250	0.55	0.13	0.52	95	0.2	0.65	0.23	435
21	EB01	Ratawi	4365	0.64	0.15	0.93	145	0.14	1.08	0.23	437
22	EB01	Ratawi	4420	0.93	0.83	1.45	156	0.36	2.28	0.89	431
23	EB01	Ratawi	4427	1.45	1.82	3.77	260	0.33	5.59	1.25	431
24	EB01	chiagara	4430	1.03	0.59	4.16	403	0.12	4.75	0.57	438
25	EB01	chiagara	4441	1.23	2.40	3.94	320	0.38	6.34	1.95	434
26	EB01	chiagara	4450	1.24	2.25	4.55	366	0.33	6.80	1.81	432
27	EB01	chiagara	4460	1.90	2.72	8.00	421	0.25	10.72	1.43	443
28	EB01	chiagara	4480	1.54	2.53	3.68	238	0.41	6.21	1.64	433
29	EB01	chiagara	4490	2.01	3.57	3.69	183	0.49	7.26	1.77	428
30	EB01	chiagara	4501	1.28	1.72	2.94	229	0.37	4.66	1.34	436
31	EB01	chiagara	4510	2.05	3.63	3.46	168	0.51	7.09	1.77	430
32	EB01	chiagara	4520	3.28	5.04	6.00	182	0.46	11.04	1.53	435

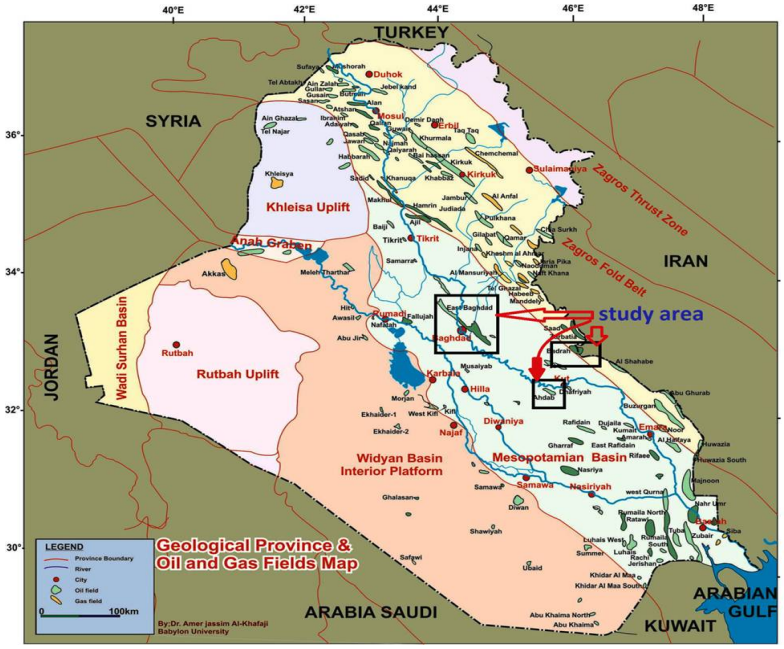

Figure 1. Shows Main Oil and Gas Fields in Iraq and the studied oil fields location of the studied area after T.K. Al-Ameri (2011).

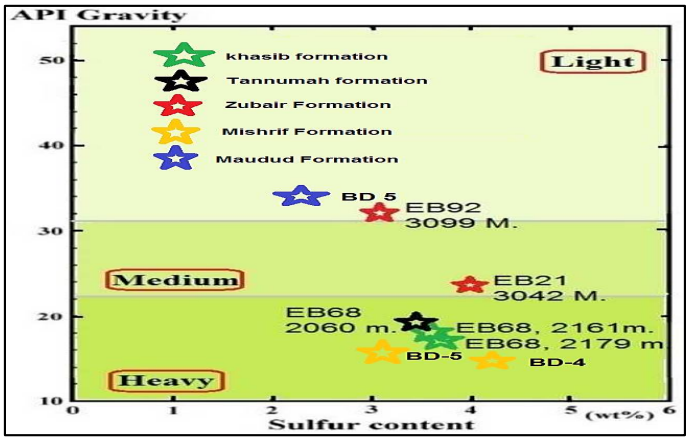

Figure 2. Crude oil characterization diagrams for study area oil fields oil character based on API and Sulfur content

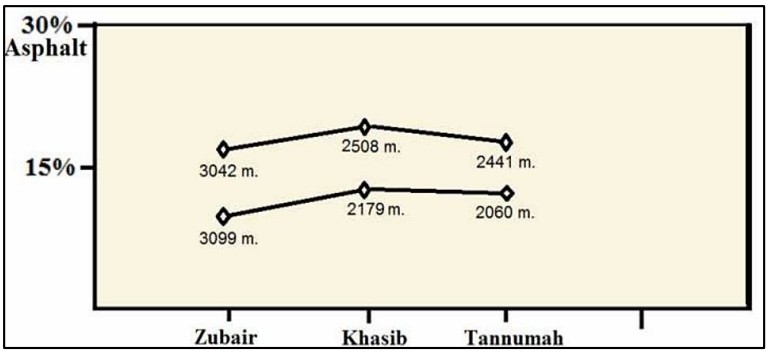

Figure 3.Crude oil characterization diagrams for study area oil fields oil character based on b- Asphalt distribution in the crude oil of selected oil wells in East Baghdad oil field, numbers in the figure are for depths.

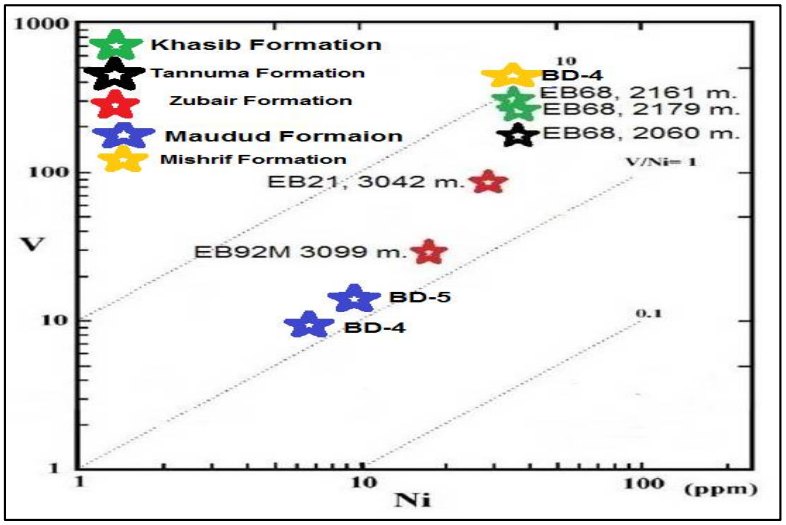

Figure 4. Crude oil characterization diagrams for study area oil fields oil character based on Ni-Vfor Bacterial phytoplancton of marine carbonate of East Baghdad oil field plotted ondiagram of the Suez Gulf.

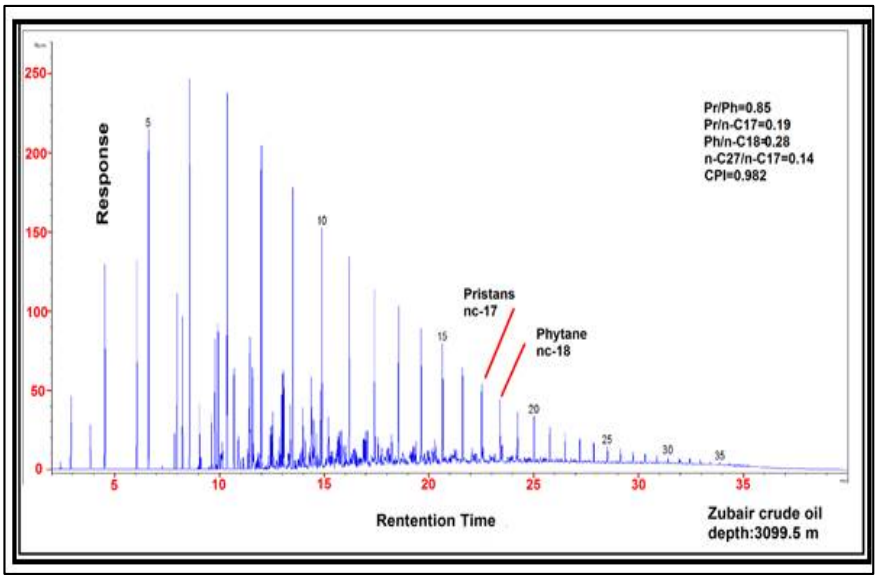

Figure 5. Examples from Geochemical Summary Sheets of the reservoir oil from studied oil fields in study area showing whole oil gaschromatogram.

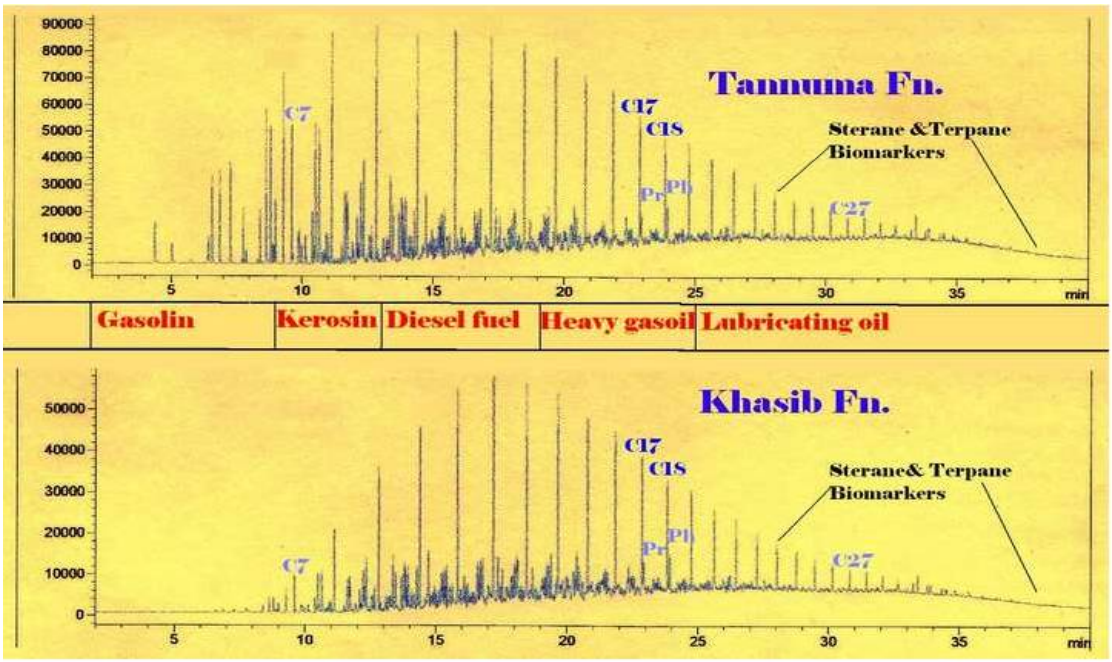

Figure 6. Crude oil characterization diagrams for study area oil fields oil character based on Suggested refined hydrocarbon products ofthe Kasib and Tannuma oils

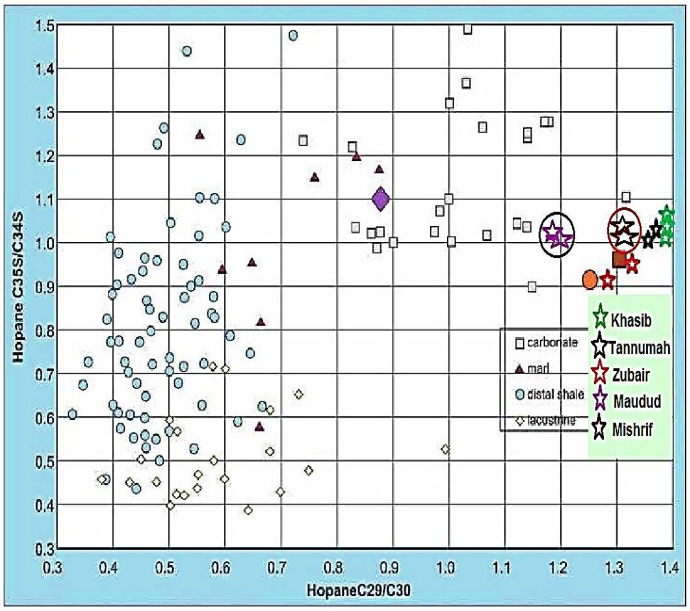

Figure 7. Biomarker diagrams of the analyzed samples for source rock type affinity of the East Baghdad oil field. Other data points represent average oil values from global petroleum systems from marine carbonate, distal marine shale, marine marl, and lacustrine shale source rocks from GeoMark Research OILS™ databaseaverage hopane ratios.

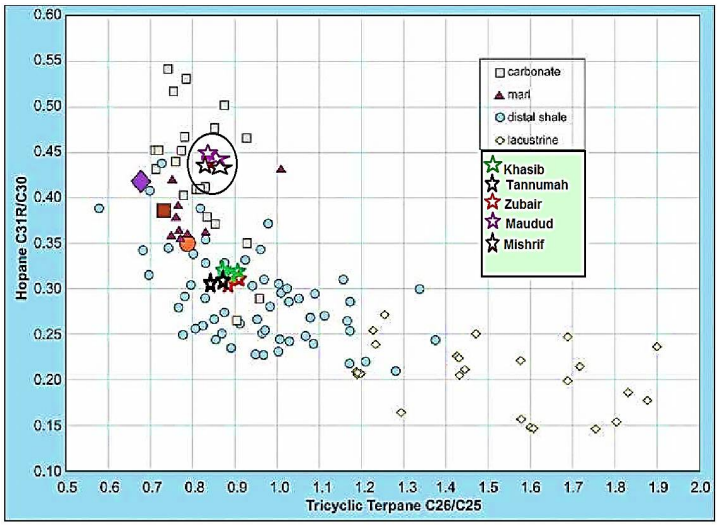

Figure 8. Biomarker diagrams of the analyzed samples for source rock type affinity of the East Baghdad oil field. Other data points represent average oil values from global petroleum systems from marine carbonate, distal marine shale, marine marl, and lacustrine shale source rocks from GeoMark Research OILS™ databaseTricyclic and Hopane ratios.

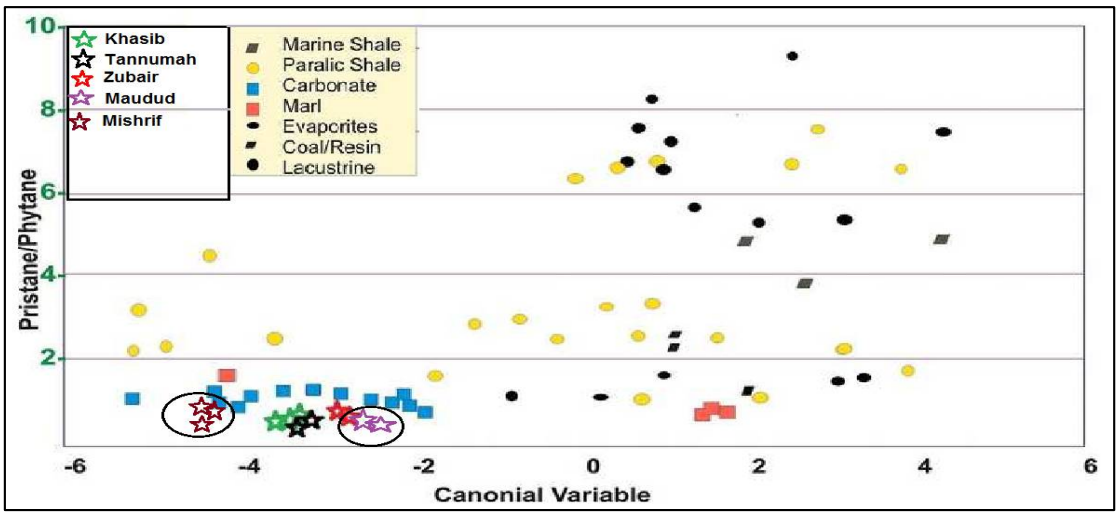

Figure 9. Biomarker diagrams of the analyzed samples for source rock type affinity of the East Baghdad oil field. Other data points represent average oil values from global petroleum systems from marine carbonate, distal marine shale, marine marl, and lacustrine shale source rocks from GeoMark Research OILS™ database, Canonical Variables versus pristane/phytane ratio.

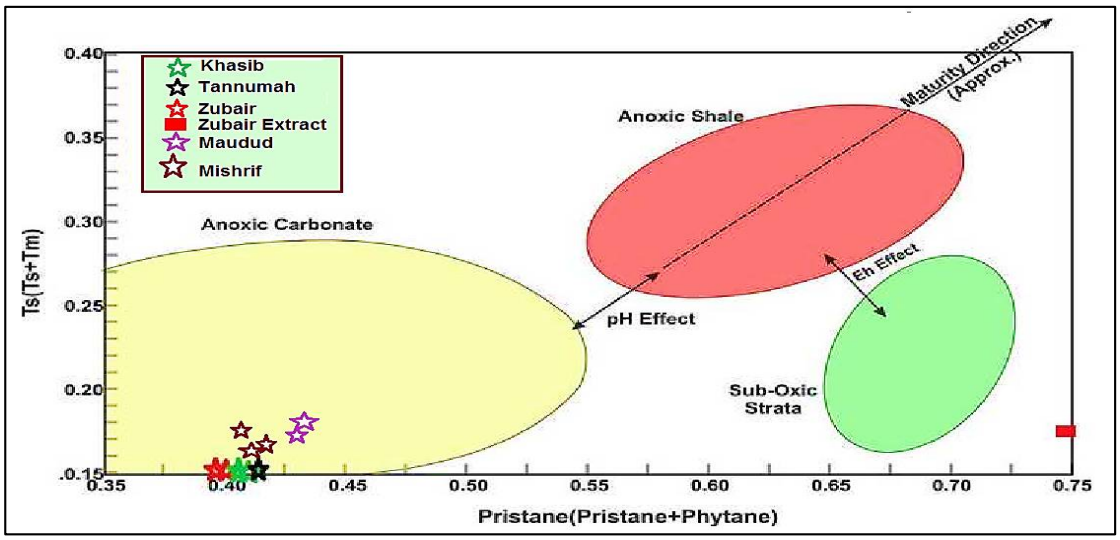

Figure 10. Biomarker diagrams of the analyzed samples for source rock type affinity of the East Baghdad oil field. Other data points represent average oil values from global petroleum systems from marine carbonate, distal marine shale, marine marl, and lacustrine shale source rocks in GeoMark Research OILS™ database Eh effect are indicated by Trisnorhopane.

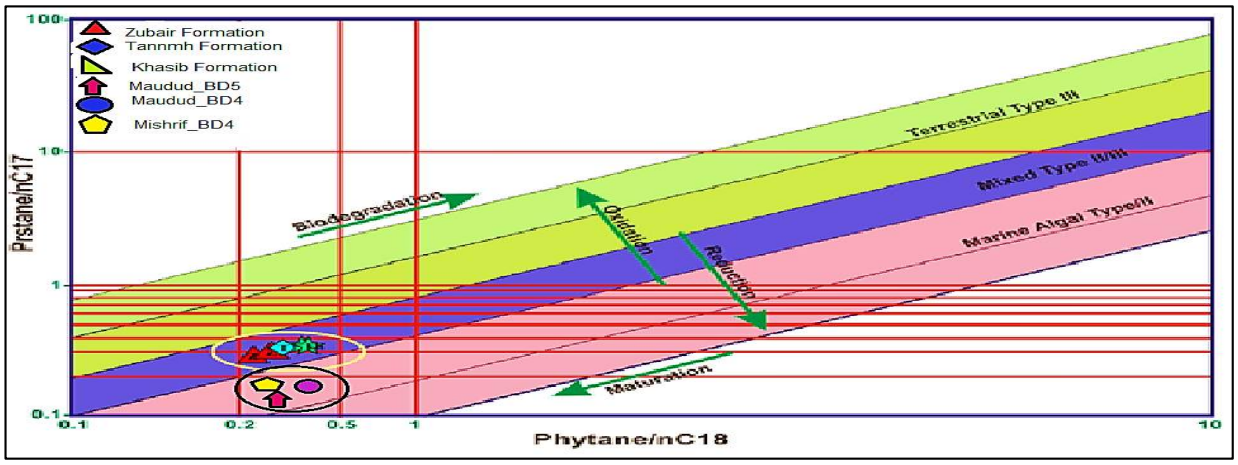

Figure 11. Pristane/ nC17 versus phytane/nC18 for Zubair, Khasib Tanuma, Maudud, and Mishrif crude oils from stady area oil fields (after Peters *et al.*, 1999 a).

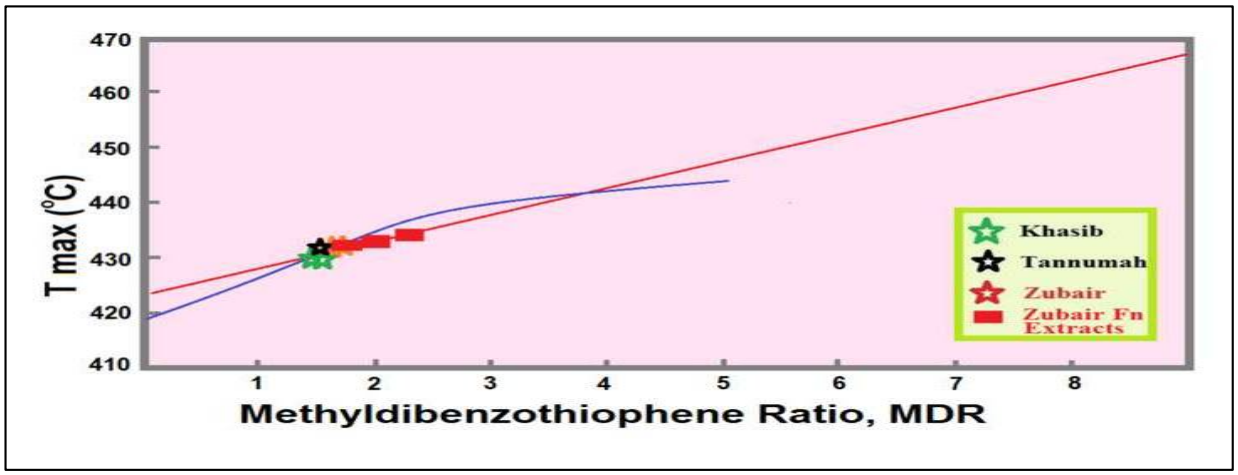

Figure 12. Maturation and organic type's diagrams with plots of the analysis data of the studied oil samples; Methyldibenzothiophene ratio (MDR) aromatic biomarkers versus Tmax.

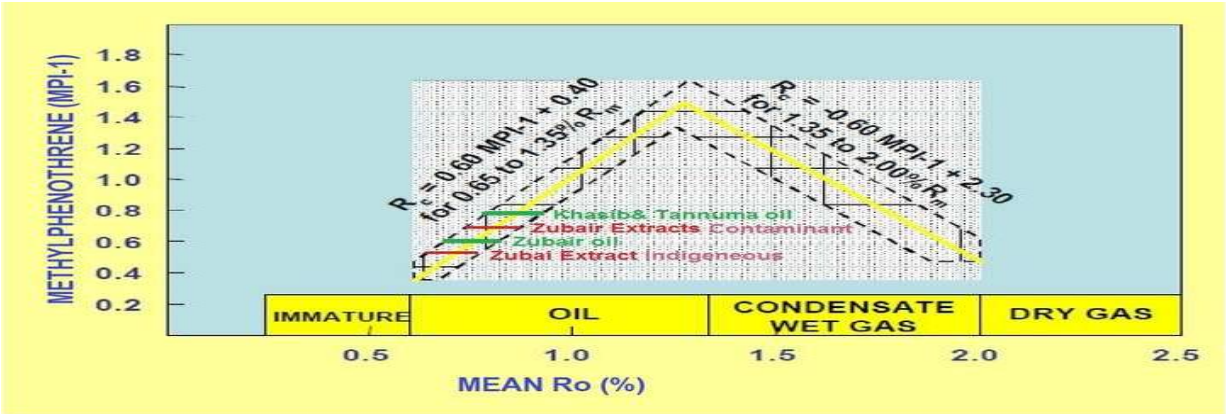

Figure 13. Maturation and organic type's diagrams with plots of the analysis data of the studied oil samples Methylphenothrene (MPI) versus mean vitrinite reflectance (%Ro) diagram.

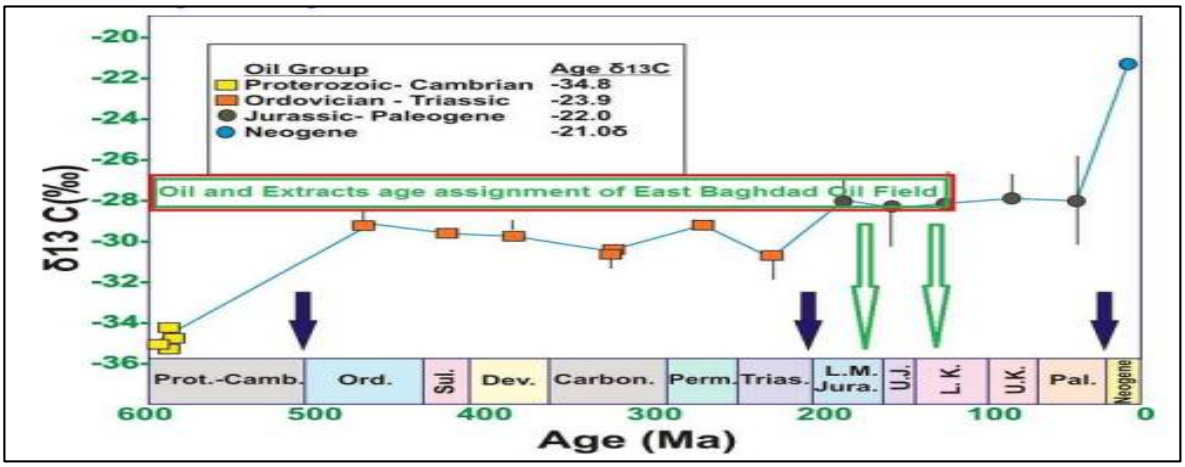

Figure 14. Source age assessments for East Baghdad oil field and extracts for the analyzed samples in this study including; a- stable carbon isotopes diagram.

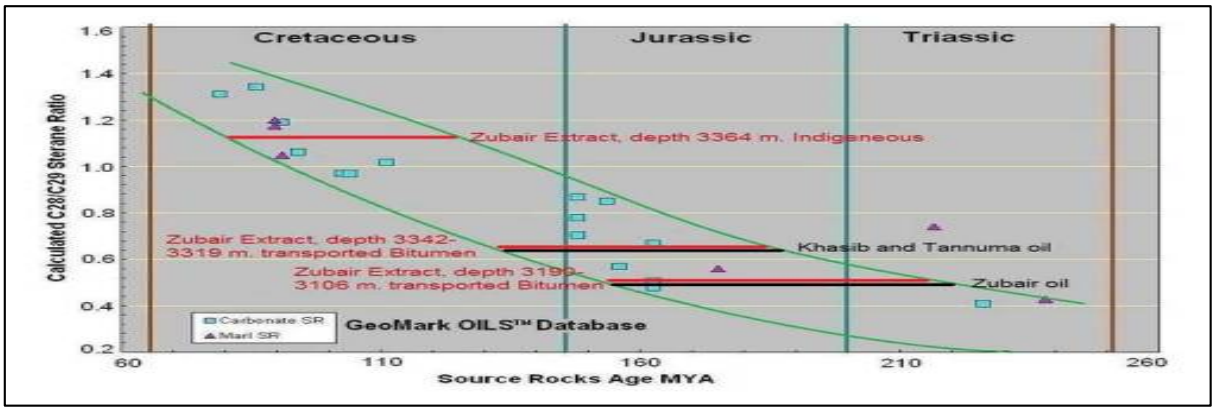

Figure 15. Source age assessments for East Baghdad oil field and extracts for the analyzed samples in this study including; Sterane ratio diagram

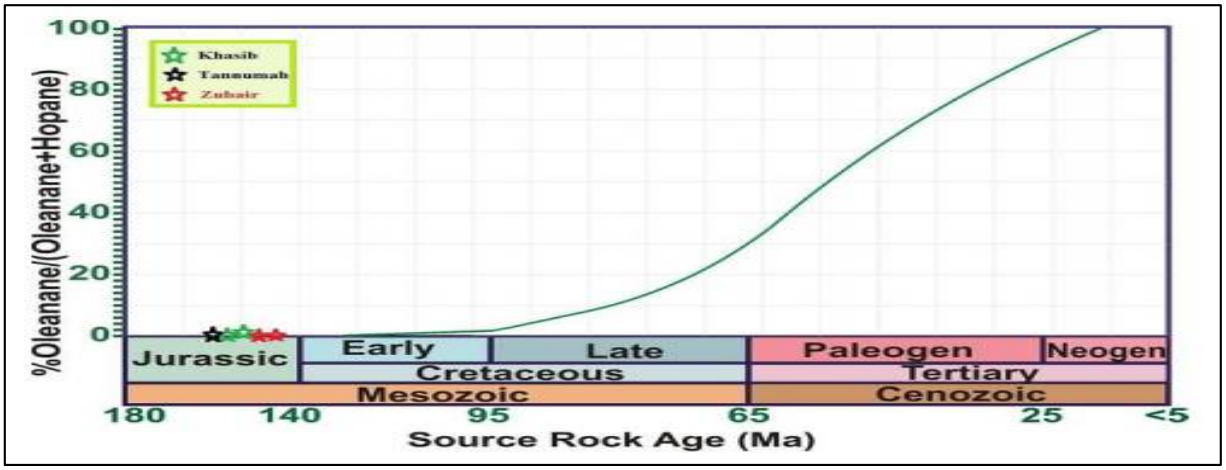

Figure 16. Source age assessments for East Baghdad oil field and extracts for the analyzed samples in this study including; Oleanane ratios in bitumen extract curve based on fossil pollen reports assigned to extant angiosperm families.

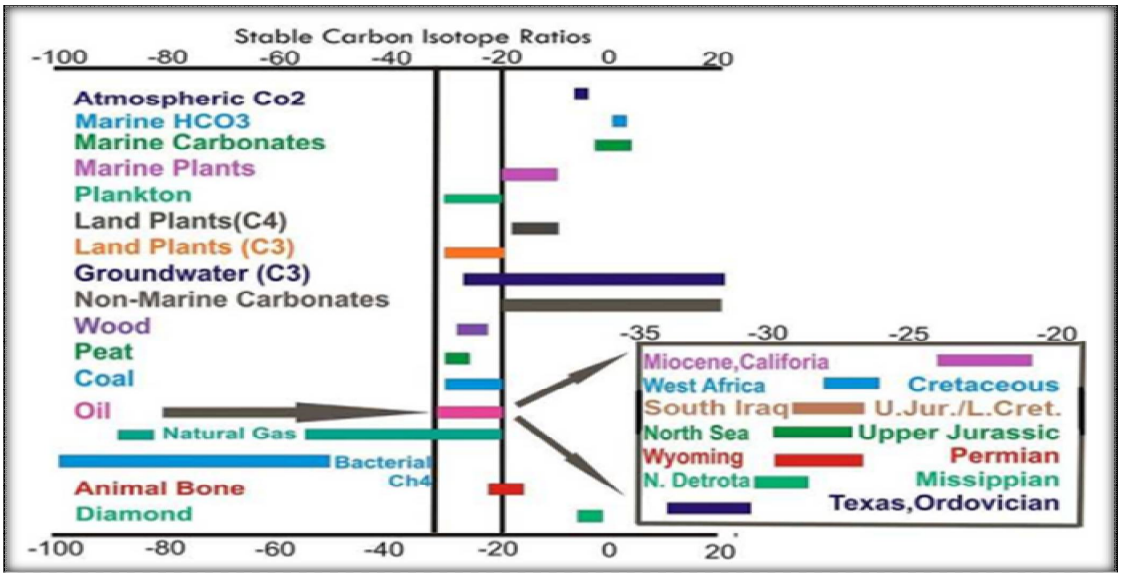

Figure 17. Source age assessments for East Baghdad oil field and extracts for the analyzed samples in this study including; stable carbon isotopes variations with age and global locations for oils and other organic matters.

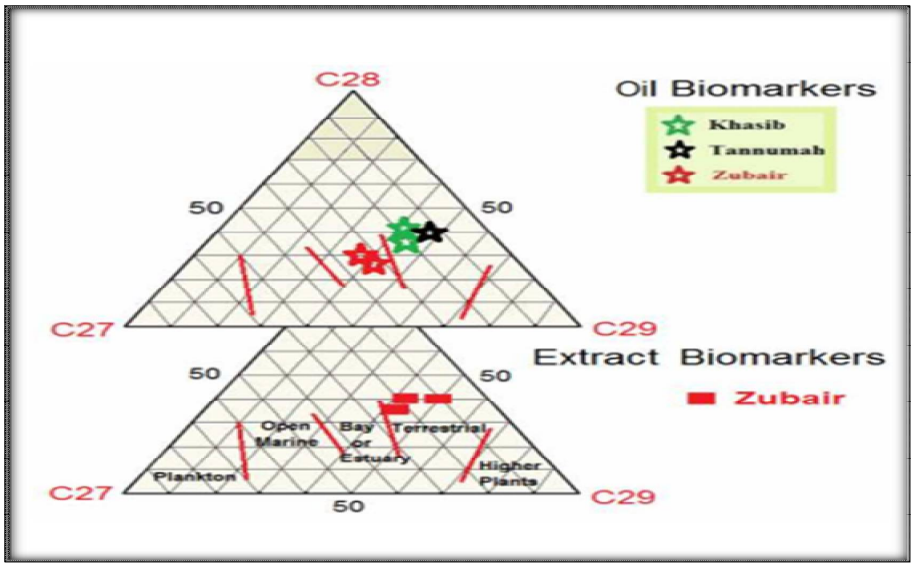

Figure 18. Oil- Source rocks correlation diagrams; Sterane triangle for oil-source correlation.

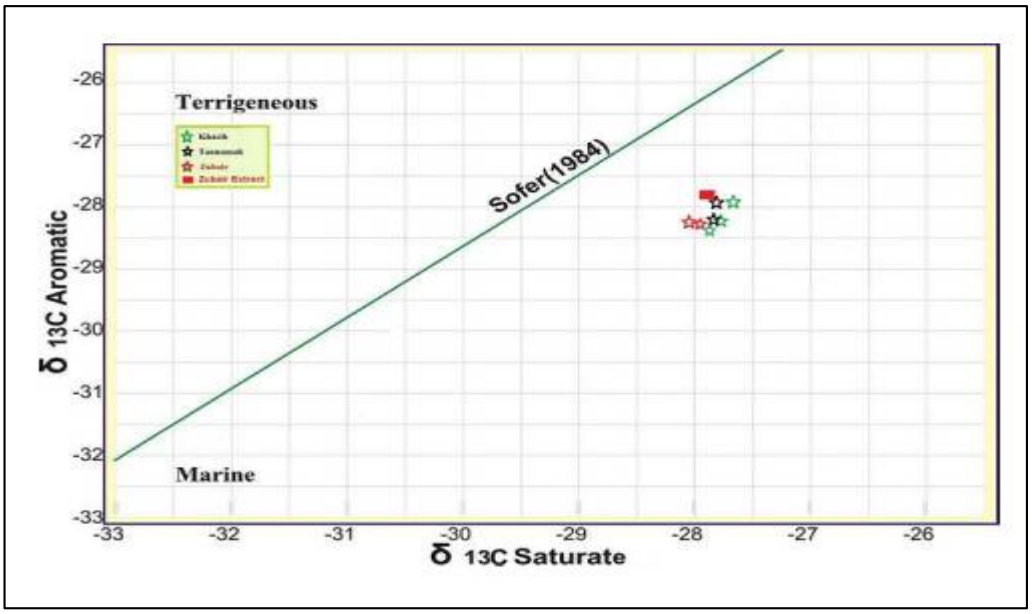

Figure 19. Oil- Source rocks correlation diagrams; isotopic oil grouping.